

HERA AND THE LHC

A workshop on the implications of HERA for LHC physics

March 2004 – March 2005

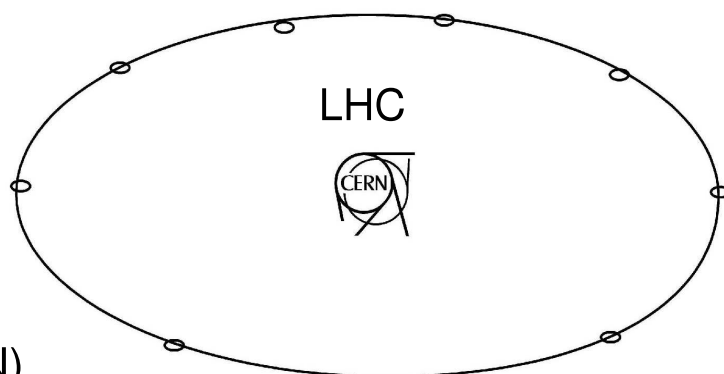
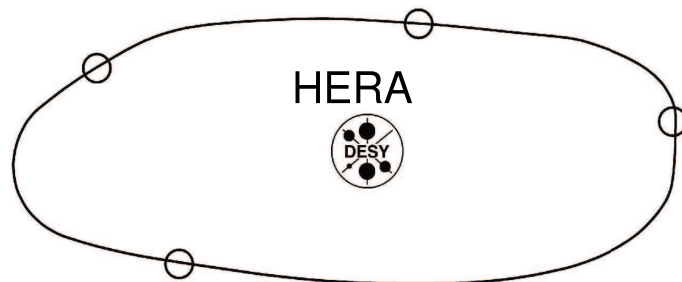
Parton density functions

Multijet final states
and energy flow

Heavy quarks

Diffraction

Monte Carlo tools



Proceedings

Editors:

A. De Roeck (CERN)

H. Jung (DESY)

Organizing Committee:

G. Altarelli (CERN), J. Blümlein (DESY), M. Botje (NIKHEF),
J. Butterworth (UCL), A. De Roeck (CERN) (chair), K. Eggert (CERN),
H. Jung (DESY) (chair), M. Mangano (CERN), A. Morsch (CERN),
P. Newman (Birmingham), G. Polesello (INFN), O. Schneider (EPFL),
R. Yoshida (ANL)

Advisory Committee:

J. Bartels (Hamburg), M. Della Negra (CERN), J. Ellis (CERN),
J. Engelen (CERN), G. Gustafson (Lund), G. Ingelman (Uppsala), P. Jenni (CERN),
R. Klanner (DESY), M. Klein (DESY), L. McLerran (BNL), T. Nakada (CERN),
D. Schlatter (CERN), F. Schrempp (DESY), J. Schukraft (CERN),
J. Stirling (Durham), W.K. Tung (Michigan State), A. Wagner (DESY),
R. Yoshida (ANL)

Contents

III Working Group 2: Multi-Jet Final States and Energy Flows	181
Introduction to multi-jet final states and energy flows	183
C. Buttar, J. Butterworth, V. Khoze, L. Lönnblad, N. Tuning	
The underlying event	192
C.M. Buttar, J.M. Butterworth, R.D. Field, C. Group, G. Gustafson, S. Hoeche, F. Krauss, A. Moraes, M.H. Seymour, A. Schalicke, P.Szczyпка, T.Sjöstrand	
Forward jets and multiple interactions	218
J. Turnau, L. Lönnblad	
Survival probability of large rapidity gaps	221
E. Gotsman, E. Levin, U. Maor, E. Naftali, A. Prygarin	
Multi-jet production and multi-scale QCD	242
Z. Czerwula, G. Davatz, A. Nikitenko, E. Richter-Was, E. Rodrigues, N. Tuning	
Unintegrated parton density functions	256
J. Collins, M. Diehl, H. Jung, L. Lönnblad, M. Lublinsky, T. Teubner	
Resummation	274
A. Banfi, G. Corcella, M. Dasgupta, Y. Delenda, G.P. Salam and G. Zanderighi	
Matching parton showers and matrix elements	288
S. Höche, F. Krauss, N. Lavesson, L. Lönnblad, M. Mangano, A. Schälicke and S. Schumann	
Constrained non-Markovian Monte Carlo modeling of the evolution equation in QCD	300
S. Jadach and M. Skrzypek	
QED\otimesQCD exponentiation and shower/ME matching at the LHC	304
B.F.L. Ward and S.A. Yost	
PHOTOS as a pocket parton shower: flexibility tests for the algorithm	309
P. Golonka and Z. Was	

Part III

Working Group 2: Multi-Jet Final States and Energy Flows

List of participants

J. R. Andersen, A. Banfi, J. Bartels, R. Bellan, M. Boonekamp, K. Boreskov, N. Brook, A. Bruni, C. Buttar, J. Butterworth, T. Carli, S. Caron, G. Cerminara, S. Chekanov, J. Collins, G. Corcella, B. Cox, Z. Czyczula, M. Dasgupta, G. Davatz, Y. Delenda, A. De Roeck, M. Diehl, R. Field, J. Forshaw, P. Golonka, E. Gotsman, G. Grindhammer, C. Group, G. Gustafson, S. Höche, S. Jadach, H. Jung, A. Kaidalov, V. Khoze, M. Klasen, H. Kowalski, F. Krauss, N. Lavesson, V. Lendermann, E. Levin, L. Lönnblad, M. Lublinsky, S. Magill, M. Mangano, U. Maor, A. Martin, A. Mastroberardino, S. Maxfield, B. Mellado, A. Moraes, E. Naftali, A. Nikitenko, R. Orava, A. Prygarin, P. Richardson, E. Richter-Was, E. Rodrigues, C. Royon, M. Ryskin, A. Sabio Vera, G. Salam, A. Savin, F.-P. Schilling, T. Schoerner-Sadenius, S. Schumann, M. Seymour, A. Shälicke, T. Sjöstrand, M. Skrzypek, W.J. Stirling, P. Szczypka, M. Tasevsky, T. Teubner, N. Tuning, J. Turnau, R. Venugopalan, B. Ward, Z. Was, B. Waugh, S.A. Yost, G. Zanderighi

Introduction to multi-jet final states and energy flows

Craig Buttar¹, Jon Butterworth², Valery Khoze³, Leif Lönnblad⁴ and Niels Tuning⁵

¹Department of Physics and Astronomy, University of Glasgow, UK; ²Department of Physics and Astronomy, University College London, UK; ³IPPP, University of Durham, UK; ⁴ Department of Theoretical Physics, Lund University, Sweden; ⁵NIKHEF, Amsterdam, The Netherlands.

Abstract

We summarize the activities of Working Group 2 of the HERA/LHC Workshop dealing with multi-jet final states and energy flows. Among the more specific topics considered were underlying event and minimum bias, rapidity gaps and survival probabilities, multi-jet topologies and multi-scale QCD, and parton shower–matrix element matching.

1 Introduction

In many ways, the LHC will become the best QCD machine ever built. It will allow us to study the production of hadrons and jets at unprecedented collision energies and will surely increase our understanding of QCD tremendously. Of course, some may argue that QCD already is a well understood and an integral part of the Standard Model, and the reason for building the LHC is to discover new phenomena, hopefully beyond the Standard Model.

However, the fact is that QCD is still not a completely understood theory. The qualitative aspects of asymptotic freedom and confinement may be under control, but the quantitative predictive power of the theory is still not at a satisfactory level. This is particularly true for the non-perturbative region, but also for the high-energy limit, where the hard scale of a process is much smaller than the total collision energy. The latter situation will be dominant in the bulk of events produced at the LHC. The triggers at the main LHC detectors will discard the majority of such events, but what is left will be processes with hard scales of around 100 GeV, which is still more than a hundred times smaller than the collision energy. And there will be significant amounts of minimum-bias data taken as well.

Except for a handful of gold-plated signals for new physics, any such search will be plagued by huge backgrounds stemming from pure QCD or other Standard Model processes involving jets. Hence, even if the study of QCD may seem to be a mundane preoccupation, it is of the utmost importance if we are to find and understand the few needles of new physics hopefully present in the immense LHC haystack.

Although the Tevatron may seem to be the obvious place to learn about QCD processes relevant for the LHC, the triggers there are typically tuned to high-scale processes, not far from the total collision energy. This means that HERA can give important additional insight, since there the situation is in some senses closer to that of the LHC, with the ratio of the typical hard scale and the total energy in DIS being $\sqrt{\langle Q^2 \rangle / S} \sim 0.01$. In addition, HERA allows us to study such processes in a more controlled environment, where one side of the collision is well constrained by our relatively precise understanding of electroweak physics.

In our Working Group we have studied in some detail which lessons about multi-jet final states and general hadronic energy flows can be learned from HERA when preparing for the analysis of LHC data. And in this brief summary we will in a few pages try to distill the progress made by almost a hundred physicists as reported in more than fifty talks in this workshop and also in almost twenty separate contributions to these proceedings. The work was broadly divided into four categories: underlying events and minimum bias; rapidity gaps and survival probabilities; multi-jet topologies and multi-scale QCD; and matrix element–parton shower matching.

The first category may not represent the most striking feature of HERA physics, but it will surely be of great importance for the LHC. And it turns out that there are many possibilities to gain further understanding of underlying events in both photoproduction and DIS at HERA.

The study of rapidity gaps and, in particular, hard diffractive scattering gained momenta when it was observed at HERA, and the suggestion to use such processes to obtain clean signals of new physics at the LHC presents exciting prospects where the experience from HERA will be very important.

Multi-scale processes have already been presented as an important connection between HERA and the LHC. This is not least true for the LHCb experiment, where the understanding of the forward region is vital, a region which has been intensely studied at HERA. Also the recent theoretical development in QCD resummation techniques, which so far have mainly been applied to e^+e^- annihilation, may provide important tools for understanding event shapes at the LHC, and the corresponding application to HERA data will be essential for this understanding.

Finally, the more technical issue of matching fixed-order tree-level matrix elements with parton shower generators as well as other theoretical improvements of such simulation programs will surely be vital for the successful understanding of data from the LHC and also here the comparison to HERA data will be essential for the tuning and validation.

It should be noted that all of these categories, presented in more detail below, have a fairly large overlap with other working groups in this workshop. The most obvious overlaps are the working groups for Diffraction and Monte Carlo simulations, but there is also overlap with the heavy flavour and parton distributions working groups.

2 Underlying events and minimum bias

An understanding of the underlying event is an interesting physics topic in its own right but is also crucial in developing robust analyses for LHC physics. The underlying event can enhance central jet production, reducing the effectiveness of the central jet veto in analyses such as the vector boson fusion Higgs channel, or reduce the isolation of leptons resulting in reduced efficiency for identifying isolated leptons. In particular for LHCb and ALICE, where the triggers typically do not mandate high-scale processes, a good understanding of underlying events and minimum-bias events is crucial.

In this workshop there were several contributions dealing with underlying events and multiple interactions. They are all described in a joint contribution to these proceedings [1]. There the event generator models in PYTHIA [2–5], HERWIG/JIMMY [6–8] and SHERPA [9] are presented together with results from tuning these and other models to available data. The contribution also includes a summary of the plenary talk by Gösta Gustafson on the theory and phenomenology underlying events and multiple scattering.

Of the models presented and studied in Ref. [1], the one implemented in PYTHIA is probably the most advanced. This model has recently been developed further, introducing a scheme for *interleaving* the multiple interaction with a transverse-momentum ordered parton shower [3]. In contrast, the default underlying event model in HERWIG is a simple parametrization of UA5 data [10]. However, HERWIG is easily interfaced to the multiple-interaction model in the JIMMY program, which is similar to the PYTHIA model in spirit, although many of the details differ. The JIMMY program has recently been improved, making the generation of events more efficient where the signal process is different from the additional multiple scattering processes. Also the SHERPA event generator is now equipped with multiple interactions. Again, this model is similar in spirit to that in PYTHIA. One interesting aspect which differs is the attempt to incorporate the multiple scatterings in the general CKKW (see Section 5 below) framework of SHERPA.

The CDF Collaboration has carried out studies of the underlying event in jet processes [11–13] and this was used to provide a tuning for PYTHIA. In Ref. [1] a new analysis is presented which has extended these studies by increasing the energy range of the leading jet from around 50 GeV to 450 GeV using E_T from the calorimeter as well as particle p_\perp measured in the tracker, and defining two-jet topologies as a subset of the leading jet to investigate the beam–beam and radiation components of the underlying event. Both PYTHIA tune-A and HERWIG/JIMMY were found to be in good agreement with the data, although both underestimate the transverse energy. The extension to higher energy scale shows that the underlying event activity increases with leading jet p_\perp i.e., the hardness of the primary scatter, but by studying the maximum and minimum activity it is seen that this rise is largely due to bremsstrahlung from the primary scattering rather than secondary interactions between the beam remnants.

The CDF analysis was carried out primarily at 1.8 TeV although some of the early 546 GeV data has also been analysed. This has meant that there is only limited information on the energy dependence of the underlying event. To cover a wider range of energy, ATLAS have used minimum-bias data from the SppS and Tevatron covering 200 GeV to 1.8 TeV in addition to the CDF underlying event data to tune PYTHIA and HERWIG/JIMMY. Comparing the predictions of minimum-bias and underlying event distributions at the LHC using the tuned PYTHIA, the tuned HERWIG/JIMMY and PHOJET [14] shows large variations, emphasizing the need to understand the energy dependence of these processes better. The energy dependence was investigated further by LHCb, again using minimum-bias data to fit the parameters required for the model of energy dependence in PYTHIA.

Both the ATLAS and LHCb analyses have the implicit assumption that minimum bias and the underlying event have the same physics origin. While CDF data supports this, it would be helpful to probe the underlying event directly over a larger range of energy scales. HERA is in a prime position to make such a contribution by studying jets from photoproduction in an energy range corresponding to centre-of-mass energies in the region of 200 GeV, fitting well with the low-energy minimum-bias data. In photoproduction, resolved photons behave like hadrons so that HERA is effectively a hadron–hadron collider. Photoproduction data shows that particle flow and multi-jet measurements require models with multiple interactions to best describe the data but detailed studies of multiple interactions have not been made. However, studies of particle and energy flow in the transverse region similar to that carried out by CDF could be made at HERA.

An interesting question is whether there is also an underlying event present in DIS at HERA. As explained in Refs. [15, 16] it is possible to relate diffraction and saturation to multiple-interaction processes also for DIS using a QCD reformulation of the so-called AGK cutting rules [17]. And since diffractive processes have been clearly seen at high Q^2 at HERA, it is reasonable to expect that multiple interactions may also be present. A good place to search for such effects is in forward-jet production at HERA. In [18] preliminary results are presented indicating that multiple-interaction effects may indeed give a noticeable increase in the measured forward-jet cross-section in resolved virtual photon processes at small x and moderate Q^2 .

The connection between multiple interactions, saturation and diffraction was also discussed in the plenary talk by Gösta Gustafson. He pointed out a possible problem with the qualitative AGK predictions for the hadronic multiplicity in multiple-interaction events. Taking the tuning of PYTHIA to CDF data at face value, there is an indication that the colour flows of secondary interactions are not independent from the primary scattering. Rather, the different colour flows seem to combine in a way where the total string length is minimized, resulting in a multiplicity which does not grow proportionally to the number of scatterings. Currently there is no theoretical understanding of this phenomenon. Gustafson also pointed out the problem that all multiple-interaction models discussed here rely on collinear factorization of the individual scatterings in a region where we expect k_\perp factorization to be the relevant formalism. In fact, using k_\perp factorization, the soft divergencies in the partonic cross section present in the conventional models may be removed, which could make the extrapolation of the model predictions to high energy more constrained.

3 Rapidity gaps and survival probabilities

A characteristic signature of diffractive processes is the existence of a large rapidity gap (LRG) in the final state, defined as a region of (pseudo-) rapidity devoid of hadronic activity. A rapidity gap may be adjacent to a leading proton or may arise between the decay products of final hadronic systems. The appearance of the rapidity gaps is intimately related to the exchange in the t -channel of objects with vacuum quantum numbers (Pomeron in the Regge theory, di-gluon Pomeron in pQCD, photon or W -mediator). The diffractive rapidity gap events have been studied in great detail at the ISR, SPS, HERA and the Tevatron. The LHC is the first collider which will have enough energy to allow the events with several ($n = 2-4$) LRGs.

The activity of our Working Group was focused mainly on the LRGs in the hard diffractive processes. For specifics of the photon and W -mediated reactions see, for example, Refs. [19–22].

An intensive discussion concerned the breakdown of factorization in hard hadronic diffractive processes. It is the consequence of unitarization effects, that both hard and Regge factorization are broken. This breakdown of factorization is experimentally seen [23] as the suppression of the single diffractive dijet cross section at the Tevatron as compared to the prediction based on HERA results. The observed suppression is in a quantitative agreement with the calculations [24] where the unitarization effects are described by multi-Pomeron exchange diagrams. The analysis of the current CDF diffractive dijet data with one or two rapidity gaps shows a good agreement with this approach. The situation with the factorization breaking in dijet photoproduction is not completely clear and further experimental and theoretical efforts are needed. A possible way to study this effect is to measure the ratio of diffractive and inclusive dijet photoproduction, see Ref. [25].

It is important to emphasize that the rapidity gap signal is very powerful but, at the same time, quite a fragile tool. We have to pay a price for ensuring such a clean environment. The gaps may easily fade away (filled by hadronic secondaries) on account of various sources of QCD ‘radiation damage’:

- (i) soft or hard rescattering between the interacting hadrons (classic screening/unitarization effects or underlying event);
- (ii) bremsstrahlung induced by the ‘active’ partons in the hard subprocesses;
- (iii) radiation originating from the small transverse distances in two-gluon Pomeron dipoles.

An essential issue in the calculation of the rate of events with LRG concerns the size of the factor W which determines the probability for the gaps to survive in the (hostile) QCD environment. As discussed in the contributions of Brian Cox [26] and Jeff Forshaw [27], this factor is a crucial ingredient for evaluation of the discovery potential of the LHC in the exclusive processes with double proton tagging.

Symbolically, the survival probability W can be written as

$$W = S^2 T^2. \quad (1)$$

S^2 is the probability that the gaps are not filled by secondary particles generated by soft rescattering, i.e., that no other interactions occur except the hard production process. Following Bjorken [28,29], who first introduced such a factor in the context of rescattering, such a factor is often called the survival probability of LRG. The second factor, T^2 , is the price to pay for not having gluon radiation in the hard production subprocess. It is related to Sudakov-suppression phenomena and is incorporated in the pQCD calculation via the skewed unintegrated parton densities. The physics of Sudakov suppression is discussed in more detail in the contribution of Jeff Forshaw to these Proceedings [27].

In some sense the soft survival factor S^2 is the ‘Achilles heel’ of the calculations of the rates of diffractive processes, since, in principle, S^2 could strongly depend on the phenomenological models for soft diffraction. This factor is not universal, but depends on the particular hard subprocess, as well as on the distribution of partons inside the proton in impact parameter space. It has a specific dependence on the characteristic momentum fractions carried by the active partons in the colliding hadrons [24].

However, the good news is that, as discussed in these Proceedings by Uri Maor et al. [30], the existing estimates of S^2 calculated by different groups for the same processes appear to be in a reasonably good agreement with each other. This is related to the fact that these approaches reproduce the existing data on high-energy soft interactions, and, thus, result in the similar profile of the optical density in the impact parameter space. Another reason results from the comparatively small role of the high-mass diffractive dissociation.

Note that it is possible to check the value of S^2 by observing double-diffractive dijet production [31]. The gap survival in the Higgs production via the WW -fusion process can be probed in Z production which is driven by the same dynamics, and has a higher cross-section, see Refs. [32,33]. Let us emphasize that it is the presence of this factor which makes the calculation infrared stable, and pQCD applicable. Neglecting the Sudakov suppression would lead to a considerable overshooting of the cross section of the hard central exclusive processes at large momentum transfer.

4 Multi-jet topologies and multi-scale QCD

In this workshop work on a wide range of topics regarding jet production and multi-scale processes has been presented [34]. It is of great interest to know what the LHC will teach us in the area of QCD, but at the same time uncertainties on the theoretical predictions for processes at the LHC should be limited as far as possible beforehand. By using the knowledge attained at HERA, our models can be sharpened and our theories can be tested.

Predictions of the event topology of $gg \rightarrow H$ at the LHC have been investigated for various parton shower models — such as PYTHIA, HERWIG and ARIADNE, that have proven their validity at HERA — and uncertainties in the event selection have been estimated [35,36]. In the parton cascade as implemented in some of these programs, the parton emissions are calculated using the DGLAP approach, with the partons ordered in virtuality. DGLAP accurately describes high-energy collisions of particles at moderate values of the Bjorken- x by resummation of the leading log terms of transverse momenta ($\alpha_s \ln Q^2$). However, to fixed order, the QCD scale used in the ladder is not uniquely defined. There are many examples where more than one hard scale plays a role in the hard scatter, such as the virtuality Q , the transverse momentum E_T of the jet, or the mass of a produced object. Also, at low values of Bjorken- x large logarithms appear ($\alpha_s \ln 1/x$), leading to large corrections.

The CCFM formalism takes this into account, describing the evolution in an angular ordered region of phase space, while reproducing DGLAP and BFKL in the appropriate asymptotic limits. The CASCADE program has implemented the CCFM formalism, describing the low- x F_2 data and forward jet data at HERA. The predictions for the jet production at the LHC have been studied, both in the context of a $gg \rightarrow H$, as well as in the context of the forward event topology at LHCb [37].

In order to get reliable predictions for exclusive final-state processes, unintegrated parton density functions $f(x, Q^2, k_\perp)$ (uPDFs) become indispensable. For example, in the small- x regime, when the transverse momenta of the partons are of the same order as their longitudinal momenta, the collinear approximation is no longer appropriate and k_\perp factorization has to be applied, with the appropriate CCFM evolution equations. In this workshop various parametrizations for unintegrated gluon densities matched to HERA F_2 data were compared to each other [38]. It is, however, still questionable if these densities are constrained enough for reliable predictions for Higgs production cross-section. Final-state measurements like photoproduction of D^* +jet events could however constrain these uPDFs further. It is argued that it is important to reformulate perturbative QCD in terms of fully unintegrated parton densities, since neglecting parton transverse momentum leads to wrong results. The HERA F_2 data has also been fitted using non-linear BFKL evolution, expressed with a universal dipole cross section, which in turn can be related to the unintegrated gluon distribution.

Finally, a theoretical description of hard diffractive processes at HERA can provide information on the so-called generalized, or skewed, gluon distribution (depending on the x of the emitted and absorbed gluon), providing for a theoretical description for diffractive Higgs production at the LHC.

The role of HERA is also emphasized in the area of resummed calculations, obtaining accurate QCD parameters such as the strong coupling, quark masses and parton distribution functions, which are vital inputs for predictions at the LHC. For example, event-shape distributions at HERA led to the finding of non-global logarithms, influencing observables at the LHC such as energy flows away from jets. Additionally, HERA data seem to confirm $1/Q$ power corrections (arising from gluon emission with transverse momentum $\sim \Lambda_{QCD}$), demonstrating that these corrections are not affected by the presence of the initial-state proton. HERA data is also used to study dijet E_T and angular spectra, in order to test NLL perturbative predictions. Finally, we have discussed whether additional small- x terms are needed to accommodate HERA DIS data, which at LHC energies would result in a broadening of the vector boson p_T spectrum.

5 Parton shower/matrix element matching

The LHC is, of course, mainly a machine for discovering new physics. But irrespective of what new phenomena may exist, we know for sure that LHC events will contain huge numbers of hadrons, and that a large fraction of these events will have many hard jets produced by standard QCD processes. Such events are interesting in their own right, but they are also important backgrounds for almost any signal of new physics. Unfortunately the standard Parton Shower (PS)-based event generators of today are not well suited to describe events with more than a couple of hard jets. The alternative is to use matrix element (ME) generator programs; this typically can generate up to six hard partons according to the exact fixed-order tree-level matrix elements. But these generators are not well suited for describing the conversion of these hard partons into jets of hadrons.

To get properly generated events it is therefore important to interface the ME generators to realistic hadronization models; this requires that also soft and collinear partons are generated according to PS models to get reliable predictions for the intra- and inter-jet structure. When adding a PS to an event from a ME generator, it is important to avoid double-counting. Hence the PS must be *vetoed* to avoid generating parton emissions above the cutoff needed to avoid divergences in the ME generator. In addition the PS assumes that the emissions are ordered in some evolution variable (scale) and uses Sudakov form factors to ensure that there was no additional emission with a scale between two generated emissions. This also generates the virtual corrections to the splittings. The ME generators, of course, have no such ordering since all diagrams are added coherently. However, there is still a need for a cutoff in some scale to regulate soft and collinear divergencies, and to naively add a PS to events from a ME generator will therefore give a strong dependence on this cutoff.

A solution to this problem was presented by Catani et al. [39]. This so-called CKKW procedure is based on using a jet reconstruction algorithm on the ME-generated event to define an ordering of the emissions and then reweight the event according to Sudakov form factors obtained from the reconstructed scales. In this way it was shown that the dependence on the ME cutoff cancels to NLL accuracy. The procedure was originally developed for e^+e^- annihilation where it was further developed in Ref. [40], but lately it has also been applied to hadron-hadron collisions [41–45] using several different parton shower models. In addition, an alternative procedure, called MLM, was developed by Mangano [46, 47] which is similar in spirit to CKKW, but which has a simpler interface between the ME and PS program.

There was some hope that during this workshop an implementation of CKKW for DIS would also be developed. This would be interesting, not least because the procedure would then be tested in a small- x environment, and comparing with such HERA data as well as with high-scale Tevatron data should then give a more reliable understanding about the uncertainties when extrapolating to the LHC. Although some progress has been made on the application to DIS [48] there was not enough time to

make a proper implementation. Instead the activities were focused on comparing the predictions of some of the programs (SHERPA [9] and MADGRAPH/MADEVENT [49]+ARIADNE [50] using CKKW, and ALPGEN [51]+PYTHIA [4] using MLM) for the case of W+jets production at the Tevatron and the LHC. This process is very interesting in its own right, but is also an important background for almost any signal of new physics at the LHC. The results are presented in these proceedings [52] and it was found that the models give fairly similar predictions for jet rates, but some differences were found, for example, for the rapidity correlation between jets and the W. The latter may be related to the fact that W production, especially at the LHC, can be considered to be a small- x process ($m_W/\sqrt{S} \sim x \sim 0.005$) and we know that there are large differences between parton shower models in this region. This emphasizes again the importance of confronting the ME+PS matching procedures with HERA DIS data also.

Possible improvements to the QCD PS approach were discussed in three other contributions to these proceedings. All of these are based on experience of Monte Carlo programs for QED resummation. One of these contributions [53] describes a new algorithm for forward evolution of the initial-state parton cascade in which the type and energy of the final parton is predefined/constrained. Contrary to the widely used backward-evolution algorithms [54], this algorithm is similar to the one used in the LDCMC generator [55] and does not need a fully evolved PDF parametrization as input.

Using an operator formalism, another contribution [56] describes what we can learn about QCD parton showers from the popular PHOTOS generator, which combines in a clever way soft photon resummation and hard collinear photon resummation in QED. Finally there is a contribution [57] which describes a more ambitious attempt to combine ME+PS calculations for both QCD and QED, preserving the proper soft gluon limit and the standard factorization of collinear singularities. All of these contributions represents work which is still in a rather early stage. Nevertheless, they signal important efforts which may lead to interesting new Monte Carlo tools for the LHC era.

6 Conclusions and outlook

In this summary we hope to have made it clear that there is a rich flora of interesting topics relating to jets and hadronic energy flows where the understanding of results from HERA will be important for the upcoming analysis of LHC data. It should also be clear that although substantial progress has been made during this workshop, we have only started to botanize among these topics. Hence, as we now thank the participants of our Working Group for all the work they have contributed to the workshop, we would also like to remind them, and also other readers of these proceedings, that there is much work still to be done.

References

- [1] C. Buttar *et al.*, *Underlying events*, these proceedings.
- [2] T. Sjöstrand and M. van Zijl, *Phys. Rev.* **D36**, 2019 (1987).
- [3] T. Sjöstrand and P. Z. Skands, *Eur. Phys. J.* **C39**, 129 (2005). [hep-ph/0408302](#).
- [4] T. Sjöstrand, and others, *Comput. Phys. Commun.* **135**, 238 (2001). [arXiv:hep-ph/0010017](#).
- [5] T. Sjöstrand, L. Lönnblad, S. Mrenna, and P. Skands (2003). [hep-ph/0308153](#).
- [6] J. Butterworth *et al.*, <http://hepforge.cedar.ac.uk/jimmy/>.
- [7] J. M. Butterworth, J. R. Forshaw, and M. H. Seymour, *Z. Phys.* **C72**, 637 (1996). [hep-ph/9601371](#).
- [8] G. Corcella *et al.*, *JHEP* **01**, 010 (2001). [hep-ph/0011363](#).
- [9] T. Gleisberg *et al.*, *JHEP* **02**, 056 (2004). [hep-ph/0311263](#).
- [10] UA5 Collaboration, G. J. Alner *et al.*, *Nucl. Phys.* **B291**, 445 (1987).
- [11] CDF Collaboration, J. Huston, *Int. J. Mod. Phys.* **A16S1A**, 219 (2001).
- [12] CDF Collaboration, T. Affolder *et al.*, *Phys. Rev.* **D65**, 092002 (2002).
- [13] CDF Collaboration, D. Acosta *et al.*, *Phys. Rev.* **D70**, 072002 (2004). [hep-ex/0404004](#).
- [14] R. Engel, *Phojet program and manual*. <http://www-ik.fzk.de/~engel/phojet.html>.
- [15] H. Kowalski, *Multiple interactions in DIS*, these proceedings.
- [16] J. Bartels, *Multiple scattering at HERA and at LHC - remarks on the AGK rules*, these proceedings.
- [17] V. A. Abramovsky, V. N. Gribov, and O. V. Kancheli, *Yad. Fiz.* **18**, 595 (1973).
- [18] J. Turnau and L. Lönnblad, *Forward jets and multiple interactions*, these proceedings.
- [19] V. A. Khoze, A. D. Martin, and M. G. Ryskin, *Eur. Phys. J.* **C23**, 311 (2002). [hep-ph/0111078](#).
- [20] V. A. Khoze, A. D. Martin, and M. G. Ryskin, *Eur. Phys. J.* **C21**, 99 (2001). [hep-ph/0104230](#).
- [21] V. A. Khoze, A. D. Martin, and M. G. Ryskin, *Eur. Phys. J.* **C18**, 167 (2000). [hep-ph/0007359](#).
- [22] V. A. Khoze, A. D. Martin, and M. G. Ryskin, *Eur. Phys. J.* **C24**, 459 (2002). [hep-ph/0201301](#).
- [23] CDF Collaboration, T. Affolder *et al.*, *Phys. Rev. Lett.* **84**, 5043 (2000).
- [24] A. B. Kaidalov, V. A. Khoze, A. D. Martin, and M. G. Ryskin, *Eur. Phys. J.* **C21**, 521 (2001). [hep-ph/0105145](#).
- [25] A. B. Kaidalov, V. A. Khoze, A. D. Martin, and M. G. Ryskin, *Phys. Lett.* **B567**, 61 (2003). [hep-ph/0306134](#).
- [26] B. Cox *et al.*, *Diffraction Higgs production: experiment*, these proceedings.
- [27] J. Forshaw, *Diffraction Higgs production: theory*, these proceedings.
- [28] J. D. Bjorken, *Int. J. Mod. Phys.* **A7**, 4189 (1992).
- [29] J. D. Bjorken, *Phys. Rev.* **D47**, 101 (1993).
- [30] U. Maor *et al.*, *Gap-survival and factorization breaking*, these proceedings.
- [31] V. A. Khoze, A. D. Martin, and M. G. Ryskin, *Eur. Phys. J.* **C14**, 525 (2000). [hep-ph/0002072](#).
- [32] H. Chehime and D. Zeppenfeld, *Phys. Rev.* **D47**, 3898 (1993).
- [33] V. A. Khoze, M. G. Ryskin, W. J. Stirling, and P. H. Williams, *Eur. Phys. J.* **C26**, 429 (2003). [hep-ph/0207365](#).
- [34] Z. Czyczula *et al.*, *Multi-jet production and multi-scale QCD*, these proceedings.
- [35] Z. Czyczula and E. Richter-Was, *MSSM Higgs production with the Yukawa bbH coupling induced mechanisms*. In [34], these proceedings.
- [36] G. Davatz and A. Nikitenko, *$gg \rightarrow H$ at the LHC: Uncertainty due to a Jet Veto*. In [34], these proceedings.

- [37] E. Rodrigues and N. Tuning, *Forward Studies with CASCADE at LHC Energies*. In [34], these proceedings.
- [38] J. Collins *et al.*, *Unintegrated parton density functions*, these proceedings.
- [39] S. Catani *et al.*, JHEP **11**, 063 (2001). [hep-ph/0109231](https://arxiv.org/abs/hep-ph/0109231).
- [40] L. Lönnblad, JHEP **05**, 046 (2002). [hep-ph/0112284](https://arxiv.org/abs/hep-ph/0112284).
- [41] F. Krauss, JHEP **08**, 015 (2002). [hep-ph/0205283](https://arxiv.org/abs/hep-ph/0205283).
- [42] S. Mrenna and P. Richardson, JHEP **05**, 040 (2004). [hep-ph/0312274](https://arxiv.org/abs/hep-ph/0312274).
- [43] F. Krauss, A. Schalicke, S. Schumann, and G. Soff, Phys. Rev. **D70**, 114009 (2004). [hep-ph/0409106](https://arxiv.org/abs/hep-ph/0409106).
- [44] N. Lavesson and L. Lönnblad, JHEP **07**, 054 (2005). [hep-ph/0503293](https://arxiv.org/abs/hep-ph/0503293).
- [45] F. Krauss, A. Schaelecke, S. Schumann, and G. Soff (2005). [hep-ph/0503280](https://arxiv.org/abs/hep-ph/0503280).
- [46] M. Mangano, *The so-called mlm prescription for me/ps matching*. <http://www-cpd.fnal.gov/personal/mrenna/tuning/nov2002/mlm.pdf>. Talk presented at the Fermilab ME/MC Tuning Workshop, October 4, 2002.
- [47] M. L. Mangano, M. Moretti, and R. Pittau, Nucl. Phys. **B632**, 343 (2002). [hep-ph/0108069](https://arxiv.org/abs/hep-ph/0108069).
- [48] C. Åberg, *Correcting the colour dipole cascade with fixed order matrix elements in deep inelastic scattering*. Diploma thesis, LU-TP 04-25 (2004).
- [49] F. Maltoni and T. Stelzer, JHEP **02**, 027 (2003). [hep-ph/0208156](https://arxiv.org/abs/hep-ph/0208156).
- [50] L. Lönnblad, Comput. Phys. Commun. **71**, 15 (1992).
- [51] M. L. Mangano, M. Moretti, F. Piccinini, R. Pittau, and A. D. Polosa, JHEP **07**, 001 (2003). [hep-ph/0206293](https://arxiv.org/abs/hep-ph/0206293).
- [52] S. Hoeche *et al.*, *Matching parton showers and matrix elements*, these proceedings.
- [53] S. Jadach and M. Skrzypek, *Constrained non-Markovian Monte Carlo modeling of the evolution equation in QCD*, these proceedings.
- [54] M. Bengtsson and T. Sjöstrand, Z. Phys. **C37**, 465 (1988).
- [55] H. Kharraziha and L. Lönnblad, JHEP **03**, 006 (1998). [hep-ph/9709424](https://arxiv.org/abs/hep-ph/9709424).
- [56] P. Golonka and Z. Was, *PHOTOS as a pocket parton shower: flexibility tests for the algorithm*, these proceedings.
- [57] B. Ward and S. Yost, *QED \otimes QCD Exponentiation and Shower/ME Matching at the LHC*, these proceedings.

The Underlying Event

*C.M. Buttar*¹, *J.M. Butterworth*², *R.D. Field*³, *C. Group*³, *G. Gustafson*⁴, *S. Hoeche*⁵, *F. Krauss*⁵,
*A. Moraes*¹, *M.H. Seymour*^{6,7}, *A. Schaliche*⁸, *P. Szczykpa*⁹, *T. Sjöstrand*^{4,7}

¹Dept. of Physics and Astronomy, University of Glasgow, UK

²Dept. of Physics and Astronomy, University College London, UK

³Dept. of Physics, University of Florida, USA

⁴Dept. of Theoretical Physics, Lund University, Sweden

⁵Institute for Theoretical Physics, Dresden University of Technology, FRG

⁶School of Physics and Astronomy, University of Manchester, UK

⁷CERN, Switzerland

⁸DESY Zeuthen, FRG

⁹Dept. of Physics, University of Bristol, UK

Abstract

The contributions to working group II: “Multi-jet final states and energy flows” on the underlying event are summarized. The study of the underlying event in hadronic collisions is presented and Monte Carlo tunings based on this are described. New theoretical and Monte Carlo methods for describing the underlying event are also discussed.

1 Introduction

The underlying event is an important element of the hadronic environment within which all physics at the LHC, from Higgs searches to physics beyond the standard model, will take place. Many aspects of the underlying event will be constrained by LHC data when they arrive. However, the physics is so complex, spanning non-perturbative and perturbative QCD and including sensitivities to multi-scale and very low- x physics, that even after LHC switch-on many uncertainties will remain. For this reason, and also for planning purposes, it is critical to have to hand sensible models containing our best physical knowledge and intuition, tuned to all relevant available data.

In this summary of several contributions to the workshop, we first outline the available models in Section 2, most of which are in use at HERA and/or the Tevatron. Recent improvements, some of which were made during the workshop, are also discussed.

Next, current work on tuning these to data is discussed. The underlying event has been extensively studied by CDF and the latest results are presented in Section 3 and compared to predictions from the PYTHIA and HERWIG+JIMMY Monte Carlo generators. The CDF tunings are compared to other tunings based on CDF data and minimum bias data and used to predict the level of underlying events at the LHC in Sections 4 and 5. These reports are very much a snapshot of ongoing work, which will be continued in the follow-up meetings of this workshop and the TeV4LHC workshop.

One major issue in extrapolating the underlying event (UE) to LHC energies is the possible energy dependence of the transverse momentum cut-off between hard and soft scatters, \hat{p}_T^{\min} . The need for such a cut-off may be avoided by using the k_{\perp} factorization scheme as discussed in Section 6, where soft emissions do not contribute to the total cross-section or to the parton density functions (PDFs), but do contribute to the properties of the event. The cross-section for a chain of partonic emission can be extracted from HERA data and can be used to predict the minijet rate or multiple interaction rate in pp or p \bar{p} collisions. The running of α_s still introduces a cut-off scale between soft and hard chains; however it has been shown that the total cross-section is insensitive to this cut-off and predictions for the mini-jet rate at the LHC are stable. The hadron multiplicity observed in the CDF underlying event data indicates that the string connections in the underlying event are made to minimise the string length. This is the

opposite to what is observed in e^+e^- collisions. The implications for this on the AGK cutting rules is discussed further in Section 6.

This summary ends with a section on conclusions and suggestions for future work.

2 Underlying event models

Several underlying event models are available, at varying stages of development and use. In this section we review the status of those discussed during the workshop.

2.1 Multiple Interactions in PYTHIA

The basic implementation of multiple interactions in PYTHIA is almost 20 years old, and many of the key aspects have been confirmed by comparisons with data. In recent years the model has been gradually improved, with junction-string topologies, with flavour-correlated multiparton densities, and with transverse-momentum-ordered showers interleaved with the multiple interactions. However, the “correct” description of colour flow still remains to be found.

The traditional PYTHIA [1,2] model for multiple interactions (MI) [3] is based on a few principles:

1. The naive perturbative QCD $2 \rightarrow 2$ cross section is divergent like dp_{\perp}^2/p_{\perp}^4 for transverse momenta $p_{\perp} \rightarrow 0$. Colour screening, from the fact that the incoming coloured partons are confined in colour singlet states, should introduce a dampening of this divergence, e.g. by a factor $p_{\perp}^4/(p_{\perp 0}^2 + p_{\perp}^2)^2$, where $p_{\perp 0}$ is a free parameter, which comes out to be of the order of 2 GeV.
2. From the thus regularized integrated interaction rate $\sigma_{\text{int}}(E_{\text{cm}}, p_{\perp 0})$ and the nondiffractive cross section $\sigma_{\text{nd}}(E_{\text{cm}})$, the average number of interactions per event can be derived as $\langle n_{\text{int}} \rangle = \sigma_{\text{int}}/\sigma_{\text{nd}}$. With no impact-parameter dependence, the actual number of interactions is given by a Poissonian with mean as above (modulo some corrections coming from $n_{\text{int}} = 0$).
3. More realistically, since hadrons are extended objects, there should be more (average) activity in central collisions than in peripheral ones. By introducing a matter distribution inside a hadron, the overlap between the two incoming hadrons can be calculated as a function of impact parameter b . The number of interactions is now a Poissonian for each b separately, with a mean proportional to the overlap. All events are required to contain at least one interaction; thereby the cross section is automatically dampened for large b . Empirically, the required hadronic impact parameter profile is more peaked at small b than in a Gaussian distribution.
4. It is natural to consider the interactions in an event in order of decreasing p_{\perp} values. Such a p_{\perp} ordering has a natural interpretation in terms of formation-time arguments. The generation procedure can conveniently be written in a language similar to that used for parton showers, with the equivalent of a Sudakov form factor being used to pick the next smaller p_{\perp} , given the previous ones. It allows the hardest interaction to be described in terms of conventional PDFs, whereas subsequent ones have to be based on modified PDFs, at the very least reduced by energy-momentum conservation effects. This also reduces the tail of events with very many interactions.
5. Technical limitations lead to several simplifications, such that only the hardest interaction was allowed to develop initial- and final state interactions, and have flavours selected completely freely.
6. Colour correlations between different scatterings cannot be predicted by perturbation theory, but have a direct consequence on the structure of events. One of the most sensitive quantities is $\langle p_{\perp} \rangle (n_{\text{charged}})$. Data here suggest a very strong colour correlation, where the total string length is essentially minimized in the final state.

For a long period of time, only one significant change was made to this scenario:

7. Originally the $p_{\perp 0}$ parameter had been assumed energy-independent. In the wake of the HERA data [4], which led to newer PDF parametrizations having a steeper small- x behaviour than previously assumed, it became necessary to let $p_{\perp 0}$ increase with energy to avoid too steep a rise of the multiplicity. Such an energy dependence can be motivated by colour screening effects [5]. A functional form $p_{\perp 0} \propto s^{\epsilon}$ with $\epsilon \sim 0.08$ is suggested by Pomeron arguments.

Several studies have been presented based on this framework. Some of the recent tuning activities are described elsewhere in this report. The PYTHIA Tune A [6] is a standard reference for much of the current Tevatron underlying-event and minimum-bias physics studies.

In recent years, an effort has been made to go beyond the framework outlined above. Several new or improved components have been introduced.

1. The fragmentation of junction-string topologies has been implemented [7]. Such topologies must be considered when at least two valence quarks are kicked out of an incoming proton beam particle. Here a proton is modelled as a Y-shaped topology, where each valence quark sits at the end of one of the three legs going out from the middle, the junction. When some ends of this Y are kicked out, also the junction is set in motion. The junction carries no energy or momentum of its own, but it is around the junction that the baryon inheriting the original baryon number will be formed. The junction rest frame is defined by having 120° between the three jets. A number of technical problems have to be overcome in realistic situations, where also gluons may be colour-connected on the three legs, thus giving more complicated space-time evolution patterns.
2. PDFs are more carefully modelled, to take into account the flavour structure of previous interactions [8], not only the overall energy-momentum constraints. Whenever a valence quark is kicked out, the remaining valence PDF of this flavour is rescaled to the new remaining number. When a sea quark is kicked out, an extra “companion” antiquark distribution contribution is inserted, thereby increasing the likelihood that also the antiquark is kicked out.
3. Also remnant flavours are more carefully considered, along with issues such as primordial k_{\perp} values and remnant longitudinal momentum sharing.
4. A few further impact-parameter possibilities are introduced.
5. New transverse-momentum-ordered showers are introduced, both for initial- and final-state radiation (ISR and FSR) [9]. On the one hand, this appears to give an improved description of (hard) multijet production. On the other hand, it allows all evolution to be viewed in terms of a common “time” ordering given by decreasing p_{\perp} values. This is especially critical for the description of MI and ISR, which are in direct competition, in the sense that both mechanisms take momentum out of the incoming beams and thereby require a rescaling of PDF’s at later “times”. This approach, with interleaved MI and ISR, is illustrated in Fig. 1.

Currently we still make use of two simplifications to the new p_{\perp} -ordered framework: (a) the inclusion of FSR is deferred until the MI and ISR have been considered in full, and (b) there is no intertwining, in which two seemingly separate higher-virtuality parton chains turns out to have a common origin when studied at lower p_{\perp} scales. Fortunately there are good reasons why neither of those omitted aspects should be so important.

There is one big remaining unsolved issue in this model, however, namely that of colour flow. If colours are only connected via the fact that the incoming beam remnants are singlets, the correct $\langle p_{\perp} \rangle (n_{\text{charged}})$ behaviour cannot be reproduced whatever variation is tried. It appears necessary to assume that some final-state colour reconnection mechanism tends to reduce the total string length almost to the minimal possible, as was required for Tune A. The most physically reasonable approach, that is yet not too time-consuming to implement, remains to be found. It is possible that also diffractive topologies will need to become a part of this game.

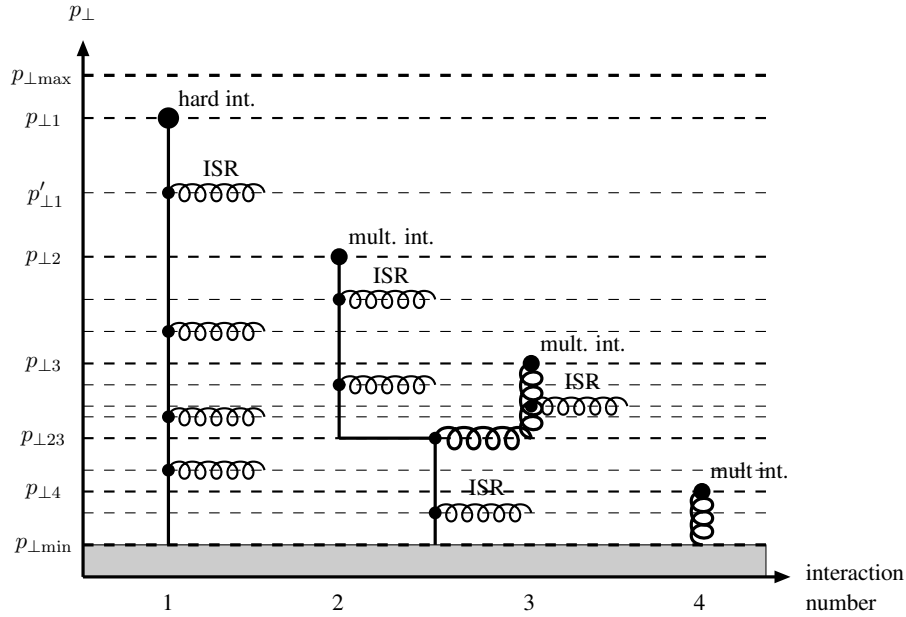


Fig. 1: Schematic figure illustrating one incoming hadron in an event with a hard interaction occurring at $p_{\perp, 1}$ and three further interactions at successively lower p_{\perp} scales, each associated with (the potentiality of) initial-state radiation, and further with the possibility of two interacting partons (2 and 3 here) having a common ancestor in the parton showers. Full lines represent quarks and spirals gluons. The vertical p_{\perp} scale is chosen for clarity rather than realism; most of the activity is concentrated to small p_{\perp} values.

Apart from this big colour issue, and the smaller ones of a complete interleaving/intertwining, PYTHIA now contains a very consistent and complete picture of both minimum-bias and underlying-event physics. It will be interesting to see how this framework fares in comparisons with data. However, if the models appears complex, this complexity is driven by necessity: all of the issues already brought up must be included in the “definitive” description, in one form or other, plus possibly some more not yet brought to light.

2.2 JIMMY

The basic ideas of the eikonal model implemented in JIMMY are discussed elsewhere [10]. The model derives from the observation that for partonic scatters above some minimum transverse momentum, \hat{p}_T^{\min} , the values of the hadronic momentum fraction x which are probed decrease as the centre-of-mass energy, s , increases, and since the proton structure function rises rapidly at small x [4], high parton densities are probed. Thus the perturbatively-calculated cross section grows rapidly with s . However, at such high densities, the probability of more than one partonic scattering in a single hadron-hadron event may become significant. Allowing such multiple scatters reduces the total cross section, and increases the activity in the final state of the collisions.

2.2.1 Model Assumptions

The JIMMY model assumes some distribution of the matter inside the hadron in impact parameter (b) space, which is independent of the momentum fraction, x . The multiparton interaction rate is then calculated using the cross section for the hard subprocess, the conventional parton densities, and the area overlap function, $A(b)$. No assumption about the behaviour of the *total* cross section is used. For cross sections other than QCD $2 \rightarrow 2$ scatters, JIMMY makes use of approximate formulae, valid when all

cross sections except QCD $2 \rightarrow 2$ are small, which is true in most cases of interest. This approximation is described in detail elsewhere [11].

2.2.2 *Standard JIMMY*

The starting point for the multiple scattering model is the assertion that, at fixed impact parameter, b , different scatters are independent and so obey Poisson statistics. It is then straightforward to show that the cross section for events in which there are n scatters of type a is given by

$$\sigma_n = \int d^2b \frac{(A(b)\sigma_a)^n}{n!} e^{-A(b)\sigma_a}, \quad (1)$$

where σ_a is the parton–parton cross section and $A(b)$ is the matter density distribution, obeying

$$\int d^2b A(b) = 1. \quad (2)$$

It is straightforward to show that the inclusive cross section for scatters of type a is σ_a and the total cross section for events with at least one scatter of type a is

$$\sigma_{\text{total}} = \int d^2b (1 - e^{-A(b)\sigma_a}). \quad (3)$$

These can then be combined to give the probability that an event has exactly n scatters of type a, given that it has at least 1 scatter of type a,

$$P_n = \frac{\int d^2b \frac{(A(b)\sigma_a)^n}{n!} e^{-A(b)\sigma_a}}{\int d^2b (1 - e^{-A(b)\sigma_a})}, \quad n \geq 1. \quad (4)$$

This is the probability distribution pretabulated (as a function of \sqrt{s}) by Jimmy.

Jimmy’s procedure can then be summarized as:

1. Give all events cross section σ_{total} .
2. In a given event, choose n according to Eq. (4).

It is interesting to note that Jimmy’s procedure, despite integrating over b once-and-for-all at initialization time, correctly reproduces the correlation between different scatters, whose physical origin is a b -space correlation: small cross section scatters are more likely to come from events with a large overlap and hence be accompanied by a larger-than-average number of large cross section scatters.

2.2.3 *Two Different Scattering Types*

We consider the possibility that there are two different scattering types, but that the cross section for the second type, σ_b , is small enough that events with more than one scatter of type b are negligible. The probability distribution for number of scatters of type a, n , in events with at least one of type b is given by [11]

$$P(n|m \geq 1) = \frac{\int d^2b \frac{(A(b)\sigma_a)^n}{n!} e^{-A(b)\sigma_a} (1 - e^{-A(b)\sigma_b})}{\int d^2b (1 - e^{-A(b)\sigma_b})}, \quad n \geq 0. \quad (5)$$

Since σ_b is small, we can expand the exponentials and obtain

$$P(n|m \geq 1) \approx \int d^2b A(b) \frac{(A(b)\sigma_a)^n}{n!} e^{-A(b)\sigma_a}, \quad n \geq 0. \quad (6)$$

Note that this expression is independent of σ_b . It is therefore ideal for implementing into JIMMY. It is useful to rewrite this equation, as follows. We redefine n to be the total number of scatters, including the one of type b (i.e. “new n ”=“old n ”+1) and rewrite, to obtain

$$P_n \approx \frac{\int d^2b n \frac{(A(b)\sigma_a)^n}{n!} e^{-A(b)\sigma_a}}{\sigma_a}, \quad n \geq 1. \quad (7)$$

Note the similarity with Eq. (4), making this form even easier to implement into Jimmy.

The Monte Carlo implementation of this procedure is straightforward:

1. Give all events cross section σ_b .
2. In a given event choose n according to Eq. (7).
3. Generate 1 scatter of type b and $n-1$ of type a.

There is one important difference between the cases in which b is distinct from a and b is a subset of a: some of the $n-1$ scatters of type a could also be of type b. Although this is a small fraction of the total, it can be phenomenologically important. As each scatter of type a is generated, a check is made as to whether it is also of type b. The m th scatter of type b generated so far is rejected with probability $1/(m+1)$. This ensures that the proposed algorithm is continuous at the boundary of b.

When using JIMMY at the LHC, the tuneable parameters are those described previously [10], with the obvious exception of those parameters which only concern the photon. Those remaining are therefore the minimum transverse momentum of a hard scatter, the proton structure, and the effective radius of the proton. Details on how to adjust these parameters can be found elsewhere [11].

2.3 Simulation of Multiple Interactions in Sherpa

Given the studies presented in the following sections, and references therein, current multi-purpose event generators rely heavily on the implementation of multiple parton interaction models to describe the final state in hadronic collisions. To allow Sherpa to provide a complete description of hadronic events, the module AMISIC++ has been developed to simulate multiple parton interactions. This module is capable of simulating multiple scatterings according to the formalism initially presented in [3] and in its current implementation acts as a benchmarking tool to cross-check new multiple interaction models [12].

The basic assumption of the multiple interaction formalism according to T. Sjöstrand and M. van Zijl is, that the differential probability $\mathcal{P}(p_\perp^{\text{out}})$ to get a (semi-)hard scattering in the underlying event is given by $\mathcal{P}(p_\perp^{\text{out}}) = \sigma_{\text{hard}}(p_\perp^{\text{out}})/\sigma_{\text{ND}}$, where p_\perp^{out} is the transverse momentum of the outgoing partons in the scattering. Since σ_{hard} is dominated by $2 \rightarrow 2$ processes, the definition of p_\perp^{out} is unambiguous. The specific feature of AMISIC++ is, that it allows for an independent Q^2 -evolution of initial and final state partons in each (semi-)hard scattering via an interface to Sherpa’s parton shower module APACIC++ [13, 14]. The key point here is, that the parton shower must then respect the initial p_\perp^{out} distribution of each (semi-)hard scattering. In particular, it must not radiate partons with $p_\perp > p_\perp^{\text{out}}$. The appropriate way to incorporate this constraint is in fact identical to the realisation of the highest multiplicity treatment in the CKKW approach [15–18]. Our proposed algorithm works as follows:

1. Create a hard scattering process according to the CKKW approach.
 - Employ a K_T jet finding algorithm in the E -scheme to define final state jets.
 - Stop the jet clustering as soon as there remains only one QCD node to be clustered.
 - Set the starting scale of the multiple interaction evolution to p_\perp of this node.
2. Select p_\perp of the next (semi-)hard interaction according to [3].
 - If done for the first time in the event, select the impact parameter b of the collision.

3. Set the jet veto scale of the parton shower to the transverse momentum p_{\perp} , selected in 2.
Start the parton shower at the QCD hard scale $\mu_{\text{QCD}}^2 = 2stu / (s^2 + t^2 + u^2)$.
4. Return to step 2.

The above algorithm works for pure QCD hard matrix elements as well as for electroweak processes in the hard scattering. In the QCD case the selected starting scale for the determination of the first additional interaction reduces to p_{\perp}^{out} and is thus equal to the original ordering parameter. In the case of electroweak core processes, like single W - or Z -boson production there is no such unique identification. On the other hand the multiple scatterings in the underlying event must not spoil jet topologies described by the hard event through, e.g., using multi-jet matrix elements. However, since the electroweak bosons may be regarded to have been radiated off QCD partons during the parton shower evolution of a hard QCD event, it is appropriate to reinterpret the hard matrix element as such a QCD+EW process, where the simplest is a 1-jet process.

An important question in conjunction with the simulation of underlying events is the assignment of colours to final state particles. In the Sherpa framework, colour connections in any hard $2 \rightarrow 2$ QCD process are chosen according to the kinematics of the process. In particular the most probable colour configuration is selected. Additionally, initial state hadrons are considered to be composed from QCD partons in such a way that the colour string lengths in the final state are minimized. In cases, where it is impossible to realise this constraint, the colour configurations of the hard matrix elements are kept but the configuration of the beam remnants is shuffled until a suitable solution is found.

Figures 2–5 show some preliminary results obtained with the above algorithm, implemented in the current Sherpa version, Sherpa-1.0.6. We compare the Sherpa prediction including multiple interactions to the one without multiple interactions and to the result obtained with PYTHIA 6.214, also including multiple interactions and employing the parameters of PYTHIA Tune A [6]. Shown are hadron-level predictions, which are uncorrected for detector acceptance, except for a uniform track finding efficiency as given in [19]. Data were taken at the Fermilab Tevatron during Run I [20]. Good agreement between the simulations and data is observed only if multiple interactions are included. The mean interaction number in Sherpa, including the hard scattering, in this case is $\langle N_{\text{hard}} \rangle = 2.08$, while for PYTHIA 6.214 it is $\langle N_{\text{hard}} \rangle = 7.35$. The lower interaction number in Sherpa can easily be understood, as a decrease of parton multiplicity in the (semi-)hard scatterings due to a rise of the parton multiplicity in the parton showers. PYTHIA 6.214 does not allow for parton showers in the (semi-)hard scatterings in the underlying event. This feature has, however, been added in PYTHIA 6.3 (see Section 2.1), and is also present in JIMMY(Section 2.2).

2.4 PHOJET

The physics model used in the MC event generator PHOJET combines the ideas of the DPM [21] with perturbative QCD to give an almost complete picture of high-energy hadron collisions [22].

PHOJET is formulated as a two-component model containing contributions from both soft and hard interactions. The DPM is used to describe the dominant soft processes and perturbative QCD is applied to generate hard interactions.

There has been very little development on PHOJET for the last few years, although it is used quite widely in minimum bias and cosmic ray physics. A major disadvantage for the LHC is that it is not part of a general purpose generator, and therefore cannot be used to generate underlying events to low cross section processes.

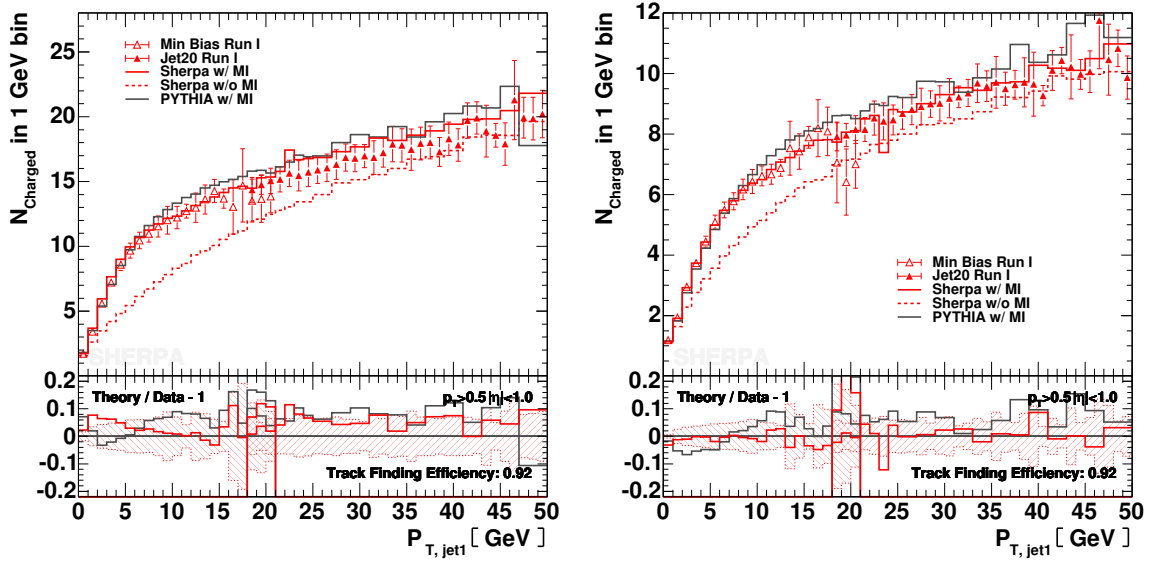


Fig. 2: Charged particle multiplicity as a function of P_T of the leading charged particle jet. The left figure shows the total charged particle multiplicity in the selected p_T - and η -range, the right one displays the same in the “Toward” region (for definitions, see Section 3 and [20]).

3 Tuning PYTHIA and HERWIG/JIMMY in Run 2 at CDF

The behaviour of the charged particle ($p_T > 0.5 \text{ GeV}/c$, $|\eta| < 1$) and energy ($|\eta| < 1$) components of the UE in hard scattering proton-antiproton collisions at 1.96 TeV has been studied at CDF. The goal is to produce data on the UE that is corrected to the particle level, so that it can be used to tune the QCD Monte-Carlo models using tools such as those described in the contributions from Group 5 of this workshop without requiring a simulation of the CDF detector. Unlike the previous CDF Run 2 UE analysis which used JetClu to define “jets” and compared uncorrected data with the QCD Monte-Carlo models after detector simulation (i.e., CDFSIM), this analysis uses the midpoint jet algorithm and corrects the observables to the particle level. The corrected observables are then compared with the QCD Monte-Carlo models at the particle level (i.e., generator level). The QCD Monte-Carlo models include PYTHIA Tune A, HERWIG and a tuned version of JIMMY.

One can use the topological structure of hadron-hadron collisions to study the UE [19,23,24]. The direction of the leading calorimeter jet is used to isolate regions of η - ϕ space that are sensitive to the UE. As illustrated in Fig. 6, the direction of the leading jet, jet#1, is used to define correlations in the azimuthal angle, $\Delta\phi$. The angle $\Delta\phi = \phi - \phi_{\text{jet}\#1}$ is the relative azimuthal angle between a charged particle (or a calorimeter tower) and the direction of jet#1. The “transverse” region is perpendicular to the plane of the hard 2-to-2 scattering and is therefore very sensitive to the UE. We restrict ourselves to charged particles in the range $p_T > 0.5 \text{ GeV}/c$ and $|\eta| < 1$ and calorimeter towers with $E_T > 0.1 \text{ GeV}$ and $|\eta| < 1$, but allow the leading jet that is used to define the “transverse” region to have $|\eta(\text{jet}\#1)| < 2$. Furthermore, we consider two classes of events. We refer to events in which there are no restrictions placed on the second and third highest P_T jets (jet#2 and jet#3) as “leading jet” events. Events with at least two jets with $P_T > 15 \text{ GeV}/c$ where the leading two jets are nearly “back-to-back” ($|\Delta\phi| > 150^\circ$) with $P_T(\text{jet}\#2)/P_T(\text{jet}\#1) > 0.8$ and $P_T(\text{jet}\#3) < 15 \text{ GeV}/c$ are referred to as “back-to-back” events. “Back-to-back” events are a subset of the “leading jet” events. The idea is to suppress hard initial and final-state radiation thus increasing the sensitivity of the “transverse” region to the “beam-beam remnants” and the multiple parton scattering component of the “underlying event”.

As illustrated in Fig. 7, we define a variety of MAX and MIN “transverse” regions which help to

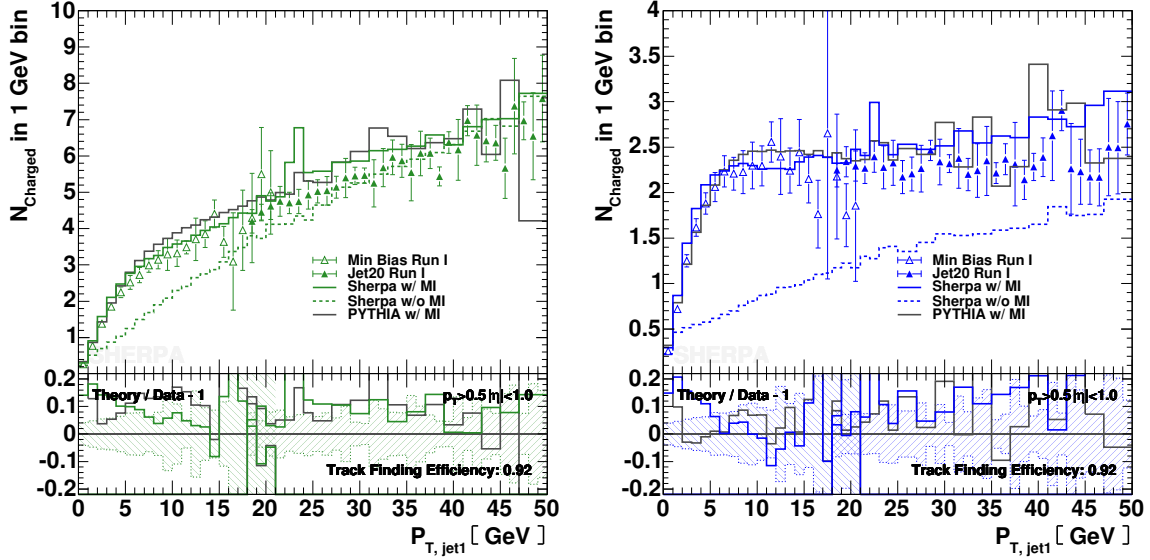


Fig. 3: Charged particle multiplicity as a function of P_T of the leading charged particle jet. The left figure shows results for the “Away” side region, the right one displays results for the “Transverse” region.

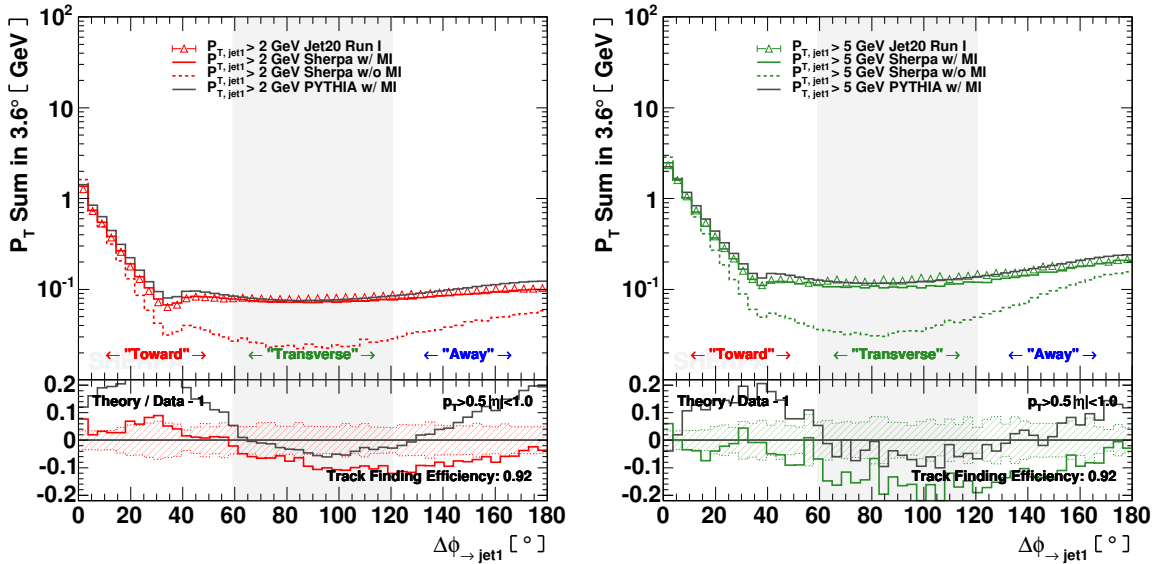


Fig. 4: Scalar P_T sum as a function of the azimuthal angle relative to the leading charged particle jet. The left figure shows results for $P_{T, \text{jet}1} > 2 \text{ GeV}$, the right one displays results for $P_{T, \text{jet}1} > 5 \text{ GeV}$.

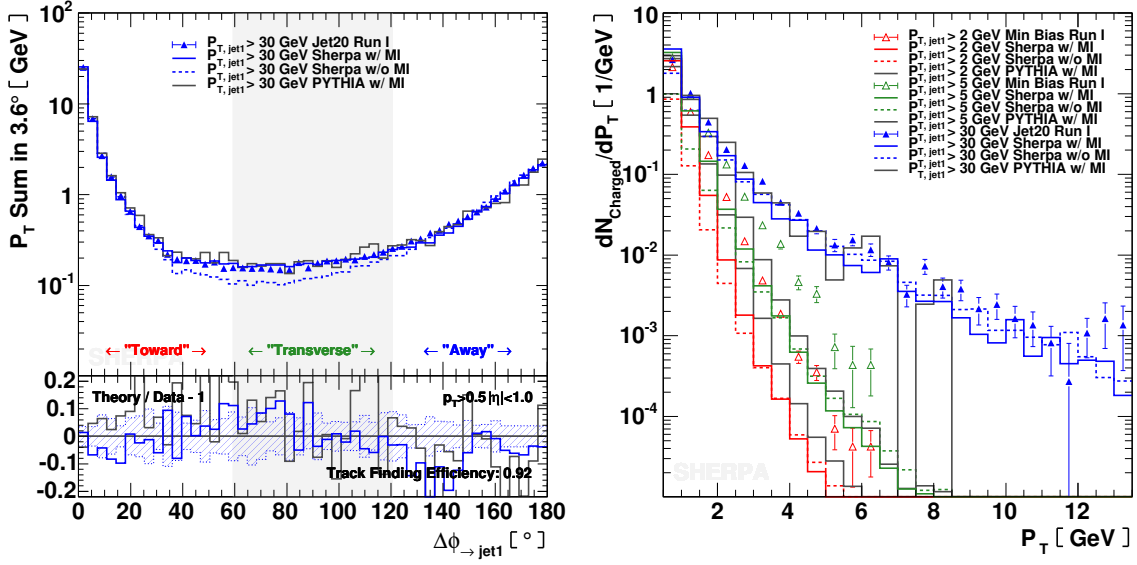


Fig. 5: Left: Scalar P_T sum as a function of the azimuthal angle relative to the leading charged particle jet for $P_{T,jet1} > 30$ GeV. Right: Charged particle multiplicity as a function of P_T in the “Transverse” region.

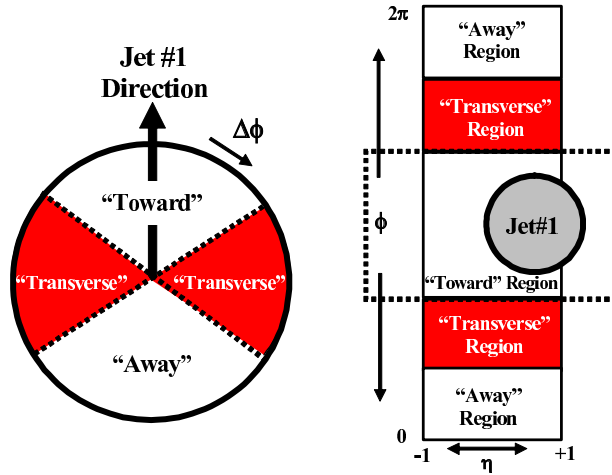


Fig. 6: Illustration of correlations in azimuthal angle ϕ relative to the direction of the leading jet (MidPoint, $R = 0.7$, $f_{merge} = 0.75$) in the event, jet#1. The angle $\Delta\phi = \phi - \phi_{jet1}$ is the relative azimuthal angle between charged particles and the direction of jet#1. The “transverse” region is defined by $60^\circ < |\Delta\phi| < 120^\circ$ and $|\eta| < 1$. We examine charged particles in the range $p_T > 0.5$ GeV/c and $|\eta| < 1$ and calorimeter towers with $|\eta| < 1$, but allow the leading jet to be in the region $|\eta(\text{jet}\#1)| < 2$.

separate the “hard component” (initial and final-state radiation) from the “beam-beam remnant” component. MAX (MIN) refer to the “transverse” region containing largest (smallest) number of charged particles or to the region containing the largest (smallest) scalar PT sum of charged particles or the region containing the largest (smallest) scalar ET sum of particles. Since we will be studying regions in η - ϕ space with different areas, we will construct densities by dividing by the area. For example, the number density, $dN_{chg}/d\phi d\eta$, corresponds to the number of charged particles ($p_T > 0.5$ GeV/c) per unit η - ϕ the PT sum density, $dPT_{sum}/d\phi d\eta$, corresponds to the amount of charged particle ($p_T > 0.5$ GeV/c) scalar PT sum per unit η - ϕ , and the transverse energy density, $dET_{sum}/d\phi d\eta$, corresponds the amount of scalar ET sum of all particles per unit η - ϕ . One expects that the “transMAX” region will pick up the

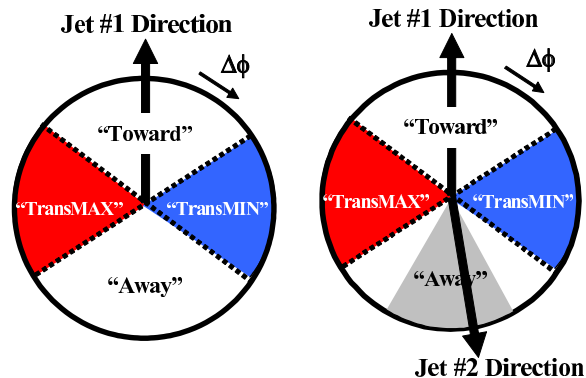


Fig. 7: Illustration of correlations in azimuthal angle ϕ relative to the direction of the leading jet (highest P_T jet) in the event, jet#1. The angle $\Delta\phi = \phi - \phi_{\text{jet}\#1}$ is the relative azimuthal angle between charged particles and the direction of jet#1. On an event by event basis, we define “transMAX” (“transMIN”) to be the maximum (minimum) of the two “transverse” regions, $60^\circ < \Delta\phi < 120^\circ$ and $60^\circ < -\Delta\phi < 120^\circ$. “transMAX” and “transMIN” each have an area in η - ϕ space of $\Delta\eta\Delta\phi = 4\pi/6$. The overall “transverse” region defined in Fig. 6 contains both the “transMAX” and the “transMIN” regions. Events in which there are no restrictions placed on the second and third highest p_T jets (jet#2 and jet#3) are referred to as “leading jet” events (*left*). Events with at least two jets with $p_T > 15$ GeV/c where the leading two jets are nearly “back-to-back” ($|\Delta\phi| > 150^\circ$) with $p_T(\text{jet}\#2)/p_T(\text{jet}\#1) > 0.8$ and $p_T(\text{jet}\#3) < 15$ GeV/c are referred to as “back-to-back” events (*right*).

hardest initial or final-state radiation while both the “transMAX” and “transMIN” regions should receive “beam-beam remnant” contributions. Hence one expects the “transMIN” region to be more sensitive to the “beam-beam remnant” component of the “underlying event”, while the “transMAX” minus the “transMIN” (i.e., “transDIF”) is very sensitive to hard initial and final-state radiation. This idea, was first suggested by Bryan Webber and Pino Marchesini [25], and implemented in a paper by Jon Pumplin [26]. This was also studied by Valeria Tano in her CDF Run 1 analysis of maximum and minimum transverse cones [27].

Our previous Run 2 UE analysis [28] used JetClu to define jets and compared uncorrected data with PYTHIA Tune A [6] and HERWIG after detector simulation (i.e., CDFSIM). This analysis uses the MidPoint jet algorithm ($R = 0.7$, $f_{\text{merge}} = 0.75$) and corrects the observables to the particle level. The corrected observables are then compared with the QCD Monte-Carlo models at the particle level (i.e., generator level). The models includes PYTHIA Tune A, HERWIG and HERWIG with a tuned version of JIMMY [10]. In addition, for the first time we study the transverse energy density in the “transverse” region.

Fig. 8 compares the data on the density of charged particles and the charged PT sum density in the “transverse” region corrected to the particle level for “leading jet” and “back-to-back” events with PYTHIA Tune A and HERWIG at the particle level. As expected, the “leading jet” and “back-to-back” events behave quite differently. For the “leading jet” case the “transMAX” densities rise with increasing $P_T(\text{jet}\#1)$, while for the “back-to-back” case they fall with increasing $P_T(\text{jet}\#1)$. The rise in the “leading jet” case is, of course, due to hard initial and final-state radiation, which has been suppressed in the “back-to-back” events. The “back-to-back” events allows a closer look at the “beam-beam remnant” and multiple parton scattering component of the UE. PYTHIA Tune A, which includes multiple parton interactions, does a better job of describing the data than HERWIG which does not have multiple parton interactions.

The “transMIN” densities are more sensitive to the “beam-beam remnant” and multiple parton interaction component of the “underlying event”. The “back-to-back” data show a decrease in the “transMIN” densities with increasing $P_T(\text{jet}\#1)$ which is described fairly well by PYTHIA Tune A (with multiple parton interactions) but not by HERWIG (without multiple parton interactions). The decrease

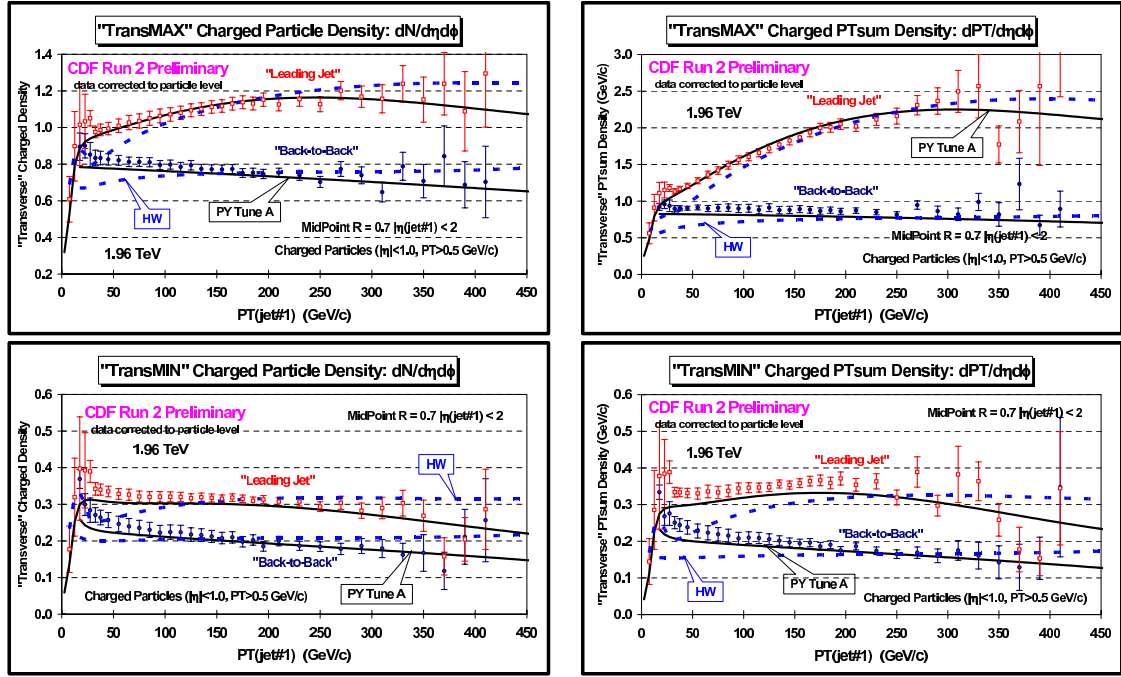


Fig. 8: Data at 1.96 TeV on (left) the density of charged particles $dN_{ch.g}/d\phi d\eta$ and (right) on the scalar PT sum density of charged particles, with $p_T > 0.5$ GeV/c and $|\eta| < 1$ in the “transMAX” region (*top*) and the “transMIN” region (*bottom*) for “leading jet” and “back-to-back” events defined in Fig. 7 as a function of the leading jet P_T compared with PYTHIA Tune A and HERWIG. The data are corrected to the particle level (with errors that include both the statistical error and the systematic uncertainty) and compared with the theory at the particle level (i.e., generator level).

of the “transMIN” densities with increasing $P_T(\text{jet}\#1)$ for the “back-to-back” events is very interesting and might be due to a “saturation” of the multiple parton interactions at small impact parameter. Such an effect is included in PYTHIA Tune A but not in HERWIG (without multiple parton interactions).

Fig. 9(left) compares the data on average p_T of charged particles in the “transverse” region corrected to the particle level for “leading jet” and “back-to-back” events with PYTHIA Tune A and HERWIG at the particle level. Again the “leading jet” and “back-to-back” events behave quite differently.

Fig. 9(right) shows the data corrected to the particle level for the scalar ET sum density in the “transverse” region for “leading jet” and “back-to-back” events compared with PYTHIA Tune A and HERWIG. The scalar ET sum density has been corrected to correspond to all particles (all p_T , $|\eta| < 1$). Neither PYTHIA Tune A nor HERWIG produce enough energy in the “transverse” region. HERWIG has more “soft” particles than PYTHIA Tune A and does slightly better in describing the energy density in the “transMAX” and “transMIN” regions.

Fig. 10(left) shows the difference of the “transMAX” and “transMIN” regions (“transDIF” = “transMAX” minus “transMIN”) for “leading jet” and “back-to-back” events compared with PYTHIA Tune A and HERWIG. “TransDIF” is more sensitive to the hard scattering component of the UE (i.e., initial and final state radiation). Both PYTHIA Tune A and HERWIG underestimate the energy density in the “transMAX” and “transMIN” regions (see Fig. 9). However, they both fit the “transDIF” energy density. This indicates that the excess energy density seen in the data probably arises from the “soft” component of the UE (i.e., beam-beam remnants and/or multiple parton interactions).

JIMMY is a model of multiple parton interaction which can be combined with HERWIG to enhance the UE thereby improving the agreement with data. Fig. 10(right) and Fig. 11(left) show the energy density and charged PT sum density, respectively, in the “transMAX” and “transMIN” regions for “lead-

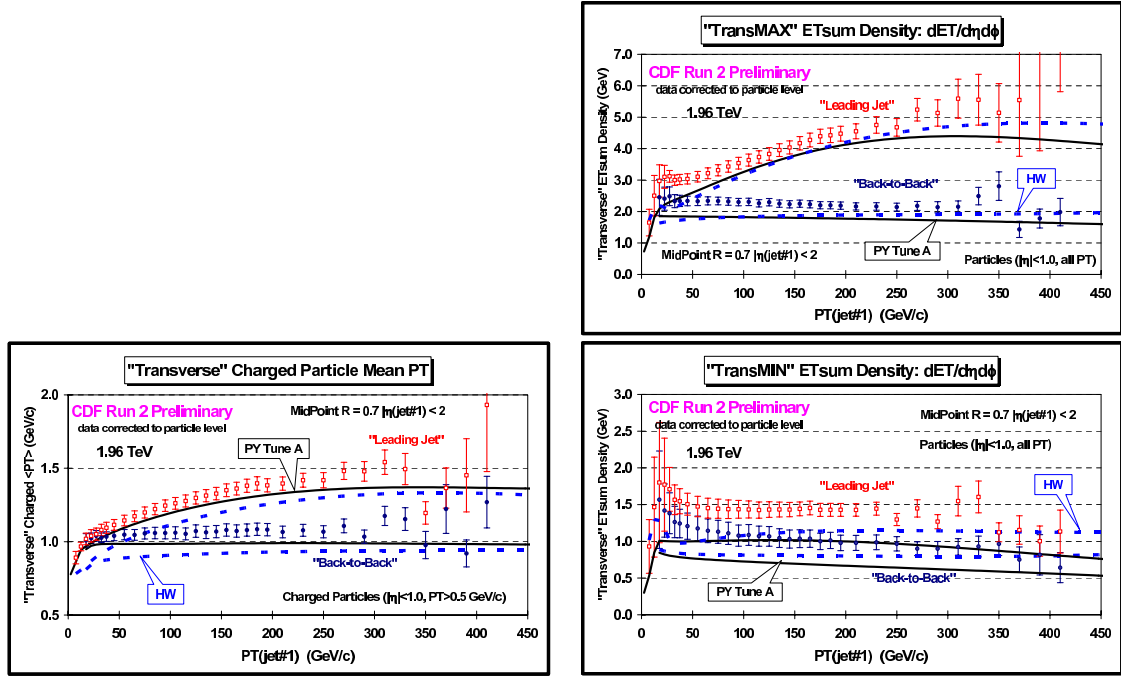


Fig. 9: On the left, data at 1.96 TeV on average transverse momentum, $\langle p_T \rangle$, of charged particles $|\eta| < 1$ in the with $p_T > 0.5$ GeV/c and $|\eta| < 1$ in the “transverse” region. On the right, scalar ET_{sum} density, $dET_{sum}/d\phi d\eta$, for particles. with $p_T > 0.5$ GeV/c and $|\eta| < 1$ in the “transMAX” region or the “transMIN” region. The “leading jet” and “back-to-back” events are defined in Fig. 7, and the data are shown as a function of the leading jet P_T and compared with PYTHIA Tune A and HERWIG. The data are corrected to the particle level (with errors that include both the statistical error and the systematic uncertainty) and compared with the theory at the particle level (i.e., generator level).

ing jet” and “back-to-back” events compared with PYTHIA Tune A and a tuned version of JIMMY. JIMMY was tuned to fit the “transverse” energy density in “leading jet” events ($PT_{JIM} = 3.25$ GeV/c). The default JIMMY ($PT_{JIM} = 2.5$ GeV/c) produces too much energy and too much charged PT_{sum} in the “transverse” region. Tuned JIMMY does a good job of fitting the energy and charged PT_{sum} density in the “transverse” region (although it produces slightly too much charged PT_{sum} at large $P_T(\text{jet}\#1)$). However, the tuned JIMMY produces too many charged particles with $p_T > 0.5$ GeV/c (see Fig. 11(right)). The particles produced by this tune of JIMMY are too soft. This can be seen clearly in Fig. 12 which shows the average charge particle p_T in the “transverse” region.

The goal of this analysis is to produce data on the UE that is corrected to the particle level so that it can be used to tune the QCD Monte-Carlo models without requiring CDF detector simulation. Comparing the corrected observables with PYTHIA Tune A and HERWIG at the particle level (i.e., generator level) leads to the same conclusions as we found when comparing the uncorrected data with the Monte-Carlo models after detector simulation [28]. PYTHIA Tune A (with multiple parton interactions) does a better job in describing the UE (i.e., “transverse” regions) for both “leading jet” and “back-to-back” events than does HERWIG (without multiple parton interactions). HERWIG does not have enough activity in the UE for $P_T(\text{jet}\#1)$ less than about 150 GeV/c, which was also observed in our published Run 1 analysis [19].

This analysis gives our first look at the energy in the UE (i.e., the “transverse” region). Neither PYTHIA Tune A nor HERWIG produce enough transverse energy in the “transverse” region. However, they both fit the “transDIF” energy density (“transMAX” minus “transMIN”). This indicates that the excess energy density seen in the data probably arises from the “soft” component of the UE (i.e., beam-

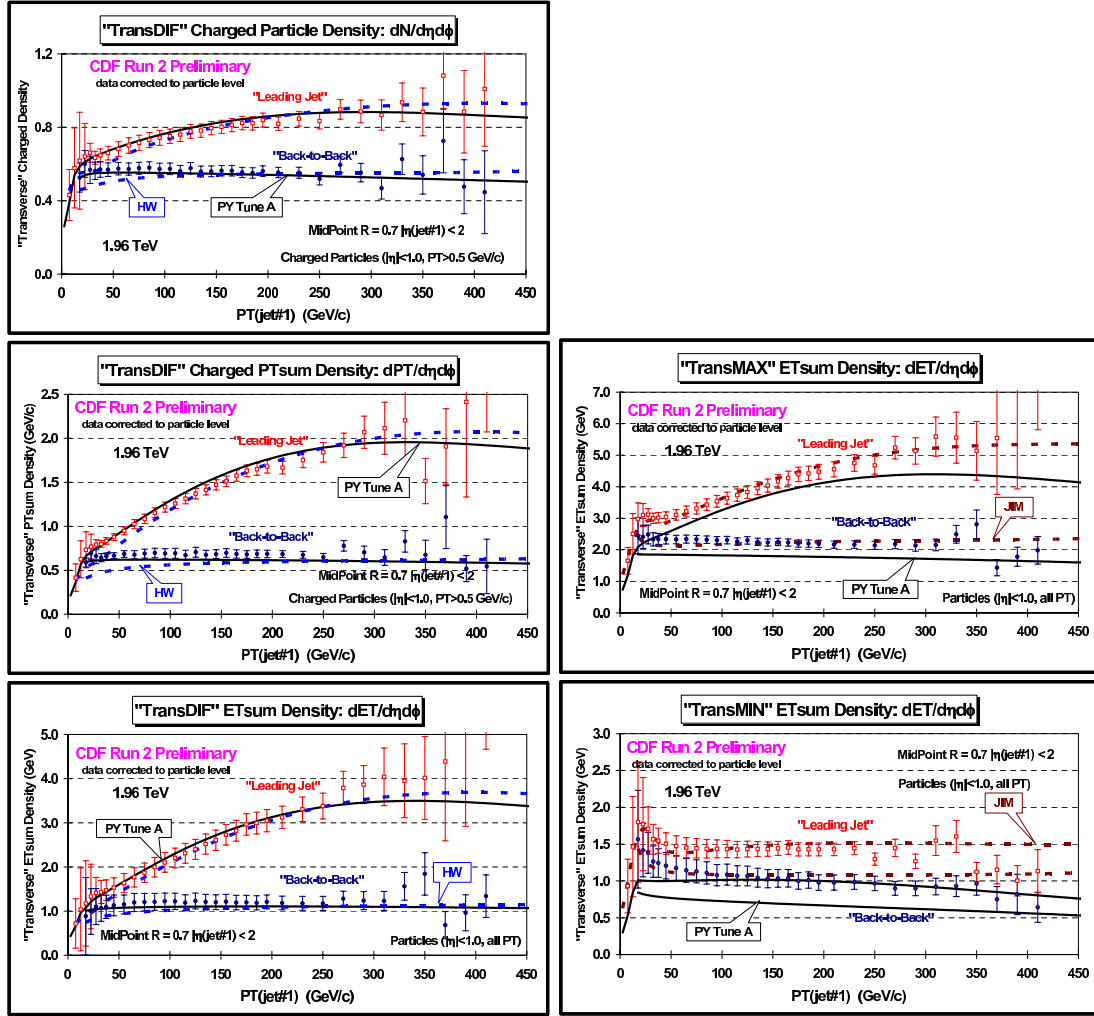


Fig. 10: Left: Data at 1.96 TeV on the difference of the “transMAX” and “transMIN” regions (“transDIF” = “transMAX”- “transMIN”) for “leading jet” and “back-to-back” events defined in Fig. 7 as a function of the leading jet P_T compared with PYTHIA Tune A and HERWIG.

Right: Data on scalar ET sum density, $dET_{sum}/d\phi d\eta$, for particles with $|\eta| < 1$ in the “transMAX” region (top) and the “transMIN” region (bottom) for “leading jet” and “back-to-back” events defined in Fig. 7 as a function of the leading jet P_T compared with PYTHIA Tune A and tuned JIMMY. JIMMY was tuned to fit the “transverse” energy density in “leading jet” events ($PT_{JIM} = 3.25 \text{ GeV}/c$). The data are corrected to the particle level (with errors that include both the statistical error and the systematic uncertainty) and compared with the theory at the particle level (i.e., generator level).

beam remnants and/or multiple parton interactions). HERWIG has more “soft” particles than PYTHIA Tune A and does slightly better in describing the energy density in the “transMAX” and “transMIN” regions. Tuned JIMMY does a good job of fitting the energy and charged PT sum density in the “transverse” region (although it produces slightly too much charged PT sum at large $P_T(\text{jet}\#1)$). However, the tuned JIMMY produces too many charged particles with $p_T > 0.5 \text{ GeV}/c$ indicating that the particles produced by this tuned JIMMY are too soft.

In summary, we see an interesting dependence of the UE on the transverse momentum of the leading jet (i.e., the Q^2 of the hard scattering). For the “leading jet” case the “transMAX” densities rise with increasing $P_T(\text{jet}\#1)$, while for the “back-to-back” case they fall with increasing $P_T(\text{jet}\#1)$. The rise in the “leading jet” case is due to hard initial and final-state radiation with $p_T > 15 \text{ GeV}/c$,

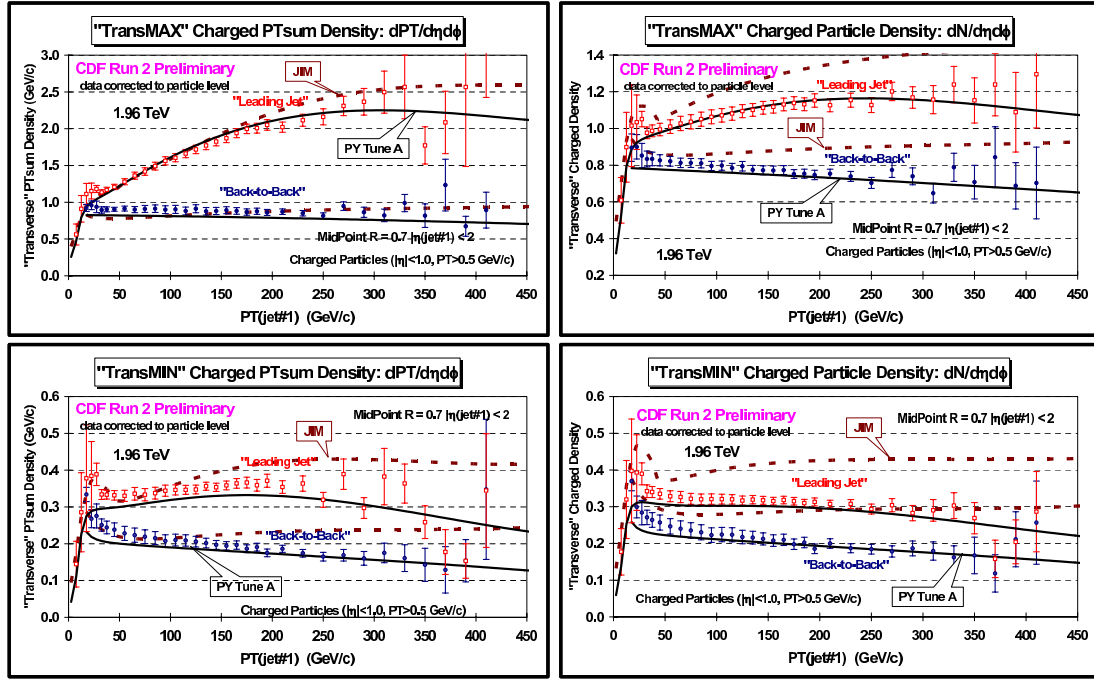


Fig. 11: Left: Data at 1.96 TeV on scalar PT sum density of charged particles, $dPT_{sum}/d\phi d\eta$, with $p_T > 0.5$ GeV/c and $|\eta| < 1$ in the “transMAX” region (top) and the “transMIN” region (bottom) for “leading jet” and “back-to-back” events defined in Fig. 7 as a function of the leading jet PT compared with PYTHIA Tune A and tuned JIMMY. JIMMY was tuned to fit the “transverse” energy density in “leading jet” events ($PT_{JIM} = 3.25$ GeV/c). Right: Data on the density of charged particles, $dN_{chg}/d\phi d\eta$, with $p_T > 0.5$ GeV/c and $|\eta| < 1$ in the “transMAX” region (top) and the “transMIN” region (bottom) for “leading jet” and “back-to-back” events defined in Fig. 2 as a function of the leading jet PT compared with PYTHIA Tune A and tuned JIMMY. JIMMY was tuned to fit the “transverse” energy density in “leading jet” events ($PT_{JIM} = 3.25$ GeV/c). The data are corrected to the particle level (with errors that include both the statistical error and the systematic uncertainty) and compared with the theory at the particle level (i.e., generator level).

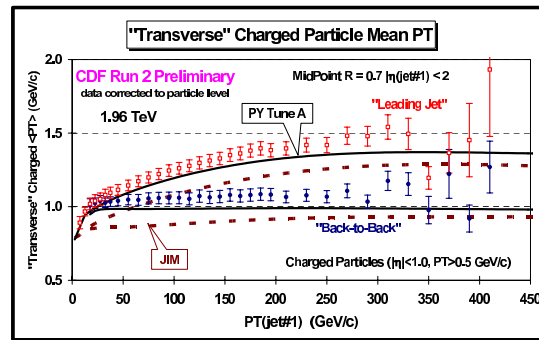


Fig. 12: Data at 1.96 TeV on average transverse momentum, $\langle p_T \rangle$, of charged particles with $p_T > 0.5$ GeV/c and $|\eta| < 1$ in the “transverse” region for “leading jet” and “back-to-back” events defined in Fig. 7 as a function of the leading jet PT compared with PYTHIA Tune A and tuned JIMMY. JIMMY was tuned to fit the “transverse” energy density in “leading jet” events ($PT_{JIM} = 3.25$ GeV/c). The data are corrected to the particle level (with errors that include both the statistical error and the systematic uncertainty) and compared with the theory at the particle level (i.e., generator level).

which has been suppressed in the “back-to-back” events. The “back-to-back” data show a decrease in the “transMIN” densities with increasing $P_T(\text{jet}\#1)$. The decrease of the “transMIN” densities with increasing $P_T(\text{jet}\#1)$ for the “back-to-back” events is very interesting and might be due to a “saturation” of the multiple parton interactions at small impact parameter. Such an effect is included in PYTHIA Tune A (with multiple parton interactions) but not in HERWIG (without multiple parton interactions). PYTHIA Tune A does predict this decrease, while HERWIG shows an increase (due to increasing initial and final state radiation).

4 Extrapolation to LHC energies

The LHCb experiment [29] is designed to measure CP violation in the B-quark sector at the LHC and expand the current studies underway at the B-factories (BaBar, Belle) and at the Tevatron (CDF, D0). At $\sqrt{s}=1.8$ TeV, 28% of all of the primary produced B-mesons in $p\bar{p}$ collisions are produced in L=1 excited states [30]. These excited states decay via the emission of a charged hadron, allowing the possibility of same-side-tagging (SST) studies. As such, it is important to simulate the production of B mesons as accurately as possible.

The production of primary produced excited meson states are not included in the default PYTHIA [31] settings and including them increases the average multiplicity of an event. An attempt to reproduce the HFAG [32] values whilst retaining the spin counting rule for B** states has been made. This note covers a preliminary re-tuning [33] of PYTHIA v6.224 including these settings.

4.1 Method

The main parameter of the multiple-interaction model in PYTHIA v6.224 is the \hat{p}_T^{\min} parameter, which defines the minimum transverse momentum of the parton-parton interactions. This effectively controls the number of parton-parton collisions and hence the average track multiplicity.

The charged particle density measured at $\eta = 0$ in the range of centre-of-mass energies, 52 GeV $< \sqrt{s} < 1800$ GeV, [34] [35] is used to tune the \hat{p}_T^{\min} parameter of PYTHIA. We define $\rho = \frac{1}{N_{ev}} \frac{dN_{ch}}{d\eta} |_{\eta=0}$ and measure ρ for a range of \hat{p}_T^{\min} values at each \sqrt{s} . The quantity $\delta = \rho_{MC} - \rho_{Data}$ is plotted against \hat{p}_T^{\min} and a linear fit performed. In Fig. 13, the re-tuned value of \hat{p}_T^{\min} at $\sqrt{s} = 900$ GeV is taken to be the point at which the fit crosses the \hat{p}_T^{\min} axis. To extrapolate \hat{p}_T^{\min} to LHC energy, a fit is performed (Figure 14) using the form suggested by PYTHIA:

$$\hat{p}_T^{\min} = \hat{p}_T^{\min}(LHC) \left(\frac{\sqrt{s}}{14TeV} \right)^{2\epsilon} \quad (8)$$

4.2 Results

Extrapolating to 14 TeV using the tuned values of $\hat{p}_T^{\min}(\sqrt{s})$ and (8), we obtain $\hat{p}_T^{\min}(LHC) = 3.34 \pm 0.13$, with $\epsilon = 0.079 \pm 0.0006$ with a corresponding central multiplicity of $\rho = 6.45 \pm 0.25$. Comparing the output of the re-tuned settings (dashed line) to the old LHCb settings (solid line), Fig. 15, 16 and 17, we find that the re-tuned settings produce a slightly lower multiplicity which affects the other distributions accordingly. Note: both the fragmentation parameters and the \hat{p}_T^{\min} parameter affect the multiplicity of a generated event. This re-tuning method varies the \hat{p}_T^{\min} parameter only i.e. it does not alter the fragmentation parameters in any fashion. Further investigations into re-tuning the fragmentation parameters using data from LEP are underway.

4.3 Conclusions

The central multiplicity values measured at CDF and UA5 are accurately reproduced using the re-tuned values for \hat{p}_T^{\min} at several \sqrt{s} . An extrapolation of \hat{p}_T^{\min} to LHC energies using a form implemented

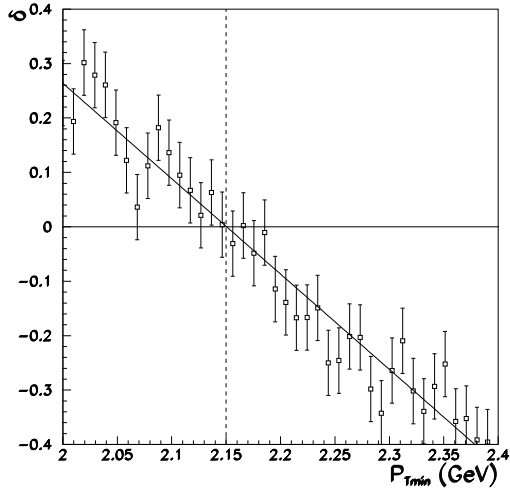


Fig. 13: Determining the value of $\hat{p}_T^{\min}(\sqrt{s} = 900\text{GeV})$, the dashed line shows the point at which $|\delta|$ is minimised.

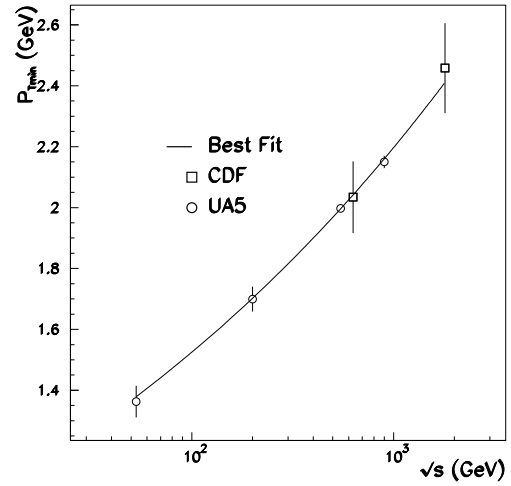


Fig. 14: The \sqrt{s} dependence of \hat{p}_T^{\min} . The curve is the result of a fit assuming the functional form of (8).

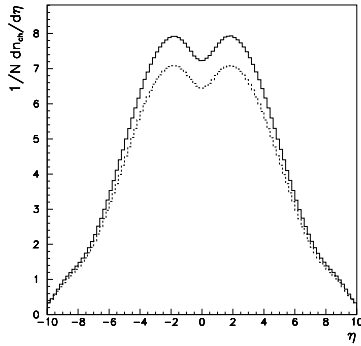


Fig. 15: η distribution at 14 TeV using the extrapolated value of $P_{T_{\text{Min}}}$

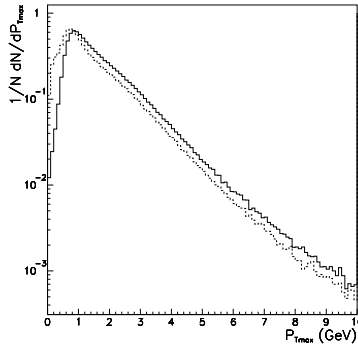


Fig. 16: $p_{\perp_{\text{max}}}$ distribution in the LHCb acceptance

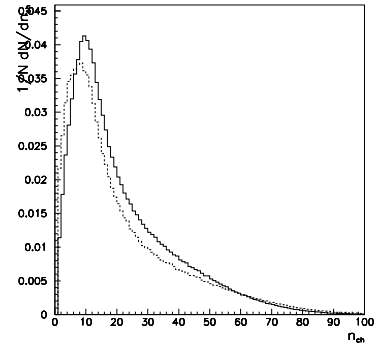


Fig. 17: Charged-stable multiplicity distribution in the LHCb acceptance.

in PYTHIA gives $\hat{p}_T^{\min}(LHC) = 3.34 \pm 0.13$, with $\epsilon = 0.079 \pm 0.0006$ with a corresponding central multiplicity of $\rho_{LHC} = 6.45 \pm 0.25$ in non-diffractive events.

5 Tuned models for the underlying event and minimum bias interactions

In this section we compare tuned MC generator models for the underlying event and minimum bias interactions. The aim of this study is to predict the event activity of minimum bias and the underlying event at the LHC. The models investigated correspond to tuned versions of PYTHIA, PHOJET and JIMMY.

5.1 Tuned models for the underlying event and minimum bias interactions

The starting point for the event generation in PYTHIA and JIMMY is the description of multiple hard interactions in the hadronic collision described in Section 2.1 (for PYTHIA 6.2), Section 2.2 for JIMMY and Section 2.4 for PHOJET.

Table 1: PYTHIA 6.214 default, ATLAS and CDF tune A parameters for minimum bias and the underlying event.

Default [31]	ATLAS [37]	CDF tune A [6]	Comments
MSTP(51)=7	MSTP(51)=7	MSTP(51)=7	CTEQ5L - selected p.d.f.
MSTP(81)=1	MSTP(81)=1	MSTP(81)=1	multiple interactions
MSTP(82)=1	MSTP(82)=4	MSTP(82)=4	complex scenario plus double Gaussian matter distribution
PARP(67)=1	PARP(67)=1	PARP(67)=4	parameter regulating initial state radiation
PARP(82)=1.9	PARP(82)=1.8	PARP(82)=2.0	$p_{t_{\min}}$ parameter
PARP(84)=0.2	PARP(84)=0.5	PARP(84)=0.4	hadronic core radius (only for MSTP(82)=4)
PARP(85)=0.33	PARP(85)=0.33	PARP(85)=0.9	probability for gluon production with colour connection to nearest neighbours
PARP(86)=0.66	PARP(86)=0.66	PARP(86)=0.95	probability to produce gluons either either as in PARP(85) or as a closed gluon loop
PARP(89)=1.0	PARP(89)=1.0	PARP(89)=1.8	energy scale (TeV) used to calculate $p_{t_{\min}}$
PARP(90)=0.16	PARP(90)=0.16	PARP(90)=0.25	power of the energy dependence of $p_{t_{\min}}$

PYTHIA and PHOJET have been shown to describe both minimum bias and underlying event data reasonably well when appropriately tuned [3, 6, 36, 37]. JIMMY is limited to the description of the underlying event; again, it has been shown capable of describing this rather well [38].

5.2 PYTHIA tunings

Several minimum bias and underlying event (UE) tunings for PYTHIA have been proposed in recent years. Ref. [37] describes how the current ATLAS tuning for PYTHIA was obtained after extensive comparisons to a variety of experimental measurements made at different colliding energies. Similar work has been done by the CDF Collaboration, although their PYTHIA tuning, CDF tune A [6], is primarily based on the description of the underlying event in jet events measured for $p\bar{p}$ at $\sqrt{s} = 1.8$ TeV.

Table 1 displays the relevant parameters tuned to the data as proposed by the ATLAS [37] and CDF [6] collaborations. For the purpose of comparison, the corresponding default values [31] are also shown in the table.

5.3 PHOJET

The parameters used in PHOJET to describe minimum bias and the underlying event can be found in Ref. [22] and are currently set as default in PHOJET1.12, which is used in this study.

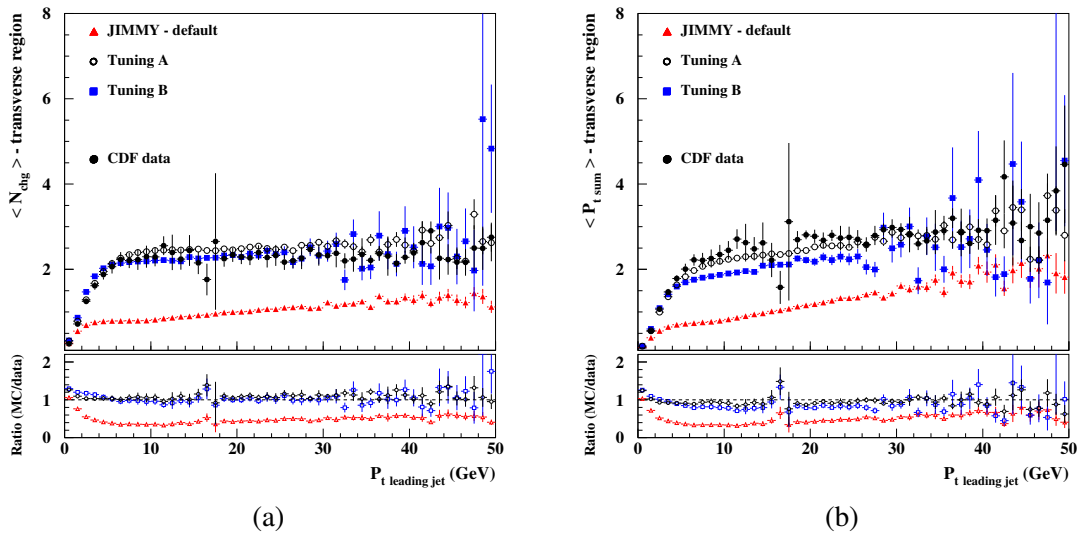
5.4 JIMMY tunings

We have tuned JIMMY to describe the UE as measured by CDF [19] and the resulting sets of parameters are shown in table 2. Figure 18 shows JIMMY predictions for the UE compared to CDF data for the average charged particle multiplicity (a) and the average p_t sum in the underlying event (b). In Fig.18 we compare JIMMY - default parameters to ‘‘Tuning A’’ and ‘‘Tuning B’’. Note that for the default parameters JIMMY does not give a correct description of the data. The other two distributions, generated with tuning A and B parameters, agree fairly well with the data.

In this study, JIMMY - tuning A and B will only be used to generate LHC predictions for the underlying event associated to jet events.

Table 2: JIMMY 4.1 default, tunings A and B parameters for the underlying event.

Default	Tuning A	Tuning B	Comments
JMUEO=1	JMUEO=0	JMUEO=0	multiparton interaction model
PTMIN=10.0	PTMIN=3.0	PTMIN=2.0	minimum p_T in hadronic jet production
PTJIM=3.0	–	–	minimum p_T of secondary scatters when JMUEO=1 or 2
JMRAD(73)=0.71	JMRAD(73)=2.13	JMRAD(73)=0.71	inverse proton radius squared
PRSOFF=1.0	PRSOFF=0.0	PRSOFF=0.0	probability of a soft underlying event


Fig. 18: JIMMY predictions for the UE compared to CDF data. (a) Average charged particles multiplicity in the UE and (b) average p_t sum in the UE.

5.5 Minimum bias interactions at the LHC

Throughout this report, minimum bias events will be associated with non-single diffractive inelastic interactions, following the experimental trend (see Ref. [37] and references therein).

For LHC collisions (pp collisions at $\sqrt{s} = 14$ TeV) the minimum bias cross-section estimated by PYTHIA 6.214, regardless of which tuning is used, is $\sigma_{nsd} = 65.7$ mb while PHOJET1.12 predicts $\sigma_{nsd} = 73.8$ mb, 12.3% greater than the former. Hence, for the same luminosity PHOJET1.12 generates more minimum bias pp collisions than PYTHIA 6.214 - tuned. We shall however, focus on the general properties per pp collision not weighted by cross-sections. The results per pp collision can later be easily scaled by the cross-section and luminosity.

Figure 19(a) shows charged particle density distributions in pseudorapidity for minimum bias pp collisions at $\sqrt{s} = 14$ TeV generated by PHOJET1.12 and PYTHIA 6.214 - ATLAS and CDF tune A. The charged particle density generated by PHOJET1.12 and PYTHIA 6.214 - CDF tune A and ATLAS at $\eta = 0$ is 5.1, 5.3 and 6.8, respectively. Contrasting to the agreement seen in previous studies for $p\bar{p}$ collisions at $\sqrt{s} = 200$ GeV, 546 GeV, 900 GeV and 1.8 TeV in Ref. [37], at the LHC PYTHIA 6.214 - ATLAS generates $\sim 25\%$ more charged particle density in the central region than PYTHIA 6.214 - CDF tune A and PHOJET1.12.

Compared to the charged particle density $dN_{ch}/d\eta$ measured by the CDF experiment at 1.8 TeV [39], PYTHIA 6.214 - ATLAS indicates a plateau rise of $\sim 70\%$ at the LHC in the central region while

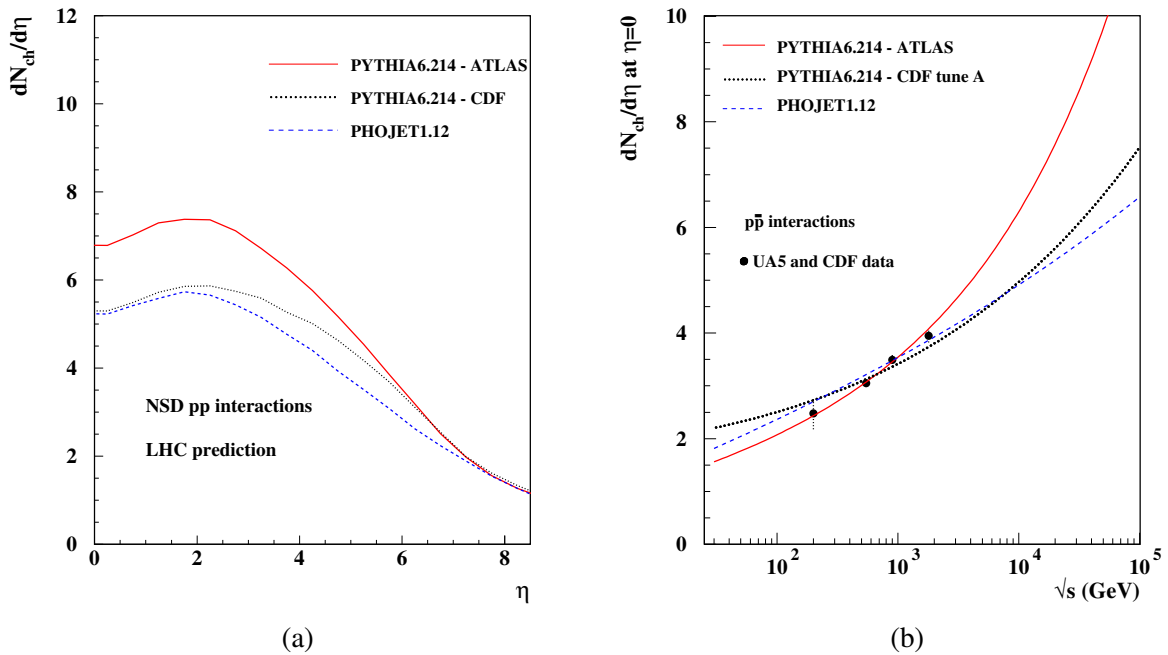


Fig. 19: (a) Charged particle density distributions, $dN_{ch}/d\eta$, for NSD pp collisions at $\sqrt{s} = 14$ TeV. (b) $dN_{ch}/d\eta$ at $\eta = 0$ for a wide range of \sqrt{s} . Predictions generated by PYTHIA 6.214, ATLAS and CDF tune A and PHOJET1.12.

PHOJET1.12 and PYTHIA 6.214 - CDF tune A suggest a smaller rise of $\sim 35\%$.

Figure 19(b) displays $dN_{ch}/d\eta$ at $\eta = 0$ plotted as a function of \sqrt{s} . For centre-of-mass energies greater than ~ 1 TeV, the multiparton interaction model employed by PYTHIA and the DPM used by PHOJET lead to multiplicity distributions with different rates of increase with the energy. PYTHIA suggests a rise dominated by the $\ln^2(s)$ term while PHOJET predicts that the dominant term gives a $\ln(s)$ rise for $dN_{ch}/d\eta$ at $\eta = 0$. The ATLAS tuning for PYTHIA gives a steeper rise than CDF tune A and PHOJET (Fig. 19(b)) indicating a faster increase in the event activity at the partonic level in the ATLAS tuning when compared to CDF tune A and PHOJET. The average charged particle multiplicity in LHC minimum bias collisions, $\langle n_{ch} \rangle$, is 69.6, 77.5 and 91.0 charged particles as predicted by PHOJET1.12, PYTHIA 6.214 - CDF tune A and ATLAS, respectively.

The $\langle p_t \rangle$ at $\eta = 0$ for charged particles in LHC minimum bias collisions predicted by PHOJET1.12 and PYTHIA 6.214 - ATLAS and CDF tune A models is 0.64 GeV, 0.67 GeV and 0.55 GeV, respectively. Generating less particles in an average minimum bias collision at the LHC, PHOJET1.12 predicts that the average p_t per particle at $\eta = 0$ is greater (or harder) than the corresponding prediction from PYTHIA 6.214 - ATLAS. However, amongst the three models, PYTHIA 6.214 - CDF tune A gives the hardest $\langle p_t \rangle$ at $\eta = 0$. The main reason for this is the increased contribution of harder parton showers used to make the model agree with the p_t spectrum of particles in the UE, and obtained by setting $PARP(67)=4$ [6].

5.6 The underlying event

Based on CDF measurements, we shall use their definition for the UE, i.e., the angular region in ϕ which is transverse to the leading charged particle jet as described in Section 3 and shown in Fig. 6. Figure 20(a) displays PYTHIA 6.214 — ATLAS and CDF tune A, and PHOJET1.12 predictions for the average particle multiplicity in the UE for pp collisions at the LHC (charged particles with $p_T > 0.5$ GeV and $|\eta| < 1$). The distributions generated by the three models are fundamentally different. Except for events

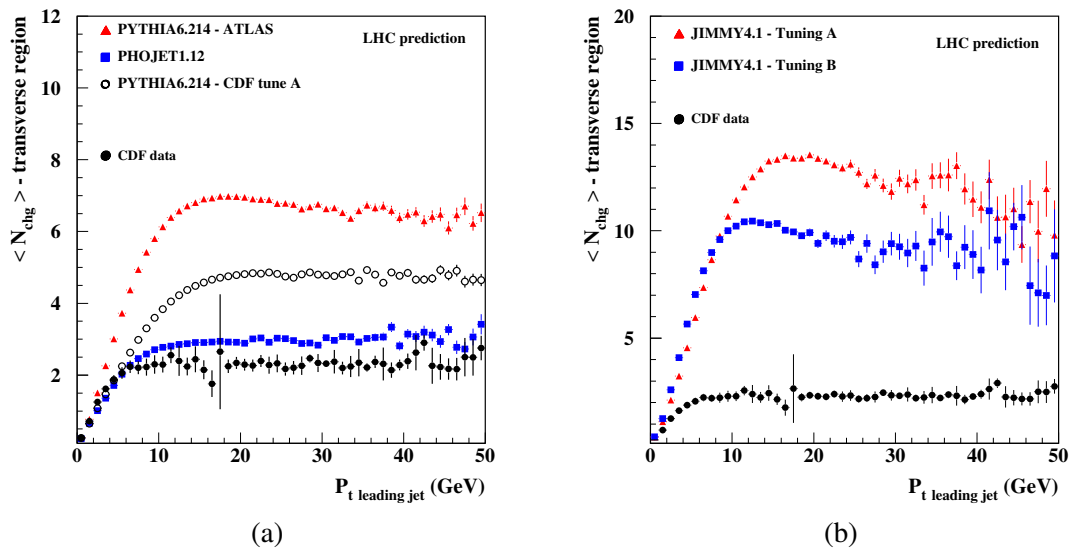


Fig. 20: (a) PYTHIA 6.214 (ATLAS and CDF tune A), PHOJET1.12 and (b) JIMMY 4.1 (tunings A and B) predictions for the average multiplicity in the UE for LHC pp collisions.

with $p_{t_{\text{jet}}} \gtrsim 3$ GeV, PYTHIA 6.214—ATLAS generates greater multiplicity in the UE than the other models shown in Fig. 20(a).

A close inspection of predictions for the UE given in Fig. 20(a), shows that the average multiplicity in the UE for $P_{t_{\text{jet}}} > 10$ GeV reaches a plateau at ~ 6.5 charged particles according to PYTHIA 6.214 - ATLAS, ~ 5 for CDF tune A and ~ 3.0 according to PHOJET1.12. Compared to the underlying event distributions measured by CDF at 1.8 TeV, PYTHIA 6.214 - ATLAS indicates a plateau rise of $\sim 200\%$ at the LHC while PYTHIA 6.214 - CDF tune A predicts a rise of $\sim 100\%$ and PHOJET1.12 suggests a much smaller rise of $\sim 40\%$.

In Fig. 20(b) we show JIMMY 4.1 - Tuning A and B predictions for the average particle multiplicity in the UE for LHC collisions. The average multiplicity in the UE for $P_{t_{\text{jet}}} > 10$ GeV reaches a plateau at ~ 12 charged particles according to JIMMY 4.1 - Tuning A, and ~ 9.0 according to JIMMY 4.1 - Tuning B. Note that, for both JIMMY tunings, the plateau rise for the average multiplicity in the UE is much greater than the ones predicted by any of the PYTHIA tunings or by PHOJET as shown in Figs. 20(a) and (b). Once again, compared to the underlying event distributions measured by CDF at 1.8 TeV, JIMMY 4.1 - Tuning A indicates a five-fold plateau rise at the LHC while JIMMY 4.1 - Tuning B - CDF suggests a four-fold rise.

5.7 Conclusion

The minimum bias and underlying event predictions for the LHC generated by models which have been tuned to the available data have been compared. In previous studies, these models have been shown to be able to describe the data distributions for these two classes of interactions. However, in this article, it has been shown that for the models detailed in tables 1 and 2, there can be dramatic disagreements in their predictions at LHC energies. This is especially evident in the distributions for the average multiplicity in the UE (Fig. 20) where, for example, PHOJET1.12 predicts that the distribution's plateau will be at ~ 3 charged particles while JIMMY 4.1 - Tuning A predicts for the same distribution, a plateau at ~ 12 .

Even though models tuned to the data have been used in this study, uncertainties in LHC predictions for minimum bias and the underlying event are still considerable. Improved models for the soft component of hadronic collisions are needed as well as more experimental information which may be

used to tune current models. Future studies should focus on tuning the energy dependence for the event activity in both minimum bias and the underlying event, which at the moment seems to be one of the least understood aspects of all the models investigated in this study.

6 Can the final state at LHC be determined from ep data at HERA?

6.1 Jets and E_{\perp} -flow

A phenomenological fit for a soft-cutoff, \hat{p}_T^{\min} , and an extrapolation to LHC energies, was discussed in sections 4.1 and 5.2. However, in the k_{\perp} -factorization formalism the soft divergence is avoided, and it is possible to predict minijets and E_{\perp} -flow from HERA data alone. Thus it is not necessary to rely on a purely phenomenological fit using $p\bar{p}$ collision data. This gives a better dynamical insight, and avoids the uncertainties associated with the extrapolation to higher energies.

High p_{\perp} jets are well described by conventional *collinear factorization*, but in this formalism the minijet cross section diverges, $\sigma_{jet} \propto 1/p_{\perp}^4$. This implies that the total E_{\perp} also diverges, and therefore a cutoff \hat{p}_T^{\min} is needed. Fits to data give $\hat{p}_T^{\min} \sim 2$ GeV growing with energy [8,9]. There is no theoretical basis for the extrapolation of \hat{p}_T^{\min} from the Tevatron to LHC, which induces an element of uncertainty in the predictions for LHC.

In the k_{\perp} -factorization formalism the off shell matrix element for the hard subcollision $k_1 + k_2 \rightarrow q_1 + q_2$ does not blow up, when the momentum exchange k_{\perp}^2 is smaller than the incoming virtualities $k_{\perp 1}^2$ and $k_{\perp 2}^2$. The unintegrated structure functions $\mathcal{F}(x, k_{\perp}^2, Q^2)$ are also suppressed for small k_{\perp} , and as a result the total E_{\perp} is not divergent but stays finite. An “effective cutoff” increases with energy, but the increase is less steep for larger energies [40].

At high energy σ_{jet} is larger than σ_{tot} , which implies that there usually are *multiple hard subcollisions* in a single event. The experimental evidence for multiple collisions has been discussed in previous sections. It includes multijet events, forward-backward correlations, the pedestal effect, and associated particles in jet events. The data also indicate that the hard subcollisions are not independent. Central collisions contain more, and peripheral collisions fewer, minijets, and the results are well described by a double Gaussian distribution in impact parameter, as suggested in ref. [3].

At high energies the pdfs needed to calculate the minijet cross section have to be evaluated in the BFKL domain of small x and low k_{\perp} . This implies that non- k_{\perp} -ordered parton chains are important. For a γ^*p collision a single local k_{\perp} -maximum corresponds to a resolved photon interaction. Similarly several local maxima in a single chain correspond to correlated hard subcollisions.

In the BFKL formalism the gluon links in the t -channel correspond to reggeized gluons, which means that soft emissions are compensated by virtual corrections. These soft emissions *do not* contribute to the parton distributions or total cross sections, but they *do* contribute to the properties of final states, and should then be added with Sudakov form factors. The CCFM model [41, 42] interpolates between DGLAP and BFKL. Here some soft emissions are included in the initial state radiation, which implies that they must be suppressed by non-eikonal form factors. The Linked Dipole Chain (LDC) model [43] is a reformulation and generalization of CCFM, in which more emissions are treated as final state emissions, in closer agreement with the BFKL picture. In the LDC formalism the chain formed by the initial state radiation is *fully symmetric* with respect to the photon end and the proton end of the ladder. This symmetry implies that the formalism is also directly applicable to hadron-hadron collisions. Thus a fit to DIS data will also give the cross section for a *parton chain* in pp collisions [44].

A potential problem is due to the fact that with a running α_s , the enhancement of small k_{\perp} implies that the result depends on a necessary cutoff Q_0 . Good fits to DIS data are possible with different Q_0 , if the input distribution $f_0(x, Q_0^2)$ is adjusted accordingly. However, although a larger cutoff gives fewer hard chains, it also implies a larger number of soft chains, in which no link has a k_{\perp} larger than Q_0 . Thus the total number of chains in pp scattering is independent of Q_0 , and therefore well determined by the fit to DIS data.

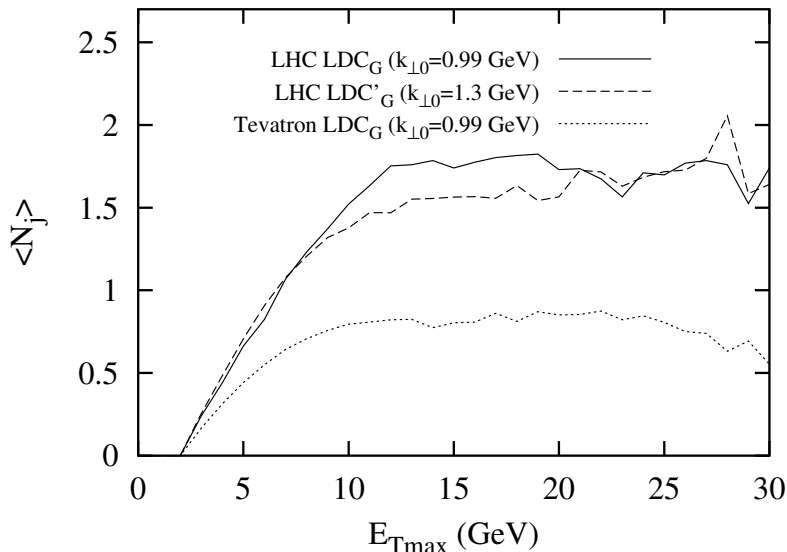


Fig. 21: The average number of minijets per event in the “minimum azimuth region”, as a function of transverse energy of the trigger jet, $E_{\perp max}$. The figure shows the result for 1.8 TeV and for LHC. The two LHC curves correspond to different values for Q_0 , showing the stability with respect to the soft cutoff.

When the fit to HERA data in this way is applied to $p\bar{p}$ scattering at the Tevatron, the predictions for *e.g.* jet multiplicity and the pedestal effect are very close to CDF’s tune A, described in Section 3. The result is insensitive to the soft cutoff Q_0 , which implies that the extrapolation to LHC energies is stable, and does not depend on an uncertain extrapolation of the low- p_{\perp} cutoff needed in a collinear formalism. As an example fig. 21 shows a prediction for the average number of minijets per event within 60° in azimuth perpendicular to a trigger jet, on the side with minimum activity.

As the LDC model is fully symmetric with respect to an interchange of the projectile and the target, the parton chains have to combine at one end at the same rate as they multiply at the other. Therefore the formalism should be suitable for studies of gluon recombination and *saturation*. This work is in progress, and some preliminary results from combining the LDC model with Mueller’s dipole formulation in transverse coordinate space [45–47] are presented in ref. [48].

6.2 Hadron multiplicities

The hadron multiplicity is much more sensitive to non-perturbative effects. This implies larger uncertainties, and models differ by factors 3-4 in their predictions for LHC (see Section 5). The CDF data also show that the data are best fitted if colours rearrange so that secondary hard scatterings give minimum extra string length, i.e. minimum extra multiplicity. This is very different from the case in e^+e^- annihilation.

In pp collisions the multiplicity of final state hadrons depends very sensitively on the colour connections between the produced partons. This implies that the result depends on soft non-perturbative effects. Multiple interactions are related to multiple pomeron exchange, which is expected to obey the Abramovskiy-Gribov-Kancheli cutting rules [49]. These rules are derived for a multiperipheral model, but a multiperipheral chain has important similarities with a gluonic chain. An essential feature is the dominance of small momentum exchanges at each vertex. The colour structure of QCD gives, however, some extra complications as discussed by J. Bartels (see the contribution by Bartels to working group 4).

The pomeron is identified by two gluon exchange, and multiple chains correspond to multi-pomeron exchange. For the example of two pomeron exchange, the AGK rules give the relative weights

1 : -4 : 2 for cutting 0, 1 or 2 pomerons. These ratios imply that the two-pomeron diagram contributes to the multiplicity *fluctuations*, but has no effect on the number of produced particles, determined by $\sum n\sigma_n$. This result can also be generalized to the exchange of more pomerons.

Similar cutting rules apply to a diagram with two pomerons attached to one proton and one pomeron to the other, connected by a central triple-pomeron coupling. In ref. [49] this and similar diagrams are, however, expected to give smaller contributions.

A hard $gg \rightarrow gg$ subcollision will imply that the two proton remnants carry colour octet charges. This is expected to give two colour triplet strings, or two cluster chains, connecting the two remnants and the two final state gluons. In the string model the strings are stretched between the remnants, with the gluons acting as kinks on the strings. These kinks can either be on different strings or both on the first or both on the second string, with equal probabilities for the three possibilities (see ref. [50]). Including initial state radiation will give extra kinks, which due to colour coherence will be connected so as to result in minimal extra string length.

Multiple collisions with two independent $gg \rightarrow gg$ scatterings would be expected to correspond to two cut pomerons, with four triplet strings stretched between the proton remnants. This would give approximately a doubled multiplicity, in accordance with the AGK cutting rules. However, the CDF data show that this is *far from reality*.

CDF's successful tune A [6] is a fit using an early PYTHIA version. Already in the analysis in ref. [3] it was realized that four strings would give too high multiplicity. Therefore in this early PYTHIA version there are three possible string connections for a secondary hard subcollision. 1) An extra closed string loop between the two final state gluons. 2) A single string between the scattered partons, which are then treated as a $q\bar{q}$ system. 3) The new hard gluons are inserted as extra kinks among the initial state radiations, in a way which corresponds to minimum extra string length. In the successful tune A the last possibility is chosen in 90% of the cases, which corresponds to *minimal extra multiplicity*. The default PYTHIA tune, which contained equal probabilities for the three cases, does not give a good fit. A more advanced treatment of pp collisions [8,9] is implemented in a new PYTHIA version (6.3) [2] (see Section 2.1). This model does, however, not work as well as Field's tune A of the older model.

Consequently two independent hard collisions do not correspond to two cut pomeron ladders stretched between the proton remnants. It also does not correspond to a cut pomeron loop in the centre. Instead it looks like a single ladder, with a higher density of gluon rungs in the central region.

How can this be understood? It raises a set of important questions: What does it imply for the AGK rules and the diffractive gap survival probability? Do rescattering and unitarity constraints (and AGK) work in the initial perturbative phase? If so, does this correspond to an initial hard collision inside a confining bag, with the final state partons colour connected in a later non-perturbative phase?

We can compare with the situation in e^+e^- -annihilation. If two gluons are emitted from the quark or antiquark legs, these gluons form a colour singlet with probability $\sim 1/N_c^2$. They could then hadronize as a separate system. Analyses of data from LEP indicate that such isolated systems are suppressed even more than by a factor $\sim 1/N_c^2$.

In conclusion we have following important questions:

- Why do the strings make the shortest connections in $\approx 100\%$ in pp and almost never in e^+e^- ?
- How do multiplicity fluctuations and the relation *diffraction* and *high multiplicity events* reflect features of AGK in ep, γp , and pp?
- Do unitarity effects and AGK cutting rules work as expected in an initial perturbative phase, and the colours recombine in a subsequent nonperturbative soft phase?
- Or is the pomeron a much more complicated phenomenon than the simple ladder envisaged by Abramovsky-Gribov-Kancheli?

7 Conclusions and the potential for HERA data

This was a very active area of discussion during the workshop. In fact, the area remains so active that firm conclusions are hard to make, and likely to be superseded on a very short timescale. Nevertheless there are some things which do seem clear.

- The underlying event is clearly an topic of substantial importance for the LHC.
- The dominant input data for understanding the underlying event comes at present from the Tevatron, with HERA data primarily featuring indirectly, though importantly, via the parton densities.
- The data strongly indicate that multiple hard scatters are required to adequately describe the final state in high energy hadron collisions.
- The UE depends on the measurement being made as demonstrated by difference between the UE in the CDF leading jet and back-to-back jet analysis.
- The colour structure of the final parton state is an unsolved problem. The CDF data indicate that ‘short strings’ are strongly favoured.
- There are large uncertainties associated with extrapolating the available models to LHC energies.

As far as the future impact of HERA data on this area goes, some ideas have been discussed in the previous section. In addition, it is worth noting that most of the models discussed here have also been used in high energy photoproduction at HERA [51], where they also improve the description of the data. No study comparable to those carried out at pp or p \bar{p} experiments is currently available. The benefits of such a study would be that (a) HERA could add another series of points in energy (around 200 GeV) to help pin down the energy dependence of the underlying event, (b) it is possible to select regions of phase space where resolved (i.e., hadronic) or direct (i.e., pointlike) photons dominate, thus effectively switching on or off the photon PDF (and thus presumably multiparton interactions) and allowing comparison between the two cases, (c) the photon is a new particle with which the physics assumptions of underlying event models can be confronted. The last of these points however also implies that a slew of new parameters will be introduced, and one may learn more about the photon this way than about underlying events themselves. Either way, it is to be hoped that such a study will be carried out before HERA finishes and LHC switches on.

References

- [1] T. Sjöstrand *et al.*, Comput. Phys. Commun. **135**, 238 (2001). hep-ph/0010017.
- [2] T. Sjöstrand *et al.*, LU TP 03-38 (2003). hep-ph/0308153.
- [3] T. Sjöstrand and M. van Zijl, Phys. Rev. **D36**, 2019 (1987).
- [4] ZEUS Collaboration, S. Chekanov *et al.*, Eur. Phys. J. **C21**, 443 (2001);
H1 Collaboration, C. Adloff *et al.*, Eur. Phys. J. **C21**, 33 (2001).
- [5] J. Dischler and T. Sjöstrand, Eur. Phys. J. direct **C3**, 2 (2001). hep-ph/0011282.
- [6] R. Field, *Min-bias and the underlying event at the tevatron and the lhc*.
http://www.phys.ufl.edu/~rfield/cdf/tunes/py_tuneA.html.
- [7] T. Sjöstrand and P. Z. Skands, Nucl. Phys. **B659**, 243 (2003). hep-ph/0212264.
- [8] T. Sjöstrand and P. Z. Skands, JHEP **03**, 053 (2004). hep-ph/0402078.
- [9] T. Sjöstrand and P. Z. Skands, Eur. Phys. J. **C39**, 129 (2005). hep-ph/0408302.
- [10] J. M. Butterworth, J. R. Forshaw, and M. H. Seymour, Z. Phys. C **72**, 637 (1996).
(Hep-ph/9601371).
- [11] J. M. Butterworth and M. H. Seymour, In preparation see
<http://www.cedar.ac.uk/hepforge/jimmy>.
- [12] S. Höche and F. Krauss, in preparation.

- [13] R. Kuhn, F. Krauss, B. Ivanyi, and G. Soff, *Comput. Phys. Commun.* **134**, 223 (2001). [hep-ph/0004270](http://arxiv.org/abs/hep-ph/0004270).
- [14] F. Krauss, A. Schälicke, and G. Soff, [hep-ph/0503087](http://arxiv.org/abs/hep-ph/0503087).
- [15] S. Catani *et al.*, *JHEP* **11**, 063 (2001). [hep-ph/0109231](http://arxiv.org/abs/hep-ph/0109231).
- [16] F. Krauss, *JHEP* **08**, 015 (2002). [hep-ph/0205283](http://arxiv.org/abs/hep-ph/0205283).
- [17] F. Krauss *et al.*, *Phys. Rev.* **D70**, 114009 (2004). [hep-ph/0409106](http://arxiv.org/abs/hep-ph/0409106).
- [18] A. Schälicke and F. Krauss, *JHEP* **07**, 018 (2005). [hep-ph/0503281](http://arxiv.org/abs/hep-ph/0503281).
- [19] CDF Collaboration, T. Affolder *et al.*, *Phys. Rev.* **D65**, 092002 (2002).
- [20] R. D. Field, http://www.phys.ufl.edu/~rfield/cdf/chgjet/chgjet_intro.html.
- [21] A. Capella *et al.*, *Phys. Rep.* **236**, 225 (1994).
- [22] R. Engel, *PHOJET manual (program version 1.05)*, June 1996.
- [23] R. Field, *Int. J. Mod. Phys.* **A16S1A**, 250 (2001).
- [24] J. Huston, *Int. J. Mod. Phys.* **A16S1A**, 219 (2001).
- [25] G. Marchesini and B. R. Weber, *Phys. Rev.* **D38**, 3419 (1988).
- [26] J. Pumplin, *Phys. Rev.* **D57**, 5787 (1998).
- [27] D. Acosta *et al.*, *Phys. Rev.* **D70**, 072002 (2004).
- [28] R. Field, *Acta Phys. Polon.* **B36**, 167 (2005).
- [29] LHCb Collaboration. CERN-LHCC-2003-030.
- [30] CDF Collaboration, T. Affolder *et al.*, *Phys. Rev.* **D64**, 072002 (2001).
- [31] T. Sjöstrand, L. Lönnblad, and S. Mrenna, *Pythia 6.2: Physics and manual*. Preprint [hep-ph/0108264](http://arxiv.org/abs/hep-ph/0108264), 2001.
- [32] Heavy Flavor Averaging Group (HFAG) (2005). [hep-ex/0505100](http://arxiv.org/abs/hep-ex/0505100).
- [33] LHCb Collaboration, P. Bartalini *et al.* (1999).
- [34] UA5 Collaboration, G. J. Alner *et al.*, *Z. Phys.* **C33**, 1 (1986).
- [35] CDF Collaboration, F. Abe *et al.*, *Phys. Rev.* **D41**, 2330 (1990).
- [36] R. Engel, *Hadronic Interactions of Photons at High Energies*, 1997. Siegen (PhD Thesis).
- [37] A. Moraes, C. Buttar, and I. Dawson, p. 46 (2005). ATL-PHYS-PUB-2005-007.
- [38] J. M. Butterworth and S. Butterworth, *Comput. Phys. Commun.* **153**, 164 (2003). See results available at <http://www.cedar.ac.uk/jetweb>, [hep-ph/0210404](http://arxiv.org/abs/hep-ph/0210404).
- [39] F. Abe *et al.*, *Phys. Rev.* **D41**, 2330 (1990).
- [40] G. Gustafson and G. Miu, *Phys. Rev.* **D63**, 034004 (2001). [hep-ph/0002278](http://arxiv.org/abs/hep-ph/0002278).
- [41] S. Catani, F. Fiorani, and G. Marchesini, *Phys. Lett.* **B234**, 339 (1990).
- [42] M. Ciafaloni, *Nucl. Phys.* **B296**, 49 (1988).
- [43] B. Andersson, G. Gustafson, and J. Samuelsson, *Nucl. Phys.* **B467**, 443 (1996).
- [44] G. Gustafson, L. Lönnblad, and G. Miu, *Phys. Rev.* **D67**, 034020 (2003). [hep-ph/0209186](http://arxiv.org/abs/hep-ph/0209186).
- [45] A. H. Mueller, *Nucl. Phys.* **B415**, 373 (1994).
- [46] A. H. Mueller and B. Patel, *Nucl. Phys.* **B425**, 471 (1994). [hep-ph/9403256](http://arxiv.org/abs/hep-ph/9403256).
- [47] A. H. Mueller, *Nucl. Phys.* **B437**, 107 (1995). [hep-ph/9408245](http://arxiv.org/abs/hep-ph/9408245).
- [48] E. Avsar, G. Gustafson, and L. Lönnblad, *JHEP* **07**, 062 (2005). [hep-ph/0503181](http://arxiv.org/abs/hep-ph/0503181).
- [49] V. A. Abramovsky, V. N. Gribov, and O. V. Kancheli, *Yad. Fiz.* **18**, 595 (1973).
- [50] G. Gustafson, *Z. Phys.* **C15**, 155 (1982).
- [51] J. M. Butterworth and M. Wing, *Rep. Prog. Phys.* **68**, 2773 (2005). [hep-ex/0509018](http://arxiv.org/abs/hep-ex/0509018).

Forward Jets and Multiple Interactions

Jacek Turnau¹, Leif Lönnblad²

¹Institute of Nuclear Physics, Polish Academy of Sciences, Cracow, Poland;

²Department of Theoretical Physics, Lund University, Sweden.

Abstract

HERA provides a unique possibility to investigate the dependence of multiple interactions on transverse interaction sizes through variation of the photon virtuality Q^2 . In order to observe effects of multiple interactions at Q^2 substantially different from zero we have to look into regions of phase space where resolved processes dominate over direct ones. The forward jet production at small values of Bjorken x is one example. PYTHIA and RAPGAP have been employed to estimate contribution of the multiple interactions to forward jet production cross section.

Comparisons of HERA photoproduction data with QCD NLO calculations for high transverse momentum jets revealed that the observed jets are not well described by the calculations. The energy flow adjacent to jets - the underlying event or jet pedestal - was found to be far above QCD expectations [1]. Similar excess of underlying energy was observed in $p\bar{p}$ data, see [2] and [3] for recent studies. It appears that both HERA and TEVATRON data can be described by adding beam remnant interactions, from soft to hard, as first proposed in ref. [4]. The remnant beam-beam interactions can result in multiple hard parton interactions (MI) thus creating additional pairs of jets. Therefore the presence of four high transverse momentum objects in the hadronic final state (e.g. four jets or prompt photon and three jets) allows searches for signatures of multi-parton interactions in a region of phase space where their effects may be maximized. The evidence of MI coming from 4-jet studies is more explicit and is not complicated by initial/final state radiation and soft beam-remnant components of the underlying event. Both ZEUS [5] and CDF [6] observed explicit double parton interactions in rough agreement with PYTHIA [4, 7] simulations.

The very interesting aspect of measurements at HERA is that variation of the photon virtuality Q^2 provides information about transverse interaction sizes. Observation of the dependence of MI on Q^2 could be important from the phenomenological point of view. In order to see MI at photon virtuality substantially different from zero we have to look into regions of phase space for deep inelastic scattering where the resolved virtual photon processes dominate over direct ones. The forward jet production at small values of Bjorken x is one example. Here one could expect that additional interactions between the remnants of the proton and resolved virtual photon would produce extra hadron multiplicity in an underlying event. Although the transverse momentum of these hadrons would be limited, they could still give a substantial effect on the rate of forward jets which have a steeply falling p_{\perp} spectrum.

The forward jet cross-section is especially interesting since it has been notoriously difficult to reproduce by standard DGLAP-based parton shower event generators. It has been shown that the description of the forward jet cross section can be improved by adding resolved virtual photon component in eg. the RAPGAP Monte Carlo [8], but the jet rates produced in the simulations are still a bit too low in the small- x region. In order to check if MI can give measurable contribution to this process we have performed a study in which we estimate MI effect using both PYTHIA 6.2 and RAPGAP 3.1. We use PYTHIA since the MI model there has been shown to be able to give a good description of underlying events and jet pedestal effects in hadron-hadron collisions and in photoproduction, and it is fairly easy to apply the same model to the resolved part of the $\gamma^* - p$ collisions. However, PYTHIA does not describe correctly the transverse energy flow in DIS at HERA above $Q^2 \approx 5 \text{ GeV}^2$. We can still use PYTHIA to estimate the relative effect of MI and we have generated forward jet cross section with H1 cuts [9]:

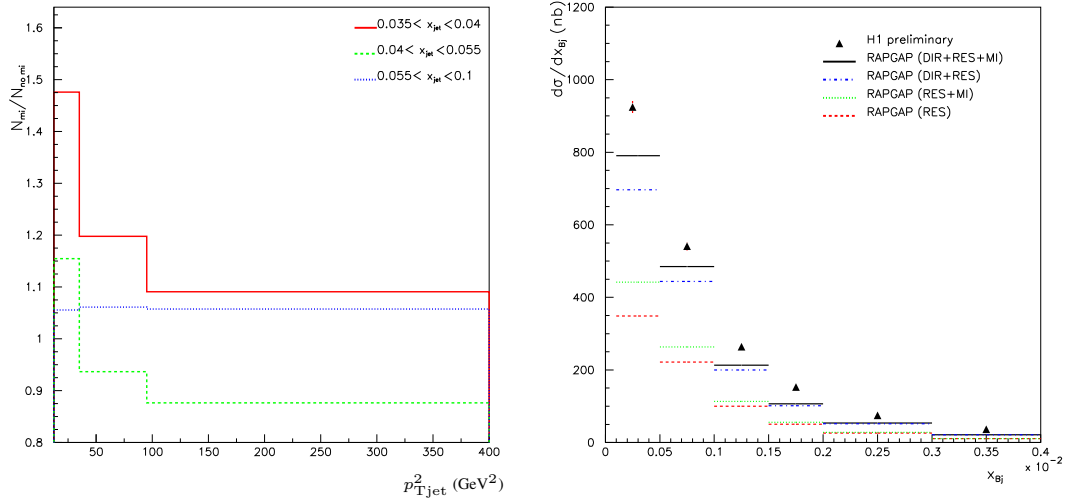


Fig. 1: Left: Ratio of forward jets with and without multiple interactions as a function of jet transverse momentum squared for three regions of proton momentum fraction carried by jet **Right:** The H1 forward jet cross section data compared with RAPGAP 3.1 simulation. Multiple interactions are included as x , Q^2 , x_{jet} and $p_{T,jet}^2$ dependent weights to resolved component, calculated using PYTHIA 6.2

($p_{T,jet} > 3.5$ GeV, $x_{jet} > 0.035$, $20^\circ > \Theta_{jet} > 7^\circ$ and $0.5 < p_{T,jet}^2/Q^2 < 5$) using PYTHIA 6.2 with default settings in γp mode (MI in mode 2) with γ^* momentum corresponding to several values of x and Q^2 within DIS kinematical phase space $0.0001 < x < 0.004$ and $5 < Q^2 < 85$ GeV 2 .

In Fig. 1 (left) we show example of the ratio of number of the forward jets with and without MI, here for $x = 0.0004$ and $Q^2 = 8$ GeV 2 , as a function of $p_{T,jet}^2$. It can be seen that effect of MI is quite substantial in the lowest $p_{T,jet}^2$ bin. Treating the above mentioned ratios as weights depending on x , Q^2 , x_{jet} and $p_{T,jet}^2$, we have generated inclusive forward jet cross section using RAPGAP 3.1 within above mentioned H1 cuts. The Fig. 1 (right) shows the result of this calculation. The inclusive forward jet cross section is enhanced by MI for about 15% in the lowest x bin, in fact improving description of the data. The effect of MI diminishes quickly with increasing x as result of decreasing contribution of the resolved photon component.

This very preliminary study suggests that Q^2 dependence of multiple interactions can be studied at HERA. This will require large statistics and an improved understanding of the underlying QCD evolution in forward jet production.

References

- [1] H1 Collaboration, I. Abt *et al.*, Phys. Lett. **B314**, 436 (1993);
ZEUS Collaboration, M.Derrick *et al.*, Phys. Lett. **B342**, 417 (1995);
H1 Collaboration, T. Ahmed *et al.*, Nucl. Phys. **B445**, 195 (1995);
G. Knies, J. Phys. G. Nucl. Part. Phys. **G19**, 1523 (1993).
- [2] CDF Collaboration, T. Affolder *et al.*, Phys. Rev. **D65**, 092002 (2002).
- [3] CDF Collaboration, R. Field, Acta Physica Polonica **B36**, 167 (2005).
- [4] T. Sjostrand and M. van Zijl, Phys. Rev. **D36**, 2019 (1987).
- [5] ZEUS Collaboration, C. Gwenlen, Acta Physica Polonica **B33**, 3123 (2002).
- [6] CDF Collaboration, F. Abe *et al.*, Phys. Rev. **D56**, 3811 (1997).
- [7] T. Sjostrand, P. Eden, C. Friberg, L. Lonnblad, G. Miu, S. Mrenna, and E. Norrbin, Comput. Phys. Commun. **135**, 238 (2001). hep-ph/0010017.

- [8] ZEUS Collaboration, J. Breitweg *et al.*, Phys. Lett. **B479**, 37 (2000);
H1 Collaboration, C. Adloff *et al.*, EPJ **C13**, 397 (2000);
L. J. H. Jung and H. Kuester, EPJ **C9**, 383 (1999).
[9] H1 Collaboration, A. Aktas *et al.*, submitted to EPJ (2005). hep-ex/0508055.

Survival Probability of Large Rapidity Gaps

E. Gotsman, E. Levin, U. Maor, E. Naftali, A. Prygarin

HEP Department, School of Physics and Astronomy, Raymond and Beverly Sackler Faculty of Exact Science, Tel Aviv University, Tel Aviv, 69978, ISRAEL.

Abstract

Our presentation centers on the consequences of s-channel unitarity, manifested by soft re-scatterings of the spectator partons in a high energy diffractive process, focusing on the calculations of gap survival probabilities. Our emphasis is on recent estimates relevant to exclusive diffractive Higgs production at the LHC. To this end, we critically re-examine the comparison of the theoretical estimates of large rapidity gap hard di-jets with the measured data, and remark on the difficulties in the interpretation of HERA hard di-jet photoproduction.

1 Introduction

A large rapidity gap (LRG) in an hadronic, photo or DIS induced final state is experimentally defined as a large gap in the $\eta - \phi$ lego plot devoid of produced hadrons. LRG events were suggested [1–4] as a signature for Higgs production due to a virtual $W - W$ fusion subprocess. An analogous pQCD process, in which a colorless exchange (“hard Pomeron”) replaces the virtual W , has a considerably larger discovery potential as it leads also to an exclusive $p + H + p$ final state. Assuming the Higgs mass to be in the range of $100 - 150 \text{ GeV}$, the calculated rates for this channel, utilizing proton tagging are promising. Indeed, LRG hard di-jets, produced via the same production mechanism, have been observed in the Tevatron [5–17] and HERA [18–29]. The experimental LRG di-jets production rates are much smaller than the pQCD (or Regge) estimates. Following Bjorken [3, 4], the correcting damping factor is called “LRG survival probability”.

The present summary aims to review and check calculations of the survival probability as applied to the HERA-Tevatron data and explore the consequences for diffractive LRG channels at LHC with a focus on diffractive Higgs production.

We distinguish between three configurations of di-jets (for details see Ref. [13–17]):

- 1) A LRG separates the di-jets system from the other non diffractive final state particles. On the partonic level this is a single diffraction (SD) Pomeron exchange process denoted GJJ.
- 2) A LRG separates between the two hard jets. This is a double diffraction (DD) denoted JGJ.
- 3) Centrally produced di-jets are separated by a LRG on each side of the system. This is a central diffraction (CD) two Pomeron exchange process denoted GJJG. This mechanism also leads to diffractive exclusive Higgs production.

We denote the theoretically calculated rate of a LRG channel by F_{gap} . It was noted by Bjorken [3, 4] that we have to distinguish between the theoretically calculated rate and the actual measured rate f_{gap}

$$f_{gap} = \langle |S|^2 \rangle \cdot F_{gap}. \quad (1)$$

The proportionality damping factor [30–33] is the survival probability of a LRG. It is the probability of a given LRG not to be filled by debris (partons and/or hadrons). These debris originate from the soft re-scattering of the spectator partons resulting in a survival probability denoted $|S_{spec}(s)|^2$, and/or from the gluon radiation emitted by partons taking part in the hard interaction with a corresponding survival probability denoted $|S_{brem}(\Delta y)|^2$,

$$\langle |S(s, \Delta y)|^2 \rangle = \langle |S_{spec}(s)|^2 \rangle \cdot \langle |S_{brem}(\Delta y)|^2 \rangle. \quad (2)$$

s is the c.m. energy square of the colliding particles and Δy is the large rapidity gap. Gluon radiation from the interacting partons is strongly suppressed by the Sudakov factor [34]. However, since this suppression is included in the perturbative calculation (see 4.3) we can neglect $\langle |S_{brem}(\Delta y)|^2 \rangle$ in our calculations. In the following we denote $\langle |S_{spec}|^2 \rangle = S^2$. It is best defined in impact parameter space (see 2.1). Following Bjorken [3,4], the survival probability is determined as the normalized integrated product of two quantities

$$S^2 = \frac{\int d^2b |M^H(s, b)|^2 P^S(s, b)}{\int d^2b |M^H(s, b)|^2}. \quad (3)$$

$M^H(s, b)$ is the amplitude for the LRG diffractive process (soft or hard) of interest. $P^S(s, b)$ is the probability that no inelastic soft interaction in the re-scattering eikonal chain results in inelasticity of the final state at (s, b) .

The organization of this paper is as follows: In Sec.2 we briefly review the role of s-channel unitarity in high energy soft scattering and the eikonal model. The GLM model [30–33] and its consequent survival probabilities [35–37] are presented in Sec.3, including a generalization to a multi channel re-scattering model [38,39]. The KKMR model [40–44] and its survival probabilities is presented in Sec.4. A discussion and our conclusions are presented in Sec.5. An added short presentation on Monte Carlo calculations of S^2 is given in an Appendix.

2 Unitarity

Even though soft high energy scattering has been extensively studied experimentally over the last 50 years, we do not have, as yet, a satisfactory QCD framework to calculate even the gross features of this impressive data base. This is just a reflection of our inability to execute QCD calculations in the non-perturbative regime. High energy soft scattering is, thus, commonly described by the Regge-pole model [45,46]. The theory, motivated by S matrix approach, was introduced more than 40 years ago and was soon after followed by a very rich phenomenology.

The key ingredient of the Regge pole model is the leading Pomeron, whose linear t -dependent trajectory is given by

$$\alpha_P(t) = \alpha_P(0) + \alpha'_P t. \quad (4)$$

A knowledge of $\alpha_P(t)$ enables a calculation of σ_{tot} , σ_{el} and $\frac{d\sigma_{el}}{dt}$, whose forward elastic exponential slope is given by

$$B_{el} = 2B_0 + 2\alpha'_P \ln\left(\frac{s}{s_0}\right). \quad (5)$$

Donnachie and Landshoff (DL) have vigorously promoted [47,48] an appealing and very simple Regge parametrization for total and forward differential elastic hadron-hadron cross sections in which they offer a global fit to all available hadron-hadron and photon-hadron total and elastic cross section data. This data, above $P_L = 10 \text{ GeV}$, is excellently fitted with universal parameters. We shall be interested only in the DL Pomeron with an intercept $\alpha_P(0) = 1 + \epsilon$, where $\epsilon = 0.0808$, which accounts for the high energy growing cross sections. Its fitted [49] slope value is $\alpha'_P = 0.25 \text{ GeV}^{-2}$.

2.1 S-channel unitarity

The simple DL parametrization is bound to violate s-channel unitarity at some energy since σ_{el} grows with energy as $s^{2\epsilon}$, modulu logarithmic corrections, while σ_{tot} grows only as s^ϵ . The theoretical problems at stake are easily identified in an impact b-space representation.

The elastic scattering amplitude is normalized so that

$$\frac{d\sigma_{el}}{dt} = \pi |f_{el}(s, t)|^2, \quad (6)$$

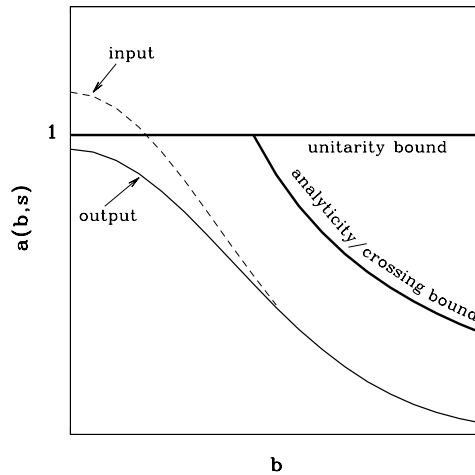


Fig. 1: A pictorial illustration of a high energy b-space elastic amplitude bounded by unitarity and analyticity/crossing. In the illustration we have an input amplitude which violates the eikonal unitarity bound and an output amplitude obtained after a unitarization procedure.

$$\sigma_{tot} = 4\pi \text{Im} f_{el}(s, 0). \quad (7)$$

The elastic amplitude in b-space is defined as

$$a_{el}(s, b) = \frac{1}{2\pi} \int d\mathbf{q} e^{-i\mathbf{q}\cdot\mathbf{b}} f_{el}(s, t), \quad (8)$$

where $t = -\mathbf{q}^2$. In this representation

$$\sigma_{tot} = 2 \int d^2b \text{Im}[a_{el}(s, b)], \quad (9)$$

$$\sigma_{el} = \int d^2b |a_{el}(s, b)|^2, \quad (10)$$

$$\sigma_{in} = \sigma_{tot} - \sigma_{el}. \quad (11)$$

As noted, a simple Regge pole with $\alpha_{\mathcal{P}}(0) > 1$ will eventually violate s-channel unitarity. The question is if this is a future problem to be confronted only at far higher energies than presently available, or is it a phenomena which can be identified through experimental signatures observed within the available high energy data base. It is an easy exercise to check that the DL model [47, 48], with its fitted global parameters, will violate the unitarity black bound (see 2.2) at very small b, just above the present Tevatron energy. Indeed, CDF reports [50] that $a_{el}(b = 0, \sqrt{s} = 1800) = 0.96 \pm 0.04$. A pictorial illustration of the above is presented in Fig.1. Note that the energy dependence of the experimental SD cross section [13–17] in the ISR-Tevatron energy range is much weaker than the power dependences observed for σ_{el} . Diffractive cross sections are not discussed in the DL model.

2.2 The eikonal model

The theoretical difficulties, pointed out in the previous subsection, are eliminated once we take into account the corrections necessitated by unitarity. The problem is that enforcing unitarity is a model dependent procedure. In the following we shall confine ourselves to a Glauber type eikonal model

[51]. In this approximation, the scattering matrix is diagonal and only repeated elastic re-scatterings are summed. Accordingly, we write

$$a_{el}(s, b) = i \left(1 - e^{-\Omega(s,b)/2} \right). \quad (12)$$

Since the scattering matrix is diagonal, the unitarity constraint is written as

$$2Im[a_{el}(s, b)] = |a_{el}(s, b)|^2 + G^{in}(s, b), \quad (13)$$

with

$$G^{in} = 1 - e^{-\Omega(s,b)}. \quad (14)$$

The eikonal expressions for the soft cross sections of interest are

$$\sigma_{tot} = 2 \int d^2b \left(1 - e^{-\Omega(s,b)/2} \right), \quad (15)$$

$$\sigma_{el} = \int d^2b \left(1 - e^{-\Omega(s,b)/2} \right)^2, \quad (16)$$

$$\sigma_{in} = \int d^2b \left(1 - e^{-\Omega(s,b)} \right), \quad (17)$$

and

$$B_{el}(s) = \frac{\int d^2b b^2 \left(1 - e^{-\Omega(s,b)/2} \right)}{2 \int d^2b \left(1 - e^{-\Omega(s,b)/2} \right)}. \quad (18)$$

From Eq.(14) it follows that $P^S(s, b) = e^{-\Omega(s,b)}$ is the probability that the final state of the two initial interacting hadrons is elastic, regardless of the eikonal rescattering chain. It is identified, thus, with $P^S(s, b)$ of Eq.(3).

Following our implicit assumption that, in the high energy limit, hadrons are correct degrees of freedom, i.e. they diagonalize the interaction matrix, Eq.(12) is a general solution of Eq.(13) as long as the input opacity Ω is arbitrary. In the eikonal model Ω is real and equals the imaginary part of the iterated input Born amplitude. The eikonalized amplitude is imaginary. Its analyticity and crossing symmetry are easily restored. In a Regge language we substitute, to this end, $s^{\alpha_P} \rightarrow s^{\alpha_P} e^{-\frac{1}{2}i\pi\alpha_P}$.

In the general case, Eq.(13) implies a general bound, $|a_{el}(s, b)| \leq 2$, obtained when $G^{in} = 0$. This is an extreme option in which asymptotically $\sigma_{tot} = \sigma_{el}$ [52]. This is formally acceptable but not very appealing. Assuming that a_{el} is imaginary, we obtain that the unitarity bound coincides with the black disc bound, $|a_{el}(s, b)| \leq 1$. Accordingly,

$$\frac{\sigma_{el}}{\sigma_{tot}} \leq \frac{1}{2}. \quad (19)$$

3 The GLM Model

The GLM screening correction (SC) model [30–33] is an eikonal model originally conceived so as to explain the exceptionally mild energy dependence of soft diffractive cross sections. It utilized the observation that s-channel unitarization enforced by the eikonal model operates on a diffractive amplitude in a different way than it does on the elastic amplitude. The GLM diffractive damping factor is identical to Bjorken's survival probability.

3.1 The GLM SC model

In the GLM model, we take a DL type Pomeron exchange amplitude input in which $\alpha_P(0) = 1 + \Delta > 0$. The simplicity of the GLM SC model derives from the observation that the eikonal approximation with a central Gaussian input, corresponding to an exponential slope of $\frac{d\sigma_{el}}{dt}$, can be summed analytically. This is, clearly, an over simplification, but it reproduces the bulk of the data well, i.e. the total and the forward elastic cross sections. Accordingly, the eikonal DL type b-space expression for $\Omega(s, b)$ is:

$$\Omega(s, b) = \nu(s) \Gamma^S(s, b), \quad (20)$$

where,

$$\nu(s) = \sigma(s_0) \left(\frac{s}{s_0} \right)^\Delta, \quad (21)$$

$$R^2(s) = 4R_0^2 + 4\alpha'_P \ln\left(\frac{s}{s_0}\right), \quad (22)$$

and the soft profile is defined

$$\Gamma^S(s, b) = \frac{1}{\pi R^2(s)} e^{-\frac{b^2}{R^2(s)}}. \quad (23)$$

It is defined so as to keep the normalization $\int d^2b \Gamma^S(s, b) = 1$.

One has to distinguish between the eikonal model input and output. The key element is that the power Δ , and ν , are input information, not bounded by unitarity, and should not be confused with DL effective power ϵ and the corresponding total cross section. Since the DL model reproduces the forward elastic amplitude, in the ISR-HERA-Tevatron range, well, we require that the eikonal model output will be compatible with the DL results. Obviously, $\Delta > \epsilon$. In a non screened DL type model with a Gaussian profile the relation $B_{el} = \frac{1}{2}R^2(s)$ is exact. In a screened model, like GLM, $B_{el} > \frac{1}{2}R^2(s)$ due to screening.

With this input we get

$$\sigma_{tot} = 2\pi R^2(s) \left[\ln\left(\frac{\nu(s)}{2}\right) + C - Ei\left(-\frac{\nu(s)}{2}\right) \right] \propto \ln^2(s), \quad (24)$$

$$\sigma_{el} = \pi R^2(s) \left[\ln\left(\frac{\nu(s)}{4}\right) + C - 2Ei\left(-\frac{\nu(s)}{2}\right) + Ei(-\nu(s)) \right] \propto \frac{1}{2}\ln^2(s), \quad (25)$$

$$\sigma_{in} = \pi R^2(s) \{ \ln[\nu(s)] + C - Ei[-\nu(s)] \} \propto \frac{1}{2}\ln^2(s). \quad (26)$$

$Ei(x) = \int_{-\infty}^x \frac{e^t}{t} dt$, and $C = 0.5773$ is the Euler constant. An important consequence of the above is that the ratio $\frac{\sigma_{el}}{\sigma_{tot}}$ is a single variable function of $\nu(s)$. In practice it means that given the experimental value of this ratio at a given energy we can obtain an "experimental" value of ν which does not depend on the adjustment of free parameters.

The formalism presented above is extended to diffractive channels through the observation, traced to Eqs.(3) and (14), that $P^S(s, b) = e^{-\Omega(s, b)}$. Accordingly, a screened non elastic diffractive cross section is obtained by convoluting its b-space amplitude square with the probability P^S .

The above has been utilized [30–33] to calculate the soft integrated single diffraction cross section. To this end, we write, in the triple Regge approximation [53], the double differential cross section $\frac{M^2 d\sigma_{sd}}{dM^2 dt}$, where M is the diffracted mass. We, then, transform it to b-space, multiply by $P^S(s, b)$ and integrate. The output $\frac{M^2 d\sigma_{sd}}{dM^2 dt}$, changes its high energy behaviour from $s^{2\Delta}$ modulu $\ln\left(\frac{s}{s_0}\right)$ (which is identical to the behaviour of a DL elastic cross section) to the moderate behaviour of $\ln\left(\frac{s}{s_0}\right)$. Note also a major difference in the diffractive b-space profile which changes from an input central Gaussian to an

output peripheral distribution peaking at higher b . Consequently, the GLM model is compatible with the Pomplin bound [54, 55].

$$\frac{\sigma_{el}(s, b) + \sigma_{diff}(s, b)}{\sigma_{tot}(s, b)} \leq \frac{1}{2}. \quad (27)$$

3.2 Extension to a multi channel model

The most serious deficiency of a single channel eikonal model is inherent, as the model considers only elastic rescatterings. This is incompatible with the relatively large diffractive cross section observed in the ISR-Tevatron energy range. To this we add a specific problematic feature of the GLM model. Whereas, σ_{tot} , σ_{el} and B_{el} are very well fitted, the reproduction of σ_{sd} , in the available ISR-Tevatron range, is poorer. A possible remedy to these deficiencies is to replace the one channel with a multi channel eikonal model, in which inelastic diffractive intermediate re-scatterings are included as well [38, 39, 56]. However, we have to insure that a multi channel model does improve the diffractive (specifically SD) predictions of the GLM model, while maintaining, simultaneously, its excellent reproductions [30–33] of the forward elastic amplitude, as well as its appealing results on LRG survival probabilities [35–37] to be discussed in 3.3.

In the simplest approximation we consider diffraction as a single hadronic state. We have, thus, two orthogonal wave functions

$$\langle \Psi_h | \Psi_d \rangle = 0. \quad (28)$$

Ψ_h is the wave function of the incoming hadron, and Ψ_d is the wave function of the outgoing diffractive system initiated by the incoming hadron. Denote the interaction operator by \mathbf{T} and consider two wave functions Ψ_1 and Ψ_2 which are diagonal with respect to \mathbf{T} . The amplitude of the interaction is given by

$$A_{i,k} = \langle \Psi_i \Psi_k | \mathbf{T} | \Psi_{i'} \Psi_{k'} \rangle = a_{i,k} \delta_{i,i'} \delta_{k,k'}. \quad (29)$$

In a 2×2 model $i, k = 1, 2$. The amplitude $a_{i,k}$ satisfies the diagonal unitarity condition (see Eq.(13))

$$2Im a_{i,k}(s, b) = |a_{i,k}(s, b)|^2 + G_{i,k}^{in}(s, b), \quad (30)$$

for which we write the solution

$$a_{i,k}(s, b) = i \left(1 - e^{-\frac{\Omega_{i,k}(s,b)}{2}} \right), \quad (31)$$

and

$$G_{i,k}^{in} = 1 - e^{-\Omega_{i,k}(s,b)}. \quad (32)$$

$\Omega_{i,k}(s, b)$ is the opacity of the (i, k) channel with a wave function $\Psi_i \times \Psi_k$.

$$\Omega_{i,k} = \nu_{i,k}(s) \Gamma_{i,k}^S(s, b) \quad (33)$$

where

$$\nu_{i,k} = \sigma_{i,k}^{S0} \left(\frac{s}{s_0} \right)^\Delta. \quad (34)$$

The factorizable radii are given by

$$R_{i,k}^2(s) = 2R_{i,0}^2 + 2R_{0,k}^2 + 4\alpha'_P \ln\left(\frac{s}{s_0}\right). \quad (35)$$

$\Gamma_{i,k}^S(s, b)$ is the soft profile of the (i,k) channel. The probability that the final state of two interacting hadron states, with quantum numbers i and k , will be elastic regardless of the intermediate rescatterings is

$$P_{i,k}^S(s, b) = e^{-\Omega_{i,k}(s,b)} = \{1 - a_{i,k}(s, b)\}^2. \quad (36)$$

In the above diagonal representation, Ψ_h and Ψ_d can be written as

$$\Psi_h = \alpha\Psi_1 + \beta\Psi_2, \quad (37)$$

$$\Psi_d = -\beta\Psi_1 + \alpha\Psi_2. \quad (38)$$

Ψ_1 and Ψ_2 are orthogonal. Since $|\Psi_h|^2 = 1$, we have

$$\alpha^2 + \beta^2 = 1. \quad (39)$$

The wave function of the final state is

$$\begin{aligned} \Psi_f = | \mathbf{T} | \Psi_h \times \Psi_h \rangle = \\ \alpha^2 a_{1,1} \{ \Psi_1 \times \Psi_1 \} + \alpha\beta a_{1,2} \{ \Psi_1 \times \Psi_2 + \Psi_2 \times \Psi_1 \} + \\ \beta^2 a_{2,2} \{ \Psi_2 \times \Psi_2 \}. \end{aligned} \quad (40)$$

We have to consider 4 possible re-scattering processes. However, in the case of a $\bar{p}p$ (or pp) collision, single diffraction at the proton vertex equals single diffraction at the antiproton vertex. i.e., $a_{1,2} = a_{2,1}$ and we end with three channels whose b-space amplitudes are given by

$$a_{el}(s, b) = \langle \Psi_h \times \Psi_h | \Psi_f \rangle = \alpha^4 a_{1,1} + 2\alpha^2\beta^2 a_{1,2} + \beta^4 a_{2,2}, \quad (41)$$

$$a_{sd}(s, b) = \langle \Psi_h \times \Psi_d | \Psi_f \rangle = \alpha\beta \{ \alpha^2 a_{1,1} + (\alpha^2 - \beta^2) a_{1,2} + \beta^2 a_{2,2} \}, \quad (42)$$

$$a_{dd}(s, b) = \langle \Psi_d \times \Psi_d | \Psi_f \rangle = \alpha^2\beta^2 \{ a_{1,1} - 2a_{1,2} + a_{2,2} \}. \quad (43)$$

In the numeric calculations one may further neglect the double diffraction channel which is exceedingly small in the ISR-Tevatron range. This is obtained by setting $a_{2,2} = 2a_{1,2} - a_{1,1}$. Note that in the limit where $\beta \ll 1$, we reproduce the single channel model.

As in the single channel, we simplify the calculation assuming a Gaussian b-space distribution of the input opacities soft profiles

$$\Gamma_{i,k}^S(s, b) = \frac{1}{\pi R_{i,k}^2(s)} e^{-\frac{b^2}{R_{i,k}^2(s)}}. \quad (44)$$

The opacity expressions, just presented, allow us to express the physical observables of interest as functions of $\nu_{1,1}$, $\nu_{1,2}$, $R_{1,1}^2$, $R_{1,2}^2$ and β , which is a constant of the model. The determination of these variables enables us to produce a global fit to the total, elastic and diffractive cross sections as well as the elastic forward slope. This has been done in a two channel model, in which σ_{dd} is neglected [38]. The main conclusion of this study is that the extension of the GLM model to a multi channel eikonal results with a very good overall reproduction of the data. The results maintain the b-space peripherality of the diffractive output amplitudes and satisfy the Pumplin bound [54, 55]. Note that since different experimental groups have been using different algorithms to define diffraction, the SD experimental points are too scattered to enable a tight theoretical reproduction of the diffractive data, see Fig.2.

3.3 Survival probabilities of LRG in the GLM model

The eikonal model simplifies the calculation of the survival probability, Eq.(3), associated with the soft re-scatterings of the spectator partons. We can, thus, eliminate the nominator and denominator terms in $|M^H(s, b)|^2$ which depend exclusively on s. In the GLM model we assume a Gaussian b-dependence for $|M^H(s, b)|^2$ corresponding to a constant hard radius R^{H^2} . This choice enables an analytic solution of Eq.(3). More elaborate choices, such as dipole or multi poles distributions, require a numerical evaluation of this equation.

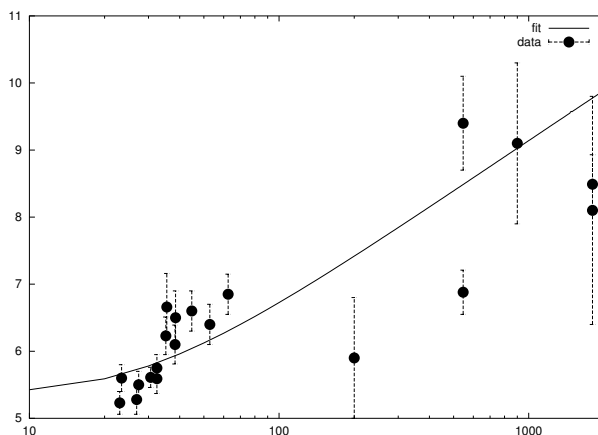


Fig. 2: Integrated SD data and a two channel model fit.

Define,

$$a_H(s) = \frac{R^2(s)}{R^{H^2}(s)} > 1. \quad (45)$$

$a_H(s)$ grows logarithmically with s . As stated, Eq.(3) can be analytically evaluated with our choice of Gaussian profiles and we get

$$S^2 = \frac{a_H(s)\gamma[a_H(s), \nu(s)]}{[\nu(s)]^{a_H(s)}}, \quad (46)$$

where $\gamma(a, \nu)$ denotes the incomplete Euler gamma function

$$\gamma(a, x) = \int_0^x z^{a-1} e^{-z} dz. \quad (47)$$

The solution of Eq.(46), at a given s , depends on the input values of R^{H^2} , R^2 and $\nu(s)$. In the GLM approach, R^{H^2} is estimated from the excellent HERA data [57–59] on $\gamma + p \rightarrow J/\Psi + p$. The values of $\nu(s)$ and $R^2(s)$ are obtained from the experimental $\bar{p}p$ data. This can be attained from a global fit to the soft scattering data [38]. Alternatively, we can obtain ν from the ratio $\frac{\sigma_{el}}{\sigma_{tot}}$ and then obtain the value of R^2 from the explicit expressions given in Eqs.(24,25,26). LHC predictions presently depend on model calculations with which this information can be obtained. Once we have determined $\nu(s)$ and $a_H(s)$, the survival probability is calculated from Eq.(46).

In the GLM three channel model we obtain for central hard diffraction of di-jets or Higgs a survival probability,

$$S_{CD}^2(s) = \frac{\int d^2b \left(\alpha^4 P_{1,1}^S \Omega_{1,1}^{H^2} + 2\alpha^2 \beta^2 P_{1,2}^S \Omega_{1,2}^{H^2} + \beta^4 P_{2,2}^S \Omega_{2,2}^{H^2} \right)}{\int d^2b \left(\alpha^4 \Omega_{1,1}^{H^2} + 2\alpha^2 \beta^2 \Omega_{1,2}^{H^2} + \beta^4 \Omega_{2,2}^{H^2} \right)}. \quad (48)$$

The hard diffractive cross sections in the (i,k) channel are calculated using the multi particle optical theorem [53]. They are written in the same form as the soft amplitudes

$$\Omega_{i,k}^{H^2} = \nu_{i,k}^H(s)^2 \Gamma_{i,k}^H(b), \quad (49)$$

where,

$$\nu_{i,k}^H = \sigma_{i,k}^{H0} \left(\frac{s}{s_0} \right)^{\Delta_H}. \quad (50)$$

As in the single channel calculation we assume that $\Gamma_{i,k}^H(b)$ is Gaussian,

$$\Gamma_{i,k}^H(b) = \frac{2}{\pi R_{i,k}^2} e^{-\frac{2b^2}{R_{i,k}^2}}. \quad (51)$$

Note, that the hard radii $R_{i,k}^{H^2}$ are constants derived from HERA J/Ψ photo and DIS production [57–59].

As it stands, a three channel calculation is not useful since σ_{dd} is very small and the 3'd channel introduces additional parameters which can not be constraint by the meager experimental information on σ_{dd} [13–17]. In a two channel model Eq.(48) reduces to

$$S_{CD}^2(s) = \frac{\int d^2b \left(P_{1,1}^S \Omega_{1,1}^{H^2} - 2\beta^2 (P_{1,1}^S \Omega_{1,1}^{H^2} - P_{1,2}^S \Omega_{1,2}^{H^2}) \right)}{\int d^2b \left(\Omega_{1,1}^{H^2} - 2\beta^2 (\Omega_{1,1}^{H^2} - \Omega_{1,2}^{H^2}) \right)}. \quad (52)$$

A new, unpublished yet, model [60], offers an explicit S^2 calculation for the exclusive $NN \rightarrow N + LRG + 2J + LRG + N$ final state, both in one and two channel eikonal models. We shall comment on its output in the next subsection.

3.4 GLM S^2 predictions

Following are a few general comments on the GLM calculations of S^2 , after which we discuss the input/output features of the single and two channel models. Our objective is to present predictions for LHC.

The only available experimental observable with which we can check the theoretical S^2 predictions is the hard LRG di-jets data obtained in the Tevatron and Hera. A comparison between data and our predictions is not immediate as the basic measured observable is f_{gap} and not S^2 . The application of the GLM models to a calculation of f_{gap} depends on an external input of a hard diffractive LRG cross section which is then corrected by S^2 as presented above. Regardless of this deficiency, the introduction of a survival probability is essential so as to understand the huge difference between the pQCD calculated F_{gap} and its experimental value f_{gap} . A direct test of the GLM predictions calls for a dedicated experimental determination of S^2 . The only direct S^2 information from the Tevatron is provided by a JGJ ratio measured by D0 [5–7] in which $\frac{S^2(\sqrt{s}=630)}{S^2(\sqrt{s}=1800)} = 2.2 \pm 0.8$. This is to be compared with a GLM ratio of $1.2 - 1.3 \pm 0.4$ presented below.

The survival probabilities of the CD, SD and DD channels are not identical. The key difference is that each of the above channels has a different hard radius. A measure of the sensitivity of S^2 to changes in ν and a_H is easy to identify in a single channel calculation which is presented in Fig.3. Indeed, preliminary CDF GJJG data [17] suggest that f_{gap} measured for this channel is moderately smaller than the rate measured for the GJJ channel.

GLM soft profile input is a central Gaussian. This is over simplified, and most models assume a power like dipole or multipole b-dependence of $\Gamma^S(s, b)$ and $\Gamma^H(s, b)$. Explicit comparisons [60] of S^2 obtained with different input profiles shows a diminishing difference between the survival probability outputs, provided their effective radii are compatible.

Regardless of the attractive simplicity of the single channel model, one should add a cautious reminder that the single channel model does not reproduce σ_{sd} well since its survival probabilities are over-estimated. Consequently, we are inclined to suspect that the S^2 values presented in Table 1 are over-estimated as well.

As we noted, the soft input can be obtained from either a model fit to the soft scattering data or directly from the measured values of $\sigma_{tot}, \sigma_{el}$ and R^{H^2} . The first method is denoted F1C and the second is denoted D1C. Note that having no LHC data, $S_{DD}^2(D1C)$, at this energy, is calculated on the

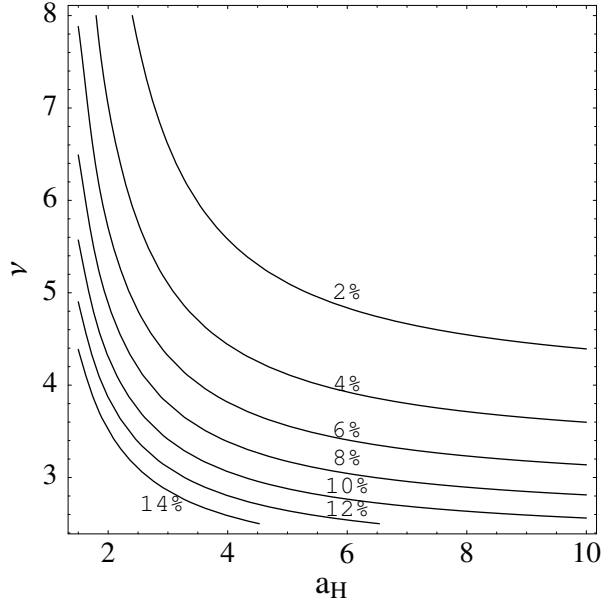


Fig. 3: A contour plot of $S^2(1C)$ against $\nu(s)$ and $a_H(s)$.

Table 1: Survival probabilities

\sqrt{s} (GeV)	$S_{CD}^2(F1C)$	$S_{CD}^2(D1C)$	$S_{SD_{incl}}^2(F1C)$	$S_{SD_{incl}}^2(D1C)$	$S_{DD}^2(F1C)$	$S_{DD}^2(D1C)$
540	14.4%	13.1%	18.5%	17.5%	22.6%	22.0%
1800	10.9%	8.9%	14.5%	12.6%	18.2%	16.6%
14000	6.0%	5.2%	8.6%	8.1%	11.5%	11.2%

basis of model estimates for the total and elastic cross sections. The constant hard radius $R^{H^2} = 7.2$ is deduced from HERA J/Ψ photoproduction forward exponential slope which shows only diminishing shrinkage [57,58]. This is a conservative choice which may be changed slightly with the improvement of the Tevatron CDF estimates [61] of R^{H^2} . The two sets of results obtained are compatible, even though, $S^2(D1C)$ is consistently lower than $S^2(F1C)$. The S^2 output presented above depends crucially on the quality of the data base from which we obtain the input parameters. The two sets of Tevatron data at 1800 GeV have a severe 10 – 15% difference resulting in a non trivial ambiguity of the S^2 output.

The global GLM two channel fit [38] reproduces the soft scattering data (including SD) remarkably well with $\beta = 0.464$. Its fitted parameters are used for the soft input required for the S^2 calculations. Our cross section predictions for LHC are: $\sigma_{tot} = 103.8 mb$, $\sigma_{el} = 24.5 mb$, $\sigma_{sd} = 12 mb$ and $B_{el} = 20.5 GeV^{-2}$. The input for the calculation of S^2 requires, in addition to the soft parameters, also the values of $\nu_{i,k}^H$ and $R_{i,k}^{H^2}$. The needed hard radii can be estimated, at present, only for the CD channel, where we associate the hard radii $R_{1,1}^H$ with the hard radius obtained in HERA exclusive J/Ψ photoproduction [57,58] and $R_{1,2}^H$ with HERA inclusive J/Ψ DIS production [59]. Accordingly, we have $R_{1,1}^{H^2} = 7.2 GeV^{-2}$, and $R_{1,2}^{H^2} = 2.0 GeV^{-2}$. We do not have experimental input to determine $\nu_{i,k}^H$. We overcome this difficulty by assuming a Regge-like factorization $\sigma_{i,k}^{H^0}/\sigma_{i,k}^{S^0} = constant$. Our predictions for the CD survival probabilities are: 6.6% at 540 GeV, 5.5% at 1800 GeV and 3.6% at 14000 GeV.

These results may be compared with a recent, more elaborate, eikonal formulation [60] aiming to calculate the survival probability of a final exclusive $N + LRG + 2J(or H) + LRG + N$ state. These calculations were done in one and two channel models. The one channel S_{CD}^2 predicted values are 14.9%

at 540 GeV , 10.8% at 1800 GeV and 6.0% at 14000 GeV . These values are remarkably similar to the GLM one channel output. In the two channel calculations the corresponding predictions are 5.1%, 4.4% and 2.7%, which are marginally smaller than the GLM two channel output numbers.

In our assessment, the two channel calculations provide a more reliable estimate of S^2 since they reproduce well the soft scattering forward data. Our estimate for the survival probability associated with LHC Higgs production is 2.5% – 4.0%.

4 The KKMR Model

The main part of this section (4.1-4.3) was written by V.A. Khoze, A.D. Martin and M. Ryskin (KMR) and is presented here without any editing.

The KKMR model calculation [40–44] of the survival probabilities is conceptually quite similar to the GLM model, in as much as unitarization is enforced through an eikonal model whose parameters provide a good reproduction of the high energy soft scattering data. However, the GLM model is confined to a geometrical calculation of S^2 for which we need just the value of R^{H^2} , without any specification of the hard dynamics. This value is an external input to the model. The KKMR model contains also a detailed pQCD calculation of the hard diffractive process, specifically, central diffractive Higgs production. Consequently, it can predict a cross section for the channel under investigation.

4.1 KKMR model for soft diffraction

The KMR description [41] of soft diffraction in high energy pp (or $p\bar{p}$) collisions embodies

- (i) *pion-loop* insertions in the bare Pomeron pole, which represent the nearest singularity generated by t -channel unitarity,
- (ii) a *two-channel eikonal* which incorporates the Pomeron cuts generated by elastic and quasi-elastic (with N^* intermediate states) s -channel unitarity,
- (iii) high-mass *diffractive dissociation*.

The KKMR model gives a good description of the data on the total and differential elastic cross section throughout the ISR-Tevatron energy interval, see [41]. Surprisingly, KMR found the bare Pomeron parameters to be

$$\Delta \equiv \alpha(0) - 1 \simeq 0.10, \quad \alpha' = 0. \quad (53)$$

On the other hand it is known that the same data can be described by a simple effective Pomeron pole with [47, 48, 62]

$$\alpha_P^{\text{eff}}(t) = 1.08 + 0.25 t. \quad (54)$$

In this approach the shrinkage of the diffraction cone comes not from the bare pole ($\alpha' = 0$), but has components from the three ingredients, (i)–(iii), of the model. That is, in the ISR-Tevatron energy range

$$“\alpha'_{\text{eff}}” = (0.034 + 0.15 + 0.066) \text{ GeV}^{-2} \quad (55)$$

from the π -loop, s -channel eikonalisation and diffractive dissociation respectively. Moreover, eikonal rescattering suppresses the growth of the cross section and so $\Delta \simeq 0.10 > \Delta_{\text{eff}} \simeq 0.08$.

Since the model [41] embodies all the main features of soft diffraction KMR expect it to give reliable predictions for the *survival probability* S^2 of the rapidity gaps against population by secondary hadrons from the underlying event, that is hadrons originating from soft rescattering. In particular, KMR predict $S^2 = 0.10$ (0.06) for single diffractive events and $S^2 = 0.05$ (0.03) for exclusive Higgs boson production, $pp \rightarrow p + H + p$, at Tevatron (LHC) energies.

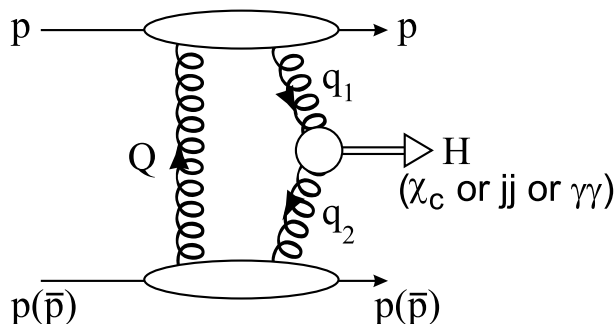


Fig. 4: Schematic diagram for central exclusive production, $pp \rightarrow p + X + p$. The presence of Sudakov form factors ensures the infrared stability of the Q_t integral over the gluon loop. It is also necessary to compute the probability, S^2 , that the rapidity gaps survive soft rescattering.

4.2 Calculation of the exclusive Higgs signal

The basic mechanism for the exclusive process, $pp \rightarrow p + H + p$, is shown in Fig. 4. The left-hand gluon Q is needed to screen the colour flow caused by the active gluons q_1 and q_2 . Since the dominant contribution comes from the region $\Lambda_{\text{QCD}}^2 \ll Q_t^2 \ll M_H^2$, the amplitude may be calculated using perturbative QCD techniques [40, 63]

$$\mathcal{M}_H \simeq N \int \frac{dQ_t^2}{Q_t^4} f_g(x_1, x'_1, Q_t^2, \mu^2) f_g(x_2, x'_2, Q_t^2, \mu^2), \quad (56)$$

where the overall normalisation constant N can be written in terms of the $H \rightarrow gg$ decay width [40, 64]. The probability amplitudes (f_g) to find the appropriate pairs of t -channel gluons (Q, q_1) and (Q, q_2) are given by the skewed unintegrated gluon densities at the hard scale μ , taken to be $0.62 M_H$. Since the momentum fraction x' transferred through the screening gluon Q is much smaller than that (x) transferred through the active gluons ($x' \sim Q_t/\sqrt{s} \ll x \sim M_H/\sqrt{s} \ll 1$), it is possible to express $f_g(x, x', Q_t^2, \mu^2)$, to single log accuracy, in terms of the conventional integrated density $g(x)$ [65–68]. The f_g 's embody a Sudakov suppression factor T , which ensures that the gluon does not radiate in the evolution from Q_t up to the hard scale $\mu \sim M_H/2$, and so preserves the rapidity gaps.

It is often convenient to use the simplified form [40]

$$f_g(x, x', Q_t^2, \mu^2) = R_g \frac{\partial}{\partial \ln Q_t^2} \left[\sqrt{T_g(Q_t, \mu)} x g(x, Q_t^2) \right], \quad (57)$$

which holds to 10–20% accuracy.¹ The factor R_g accounts for the single log Q^2 skewed effect [67]. It is found to be about 1.4 at the Tevatron energy and about 1.2 at the energy of the LHC.

4.3 The Sudakov factor

The Sudakov factor $T_g(Q_t, \mu)$ reads [65, 66, 69]

$$T_g(Q_t, \mu) = \exp \left(- \int_{Q_t^2}^{\mu^2} \frac{\alpha_S(k_t^2)}{2\pi} \frac{dk_t^2}{k_t^2} \left[\int_{\Delta}^{1-\Delta} z P_{gg}(z) dz + \int_0^1 \sum_q P_{qg}(z) dz \right] \right), \quad (58)$$

with $\Delta = k_t/(\mu + k_t)$. The square root arises in (57) because the (survival) probability not to emit any additional gluons is only relevant to the hard (active) gluon. It is the presence of this Sudakov factor which makes the integration in (56) infrared stable, and perturbative QCD applicable².

¹In the actual computations a more precise form, as given by Eq. (26) of [68], was used.

²Note also that the Sudakov factor inside t integration induces an additional strong decrease (roughly as M^{-3} [44]) of the cross section as the mass M of the centrally produced hard system increases. Therefore, the price to pay for neglecting this suppression effect would be to considerably overestimate the central exclusive cross section at large masses.

Table 2: Compilation of S^2 values obtained in the KKMR model

\sqrt{s} (GeV)	S_{2C}^2 (CD)	S_{2C}^2 (SD _{incl})	S_{2C}^2 (DD)
540	6.0%	13.0%	20.0%
1800	4.5%	10.0%	15.0%
14000	2.6%	6.0%	10.0%

It should be emphasized that the presence of the double logarithmic T -factors is a purely classical effect, which was first discussed in 1956 by Sudakov in QED. There is strong bremsstrahlung when two colour charged gluons ‘annihilate’ into a heavy neutral object and the probability not to observe such a bremsstrahlung is given by the Sudakov form factor³. Therefore, any model (with perturbative or non-perturbative gluons) must account for the Sudakov suppression when producing exclusively a heavy neutral boson via the fusion of two coloured particles.

More details of the role of the Sudakov suppression can be found in J. Forshaw’s review in these proceedings [34]. Here KMR would like to recall that the T -factors in [44, 70] were calculated to *single* log accuracy. The collinear single logarithms were summed up using the DGLAP equation. To account for the ‘soft’ logarithms (corresponding to the emission of low energy gluons) the one-loop virtual correction to the $gg \rightarrow H$ vertex was calculated explicitly, and then the scale $\mu = 0.62 M_H$ was chosen in such a way that eq.(58) reproduces the result of this explicit calculation. It is sufficient to calculate just the one-loop correction since it is known that the effect of ‘soft’ gluon emission exponentiates. Thus (58) gives the T -factor to single log accuracy.

In some sense, the T -factor may be considered as a ‘survival’ probability not to produce any hard gluons during the $gg \rightarrow H$ fusion subprocess. However, it is not just a number (i.e. a numerical factor) which may be placed in front of the integral (the ‘bare amplitude’). Without the T -factors hidden in the unintegrated gluon densities f_g the integral (56) diverges. From the formal point of view, the suppression of the amplitude provided by T -factors is infinitely strong, and without them the integral depends crucially on an ad hoc infrared cutoff.

4.4 Summary of KKMR S^2 predictions

Table 2 shows a compilation of S^2 values in the KKMR model. A comparison with the corresponding GLM two channel model is possible only for the available GLM CD channel, where, the KKMR output is compatible with GLM. KKMR SD and DD output are compatible with the corresponding GLM single channel numbers. Overall, we consider the two models to be in a reasonable agreement.

A remarkable utilization of the KKMR model is attained when comparing the HERA [18–27] and CDF [8–12, 17] di-jets diffractive structure functions derived for the dynamically similar GJJ channels. To this end, the comparison is made between the kinematically compatible HERA $F_{jj}^D(Q^2 = 75 \text{ GeV}^2, \beta)$ and the CDF $F_{jj}^D(< E_T^2 \geq 75 \text{ GeV}^2, \beta)$. The theoretical expectation is that $F_{jj}^D(\beta)$, as measured by the two experiments, should be very similar. As can be seen in Fig.5, the normalizations of the two distributions differ by approximately an order of magnitude and for very small $\beta < 0.15$ there is a suggestive change in the CDF distribution shape. This large discrepancy implies a breaking of QCD and/or Regge factorization. Reconsidering, it is noted, that HERA DIS data is measured at a high Q^2 where the partonic interactions induced by the highly virtual photon are point like and, hence, $S^2 = 1$. On the other hand, CDF GJJ measurement is carried out at 1800 GeV and, as we saw, its survival prob-

³It is worth mentioning that the $H \rightarrow gg$ width and the normalization factor N in (56) is an ‘inclusive’ quantity which includes all possible bremsstrahlung processes. To be precise, it is the sum of the $H \rightarrow gg + ng$ widths, with $n=0,1,2,\dots$. The probability of a ‘purely exclusive’ decay into two gluons is nullified by the same Sudakov suppression.

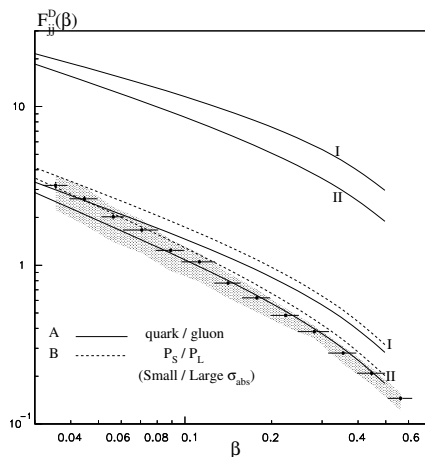


Fig. 5: The predictions for the diffractive di-jets production at the Tevatron (lower lines), obtained from two alternative sets of HERA diffractive parton distributions I and II, compared with the CDF data (shaded area). The upper lines correspond to the Tevatron prediction neglecting the survival probability correction.

ability is rather small. The convolution between the HERA determined GJJ $F_{jj}^D(\beta)$ and the β dependent survival probabilities, as calculated by KKMR, provides the $F_{jj}^D(\beta)$ distribution corrected for the soft rescattering of the spectator partons. This is shown in Fig.5 and provides an impressive reproduction of the experimental distribution. We were informed [71] that this analysis was successfully redone with an updated H1 produced structure function distribution.

The weak element in the above analysis is that it is crucially dependent on the H1 determined $F_{jj}^D(\beta)$ distribution. ZEUS has constructed a somewhat different structure function. Clearly, a very different experimental determination of $F_{jj}^D(\beta)$, such as been recently suggested by Arneodo [72], will re-open this analysis for further studies, experimental and theoretical.

4.5 A Comparison between KKMR and GLM

The approach of GLM and KKMR to the calculation of forward soft scattering in the ISR-Tevatron range are basically similar. Both models utilize the eikonal model assuming different input soft profiles which have, nevertheless, compatible effective radii. There are, though, a few particular differences between the two sets of calculations:

- 1) The GLM model, with a Gaussian soft profile, is applicable only in the forward cone ($|t| < 0.3 GeV^2$), where we have most of the data of interest. KKMR use a multipole power behaviour profile which enables applicability over a, somewhat, wider t range, $|t| < 0.5 GeV^2$. Note that, the GLM output is not significantly changed with a multipole power behaviour profile provided its radii are compatible with the Gaussian input [60].
- 2) The GLM input Pomeron trajectory is specified by $\Delta = 0.12$ and $\alpha'_{\mathcal{P}} = 0.2$. These evolve due to eikonalisation to an effective output of $\epsilon = 0.08$ and $\alpha'_{\mathcal{P}} = 0.25$. Note that, Δ is obtained in GLM as a fitted output parameter. In KKMR, the relatively high input $\Delta \simeq 0.2$ is theoretically tuned by a pion loop renormalization resulting in an input value of $\Delta \simeq 0.1$. KKMR have a more elaborate treatment of $\alpha_{\mathcal{P}}(t)$ than GLM, resulting, nevertheless, with forward cone output predictions similar to GLM. However, KKMR accounts for a somewhat wider t range than GLM and reproduces the t dependence of B_{el} well. Similar results are obtained in a GLM version [39,56] in which the soft profile is given by a dipole distribution. KKMR can predict a few differential properties of S^2 , which are beyond the scope of GLM.

- 3) Both models treat the high mass diffraction with the triple Pomeron formalism [53]. In GLM the final SD cross section is obtained by a convolution of the input $\frac{d\sigma_{sd}}{d^2b}$ with $P^S(s, b)$. In KKMR the treatment of the SD amplitude is more elaborate, ending, though, with no detailed SD data reconstruction which is presented in GLM.
- 4) The LHC predictions of the two models for cross sections and slopes are compatible, with the exception of σ_{dd} which is neglected in GLM and acquires a significant KKMR predicted value of $9.5 mb$.

GLM is a geometrical model where both the input hard LRG non corrected matrix element squared and the soft elastic scattering amplitude, are approximated by central Gaussians in b -space. This property enables us to easily calculate the survival probabilities which depend on ν , R^2 and R^{H^2} in a single channel input, and on $\nu_{i,k}$, $R_{i,k}^2$ and $R_{i,k}^{H^2}$ in a two channel input. As we have noted, the GLM model, on its own, cannot provide a calculation of F_{gap} and f_{gap} as it needs the hard radii as an external input. The KKMR model is more sophisticated. This is attributed to the fact that the hard diffractive LRG process is explicitly calculated in pQCD, hence the non corrected F_{gap} and the corrected f_{gap} and F_{jj}^D are model predictions. As we have just noted, given the hard diffractive matrix element, the actual calculation of the diffractive LRG survival probability damping is almost identical to GLM. Keeping this basic observation in mind, it is constructive to compare the features of the two models with a special interest on the input assumptions and output differences of the two models.

The main difference between the two models is reflected in the level of complexity of their inputs. GLM soft input is obtained from a simple eikonal model for the soft forward scattering, to which we add the hard radii which are derived from the HERA data. KKMR calculations of P^S are equally simple. The calculation of the hard sector matrix elements are, naturally, more cumbersome. Given HERA $F_{jj}^D(Q^2, \beta)$, a Tevatron diffractive F_{jj}^D in which $\langle E_T \rangle$ and Q^2 are comparable, can be calculated, parameter free, without the need to calculate the hard amplitude. But this is a particular case and, in general, the KKMR calculation depends on an extended parameter base, such as the the input p.d.f. and pQCD cuts. These input parameters are not constrained tightly enough.

The elaborate structure of the KKMR model provides a rich discovery potential which is reflected in the model being able to define and calculate the dependence of S^2 not only on b , but also on other variables, notably β , and experimental cuts such as the recoil proton transverse momentum. GLM depends on the hard radii external information obtained from HERA data. It lacks the potential richness of KKMR. GLM can serve, though, as a standard through which we can compare different unitarized models. Given such a model, we can extract effective values for ν , R^2 and R^{H^2} and proceed to a simple calculation of S^2 . We shall return to this proposed procedure in the final discussion.

Even though both GLM and KKMR are two channel models, they are dynamically different. GLM two channel formulation relates to the diversity of the intermediate soft re-scatterings, i.e. elastic and diffractive for which we have different soft amplitudes $a_{i,k}$, each of which is convoluted with a different probability $P_{i,k}^S$ which depends on a different interaction radius $R_{i,k}^2$. In the KKMR model the two channels relate to two different dynamical options of the hard process. In model A the separation is between valence and sea interacting partons. In model B the separation is between small and large dipoles. The two models give compatible results. The key point, though, is that the KKMR opacities $\Omega_{i,k}$, in the definition of $P_{i,k}^S$, differ in their normalization, but have the same b -dependence. Regardless of this difference the output of the GLM and KKMR models is reasonably compatible. The compatibility between GLM and KKMR is not surprising since the explicit KKMR calculation of the hard LRG amplitude is approximated relatively well by the GLM simple Gaussian.

Our final conclusion is that the two model output sets are compatible. The richness of the KKMR model has a significant discovery potential lacking in GLM. On the other hand, the GLM simplicity makes it very suitable as a platform to present different models in a uniform way, which enables a transparent comparison.

5 Discussion

As we shall see, at the end of this section, there is no significant difference between the values of σ_{tot} predicted by DL and GLM up to the top Cosmic Rays energies. This is, even though, DL is a Regge model without unitarity corrections. The explanation for this "paradox" is that the DL amplitude violations of s-unitarity are confined, even at super high energies, to small b which does not contribute significantly to σ_{tot} . Note, though, that $\frac{\sigma_{el}}{\sigma_{tot}}$ grows in DL like s^ϵ whereas in GLM its growth is continuously being moderated with increasing s (see table in 5.3). The DL model predicts that S^2 is identical to unity or very close to it in the DL high- t model where a weak PP cut is added. The need for survival probabilities so as to reproduce the the experimental soft SD cross section values and the hard di-jets rates, is the most compelling evidence in support of unitarization at presently available energies. As such, the study of high energy soft and hard diffraction serves as a unique probe substantiating the importance of s-channel unitarity in the analysis of high energy scattering.

5.1 S^2 in unitarized models

Most, but not all, of the unitarized models dealing with LHC S^2 predictions have roughly the same S^2 values. This calls for some clarifications. The first part of our discussion centers on the correlated investigation of two problems:

- 1) How uniform are the output predictions of different unitarization procedures?
- 2) How sensitive are the eikonal calculations to the details of the eikonal model they use?

We start with two non eikonal models which have contradictory predictions.

The first is a model suggested by Troshin and Tyurin [52]. In this model the single channel unitarity constraint (Eq.(13)) is enforced with an asymptotic bound where $G_{in} = 0$ and $|a_{el}| = 2$ i.e. asymptotically, $\sigma_{tot} = \sigma_{el}$ and $P^S(s, b) = 1$. The parameters of the model are set so as to obtain a "normal" survival probability monotonically decreasing with energy up to about $2500 GeV$ where it changes its behavior and rises monotonically to its asymptotic limit of 1. Beside the fact that the model has a legitimate but non appealing asymptotics, its main deficiency is that it suggests a dramatic change in the systematics of S^2 without being able to offer any experimental signature to support this claim. Regardless of this criticism, this is a good example of a proper unitarity model whose results are profoundly different from the eikonal model predictions.

Another non eikonal procedure is Goulianos flux renormalization model [17]. This is a phenomenological model which formally does not enforce unitarity, but rather, a bound of unity on the Pomeron flux in diffractive processes. Note that, the Pomeron flux is not uniquely defined so this should be regarded as an ad hoc parametrization. Nevertheless, it has scored an impressive success in reproducing the soft and hard diffractive data in the ISR-Tevatron range. The implied survival probabilities of this procedure are compatible with GLM and KKMR. However, the model predicts suppression factors for the diffractive channels which are t -independent and, thus, b -independent. The result is that, even though the output diffractive cross section is properly reduced relative to its input, there is no change of the output profile from its input Gaussian form. Consequently, the Pumplin bound is violated. We are informed that Goulianos plans to improve his model by eikonalizing the output of his present model.

As noted, there are a few eikonal models on the market [73–80], and their predictions are compatible with GLM and KKMR. Reconsidering the procedure of these calculations, their compatibility is not surprising once we translate their input to a GLM format. The GLM eikonal S^2 calculation has two input sectors in either a single or a two channel version. They are the soft ν and R^2 , and the hard radius R^{H^2} . Since the soft input is based on a fit of the soft scattering data base, the potential variance in the soft parameters is relatively small. The input hard radius is obtained from either the HERA data or a theoretical calculation, be it a pQCD diagram or a Regge model. All in all, this is a reasonably stable input. In this context, it is interesting to discuss the eikonal model of Block and Halzen [73], where

the calculated survival probabilities for Higgs production through W-W fusion are seemingly too high, $S^2(540) = 27\%$, $S^2(1800) = 21\%$ and $S^2(14000) = 13\%$. Even though, Higgs production is a CD process, the above S^2 values are in agreement with the KKMR calculations of S_{DD}^2 with a relatively high $R^{H^2} = 11 \text{ GeV}^{-2}$. In a proper S_{CD}^2 calculation, these high S^2 values correspond to an even higher $R^{H^2} \simeq 20 \text{ GeV}^{-2}$, which is far too high as an estimate of the hard radius of $WW \rightarrow H$. A possible interpretation of Block-Halzen results is to associate them with a soft, rather than a hard, LRG CD process. This would couple with the non screened interpretation of CD Higgs through the soft CEM model [74, 75], which predicts very high S^2 values. Since the CEM model is not screened we may, as well, assign a survival probability to its output result. This translates into $S_{CD}^2 = S_{BH}^2 S_{CEM}^2$, providing rather reasonable one channel predictions, $S_{CD}^2(540) = 18.9\%$ and $S_{CD}^2(1800) = 7.2\%$.

Obviously, each of the eikonal models, quoted above has its own particular presentation and emphasis. They do, however, have compatible results reflecting the observation that their input translates into similar values of ν , R^2 and R^{H^2} .

5.2 Compatibility between HERA and the Tevatron di-jets data

Much attention has been given recently to the compatibility between the Tevatron and HERA DIS GJJ data. The starting point made by KKMR and CDF is that rather than depend on a p.d.f. input to calculate F_{gap} , we may use, the GJJ di-jets diffractive structure function, F_{jj}^D , inferred from HERA DIS data [18–27] and associate it with the F_{jj}^D derived from the Tevatron GJJ data. As it stands, this procedure ignores the role of the survival probability. Consequently, F_{jj}^D obtained from the Tevatron is an order of magnitude smaller than the HERA output [8–12, 17, 40–44]. This result led to speculations about a possible breaking of QCD or Regge factorization or both. Once the Tevatron di-jets diffractive structure function is rescaled by the appropriate survival probability, the compatibility between the Tevatron and HERA DIS diffractive data is attained. The conclusion of this analysis is that the breaking of factorization is attributed to the soft re-scatterings of the the colliding projectiles. Additional hard contribution to the factorization breaking due to gluon radiation is suppressed by the Sudakov factor included in the pQCD calculation (see 4.3).

One should note, though, that the H1 determination [18–27] of F_{jj}^D is not unique. Arneodo [72] has suggested a different F_{jj}^D output based on HERA di-jets data which has a different normalization and β dependences. Should this be verified, there might well be a need to revise the KKMR calculations.

The evolution of HERA F_{jj}^D from high Q^2 DIS to $Q^2 = 0$ di-jets photoproduction has raised additional concern with regard to the validity of the factorization theorems [28, 29]. This is a complicated analysis since one has to be careful on two critical elements of the calculations:

- 1) The determination of the ratio between direct and resolved exchanged photon (real or virtual). This is a crucial element of the theoretical calculation since survival probability is applicable only to the resolved photon component. For very high Q^2 data the hard scattering process with the target partons is direct. At $Q^2 = 0$ there is a significant resolved photon contribution.
- 2) For di-jets production there is a big difference between the LO and the NLO pQCD calculated cross sections [81–83]. Since the HERA analysis compares the pQCD calculation with the di-jets measured cross section the normalization and shape of the theoretical input is most crucial in the experimental comparison between the high Q^2 and $Q^2 = 0$ data.

On the basis of a NLO calculation, Klasen and Kramer [81, 82] conclude that they can reproduce the photoproduction data with $S^2 = 0.34$, applied to the resolved sector. This survival probability is in agreement with KKMR and GLM calculations.

Regardless of the above, preliminary photoproduction GJJ HERA data [28, 29] suggest that both the direct and resolved photon sectors are suppressed at $Q^2 = 0$. A verification of this observation has

Table 3: GLM two-channel predictions at a few energies

\sqrt{s} [GeV]	σ_{tot}^{DL} [mb]	σ_{tot}^{GLM} [mb]	σ_{el}^{GLM} [mb]	σ_{sd}^{GLM} [mb]	B_{el}^{GLM} [GeV ⁻²]	$S_{CD}^{GLM^2}$
540	60.1	62.0	12.3	8.7	14.9	0.066
1800	72.9	74.9	15.9	10.0	16.8	0.055
14000	101.5	103.8	24.5	12.0	20.5	0.036
30000	114.8	116.3	28.6	12.7	22.0	0.029
60000	128.4	128.7	32.8	13.2	23.4	0.023
90000	137.2	136.5	35.6	13.5	24.3	0.019
120000	143.6	142.2	37.6	13.7	24.9	0.017

severe consequences for our understanding of the evolution of the diffractive structure function from DIS to photoproduction. It does not directly relate, though, to the issue of soft survival probability which apply, per definition, only to the resolved photon sector. The suggested effect in the direct photon sector should, obviously be subject to a good measure of caution before being substantiated by further independent analysis.

5.3 Diffraction at energies above the LHC

We end with Table 3, which shows the GLM two channel predictions for energies including the LHC, and up to the top Cosmic Rays energies. The, somewhat, surprizing observation is that the GLM calculated total cross sections are compatible with the DL simple Regge predictions all over the above energy range. This is a reflection of the fact that even at exceedingly high energies unitarization reduces the elastic amplitude at small enough b values to be relatively insensitive to the calculation of σ_{tot} . On the other hand, we see that σ_{el} becomes more moderate in its energy dependence and σ_{el}/σ_{tot} which is 23.6% at the LHC is no more than 26.4% at the highest Cosmic Rays energy, 120 TeV . The implication of this observation is that the nucleon profile becomes darker at a very slow rate and is grey (well below the black disc bound) even at the highest energy at which we can hope for a measurement. A check of our results at the Planck scale shows $\sigma_{tot} = 1010 mb$ and the profile to be entirely black. i.e., $\frac{\sigma_{el}}{\sigma_{tot}} = \frac{1}{2}$. σ_{sd} is even more moderate in its very slow rise with energy. The diminishing rates for soft and hard diffraction at exceedingly high energies are a consequence of the monotonic reduction in the values of S^2 with a Planck scale limit of $S^2 = 0$. This picture is bound to have its effect on Cosmic Rays studies.

Our LHC predictions are compatible with KMR. Note, though, that: i) σ_{sd}^{GLM} is rising slowly with s gaining 20% from the Tevatron to LHC. KMR has a much faster rise with energy, where, σ_{sd}^{KMR} is gaining 77% – 92% over the same energy interval. ii) At the LHC $B_{el}^{GLM} = 20.5 GeV^{-2}$, to be compared with a DL slope of 19 GeV^{-2} and a KMR slope of 22 GeV^{-2} . The GLM 30 TeV cross sections are compatible with Block-Halzen.

6 Acknowledgements

We are very thankful to our colleagues Valery Khoze, Alan Martin, Misha Ryskin and Leif Lönnblad, who generously contributed to **Section 4** and the **Appendix**. Needless to say, they bear no responsibility for the rest of this review.

Appendix: Monte Carlo modeling of gap survival

The following was contributed by Leif Lönnblad and is presented without any editing.

An alternative approach to gap survival and factorization breaking is to implement multiple interactions in Monte Carlo event generators. These models are typically based on the eikonalization of the partonic cross section in hadronic collisions and can be combined with any hard sub process to describe the additional production of hadrons due to secondary partonic scatterings. Some of these programs, such as PYTHIA [84, 85] and HERWIG/JIMMY [86–88], are described in some detail elsewhere in these proceedings [89]. Common for all these models is that they include exact kinematics and flavour conservation, which introduces some non-trivial effects and makes the multiple scatterings process-dependent. Also, the predictions of the models are very sensitive to the cutoff used to regularize the partonic cross section and to the assumptions made about the distribution of partons in impact parameter space. Nevertheless, the models are quite successful in describing sensitive final-state observables such as multiplicity distributions and jet-pedestal effects [89]. In particular this is true for the model in PYTHIA which has been successfully tuned to Tevatron data⁴ by Rick Field [90], the so-called *CDF tune A*.

The PYTHIA model does not make any prediction for the energy dependence of the total cross section - rather this is an input to the model used to obtain the distribution in the number of multiple interactions. PYTHIA can, however, make predictions for gap survival probabilities. This was first done for Higgs production via W-fusion [2], and amounts to simply counting the fraction of events which do not have any additional scatterings besides the W-fusion process. The basic assumption is that any additional partonic scattering would involve a colour exchange which would destroy any rapidity gap introduced by W-fusion process. Since PYTHIA produces complete events, these can also be directly analyzed with the proper experimental cuts. A similar estimate was obtained for the gaps between jets process, both for the Tevatron and HERA case [91].

Recently, PYTHIA was used to estimate gap survival probabilities also for the case of central exclusive Higgs production [92]. As in the case of gaps between jets, the actual signal process is not implemented in PYTHIA, so direct analysis with proper experimental cuts was not possible. Instead a similar hard sub process was used (standard inclusive Higgs production via gluon fusion in this case) and the fraction of events without additional secondary partonic scatterings was identified with the gap survival probability. Using the *CDF tune A* the gap survival probability was estimated to be 0.040 for the Tevatron and 0.026 for the LHC. This is remarkably close both to the values used in [64] obtained in the KKMR model [43], and to the GLM values presented in section 3.4 especially the two-channel ones obtained in [60].

References

- [1] Y. L. Dokshitzer, S. I. Troian, and V. A. Khoze, *Sov. J. Nucl. Phys.* **46**, 712 (1987).
- [2] Y. L. Dokshitzer, V. A. Khoze, and T. Sjöstrand, *Phys. Lett.* **B274**, 116 (1992).
- [3] J. D. Bjorken, *Int. J. Mod. Phys.* **A7**, 4189 (1992).
- [4] J. D. Bjorken, *Phys. Rev.* **D47**, 101 (1993).
- [5] D0 Collaboration, S. Abachi *et al.*, *Phys. Rev. Lett.* **72**, 2332 (1994).
- [6] D0 Collaboration, S. Abachi *et al.*, *Phys. Rev. Lett.* **76**, 734 (1996). [hep-ex/9509013](#).
- [7] D0 Collaboration, B. Abbott *et al.*, *Phys. Lett.* **B440**, 189 (1998). [hep-ex/9809016](#).
- [8] CDF Collaboration, F. Abe *et al.*, *Phys. Rev. Lett.* **74**, 855 (1995).
- [9] CDF Collaboration, F. Abe *et al.*, *Phys. Rev. Lett.* **80**, 1156 (1998).
- [10] CDF Collaboration, F. Abe *et al.*, *Phys. Rev. Lett.* **81**, 5278 (1998).
- [11] CDF Collaboration, T. Affolder *et al.*, *Phys. Rev. Lett.* **84**, 5043 (2000).
- [12] CDF Collaboration, T. Affolder *et al.*, *Phys. Rev. Lett.* **85**, 4215 (2000).
- [13] K. Goulios (2003). [hep-ph/0306085](#).
- [14] K. Goulios, *J. Phys.* **G26**, 716 (2000). [hep-ph/0001092](#).

⁴Note that the model in PYTHIA has recently been revised [89]. However, the reproduction of Tevatron data is not as good for the revised model.

- [15] CDF Collaboration, K. Goulios, Nucl. Phys. Proc. Suppl. **99A**, 37 (2001). hep-ex/0011059.
- [16] K. Goulios (2004). hep-ph/0407035.
- [17] K. Goulios. Private communication to UM.
- [18] ZEUS Collaboration, M. Derrick *et al.*, Phys. Lett. **B315**, 481 (1993).
- [19] ZEUS Collaboration, M. Derrick *et al.*, Z. Phys. **C68**, 569 (1995). hep-ex/9505010.
- [20] ZEUS Collaboration, M. Derrick *et al.*, Phys. Lett. **B356**, 129 (1995). hep-ex/9506009.
- [21] ZEUS Collaboration, M. Derrick *et al.*, Phys. Lett. **B369**, 55 (1996). hep-ex/9510012.
- [22] ZEUS Collaboration, J. Breitweg *et al.*, Eur. Phys. J. **C6**, 43 (1999). hep-ex/9807010.
- [23] H1 Collaboration, T. Ahmed *et al.*, Nucl. Phys. **B429**, 477 (1994).
- [24] H1 Collaboration, T. Ahmed *et al.*, Phys. Lett. **B348**, 681 (1995). hep-ex/9503005.
- [25] H1 Collaboration, C. Adloff *et al.*, Z. Phys. **C76**, 613 (1997). hep-ex/9708016.
- [26] F.-P. Schilling, *Measurement and nlo dglap qcd interpretation of diffractive deep-inelastic scattering at hera*. Paper 089 submitted to EPS 2003 Conf. Aachen.
- [27] A. A. Savin. Prepared for NATO Advanced Research Workshop on Diffraction 2002, Alushta, Ukraine, 31 Aug - 6 Sep 2002.
- [28] H. Abramowicz, ECONF **C0406271**, MONT04 (2004). hep-ex/0410002.
- [29] O. Gutsche, *Dijets in diffractive photoproduction and deep-inelastic scattering at hera*. Contribution No. 6-0177 submitted to ICHEP04, Beijing Aug 2004.
- [30] E. Gotsman, E. M. Levin, and U. Maor, Z. Phys. **C57**, 677 (1993). hep-ph/9209218.
- [31] E. Gotsman, E. M. Levin, and U. Maor, Phys. Rev. **D49**, 4321 (1994). hep-ph/9310257.
- [32] E. Gotsman, E. M. Levin, and U. Maor, Phys. Lett. **B353**, 526 (1995). hep-ph/9503394.
- [33] E. Gotsman, E. M. Levin, and U. Maor, Phys. Lett. **B347**, 424 (1995). hep-ph/9407227.
- [34] J. Forshaw, *Diffractive Higgs production: theory*. These Proceedings.
- [35] E. Gotsman, E. M. Levin, and U. Maor, Phys. Lett. **B309**, 199 (1993). hep-ph/9302248.
- [36] E. Gotsman, E. Levin, and U. Maor, Nucl. Phys. **B493**, 354 (1997). hep-ph/9606280.
- [37] E. Gotsman, E. Levin, and U. Maor, Phys. Lett. **B438**, 229 (1998). hep-ph/9804404.
- [38] E. Gotsman, E. Levin, and U. Maor, Phys. Lett. **B452**, 387 (1999). hep-ph/9901416.
- [39] E. Gotsman, E. Levin, and U. Maor, Phys. Rev. **D60**, 094011 (1999). hep-ph/9902294.
- [40] V. A. Khoze, A. D. Martin, and M. G. Ryskin, Eur. Phys. J. **C14**, 525 (2000). hep-ph/0002072.
- [41] V. A. Khoze, A. D. Martin, and M. G. Ryskin, Eur. Phys. J. **C18**, 167 (2000). hep-ph/0007359.
- [42] V. A. Khoze, A. D. Martin, and M. G. Ryskin, Eur. Phys. J. **C19**, 477 (2001). hep-ph/0011393.
- [43] A. B. Kaidalov, V. A. Khoze, A. D. Martin, and M. G. Ryskin, Eur. Phys. J. **C21**, 521 (2001). hep-ph/0105145.
- [44] A. B. Kaidalov, V. A. Khoze, A. D. Martin, and M. G. Ryskin, Eur. Phys. J. **C33**, 261 (2004). hep-ph/0311023.
- [45] P. D. B. Collins, *An Introduction to Regge Theory and High-Energy Physics*. Cambridge 1977, 445p.
- [46] L. e. Caneschi, *Current physics sources and comments vol. 3: Regge theory of low p_t hadronic interactions*. North Holland Pub (1989).
- [47] A. Donnachie and P. V. Landshoff, Phys. Lett. **B296**, 227 (1992). hep-ph/9209205.
- [48] A. Donnachie and P. V. Landshoff, Z. Phys. **C61**, 139 (1994). hep-ph/9305319.
- [49] M. M. Block, K. Kang, and A. R. White, Int. J. Mod. Phys. **A7**, 4449 (1992).
- [50] CDF Collaboration, F. Abe *et al.*, Phys. Rev. **D50**, 5535 (1994).
- [51] T. T. Chou and C.-N. Yang, Phys. Rev. **170**, 1591 (1968).
- [52] S. M. Troshin and N. E. Tyurin, Eur. Phys. J. **C39**, 435 (2005). hep-ph/0403021.
- [53] A. H. Mueller, Phys. Rev. **D2**, 2963 (1970).

- [54] J. Pumplin, Phys. Rev. **D8**, 2899 (1973).
- [55] J. Pumplin, Phys. Scripta **25**, 191 (1982).
- [56] T. Gitman. TAU M.Sc. Thesis, unpublished (2003).
- [57] H1 Collaboration, C. Adloff *et al.*, Phys. Lett. **B483**, 23 (2000). hep-ex/0003020.
- [58] ZEUS Collaboration, S. Chekanov *et al.*, Eur. Phys. J. **C24**, 345 (2002). hep-ex/0201043.
- [59] H. Kowalski and D. Teaney, Phys. Rev. **D68**, 114005 (2003). hep-ph/0304189.
- [60] E. Gotsman, H. Kowalski, E. Levin, U. Maor, and A. Prygarin. Preprint in preparation (2005).
- [61] CDF Collaboration, F. Abe *et al.*, Phys. Rev. Lett. **79**, 584 (1997).
- [62] A. Donnachie and P. V. Landshoff, Nucl. Phys. **B231**, 189 (1984).
- [63] V. A. Khoze, A. D. Martin, and M. G. Ryskin, Phys. Lett. **B401**, 330 (1997). hep-ph/9701419.
- [64] V. A. Khoze, A. D. Martin, and M. G. Ryskin, Eur. Phys. J. **C23**, 311 (2002). hep-ph/0111078.
- [65] M. A. Kimber, A. D. Martin, and M. G. Ryskin, Phys. Rev. **D63**, 114027 (2001). hep-ph/0101348.
- [66] M. A. Kimber, A. D. Martin, and M. G. Ryskin, Eur. Phys. J. **C12**, 655 (2000). hep-ph/9911379.
- [67] A. G. Shuvaev, K. J. Golec-Biernat, A. D. Martin, and M. G. Ryskin, Phys. Rev. **D60**, 014015 (1999). hep-ph/9902410.
- [68] A. D. Martin and M. G. Ryskin, Phys. Rev. **D64**, 094017 (2001). hep-ph/0107149.
- [69] G. Watt, A. D. Martin, and M. G. Ryskin, Eur. Phys. J. **C31**, 73 (2003). hep-ph/0306169.
- [70] A. B. Kaidalov, V. A. Khoze, A. D. Martin, and M. G. Ryskin, Eur. Phys. J. **C31**, 387 (2003). hep-ph/0307064.
- [71] V. Khoze. Private communication to UM, July 2005.
- [72] M. Arneodo. Talk at HERA/LHC CERN Meeting and private communication to UM, Oct. 2004.
- [73] M. M. Block and F. Halzen, Phys. Rev. **D63**, 114004 (2001). hep-ph/0101022.
- [74] O. J. P. Eboli, E. M. Gregores, and F. Halzen, Phys. Rev. **D61**, 034003 (2000). hep-ph/9908374.
- [75] O. J. P. Eboli, E. M. Gregores, and F. Halzen, Nucl. Phys. Proc. Suppl. **99A**, 257 (2001).
- [76] L. Frankfurt, M. Strikman, and C. Weiss, Annalen Phys. **13**, 665 (2004). hep-ph/0410307.
- [77] L. Frankfurt, M. Strikman, C. Weiss, and M. Zhalov (2004). hep-ph/0412260.
- [78] V. A. Petrov and R. A. Ryutin, Eur. Phys. J. **C36**, 509 (2004). hep-ph/0311024.
- [79] A. Bialas, Acta Phys. Polon. **B33**, 2635 (2002). hep-ph/0205059.
- [80] A. Bialas and R. Peschanski, Phys. Lett. **B575**, 30 (2003). hep-ph/0306133.
- [81] M. Klasen and G. Kramer, Eur. Phys. J. **C38**, 93 (2004). hep-ph/0408203.
- [82] M. Klasen and G. Kramer, Phys. Rev. Lett. **93**, 232002 (2004). hep-ph/0410105.
- [83] A. B. Kaidalov, V. A. Khoze, A. D. Martin, and M. G. Ryskin, Phys. Lett. **B567**, 61 (2003). hep-ph/0306134.
- [84] T. Sjöstrand and M. van Zijl, Phys. Rev. **D36**, 2019 (1987).
- [85] T. Sjöstrand, and others, Comput. Phys. Commun. **135**, 238 (2001). hep-ph/0010017.
- [86] G. Corcella *et al.*, JHEP **01**, 010 (2001). hep-ph/0011363.
- [87] J. M. Butterworth, J. R. Forshaw, and M. H. Seymour, Z. Phys. **C72**, 637 (1996). hep-ph/9601371.
- [88] J. Butterworth *et al.* <http://jetweb.hep.ucl.ac.uk/JIMMY>.
- [89] C. Buttar *et al.*, *Underlying events*. These Proceedings.
- [90] R. Field, *Min-bias and the underlying event at the tevatron and the lhc*. http://www.phys.ufl.edu/~rfield/cdf/FNAL_Workshop_10-4-02.pdf. Talk presented at the Fermilab ME/MC Tuning Workshop, October 4, 2002.
- [91] B. Cox, J. Forshaw, and L. Lönnblad, JHEP **10**, 023 (1999). hep-ph/9908464.
- [92] L. Lönnblad and M. Sjödal, JHEP **05**, 038 (2005). hep-ph/0412111.

Multi-Jet Production and Multi-Scale QCD

Z. Czyczula^{1,2}, G. Davatz³, A. Nikitenko⁴, E. Richter-Was^{1,5,*}, E. Rodrigues⁶, N. Tuning⁶

¹ Institute of Physics, Jagiellonian University, Krakow, Poland

² Niels Bohr Institute, University of Copenhagen, Copenhagen, Denmark

³ Institute for Particle Physics, ETH Zürich, Switzerland

⁴ Imperial College, London, UK

⁵ Institute of Nuclear Physics PAN, Krakow, Poland

⁶ NIKHEF, Amsterdam, The Netherlands

Abstract

We summarize the contributions in Working Group II on “Multi-jet final states and energy flows” related to the topic of jet production, multi-jet topologies and multi-scale QCD. Different parton shower models will lead to systematic differences in the event topology. This may have a significant impact on predictions for the LHC. Here we will look at a few examples, such as the acceptance of $H \rightarrow \tau\tau$ events and in applying a jet veto in the non-hadronic $H \rightarrow WW \rightarrow l\nu l\nu$ decay channel. We also study the effect of CCFM evolution on the jet veto and on the event topology at the LHC in the forward region. Finally, we show that the choice of the QCD scale leads to large uncertainties in e.g. the $H \rightarrow \tau\tau$ analysis.

1 Introduction

In simulating high-energy interactions, the sequence of branchings such as $q \rightarrow qg$, can be modelled by calculating the exact amplitude of the Feynman diagrams, known as the matrix-element method, or, alternatively, can be modelled using the parton-shower approach. Matrix elements are in principle the exact approach but lead to increasingly complicated calculations in higher orders, and are therefore only used for specific exclusive physics applications, such as background estimates with multiple hard jets (see also [1]).

Since no exact way of treating partonic cascades exist, various Monte Carlo programs model the parton showers in different ways. In HERWIG [2] the parton showers are performed in the soft or collinear approximation, treating the soft gluon emission correctly. The shower is strictly angular ordered, where the angle between emitted partons is smaller at each branching. The hardest gluon emission is then matched to the first order matrix-element. This matrix-element correction has recently been implemented for $gg \rightarrow H$, leading to harder jets, and thus a more stringent jet veto in e.g. the non-hadronic decay $H \rightarrow WW \rightarrow l\nu l\nu$, where the jet veto is crucial to reduce the top background. PYTHIA [3] applies the collinear algorithm with the cascade ordered according to the virtuality Q^2 . Corrections to the leading-log picture using an angular veto, lead to an angular ordering of subsequent emissions. The initial parton branchings are weighted to agree with matrix-elements. ARIADNE [4] on the other hand, does not emit gluons from single partons, but rather from the colour dipoles between two dipoles, thus automatically including the coherence effects approximated by angular ordering in HERWIG. From the resulting two dipoles softer emission occurs, resulting in a p_T ordering of subsequent emissions. ARIADNE has proven to predict the event shapes at HERA accurately [5], and could be explored more widely for simulation studies for the LHC.

The way parton showers are implemented affects the emission of soft gluons, and therefore affect both the transverse momentum of the produced Higgs, as well as the p_T of the balancing jets. In the

* Supported in part by the Polish Government grant KBN 1 P03 091 27 (years 2004-2006) and by the EU grant MTKD-CT-2004-510126, in partnership with the CERN Physics Department.

following we will discuss the effect of the different parton showers on the selection of $H \rightarrow \tau\tau$ by applying angular cuts on the jets and on the selection of $H \rightarrow WW \rightarrow l\nu l\nu$ by rejecting events with jets with large p_T .

Both PYTHIA and HERWIG are general purpose leading order (LO) parton shower Monte Carlo programs, based on LO matrix elements. MC@NLO [6] on the other hand, uses exact next-to-leading order (NLO) calculations and is matched to the HERWIG parton shower Monte Carlo. Its total cross section is normalized to NLO predictions. The different predictions of these programs for the high part of the transverse momentum spectrum of the Higgs will be described in detail.

In the parton cascade as implemented in e.g. PYTHIA, the parton emissions are calculated using the DGLAP approach [7], with the partons ordered in virtuality. DGLAP accurately describes high-energy collisions of particles at moderate values of the Bjorken- x by resummation of the leading log terms of transverse momenta $((\alpha_s \ln Q^2)^n)$. However, to fixed order, the QCD scale used in the ladder is not uniquely defined. Different choices of the scale lead to large differences in the average transverse momentum of the Higgs in e.g. the processes $gb \rightarrow bH$ and $gg \rightarrow bbH$.

In the CCFM formalism [8] there is no strict ordering along the parton ladder in transverse energy, contrary to the DGLAP formalism. The CASCADE Monte Carlo program [9] has implemented the CCFM formalism, inspired by the low- x F_2 data and forward jet data from HERA, and became recently available for pp scattering processes. Until now, CASCADE only includes gluon chains in the initial state cascade. Different sets of unintegrated gluon densities are available, which all describe HERA data equally well [9]. Note, however, that it is questionable if these densities are constrained enough for Higgs production, as discussed elsewhere in these proceedings [10].

CCFM is expected to provide a better description of the gluon evolution at very low values of x compared to DGLAP, as it also takes leading-logs of longitudinal momenta $((\alpha_s \ln x)^n)$ into account. Since the partons at the bottom of the ladder (furthest away from the hard scatter) are closest in rapidity to the outgoing proton, effects might be expected in the forward region. The event topology in terms of jets and charged multiplicity is investigated at rapidities $2 < \eta < 5$, corresponding to the acceptance of the LHCb detector.

2 MSSM Higgs production with the Yukawa bbH coupling induced mechanisms

In the MSSM, the Yukawa coupling of the heavy neutral Higgs bosons to the bottom quarks is strongly enhanced for large $\tan(\beta)$ with respect its SM value, which makes the Higgs boson production in association with bottom quarks the primary production mechanism in LHC pp collisions. Currently, the inclusive cross section for this process is under good control up to NNLO, both in the so called fixed-flavour-scheme (FFS) and varying-flavour-scheme (VFS). The impressive level of theoretical uncertainty in the order of 15% is achieved on the predictions for the total cross-section for $m_H=120$ GeV [11, 12].

The observability potential for the $H \rightarrow \tau\tau$ channel [13] is, however, very sensitive to the topology of the events, due to the reconstruction of the invariant mass of the tau-pair, using the collinear approximation of τ -leptons decay, in order to account for the neutrino momenta. The impact of the event topology on the final acceptance of the signal has been discussed elsewhere [14]. Here, we pursue the subject further and we study more quantitatively the systematic effects from the parton shower model and the choice of the QCD scale selected in the event generation.

Currently available Monte Carlo generators for the Higgs boson production are based on the LO matrix elements, with the QCD part of physics event simulated with a parton shower approach. Clearly, the kinematics of the Higgs boson (and therefore the final acceptance for the signal) depends strongly on the algorithm used to simulate the QCD cascade. At tree level, the following exclusive processes have been studied, combining the observability of events with and without spectator b-tagged jets accompanying the reconstructed tau-pair: $gb \rightarrow bH$ (VFS), $gg \rightarrow b\bar{b}H$ (FFS), $b\bar{b} \rightarrow H$ (VFS) and $gg \rightarrow H$.

For the purpose of the discussion presented here we have studied the SM Higgs boson production

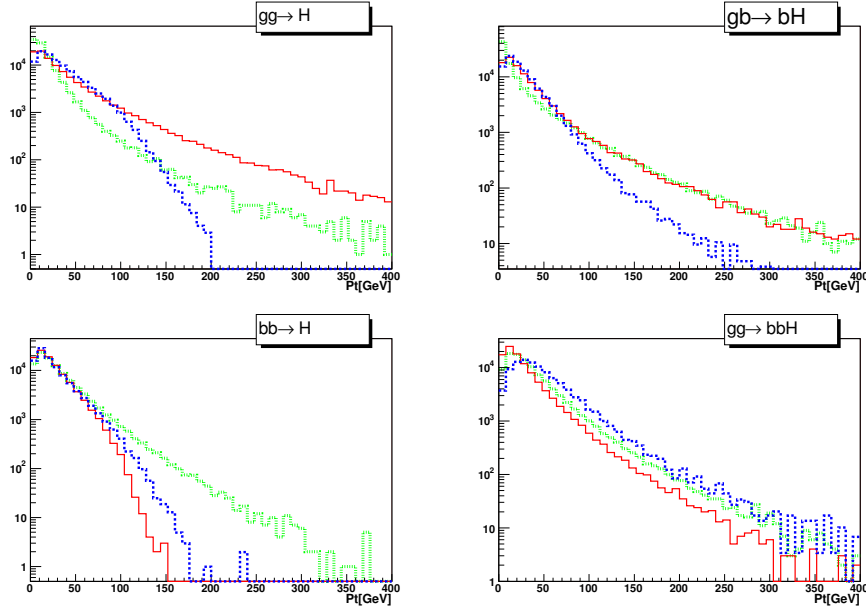


Fig. 1: The transverse momenta of the Higgs boson, p_T^{Higgs} for 3 different shower models for each production mechanism. The red solid line represents PYTHIA, the dashed green line ARIADNE and the dotted blue line HERWIG events. The vertical scale gives the number of events per bin, and a total of 10^5 events have been generated with each program.

with a mass of 120 GeV, decaying into a tau pair, where one tau decays hadronically and one leptonically. The reconstruction of the Higgs boson mass and the selection criteria were performed at the level of generated particles (leptons, hadrons) or, where necessary (missing energy, b-jets), on objects reconstructed from simplified simulation of the detector response [15].

2.1 Systematics from the choice of parton shower model

As discussed in the introduction, the various parton shower models predict different spectra of the transverse momentum, p_T^{Higgs} , of the produced Higgs boson. This leads to a large variation in the prediction for the fraction of accepted events. The obvious starting point for the discussion is the Higgs boson transverse momentum spectra in complete physics events¹. In case of the $2 \rightarrow 2$ and $2 \rightarrow 3$ processes, the p_T of the Higgs boson arises predominantly from matrix elements, whereas in the $2 \rightarrow 1$ events p_T^{Higgs} purely comes from the parton shower. Therefore, the Higgs transverse momentum spectra differ significantly for different models of the QCD cascade. Figure 1 shows these spectra for each production mechanism².

Clearly, the spectra of the Higgs boson transverse momenta show substantial dependence not only on the topology of the hard process, but also on the shower model used in the simulation of the event. The shower model as implemented in PYTHIA includes hard matrix element corrections for inclusive gluon-gluon fusion, $gg \rightarrow H$, hence leading to a harder spectrum compared to the one obtained from the standard HERWIG shower. In this production mode the shower model from ARIADNE fails because of the missing splitting kernel for $g \rightarrow q\bar{q}$. On the other hand, the ARIADNE model predicts the hardest spectra for the process $b\bar{b} \rightarrow H$. In this production channel, predictions from PYTHIA and HERWIG

¹The AcerMC 2.4 framework [16] with interfaces to PYTHIA 6.2, ARIADNE 4.12 and HERWIG 6.5 was used to generate events and AcerDET [15] was used to simulate the detector performance.

²The CTEQ5L parton density functions were used in all simulations. It has been checked that both final acceptance of the signal and the mean Higgs boson transverse momentum is almost independent of the pdf parametrization. Uncertainties below 10% are observed by using CTEQ5L, CTEQ6L, MRST2001 interfaced with LHAPDF [17]).

Table 1: The average transverse momenta of the Higgs boson and acceptance of selection criteria for different hard processes and parton shower models. Events were generated with default initialization of these generators. Columns marked PY, AR and HW denote results from PYTHIA, ARIADNE and HERWIG shower model respectively.

Hard process	gg \rightarrow H			b \bar{b} \rightarrow H		
Shower model	PY	AR	HW	PY	AR	HW
$\langle p_T^{\text{Higgs}} \text{ (generated)} \rangle$ (GeV)	37.2	X	32.2	23.1	29.9	24.6
$\langle p_T^{\text{Higgs}} \text{ (accepted)} \rangle$ (GeV)	129.4	X	75.27	58.6	91.64	68.4
basic selection	14.2%	X	12.7%	12.8%	13.8%	11.8%
+($\cos(\phi) > -0.9$, $ \sin(\phi) > 0.2$)	5.5%	X	4.5%	2.9%	4.3%	2.7%
+($p_T^{\text{miss}} > 30$ GeV, $m_T^{\text{lep-miss}} < 50$ GeV)	3.8%	X	2.3%	1.4%	2.3%	1.5%
+(mass window: 120 ± 20 GeV)	2.4%	X	1.3%	0.6%	1.3%	0.6%
+(1 tagged b-jet)				0.4%	1.0%	0.4%
Hard process	gb \rightarrow bH			gg \rightarrow b \bar{b} H		
Shower model	PY	AR	HW	PY	AR	HW
$\langle p_T^{\text{Higgs}} \text{ (generated)} \rangle$ [GeV]	32.5	26.0	26.9	27.2	35.8	47.4
$\langle p_T^{\text{Higgs}} \text{ (accepted)} \rangle$ [GeV]	125.1	133.9	82.1	95.0	99.6	105.3
basic selection	13.3%	12.6%	11.7%	13.0%	13.6%	12.1%
+($\cos(\phi) > -0.9$, $ \sin(\phi) > 0.2$)	4.4%	3.4%	3.2%	3.5%	5.1%	6.7%
+($p_T^{\text{miss}} > 30$ GeV, $m_T^{\text{lep-miss}} < 50$ GeV)	2.7%	2.4%	1.7%	2.0%	2.9%	3.8%
+(mass window: 120 ± 20 GeV)	1.7%	1.5%	0.9%	1.1%	1.8%	2.6%
+(1 tagged b-jet)	1.3%	1.4%	0.6%	0.9%	1.2%	2.1%

are in quite good agreement. However, almost a factor of two difference for the prediction of the mean transverse momenta can be reported between PYTHIA and HERWIG in $gg \rightarrow b\bar{b}H$ process.

Numerical values for the average Higgs boson transverse momentum in different production processes and parton shower models are given in Table 1. It is important to stress that these results were obtained with default settings of the parameters for each parton shower model.

The steps of the analysis that lead to the reconstruction of the tau-pair invariant mass are indicated in Table 1, including the acceptances for all the discussed production processes and parton shower models. They consist of the basic selection (including the trigger and p_T and $|\eta|$ cuts on the lepton and jet), and the additional selection that is needed to improve the mass resolution of the accepted tau-pair. The acceptance of the signal after the basic selection is rather stable, at the level of 12%-14% depending on the production mechanism. The significant differences start to appear when a cut on the angle between the lepton and hadron is applied. A difference of almost a factor two is observed for the $b\bar{b} \rightarrow H$ production process with the parton shower from the HERWIG or ARIADNE model, respectively.

For the final acceptance values, the uncertainty from the parton shower model varies between 85% for inclusive gluon fusion to 135% for $gg \rightarrow b\bar{b}H$ (between HERWIG and PYTHIA models). In the case of the Higgs production through $b\bar{b} \rightarrow H$, predictions from HERWIG and PYTHIA models are in excellent agreement. However, the prediction of the acceptance in this production channel differs by 115% if the parton shower from ARIADNE is used. For the $gb \rightarrow bH$ production mechanism, the uncertainty due to the shower model from either PYTHIA or HERWIG is about 90%.

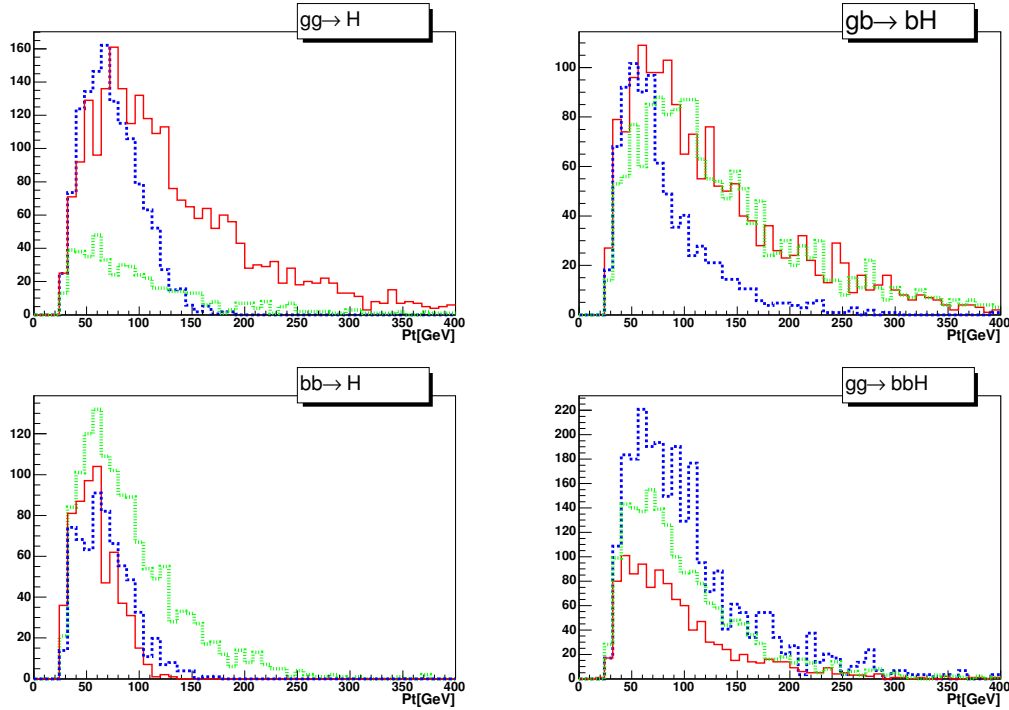


Fig. 2: Same as Fig. 1 but after selection presented in Table 1. The vertical scale is in number of events entering given bin after selection procedure, in each case 10^5 events were initially generated.

The systematic theoretical uncertainty on the predictions for the final acceptance ranges from 85% to 135% for the three different shower models studied here. The uncertainty is even larger, when the requirement of an additional tagging b-jet is introduced, up to 170% for $bb \rightarrow H$ ³. Figure 2 shows the Higgs boson transverse momentum for those events that passed all selection criteria. As can be observed, the selection criteria rejected most of events with $p_T^{\text{Higgs}} < 40$ GeV.

2.2 Systematics from the choice of QCD scale

Having considered here the available Monte Carlo generators with the overall precision of the leading order only, large uncertainties are expected for the predictions coming from different scale choices. Here we concentrate only on the effects on the event topology, neglecting the effects from the choice of the QCD scale on the total cross-section. Table 2 shows the Higgs boson mean transverse momentum and final acceptance of the signal for $2 \rightarrow 2$ and $2 \rightarrow 3$ processes for some possible choices in PYTHIA and ARIADNE. The Q^2 value sets the scale not only for the hard scattering process, but also for the initial state parton shower. For the $2 \rightarrow 1$ production, the Q^2 scale is naturally set to be the mass of the Higgs boson mass. The uncertainty in the acceptance due to scale choice for the $gg \rightarrow b\bar{b}H$ production mechanism is about 60% in the case of PYTHIA and 25% in the case of ARIADNE parton shower model. For the exclusive process $gb \rightarrow bH$, the uncertainties are 75% and 100%, respectively.

3 $gg \rightarrow H$ at the LHC: Uncertainty due to a Jet Veto

In the Higgs mass range between 155 and 180 GeV, $H \rightarrow W^+W^- \rightarrow \ell\nu\ell\nu$ is considered to be the main Higgs discovery channel [18, 19]. The signal consists of two isolated leptons with large missing E_T and

³It should be stressed, that the problem of the efficiency of b-jet tagging was not touched upon, nor was the problem of the efficiency for the reconstruction of the τ -jet. Discussing these effects, very important for complete experimental analysis, would complicate the problem and dilute the aim of the phenomenological studies presented here.

Table 2: The average transverse momenta of the Higgs boson and acceptance of selection criteria for different scale choices. Events were generated with default initialization of these generators. Events marked PY and AR denote results from PYTHIA and ARIADNE shower model respectively.

Hard process	gb \rightarrow bH			gg \rightarrow bbH			
	default	\hat{s}	$\frac{2\hat{s}\hat{t}\hat{u}}{\hat{s}^2+\hat{t}^2+\hat{u}^2}$	default	m_b^2	m_b^2	\hat{s}
$\langle Q \rangle$ (GeV)	94	257	49	27	4.8	120	255
$\langle p_T^{\text{Higgs}} \text{ (generated)} \rangle$ (GeV)[PY]	32.5	42.7	43.2	27.2	29.8	32.1	36.2
Acceptance (%) [PY]	1.7	2.6	2.96	1.1	1.3	1.4	1.8
$\langle p_T^{\text{Higgs}} \text{ (generated)} \rangle$ (GeV)[AR]	26.0	25.5	44.9	35.8	38.	35.3	34.5
Acceptance (%) [AR]	1.5	1.6	3.1	1.8	2.1	1.7	1.7

with a small opening angle in the plane transverse to the beam, due to spin correlations of the W -pair. In order to reduce the top background, a jet veto has to be applied. The signal over background ratio is found to be around 2:1 for Higgs masses around 165 GeV. For lower and higher Higgs masses, the signal over background ratio decreases slightly [19]. The experimental cross section σ_{meas} of the Higgs signal and other final states is given by:

$$\sigma_{meas} = N_s / (\epsilon_{sel} \times L_{pp}), \quad (1)$$

with N_s being the number of signal events, ϵ_{sel} the efficiency after all signal selection cuts are applied and L_{pp} the proton-proton luminosity. In order to get an estimate of the cross section uncertainty, the statistical and systematic uncertainties have to be determined. The systematic uncertainties come from the experimental selection, background and luminosity uncertainties. As the signal over background ratio is small in the channel under study, the systematic uncertainties should be known precisely. This study concentrates on the uncertainty of the signal efficiency due to the jet veto, by studying the systematics using different Monte Carlo simulations. To do so, four different parton-shower Monte Carlo programs were used, as described in the introduction. The effect of different parton shower models are discussed by comparing PYTHIA 6.225 [3] and HERWIG 6.505 [2], whereas the comparison to MC@NLO 2.31 [6] leads to an uncertainty estimate of higher-order effects⁴. Then, also CASCADE 1.2009 [9] is studied to compare the DGLAP approach to the CCFM formalism.

Jets are reconstructed using an iterative cone algorithm with a cone size of 0.5. The leading particle (seed) of the jet is required to have a p_T larger than 1 GeV. The pseudo-rapidity $|\eta|$ of the jet should be smaller than 4.5, corresponding to the CMS detector acceptance [20]. The event is rejected if it contains a jet with a p_T higher than 30 GeV. The Higgs mass for this study was chosen to be 165 GeV, corresponding to the region of phase space with the highest signal over background ratio. First, all events are studied without considering the underlying event. Finally, PYTHIA is also studied including different underlying event schemes.

3.1 Matrix Element Corrections

At leading order, the transverse momentum of the Higgs boson, p_T^{Higgs} , is zero. However, parton shower Monte Carlos emit soft gluons which balance the Higgs and introduce a transverse momentum in LO parton shower Monte Carlos. As the Higgs is balanced by jets, the transverse momentum is very sensitive to the jet veto and therefore also the efficiency of a jet veto depends strongly on p_T^{Higgs} .

In Fig. 3, the normalized p_T^{Higgs} spectra are shown for PYTHIA, HERWIG and MC@NLO. HERWIG and MC@NLO are very similar at low p_T , as can be seen on the linear scale, which is to be expected as the soft and collinear emissions of MC@NLO are treated by HERWIG. Figure 4 shows that PYTHIA

⁴In the following, HERWIG and PYTHIA use the pdf-set CTEQ5L, whereas MC@NLO uses CTEQ5M.

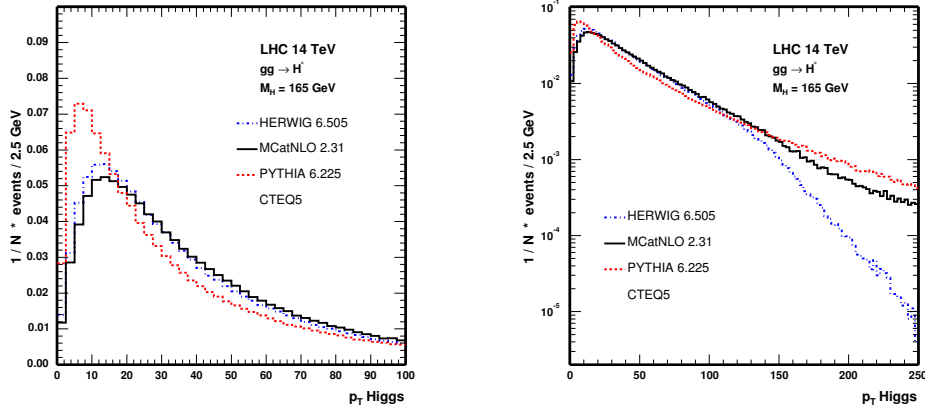


Fig. 3: p_T^{Higgs} spectra for PYTHIA, HERWIG and MC@NLO in linear and logarithmic scale.

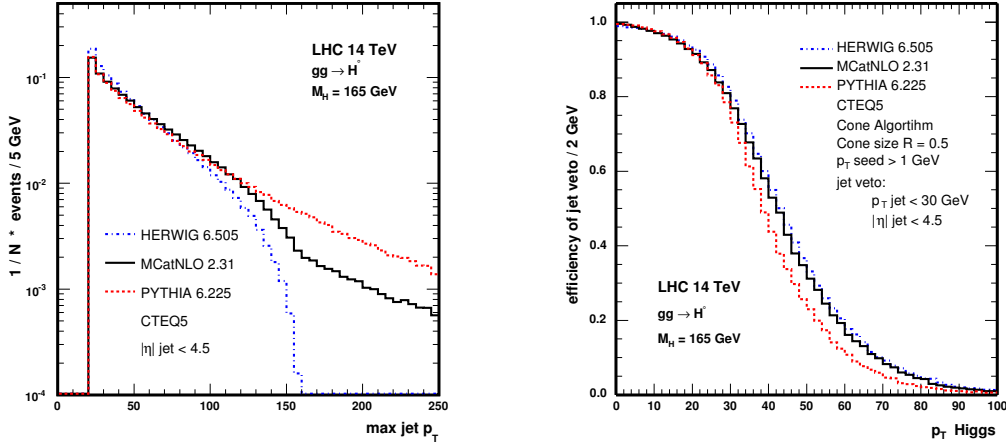


Fig. 4: p_T of the leading jet for PYTHIA, HERWIG and MC@NLO

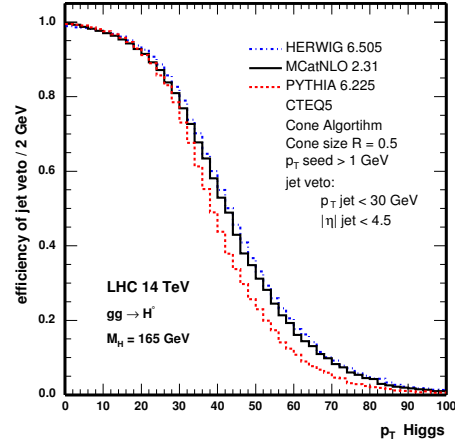


Fig. 5: Efficiency of the jet veto of 30 GeV as a function of p_T^{Higgs} .

predicts a softer leading jet spectrum than HERWIG and therefore also a softer p_T^{Higgs} spectrum. HERWIG implements angular ordering exactly and thus correctly sums the LL (Leading Log) and part of the $N^k LL$ (Next-to-Leading Log) contributions. However, the current version of HERWIG available does not treat hard radiations in a consistent way. Hence the spectrum drops quickly at high p_T , see Fig. 3b). PYTHIA on the other hand does not treat angular ordering in an exact way, but includes hard matrix element corrections. Therefore PYTHIA looks more similar to MC@NLO at high p_T . MC@NLO correctly treats the hard radiation up to NLO, combining the high p_T spectrum with the soft radiation of HERWIG.

In Fig. 5, the efficiency of the jet veto is shown for the three different Monte Carlos as a function of p_T^{Higgs} . One observes a strong dependency of p_T^{Higgs} on the jet veto. Once a jet veto is defined, the efficiency starts to drop quickly as soon as p_T^{Higgs} is close to the p_T used to define a jet veto. However, as the transverse momentum of the Higgs can be balanced by more than one jet, the efficiency is not zero above this value.

G. Corcella provided a preliminary version of HERWIG including hard matrix element corrections for $gg \rightarrow H$ [21]. The hard matrix element corrections lead to harder jets, see Fig. 6, and therefore the jet

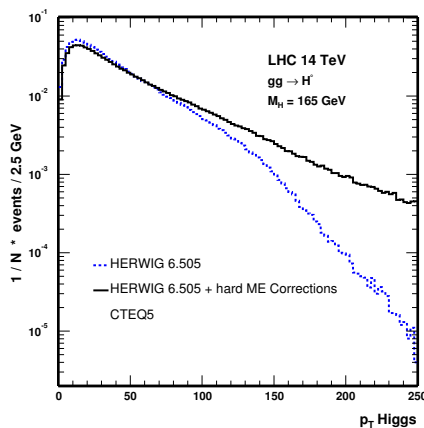


Fig. 6: HERWIG with and without hard Matrix Element Corrections, logarithmic scale.

Table 3: Efficiency of jet veto for MC@NLO, PYTHIA, HERWIG, HERWIG + ME Corrections and CASCADE

	Efficiency for events with a p_T Higgs between 0 and 80 GeV	Inclusive efficiency (all events)
MC@NLO 2.31	0.69	0.58
PYTHIA 6.225	0.73	0.62
HERWIG 6.505	0.70	0.63
HERWIG 6.505 + ME Corrections	0.68	0.54
CASCADE 1.2009	0.65	0.55

veto is more effective. At high p_T , PYTHIA and HERWIG now show very similar predictions. Table 3 shows the efficiencies of the jet veto of 30 GeV for MC@NLO, PYTHIA and HERWIG with and without matrix element corrections. In addition, the numbers for CASCADE are shown, which will be discussed in more detail later. In the first row, the number of the efficiency for p_T^{Higgs} between 0 and 80 GeV is shown. The second column shows the inclusive efficiency for all events. One has to keep in mind that after all selection cuts, only the low p_T region is important [19].

In order to estimate the effect from the detector resolution on the jet veto, the E_T of the jet is smeared with the jet resolution of e.g. CMS, as given by [20]:

$$\Delta E_T / E_T = 118\% / \sqrt{E_T} + 7\%. \quad (2)$$

More jets at initially low p_T are shifted to higher p_T than vice versa, as the jets are generally soft. However, the effect of the smearing is limited and the difference between the smeared and unsmeared case is smaller than 1%.

In the last years, a lot of progress has been made in understanding the Higgs boson production and decays on a theoretical basis. The gluon fusion cross section has been calculated up to NNLO [22]. Such corrections are known to increase the LO cross section by a factor of more than two. In order to include these higher order corrections in a parton shower Monte Carlo, each event is reweighted with its corresponding p_T -dependent effective K-factor (which includes all selection cuts) [19]. This technique can be applied to other processes which are sensitive to jet activity, e.g. the WW background for this channel. The result is an overall effective K-factor of 2.04 for a Higgs mass of 165 GeV, which is only

Table 4: Efficiency numbers for different underlying event tunings in PYTHIA.

	Efficiency for events with a p_T Higgs between 0 and 80 GeV	Inclusive efficiency (all events)
PYTHIA no UE	0.730	0.620
PYTHIA default	0.723	0.613
ATLAS tune	0.706	0.600
CDF tune	0.709	0.596

about 15% lower than the inclusive K-factor (without any cuts) for the same mass. This reweighting method allows to optimize the selection cuts and thus also helps to improve the discovery potential. We observe that the uncertainty of the jet veto efficiency does not change significantly including those higher order corrections.

3.2 Underlying Event

So far all events were generated without considering the underlying event. However, to study a jet veto, it is important to consider also the effect of the underlying event. Therefore, PYTHIA was studied with different underlying event tuning schemes, which are the ATLAS Tune [23], CDF Tune A [24] and PYTHIA default (MSTP(81)=1, MSTP(82)=3 [3]). The different tunings lead to approximately the same efficiency, and also the difference in the efficiency with and without underlying event is smaller than 1%, see Table 4.

3.3 Comparing to CCFM evolution

Finally, we compared the PYTHIA, HERWIG and MC@NLO predictions with the ones obtained using CASCADE. One has to keep in mind that this Monte Carlo is dedicated to low- x physics, and is about to be released for LHC physics applications. There were many improvements implemented during this workshop. In Fig. 7, the p_T^{Higgs} spectra for PYTHIA, HERWIG+ME Corrections, MC@NLO and CASCADE are shown. The prediction from CASCADE lies within the ones from PYTHIA and HERWIG. When looking at different p_T regions, one generally observes that CASCADE produces more jets compared to the other Monte Carlos, and the jets are harder. The jet veto efficiency as a function of the p_T of the Higgs is shown in Fig. 8, indicating that the main differences are in the low p_T range and that the efficiency for CASCADE is slightly smaller than unity at a p_T^{Higgs} of zero. A reason for this is that the Higgs boson is balanced by more than one jet, with at least one of the jets with a p_T higher than 30 GeV and thus vetoed. For the same reason, the efficiency in general is lower than for the other Monte Carlo programs at low p_T^{Higgs} . Results in the high p_T region have to be studied carefully.

4 Forward Studies with CASCADE at LHC Energies

The applicability of DGLAP evolution [7] is known to be limited in the very forward region, that is at small values of Bjorken- x , where $\ln(x)$ terms are expected to become large [25]. Since the partons at the bottom of the ladder (furthest away from the hard scatter) are closest in rapidity to the outgoing proton, effects might be expected in the forward region. The CCFM evolution [8] takes these BFKL-like terms into account, and is implemented in the CASCADE Monte Carlo program [9].

We have studied the topology of forward particle and jet production in the LHCb detector at the LHC. LHCb is a forward spectrometer covering roughly the forward region $1.8 < \eta < 4.9$ [26]. Its main goal is the study of CP violation in the B -meson sector and the measurement of rare B -decays. But its very nature makes LHCb a suitable environment for QCD forward studies.

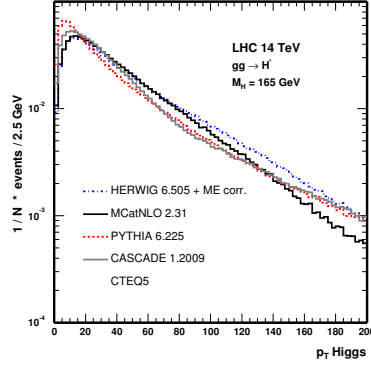
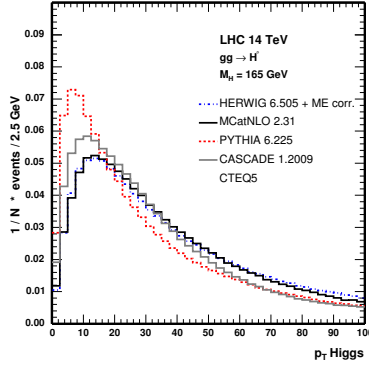


Fig. 7: p_T^{Higgs} Higgs of PYTHIA, HERWIG + ME Corrections, MC@NLO and CASCADE, linear and logarithmic scale.

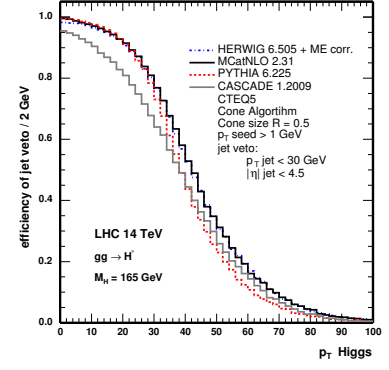


Fig. 8: Efficiency as a function of p_T for PYTHIA, HERWIG+ME Corrections, MC@NLO and CASCADE.

The usage of another Monte Carlo program in LHCb is important in order to estimate the uncertainty on the PYTHIA [3] predictions. In particular, the track multiplicity seen in the detector is an important factor to take into account, as it affects the performance of the trigger, the tracking and the B -tagging. But here we will concentrate on another aspect: the study of the QCD evolution itself, proving that LHCb has the potential to be a natural test bed of QCD in the forward region, complementing the studies done at present at the Tevatron and the future studies to be made with the central detectors – ATLAS and CMS – at the LHC. The predictions in the forward region as given by CASCADE are here compared with that of PYTHIA, the default Monte Carlo generator used in LHCb. This is a “natural” way to test CCFM versus DGLAP QCD evolution in the region of the phase space where differences are most likely to show.

In what follows we will compare both predictions for the event kinematics and topology, and the particle and jet production. We used CASCADE version 1.2009 “out of the box” and PYTHIA 6.227 with the LHCb tune. We used for the comparisons a sub-sample of the QCD processes of PYTHIA, as CASCADE only includes (unintegrated) gluons. PYTHIA was run with the only sub-processes $fg \rightarrow fg$, $gg \rightarrow ff$ and $gg \rightarrow gg$, and multiple interactions (MI) were also switched off, since they are as yet not implemented in CASCADE; this version is denoted “*PYTHIA gluon*” in the plots. Another configuration named “*PYTHIA gluon incl MI*” has the multiple interactions switched on, for a cross-check of the influence of such inclusion. All the plots refer to minimum bias events.

4.1 Event Kinematics

Figure 9 shows the kinematic variables Q^2 and Bjorken- x variables x_1 and x_2 (referring to both LHC proton beams of energy E_p), using the definitions given below. For PYTHIA the standard definitions from the PYPARS common block were used:

$$x_1 = \text{PARI}(33) \quad x_2 = \text{PARI}(34);$$

$$Q^2 = \text{PARI}(18),$$

whereas for CASCADE we set ⁵:

$$x_{1,2} = \frac{(E + |p_z|)_{in. parton 1,2}}{2E_p};$$

⁵The two incoming partons in the hard interaction are obtained from the variables NIA1 and NIA2, corresponding to the positions 4 and 6 in the CASCADE event record, whereas the outgoing partons are at positions 7 and 8.

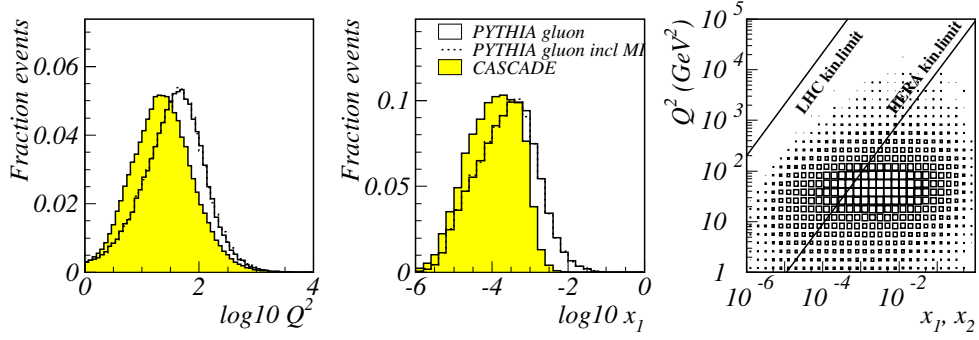


Fig. 9: Comparison between CASCADE and PYTHIA for the general event kinematics variables (refer to the text for the definitions). Note that $x_1 < x_2$ by construction.

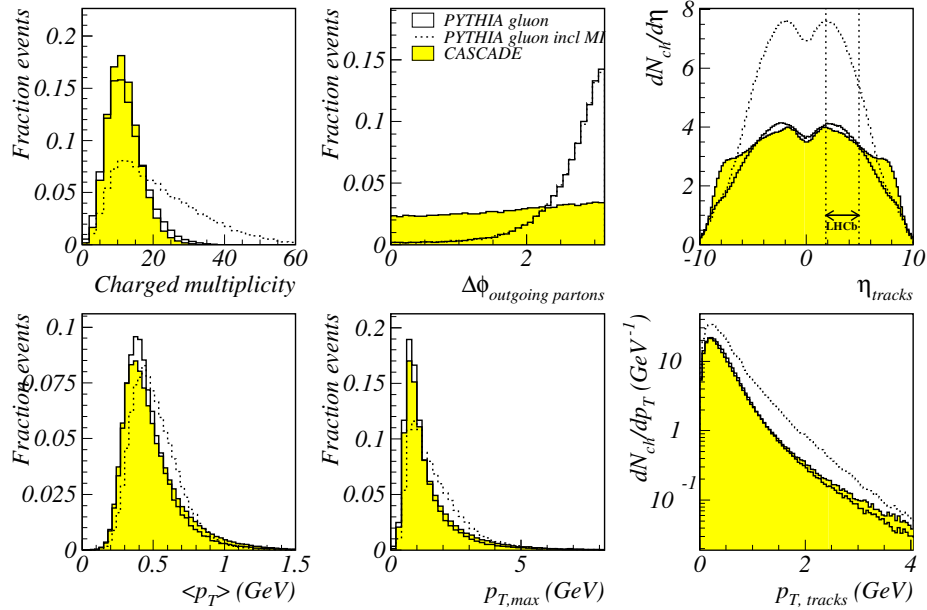


Fig. 10: Comparison between CASCADE and PYTHIA for general event variables, and between charged tracks variables in the region of the LHCb acceptance defined as $1.8 < \eta < 4.9$. No acceptance cuts are applied on the $\Delta\phi$ and η_{tracks} distributions.

$$Q^2 = p_{T, out. parton}^2.$$

There is a reasonable agreement between both Monte Carlo programs, although a direct comparison seems difficult and unnatural given the definitions above. The phase space spanned by the kinematic variables $x_{1,2}$ and Q^2 is shown also in Fig. 9 for PYTHIA.

4.2 Forward Particle Production

Some general event variables are compared in Fig. 10 in the region of the LHCb acceptance, $1.8 < \eta < 4.9$, including the charged track multiplicity, the acoplanarity ($\Delta\phi$) of the outgoing partons, the average track transverse momentum in the event $\langle p_T \rangle$ and the maximum track transverse momentum $p_{T,max}$. The predictions from both Monte Carlo programs agree well – neglecting the multiple interactions in PYTHIA – likely because the same final state parton showering is performed. The effect of including the multiple interactions is seen mainly in the event multiplicity, as expected. Interesting is the distribution of the acoplanarity of the two outgoing partons: PYTHIA predicts a strong (anti-)correlation whereas CASCADE exhibits a distribution that is nearly flat.

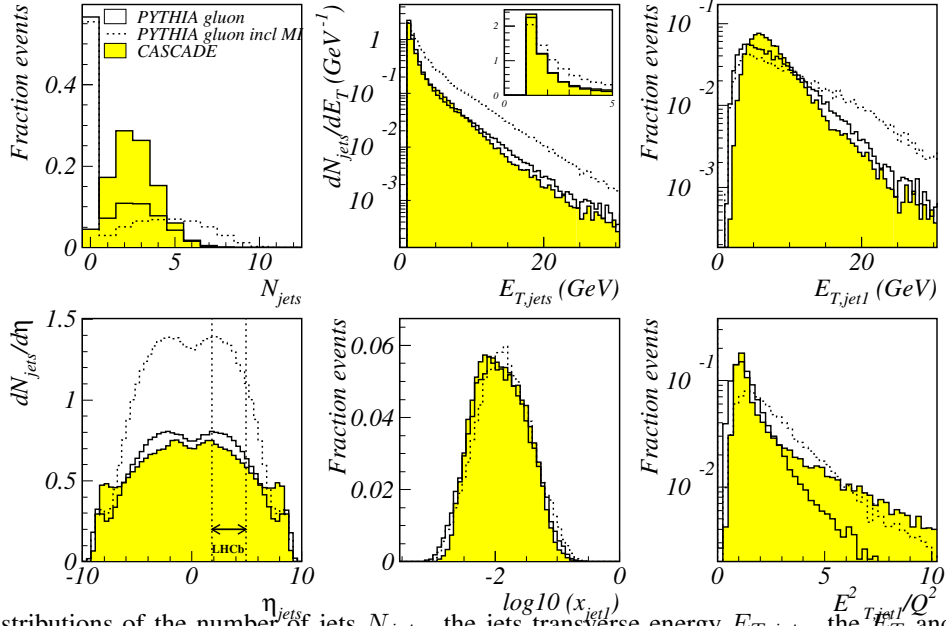


Fig. 11: Distributions of the number of jets N_{jets} , the jets transverse energy $E_{T,jets}$, the E_T and x_{jet} of the highest- E_T jet, $jet1$, all in the LHCb acceptance. Also the number of jets per unit pseudorapidity is shown. The distribution of the ratio of $E_{T,jet}^2/Q^2$ in the LHCb acceptance shows a comparison of the two scales. Jets were selected with $E_{T,jet} > 1$ GeV.

The number of charged tracks per unit rapidity, $dN/d\eta_{tracks}$, and the differential distribution of the number of charged tracks (in the LHCb acceptance) as a function of the transverse momentum $p_{T,tracks}$ are also included in Fig. 10. Note that these 2 distributions were normalized to the mean track multiplicity in the full and LHCb acceptance, respectively. The p_T distributions compare very well, leading us to conclude that the general hard dynamics of the event is predicted in a rather similar way by both programs. CASCADE however, produces more forward tracks than PYTHIA, as the η -distribution is clearly flatter than the rather steep distribution of PYTHIA. This is particularly true in the region $5 < \eta < 8$, just beyond the acceptance of the LHCb spectrometer – shown between the 2 vertical dashed lines –, but could make LHCb a candidate environment to discriminate between the two predicted forward behaviours.

4.3 Forward Jet Production

We have also looked at jet production. Jets were found in the laboratory frame with the KTCLUS algorithm on all stable hadrons, in the longitudinally invariant inclusive mode. We looked at the jet production in the LHCb acceptance with a rather loose selection of $E_{T,jets} > 1$ GeV. The number of jets found in PYTHIA or CASCADE is shown in Fig. 11. The number of events with no jets satisfying $E_{T,jet} > 1$ GeV inside $1.8 < \eta < 4.9$ is much larger for PYTHIA. In other words, CASCADE predicts a jet cross-section larger than PYTHIA, a fact already shown by the HERA experiments in low- x jet analyses. This difference leads us to believe that strong angular ordering in CASCADE favours a “clustered production” of particles and therefore the production of jets, whereas PYTHIA tends to give a more spreaded transverse energy flow. Furthermore, though the effect is small, we already saw from Fig. 10 that the highest- p_T track is somewhat softer in PYTHIA compared to CASCADE.

The rapidity distribution and the transverse energy distribution of the jets is also shown in Fig. 11; they have been normalized to the average number of jets per event in the full acceptance and LHCb acceptance, respectively. PYTHIA and CASCADE predict similar jets in the LHCb acceptance, but the inclusion of multiple interactions gives a harder spectrum.

Also shown are the event distributions in the LHCb acceptance of the highest- E_T jet in the event, $E_{T,jet1}$, and the energy fraction of the proton carried by the highest- E_T jet, $x_{jet1} = E_{jet1}/E_p$. The hardest jet in the event is on average harder in CASCADE compared to PYTHIA. The distributions of x_{jet} and $E_{T,jet}^2/Q^2$ are interesting in that they correspond to variables now in standard use within the HERA experiments as a means of selecting samples where forward effects are expected. Indeed both experiments have published a series of “forward QCD” analyses [25] applying cuts of the kind $E_{T,jet}^2 \sim Q^2$ and $x_{jet} \gg x_{Bjorken}$. The phase space is selected such that it suppresses jet production via DGLAP evolution and enhances production from BFKL dynamics:

- DGLAP evolution is suppressed in the small phase space for Q^2 evolution requiring $E_{T,jet}^2 \sim Q^2$;
- CCFM evolution enhanced when large phase space for x evolution requiring $x_{jet} \gg x_{Bjorken}$.

At the LHC such a selection becomes rather delicate, since there are two proton beams and the comparison of x_{jet} with $x_{Bjorken}$ gets an ambiguity between the choice of x_1 or x_2 . A way out – though it lowers significantly the statistics – would be to make the selection based on $x_{jet} \gg \max(x_1, x_2)$. From the distributions presented in this paper we are lead to believe that such a forward selection is indeed possible. But we leave this issue open for further investigation.

5 Summary

Various ways of treating parton showers have been compared, as implemented by the HERWIG, PYTHIA and ARIADNE Monte Carlo programs. We have studied the uncertainties that arise from these different models to the p_T -spectrum of the jets, and the p_T -spectrum of the Higgs boson.

The theoretical systematic uncertainty on predictions for inclusive cross section at NNLO for Higgs production with bbH Yukawa coupling is under good theoretical control with an uncertainty of about 15% for a Higgs mass around 120 GeV. However, the predictions for the exclusive cross section determined by the event selection of a simplified experimental analysis indicates at present an order by magnitude larger uncertainty in e.g. $H \rightarrow \tau\tau$ events. Uncertainties due to the shower model can reach 170% and depend strongly on the production mechanism. Another factor of two arises from the choice of the QCD scale. Higher order Monte Carlo generators will therefore be mandatory to achieve better precision on the theoretical predictions.

On the other hand, the uncertainty of the jet veto efficiency in the $H \rightarrow WW \rightarrow l\nu l\nu$ decay channel by using different Monte Carlo generators in the $gg \rightarrow H$ process is estimated to be around 10%. Including higher order QCD corrections does not enhance the uncertainty significantly. Also the effect of including a realistic jet- E_T resolution is very small. The effect of including an underlying event in the simulation is smaller than 1%, and does not vary significantly for various tuning models.

Furthermore we have studied the predictions at the LHC using the CCFM formalism as implemented in the full hadron level Monte Carlo generator. We conclude that CASCADE produces more and harder jets compared to the other Monte Carlo programs, leading to a bigger uncertainty of the jet veto efficiency in the small p_T^{Higgs} range. In the forward region larger differences are expected between the DGLAP and CCFM approach, but in the moderate forward rapidity range $2 < \eta < 5$, as covered by the LHCb detector, a fairly good agreement between CASCADE and PYTHIA is observed for most of the distributions looked at, and despite their different philosophies. However, this result has to be treated with care, as the program is only recently developed for proton physics at such high energies as produced in the future LHC. It also comes out of this simple study that CASCADE is indeed a potential Monte Carlo tool to use for QCD studies at the LHC in the forward region. In the future one should further investigate regions of phase space where large differences in behaviour are expected at the LHC from DGLAP and BFKL dynamics. LHCb seems a natural experimental environment in which to study such differences.

Finally, we would like to encourage the community by stating that it is very interesting and instruc-

tive to study the predictions at the LHC by using tools developed and tuned at HERA, such as the CCFM Monte Carlo CASCADE, and by using parton shower models such as ARIADNE, that have proven their validity at HERA.

References

- [1] S. Höche *et al.*, *Matching parton showers and matrix elements*. These proceedings.
- [2] G. Corcella *et al.*, JHEP **0101**, 010 (2001).
- [3] T. Sjöstrand *et al.*, Comput. Phys. Commun. **135**, 238 (2001).
- [4] L. Lönnblad, Comput. Phys. Commun. **71**, 15 (1992).
- [5] ZEUS Collaboration, S. Chekanov *et al.*, Eur. Phys. J. **C27**, 531 (2003).
- [6] S. Frixione and B. Webber, JHEP **0206**, 029 (2002).
- [7] V. Gribov and L. Lipatov, Sov. J. Nucl. Phys. **15**, 438 and 675 (1971);
G. Altarelli and G. Parisi, Nucl. Phys. **B126**, 298 (1977);
Y. L. Dokshitzer, Sov. Phys. JETP **46**, 641 (1977).
- [8] M. Ciafaloni, Nucl. Phys. **B296**, 49 (1988);
S. Catani, F. Fiorani, and G. Marchesini, Nucl. Phys. **B336**, 18 (1990).
- [9] H. Jung, Comput. Phys. Commun. **143**, 100 (2002).
- [10] J. Collins *et al.*, *Unintegrated parton density functions*. These proceedings.
- [11] R. Harlander and W. Kilgore, Phys. Rev. **D68**, 013001 (2003).
- [12] J. Campbell, R. K. Ellis, F. Maltoni, and S. Willenbrock, Phys. Rev. **D67**, 095002 (2003).
hep-ph/0204093.
- [13] ATLAS Collaboration, *Detector performance and physics potential TDR*, 1999.
CERN-LHCC-99-15, vol.II, ch.19.
- [14] E. Richter-Was, T. Szymocha, and Z. Was, Phys. Lett. **B589**, 125 (2004). hep-ph/0402159.
- [15] E. Richter-Was, *AcerDET: a particle level fast simulation and reconstruction package for phenomenological studies on high p_t physics at LHC*. Preprint hep-ph/0207355, 2002.
- [16] B. Kersevan and E. Richter-Was, *The Monte Carlo event generator AcerMC 2.0 with interfaces to PYTHIA 6.2 and HERWIG 6.5*. Preprint hep-ph/0405247, 2004.
- [17] *LHAPDF online manual*, available on <http://durpdg.dur.ac.uk/lhapdf>.
- [18] M. Dittmar and H. Dreiner, Phys. Rev. **D55**, 167 (1997).
- [19] G. Davatz, G. Dissertori, M. Dittmar, M. Grazzini, and F. Pauss, JHEP **05**, 009 (2004).
- [20] CMS Collaboration, *CMS TDR 6.2*, 2002. CERN-LHCC-2002-26, ch.15, p.317.
- [21] G. Corcella and S. Moretti, Phys. Lett. **B590**, 249 (2004).
- [22] S. Catani, D. de Florian, and M. Grazzini, JHEP **0105**, 025 (2001);
R. V. Harlander and W. B. Kilgore, Phys. Rev. **D64**, 013015 (2001);
R. V. Harlander and W. B. Kilgore, Phys. Rev. Lett. **88**, 201801 (2002);
C. Anastasiou and K. Melnikov, Nucl. Phys. **B646**, 220 (2002);
C. Anastasiou and K. Melnikov, Phys. Rev. Lett. **93**, 262002 (2004);
J. S. V. Ravindran and W. L. van Neerven, Nucl. Phys. **B665**, 325 (2003).
- [23] I. D. A. Moraes, C. Buttar and P. Hodgson, available on
<http://amoraes.home.cern.ch/amoraes/>. ATLAS internal notes.
- [24] R. Field, available on <http://www.phys.ufl.edu/rfield/cdf/>. CDF Note 6403.
- [25] ZEUS Collaboration, S. Chekanov *et al.* (2005). hep-ex/0502029;
H1 Collaboration, C. Adloff *et al.*, Nucl. Phys. **B38**, 3 (1999).
- [26] LHCb Collaboration, *LHCb reoptimized detector design and performance TDR*, 2003.
CERN-LHCC-2003-030.

Unintegrated parton density functions

John Collins¹, Markus Diehl², Hannes Jung², Leif Lönnblad³, Michael Lublinsky⁴, Thomas Teubner⁵

¹ Physics Department, Penn State University, U.S.A.

² Deutsches Elektronen-Synchrotron Hamburg, FRG

³ Department of Theoretical Physics, Lund University, Sweden

⁴ University of Connecticut, U.S.A.

⁵ University of Liverpool, U.K

Abstract

An overview on activities to determine unintegrated parton density functions is given and the concept and need for unintegrated PDFs is discussed. It is also argued that it is important to reformulate perturbative QCD results in terms of fully unintegrated parton densities, differential in all components of the parton momentum. Also the need for non-linear BFKL evolution is discussed and results using the BK equation supplemented by DGLAP corrections at short distances is reviewed. Finally the use unintegrated generalized parton distributions for hard diffractive processes is discussed.

1 Unintegrated parton density functions¹

The parton distributions of hadrons still cannot be calculated from first principles, but have to be determined experimentally. However, once the initial distributions $f_i^0(x, \mu_0^2)$ at the hadronic scale ($\mu^2 \sim 1 \text{ GeV}^2$) are determined, different approximations allow to calculate the parton density functions (PDFs) for different kinematic regions:

- DGLAP [1–4] describes the evolution with the scale μ^2
- BFKL [5–7] describes the evolution in the longitudinal momenta x
- CCFM [8–11] describes the evolution in an angular ordered region of phase space while reproducing DGLAP and BFKL in the appropriate asymptotic limits

The different evolution equations attempt to describe different regions of phase space on the basis of in perturbative QCD (pQCD).

1.1 Introduction to uPDFs and k_\perp factorization

In the collinear factorization ansatz the cross sections are described by x -dependent density functions $f_i(x, \mu^2)$ of parton i at a given factorization scale μ convoluted with an (on-shell) coefficient function (matrix element):

$$\sigma(a + b \rightarrow X) = \int dx_1 dx_2 f_i(x_1, \mu^2) f_j(x_2, \mu^2) \hat{\sigma}_{ij}(x_1, x_2, \mu^2) \quad (1)$$

with $\hat{\sigma}_{ij}(x_1, x_2, \mu^2)$ being the hard scattering process for the partons $i + j \rightarrow X$. In this equation we have left implicit all external kinematic variables, keeping only the variables used in the parton densities. This ansatz is very successful in describing inclusive cross sections, such as the structure function $F_2(x, Q^2)$ at HERA or the inclusive production of vector bosons or Drell-Yan in proton proton collisions. The free parameters of the starting distributions $f_i^0(x, \mu_0^2)$ are determined such that after a DGLAP evolution to the scale $\mu^2 = Q^2$ and convolution with the coefficient functions the measured structure function

¹Authors: Hannes Jung and Leif Lönnblad.

$F_2(x, Q^2)$ at HERA (and, usually, some other cross sections, e.g., in hadron-hadron and neutrino-hadron scattering) are best described.

However, as soon as, for example, final-state processes are considered, the collinear factorization ansatz becomes more and more unreliable, because neglecting the transverse momenta of the partons during the (DGLAP) evolution leads to inconsistencies, as will be discussed in more detail in section 2. Collinear factorization is only appropriate when (a) the transverse momentum (and virtuality) of the struck parton(s) can be neglected with respect to Q , and (b) the integrals over these variables can be treated as independent and unrestricted up to the scale Q . (Certain complications concerning high transverse momentum partons are correctly treated by NLO and higher corrections to the hard scattering.) When these requirements are not met, a more general treatment using unintegrated parton densities (uPDFs) is better.

For example, in the small x regime, when the transverse momenta of the partons are of the same order as their longitudinal momenta, the collinear approximation is no longer appropriate and high energy or k_\perp - factorization has to be applied, with the appropriate BFKL or CCFM evolution equations. Cross sections are then k_\perp - factorized [12–15] into an off-mass-shell (k_\perp - dependent) partonic cross section $\hat{\sigma}(x_1, x_2, k_{\perp 1}, k_{\perp 2})$ and a k_\perp - unintegrated parton density function (uPDF) $\mathcal{F}(z, k_\perp)$:

$$\sigma = \int dx_1 dx_2 d^2 k_{\perp 1} d^2 k_{\perp 2} \hat{\sigma}_{ij}(x_1, x_2, k_{\perp 1}, k_{\perp 2}) \mathcal{F}(x_1, k_{\perp 1}) \mathcal{F}(x_2, k_{\perp 2}) \quad (2)$$

The unintegrated gluon density $\mathcal{F}(z, k_\perp)$ is described by the BFKL evolution equation in the region of asymptotically large energies (small x). It is important to note that only when the k_\perp dependence of the hard scattering process $\hat{\sigma}$ can be neglected, i.e. if $\hat{\sigma}(x_1, x_2, k_{\perp 1}, k_{\perp 2}) \sim \hat{\sigma}(x_1, x_2, 0, 0)$, then the k_\perp integration can be factorized and an expression formally similar to eq.(1) is obtained.

An appropriate description valid for both small and large x , is given by the CCFM evolution equation, resulting in an unintegrated gluon density $\mathcal{A}(x, k_\perp, \mu)$, which is a function also of the additional evolution scale μ . This scale is connected to the factorization scale in the collinear approach.

Further examples where uPDFs are needed are the Drell-Yan and related processes at low transverse momentum, as in the CSS formalism [16]. However, the relation between CSS method (which does not need small x) and k_\perp -factorization of the BFKL/CCFM kind (for small x) has not yet been properly worked out.

1.2 Extraction and determination of uPDFs

In this section we will review how measurements of uPDFs have been extracted from DIS data at small x , mostly from the inclusive structure function F_2 . For measurements of the uPDFs in Drell-Yan processes using the CSS formalism, see [17].

From the DIS data, the uPDF can be obtained by adjusting the non-perturbative input distribution $f_i^0(x, \mu_0^2)$ and the free parameters of the perturbative evolution such that after convolution with the appropriate off-shell matrix element (according to eq.(2)) a measured cross section is best described.

Applying k_\perp -factorization to determine the uPDF from DIS data until now mainly the inclusive structure function measurements of $F_2(x, Q^2)$ at HERA have been used. The exceptions are those which are simply derivatives of integrated PDFs, which then neglects fully the transverse momentum dependence of the matrix element. Extracting a uPDF from the integrated PDF is appropriate only if the k_\perp -dependence of the hard scattering process $\hat{\sigma}$ in eq.(2) can be neglected. In addition, contributions from $k_\perp > \mu$, which are present in a full calculation, are entirely neglected. It thus can only provide an estimate of the proper kinematics in the collinear approach, which is otherwise fully neglected when using integrated PDFs.

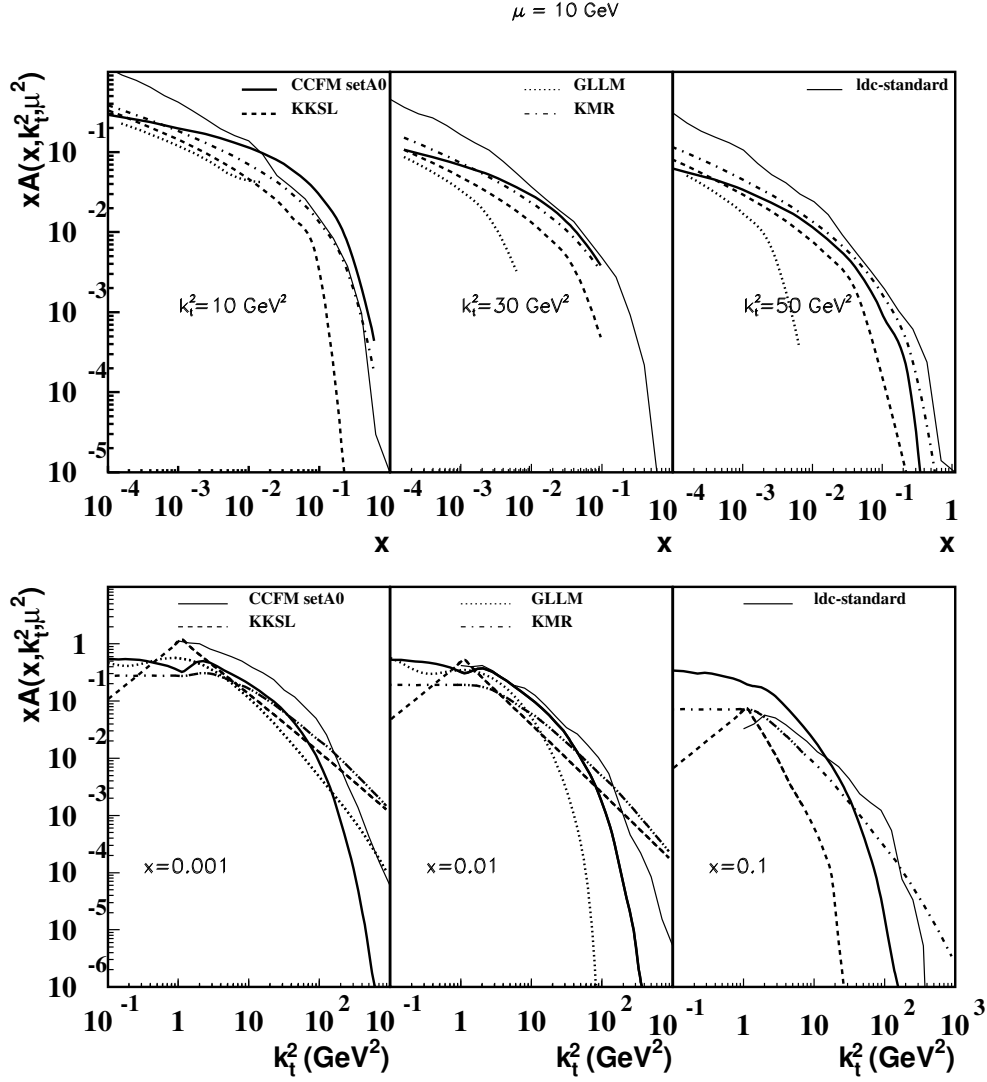


Fig. 1: Comparison of different uPDFs at $\mu = 10 \text{ GeV}$.

Here we compare some of these parameterizations which have been obtained in different ways:

- **CCFM set A0** was obtained using CCFM evolution in [18, 19].
- **LDC standard** was similarly obtained in [20] using LDC evolution [21], which is a reformulation and generalization of CCFM.
- **KKSL** [22] was obtained from a combined BFKL and DGLAP evolution following [23].
- **GLLM** [24] was obtained applying the BK equation to HERA F_2 measurements, as described in Section 3.
- **KMR** is one of the more advanced derivatives of integrated PDFs, using Sudakov form factors [25].

In Fig. 1 we show a comparison of the different uPDFs as a function of x and k_{\perp} at a factorization scale $\mu = 10 \text{ GeV}$. All the parameterizations are able to describe the measured $F_2(x, Q^2)$ in the small x range reasonably well, with a $\chi^2/ndf \sim 1$. In Fig. 2 the same uPDFs are compared at a factorization scale which is relevant at LHC energies, e.g. for inclusive Higgs production ($\mu = 120 \text{ GeV}$). One should note that the uPDFs from KKSL and GLLM have no explicit factorization scale dependence, therefore they are the same as in Fig 1.

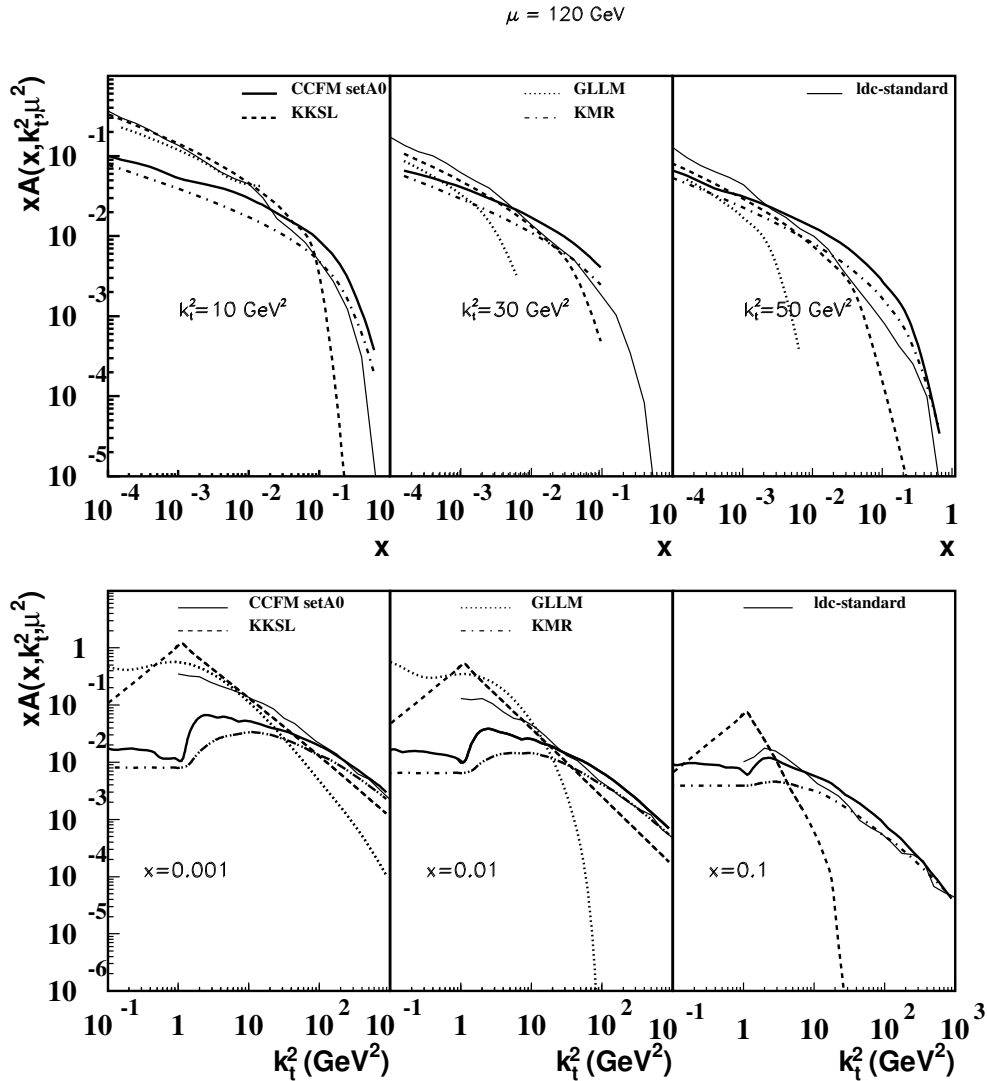


Fig. 2: Comparison of different uPDFs at $\mu = 120 \text{ GeV}$.

1.3 Extrapolation to LHC energies

All the parameterizations of uPDFs considered in this report give a fairly good fit to HERA F_2 data. This means that they are well constrained mainly in the region of small x and relatively small Q^2 , where the bulk of the HERA data is concentrated. For higher x and Q^2 , a fit to HERA data is less constraining, and indeed some of the parameterizations based on the CCFM and LDC evolution of the gluon alone are only fitted in the small- x region (typically $x < 0.01$, $Q^2 < 100 \text{ GeV}^2$).

When evolving the uPDFs to apply them to the processes of main interest at the LHC, such as Higgs production, this is a serious concern. Although the x -values in such processes are typically below 0.01, the scales involved are of the order of 10^4 GeV^2 or more. Through the evolution one then becomes sensitive to larger x -values at lower scales where the current parameterizations are less constrained.

A notable exception is the KMR [25] densities which are obtained from a global fit of integrated PDFs, which should give reliable prediction at LHC at least for integrated observables such as the inclusive Higgs cross section. In contrast, it was shown in [20] that the CCFM [8–11] and LDC [21] evolved uPDFs have unreasonably large uncertainties for such cross sections. On the other hand it was also shown in [20] that there are some questions about the constraint of the actual k_{\perp} distribution of the KMR uPDFs resulting eg. in a too soft p_{\perp} spectrum of W or Z production at the Tevatron for small transverse

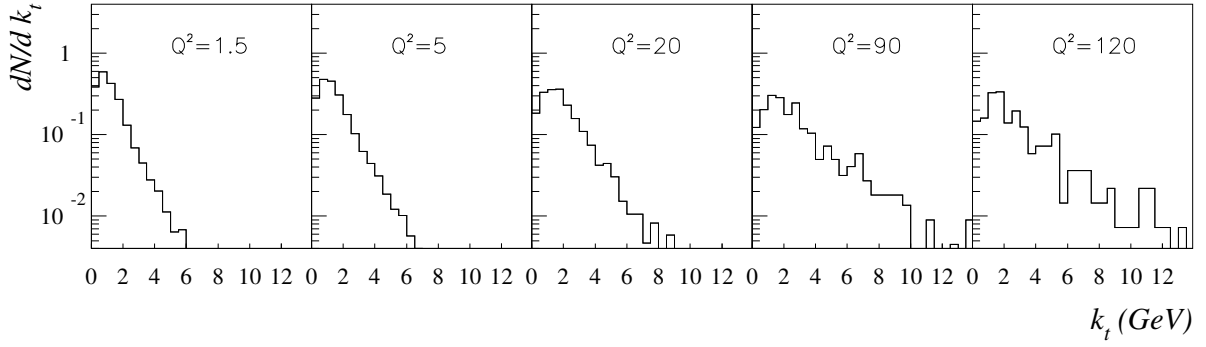


Fig. 3: k_{\perp} distribution in different Q^2 bins used in $F_2(x, Q^2)$ at HERA.

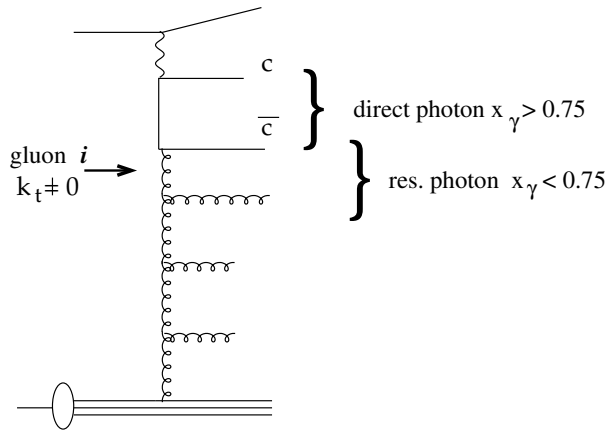


Fig. 4: Diagram of charm photoproduction, showing the sensitivity to the gluon transverse momentum

momenta. Hence, although the KMR prediction for inclusive quantities may be reliable at the LHC, the predictions of eg. the detailed distribution of low- p_{\perp} Higgs may be questionable.

What is needed is clearly to obtain fits of the uPDFs, not only to HERA F_2 data, but also to observables more sensitive to higher x and Q^2 values, as well as to observables directly sensitive to the k_{\perp} distribution. To obtain such global fits there is a need for both theoretical and phenomenological developments. Examples of the former is the inclusion of quarks in the CCFM evolution, while the latter involves the development of k_{\perp} -sensitive observables, where HERA data at small x , such as forward jet or heavy quark production, will play an important role, as discussed in the following.

1.4 Global uPDF fits

Until now the uPDFs obtained from DIS were only determined and constrained by the inclusive structure function $F_2(x, Q^2)$. It is clear that the inclusive measurements are not very sensitive to the details of the k_{\perp} dependence. In Fig. 3 we show the k_{\perp} distribution of the gluon in $\gamma^* g^* \rightarrow q\bar{q}$ which is the relevant process for F_2 at small x . The k_{\perp} -distributions in Fig. 3 are obtained with CASCADE [26,27] using the CCFM uPDFs. The bins in Q^2 are typical for HERA F_2 measurements. It is interesting to observe that even at large Q^2 essentially only the small k_{\perp} region is probed by F_2 .

A larger lever arm for the k_{\perp} distribution can be obtained with photoproduction of $D^* + \text{jet}$ events at HERA. In Fig. 4 the relevant diagram is shown. The quantity x_{γ} , normally designed to separate direct from resolved photon processes, can be also used to distinguish small and large k_{\perp} - regions. The region of large x_{γ} corresponds to measuring jets coming from the quark-box. The region of small x_{γ}

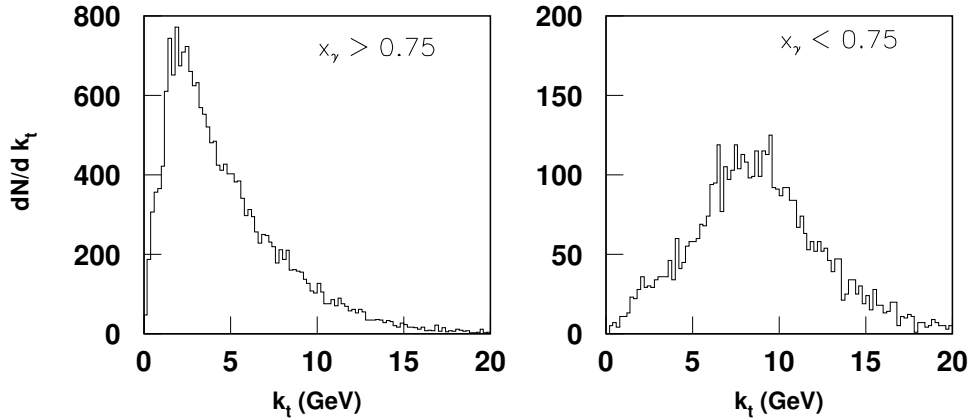


Fig. 5: k_{\perp} distribution in different x_{γ} bins obtained from D^* +jet photo-production at HERA.

corresponds to the situation where one of the jets originates from a gluon, as indicated in Fig. 4. Thus, the transverse momentum of the gluon i can be probed, as shown in Fig. 5 for two different regions of x_{γ} using CASCADE. It is interesting to note that the average k_{\perp} distribution for bottom production at the Tevatron is similar to what it shown in Fig. 5.

To further constrain the uPDF it would be desirable to perform a common fit to inclusive measurements like F_2 and simultaneously to final state measurements.

Once the data sets and the sensitivity to the uPDFs have been identified, a systematic error treatment of the data used in the uPDF fits can be performed. Until now, the uPDFs are not really the result of a fit but rather a proof that the uPDF is consistent with various measurements.

A uPDF fit would require a systematic variation of the parameters used to specify the non-perturbative input gluon distribution as well as a systematic treatment of the experimental systematic uncertainties. Only then an uncertainty band of the uPDFs can be given. To consider the uncertainty of the uPDF given from the spread of different available parameterizations is a very rough estimate.

1.5 Outlook and Summary

Clearly, the extraction of uPDFs from data is still in its infancy, especially if compared to the well developed industry of fitting integrated PDFs. The uPDFs are only leading order parameterizations, they have mainly been fitted to F_2 data at small x , and besides the KMR and LDC parameterizations, no attempts have been made to obtain unintegrated quark densities. Taken together, this means that the applicability to LHC processes are uncertain. However, the field is maturing and we hope to soon be able to do more global uPDF fits which will greatly enhance the reliability of the predictions for the LHC. In doing so the small- x data from HERA will be very important, but also eg. Tevatron data will be able to provide important constraints.

2 Need for fully unintegrated parton densities²

2.1 Introduction

Conventional parton densities are defined in terms of an integral over all transverse momentum and virtuality for a parton that initiates a hard scattering. While such a definition of an integrated parton density is appropriate for very inclusive quantities, such as the ordinary structure functions F_1 and F_2 in DIS, the definition becomes increasingly unsuitable as one studies less inclusive cross sections. Associated

²Authors: John Collins and Hannes Jung.

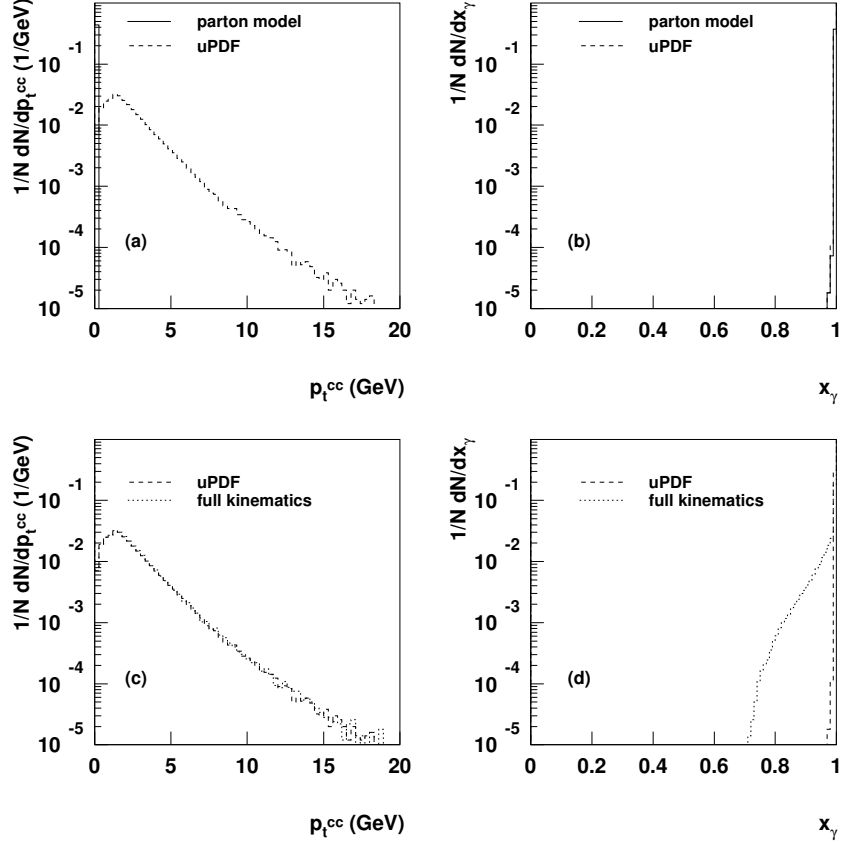


Fig. 6: (a) and (b): comparison between use of simple LO parton model approximation and of the use of k_\perp densities for the p_T of $c\bar{c}$ pairs in photoproduction, and for the x_γ . (c) and (d): comparison of use of k_\perp densities and full simulation.

with the use of integrated parton densities are approximations on parton kinematics that can readily lead to unphysical cross sections when enough details of the final state are investigated.

We propose that it is important to the future use of pQCD that a systematic program be undertaken to reformulate factorization results in terms of fully unintegrated densities, which are differential in both transverse momentum and virtuality. These densities are called “doubly unintegrated parton densities” by Watt, Martin and Ryskin [28, 29], and “parton correlation functions” by Collins and Zu [30]; these authors have presented the reasoning for the inadequacy, in different contexts, of the more conventional approach. The new methods have their motivation in contexts such as Monte-Carlo event generators where final-state kinematics are studied in detail. Even so, a systematic reformulation for other processes to use unintegrated densities would present a unified methodology.

These methods form an extension of k_\perp -factorization. See Sec. 1 for a review of k_\perp -factorization, which currently involves two different formalisms, the BFKL/CCFM methods [5–11] and the CSS method [16].

2.2 Inadequacy of conventional PDFs

The problem that is addressed is nicely illustrated by considering photoproduction of $c\bar{c}$ pairs. In Figs. 6, we compare three methods of calculation carried out within the CASCADE event generator [26, 27]:

- Use of a conventional gluon density that is a function of parton x alone.
- Use of a k_\perp density that is a function of parton x and k_\perp . These are the “unintegrated parton densities” (uPDFs) that are discussed in Sec. 1

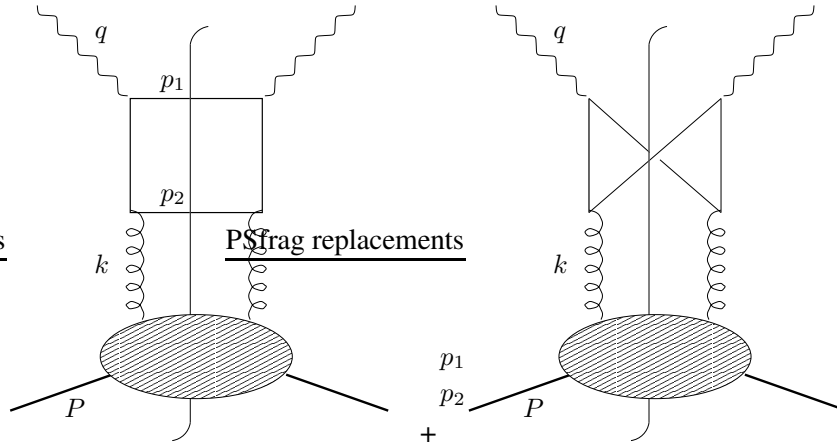


Fig. 7: Photon-gluon fusion.

- Use of a doubly unintegrated density that is a function of parton x , k_{\perp} and virtuality, that is, of the complete parton 4-momentum.

The partonic subprocess in all cases is the lowest order photon-gluon-fusion process $\gamma + g \rightarrow c + \bar{c}$ (Fig. 7). Two differential cross sections are plotted: one as a function of the transverse momentum of the $c\bar{c}$ pair, and the other as a function of the x_{γ} of the pair. By x_{γ} is meant the fractional momentum of the photon carried by the $c\bar{c}$ pair, calculated in the light-front sense as

$$x_{\gamma} = \frac{\sum_{i=c,\bar{c}}(E_i - p_{zi})}{2yE_e} = \frac{p_{c\bar{c}}^-}{q^-}.$$

Here E_e is the electron beam energy and the coordinates are oriented so that the electron and proton beams are in the $-z$ and $+z$ directions respectively.

In the normal parton model approximation for the hard scattering, the gluon is assigned zero transverse momentum and virtuality, so that the cross section is restricted to $p_{Tc\bar{c}} = 0$ and $x_{\gamma} = 1$, as shown by the solid lines in Fig. 6(a,b). When a k_{\perp} dependent gluon density is used, quite large gluonic k_{\perp} can be generated, so that the $p_{Tc\bar{c}}$ distribution is spread out in a much more physical way, as given by the dashed line in Fig. 6(a). But as shown in plot (b), x_{γ} stays close to unity. Neglecting the full recoil mass m_{rem} (produced in the shaded subgraph in Fig 7) is equivalent of taking $k^2 = -k_{\perp}^2/(1-x)$ with k^2 being the virtuality of the gluon in Fig. 7, k_{\perp} its transverse momentum and x its light cone energy fraction. This gives a particular value to the gluon's k^- . When we also take into account the correct virtuality of gluon, there is no noticeable change in the $p_{Tc\bar{c}}$ distribution — see Fig. 6(c) (dashed line) — since that is already made broad by the transverse momentum of the gluon. But the gluon's k^- is able to spread out the x_{γ} distribution, as in Fig. 6(d) with the dashed line. This is equivalent with a proper treatment of the kinematics and results in $k^2 = -(k_{\perp}^2 + xm_{\text{rem}}^2)/(1-x)$, where m_{rem} is the invariant mass of the beam remnant, the part of the final state in the shaded blob in Fig. 7. This change can be particularly significant if x is not very small.

Note that if partons are assigned approximated 4-momenta during generation of an event in a MC event generator, the momenta need to be reassigned later, to produce an event that conserves total 4-momentum. The prescription for the reassignment is somewhat arbitrary, and it is far from obvious what constitutes a correct prescription, especially when the partons are far from a collinear limit. A treatment with fully unintegrated PDFs should solve these problems.

If, as we claim, an incorrect treatment of parton kinematics changes certain measurable cross sections by large amounts, then we should verify directly that there are large discrepancies in the distributions in partonic variables themselves. We see this in Fig. 8. Graph (a) plots the gluonic transverse

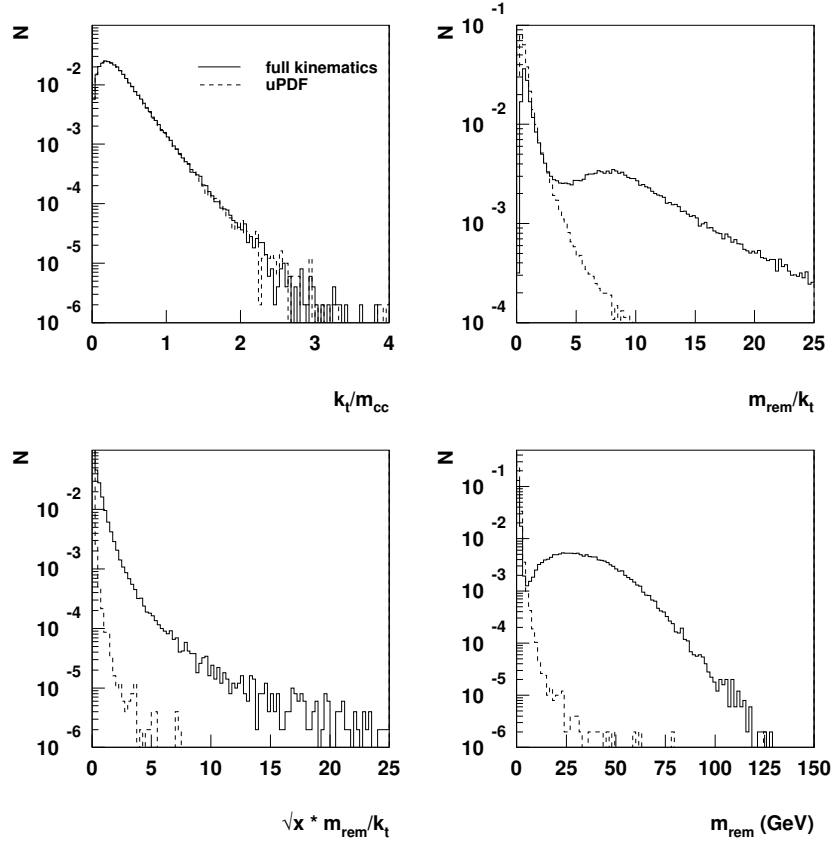


Fig. 8: Comparison of distributions in partonic variables between calculations with full parton kinematics and with ordinary unintegrated PDFs.

momentum divided by the charm-pair mass. As is to be expected, the typical values are less than one, but there is a long tail to high values. But the use of full parton kinematics does not have much of an effect, the unintegrated parton distributions already providing realistic distributions in transverse momentum.

On the other hand, a simple collinear approximation for showering sets the remnant mass, m_{rem} , to zero. As can be seen from the formulae for the gluon virtuality, this only provides a good approximation to the gluon kinematics if m_{rem} is much less than k_{\perp} . In reality, as we see from graph (b), there is a long tail to large values of m_{rem}/k_{\perp} , and the tail is much bigger when correct kinematics are used. A more correct comparison uses xm_{rem}^2 , with an extra factor of x . Even then, there is a large effect, shown in graph (c). The vertical scale is logarithmic, so the absolute numbers of events are relatively small, but the tail is broad. Finally, graph (d) shows that the distribution in m_{rem} itself is very broad, extending to many tens of GeV. This again supports the argument that unless a correct treatment of parton kinematics is made, very incorrect results are easily obtained.

It is important to note that, for the cross sections themselves, the kinematic variables used in Fig. 6 are normal ones that are in common use. Many other examples are easily constructed. Clearly, the use of the simple parton-model kinematic approximation gives unphysically narrow distributions. The correct physical situation is that the gluon surely has a distribution in transverse momentum and virtuality, and for the considered cross sections neglect of parton transverse momentum and virtuality leads to wrong results. It is clearly better to have a correct starting point even at LO, for differential cross sections such as we have plotted.

2.3 Kinematic approximations

The standard treatment of parton kinematics involves replacing the incoming parton momentum k by its plus component only: $k^\mu \mapsto \hat{k}^\mu \equiv (k^+, 0, 0_T)$. There are actually two parts to this. The first is to neglect the $-$ and transverse components of k with respect to the large transverse momenta in the calculation of the numerical value of the hard-scattering amplitude; this is a legitimate approximation, readily corrected by higher order terms in the hard scattering. The second part is to change the kinematics of the final-state particles, p_1 and p_2 , so that their sum is q plus the approximated gluon momentum. It is this second part that is problematic, for it amounts to the replacement of the momentum conservation delta function $\delta^{(4)}(k + q - p_1 - p_2)$ by $\delta^{(4)}(\hat{k} + q - p_1 - p_2)$. These delta-functions are infinitely different, point-by-point. Only when integrated with a sufficiently smooth test function can they be regarded as being approximately the same, as in a fully inclusive cross section.

In an event generator, the effect is to break momentum conservation, which is restored by an ad hoc correction of the parton kinematics. Note that the change of parton kinematics is only in the hard scattering, i.e., in the upper parts of the graphs. Parton kinematics are left unaltered within the parton density part, and the integrals over k_\perp and virtuality are part of the standard definition of integrated PDFs.

The situation is ameliorated by inclusion of NLO terms, and perhaps also by some kind of resummation. But these do not correct the initial errors in the approximation, and lead to a very restricted sense in which the derivation of the cross section can be regarded as valid. Furthermore, when much of the effect of NLO terms is to correct the kinematic approximations made in LO, this is an inefficient use of the enormous time and effort going into NLO calculations. A case in point is the BFKL equation, where 70% of the (large) NLO corrections are accounted for [31] by the correction of kinematic constraints in the LO calculation.

2.4 Conclusions

The physical reasoning for the absolute necessity of fully unintegrated densities is, we believe, unquestionable. Therefore it is highly desirable to reformulate perturbative QCD methods in terms of doubly unintegrated parton densities from the beginning. A full implementation will be able to use the full power of calculations at NLO and beyond.

Among other things, a full implementation, as in [30], will provide extra factorization formulae for obtaining the values of the unintegrated densities at large parton transverse momentum and virtuality. This will incorporate all possible perturbatively calculable information, so that the irreducible nonperturbative information, that must be obtained from data, will be at low transverse momentum and virtuality. In addition, the implementation will quantify the relations to conventional parton densities. With the most obvious definitions, the integrated PDFs are simple integrals of the unintegrated densities. However, in full QCD a number of modifications are required [30, 32], so that the relations between integrated and unintegrated PDFs are distorted.

The fact that we propose new and improved methods does not invalidate old results in their domain of applicability. The work of Watt, Martin and Ryskin, and of Collins and Zu provides a start on this project; but much remains to be done to provide a complete implementation in QCD; for example, there is as yet no precise, valid, and complete gauge-invariant operator definition of the doubly unintegrated densities in a gauge theory.

The outcome of such a program should have the following results:

1. Lowest order calculations will give a kinematically much more realistic description of cross sections. This may well lead to NLO and higher corrections being much smaller numerically than they typically are at present, since the LO description will be better.

2. It will also obviate the need for separate methods (resummation or the CSS technique), which are currently applied to certain individual cross sections like the transverse-momentum distribution for the Drell-Yan process. All these and others will be subsumed and be given a unified treatment.
3. A unified treatment will be possible for both inclusive cross sections using fixed order matrix element calculations and for Monte-Carlo event generators.
4. For a long-term theoretical perspective, the doubly unintegrated distributions will interface to methods of conventional quantum many-body physics much more easily than regular parton densities, whose definitions are tuned to their use in ultra-relativistic situations.

This program is, of course, technically highly nontrivial if it is to be used in place of conventional methods with no loss of predictive power. A start is made in the cited work.

Among the main symptoms of the difficulties are that the most obvious definition of a fully unintegrated density is a matrix element of two parton fields at different space-time points, which is not gauge-invariant. It is often said that the solution is to use a light-like axial gauge $A^+ = 0$. However, in unintegrated densities, this leads to divergences — see [32] for a review — and the definitions need important modification, in such a way that a valid factorization theorem can be derived.

We also have to ask to what extent factorization can remain true in a generalized sense. Hadron-hadron collisions pose a particular problem here, because factorization needs a quite nontrivial cancellation arising from a sum over final-state interactions. This is not compatible with simple factorization for the exclusive components of the cross section, and makes a distinction between these processes and exclusive components of DIS, for example.

3 PDF extrapolation to LHC energies based on combined BK/DGLAP equations ³

3.1 Introduction

In recent years it became clear that the DGLAP evolution is likely to fail in certain kinematics associated with the *low x* domain. This might be a dangerous problem for certain DGLAP based predictions made for the LHC. The reasons for the failure are well known.

- DGLAP predicts a very steep rise of gluon densities with energy. If not suppressed this rise will eventually violate unitarity.
- The leading twist evolution breaks down when higher twists become of the same order as the leading one. We have to recall here that higher twists are estimated to rise with energy much faster than the leading one [33].
- The DGLAP evolution is totally unable to describe physics of low photon virtualities.

It is most important to stress that NLO corrections are in principal unable to solve any of the above problems, though they can potentially help to delay their onset.

Fortunately, a solution to the low *x* problem does exist. We have to rely on a nonlinear evolution based on the BFKL dynamics. So far the best candidate on the market is the Balitsky-Kovchegov (BK) equation [34, 35], which is a nonlinear version of the LO BFKL equation. Compared to the DGLAP equation it has the following advantages:

- it accounts for saturation effects due to high parton densities.
- it sums higher twist contributions.
- it allows an extrapolation to large distances.

Though the BK evolution takes care of the low *x* domain, it misses the essential part of the short distance physics correctly accounted for by the DGLAP evolution. The reason is that the BFKL kernel

³Author: Michael Lublinsky.

involves the $1/z$ part only of the full gluon-gluon splitting function $P_{gg}(z)$. Thus we have to develop a scheme which in a consistent manner would use elements of both the equations. Such scheme was proposed in Ref. [36] and realized in a successful fit to F_2 data in Ref. [37].

One of the main problems of the DGLAP evolution is a necessity to specify the x dependence of the distributions in the initial conditions of the evolution. The scheme which we propose generally avoids this problem and thus can be used for future more elaborated analysis including NLO corrections and the quark sector.

At low x it is very convenient to use the dipole picture. In this approach the structure function F_2 can be expressed through the universal dipole cross section σ^{dipole} :

$$F_2(y, Q^2) = \frac{Q^2}{4\pi^2} \int d^2 r \int dz P^{\gamma^*}(Q^2; r, z) \sigma^{dipole}(r, y). \quad (3)$$

with the probability to find a dipole of the transverse size r in the photon's wavefunction given by

$$P^{\gamma^*}(Q^2; r, z)^2 = \frac{N_c}{2\pi^2} \sum_{f=1}^3 Z_f^2 \{ (z^2 + (1-z)^2) a^2 K_1^2(ar) + 4Q^2 z^2 (1-z)^2 K_0^2(ar) \},$$

where $a^2 = Q^2 z(1-z)$, Z_f are the quark charges, and K_i the standard modified Bessel functions.

The dipole cross section is determined through the evolution of the imaginary part of the dipole target elastic amplitude N subsequently integrated over the impact parameter b (in the analysis of Ref. [37] the dependence on b was modeled):

$$\sigma^{dipole}(r, y) = 2 \int d^2 b N(r, y; b).$$

In our approach, the amplitude \tilde{N} is given by a sum of two terms

$$N = \tilde{N} + \Delta N$$

The first term \tilde{N} follows from the solution of the BK equation whereas ΔN is a DGLAP correction to it (Fig. 9). The strategy of the fit is the following. We trust the DGLAP evolution for x above $x_0 = 10^{-2}$. The gluon density obtained as a result of this evolution is then used as a initial condition for the low x evolution based on the BK equation. In practice the CTEQ6 gluon was used as an input. The large distance behavior was extrapolated using the method proposed in Ref. [38]. The extrapolation is based on the geometrical scaling [39], a phenomenon experimentally observed by HERA. The BK evolved function N is fitted to the low Q^2 data, with the effective proton size being the only fitting parameter entering the b dependence ansatz. As the last step, the DGLAP correction ΔN is switched on and computed by solving a DGLAP-type equation. An inhomogeneous N -dependent term in the equation acts as a source term for ΔN . This allows to have zero initial condition for the DGLAP correction. ⁴

3.2 Results

We skip most of the technical details reported in Ref. [37] and present a result of the fit with $\chi^2/d.o.f. \simeq 1$. Fig. 10 displays the results vs. a combined set of experimental data for x below 10^{-2} . The solid line is the final parameterization. The dashed line on plot (b) is the result without DGLAP corrections added. Figure 11, a presents our results for the logarithmic derivative of F_2 with respect to $\ln x$. This graph illustrates the hard-soft pomeron transition as a result of multiple rescattering of the BFKL pomeron. The intercept decreases from the LO BFKL intercept of the order 0.3 to the hadronic value of the order 0.1. As clearly observed from Fig. 11a, the intercept depends strongly on the photon virtuality Q^2 and decreases towards hadronic value when the virtuality decreases. If we further increase the energy, the

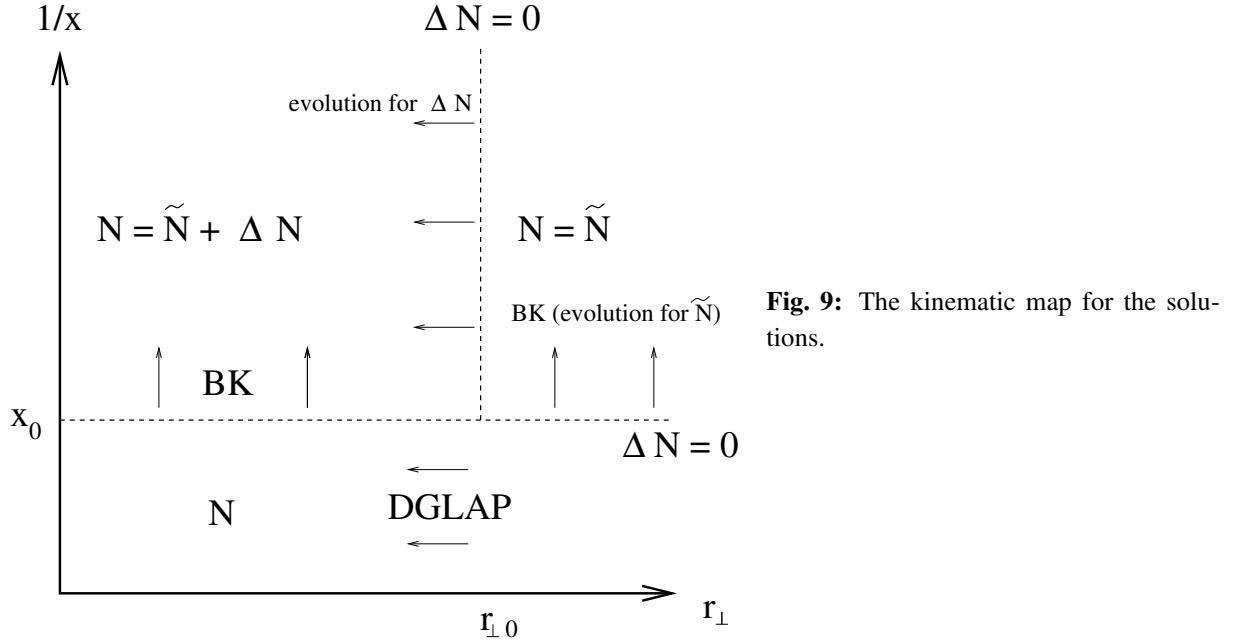


Fig. 9: The kinematic map for the solutions.

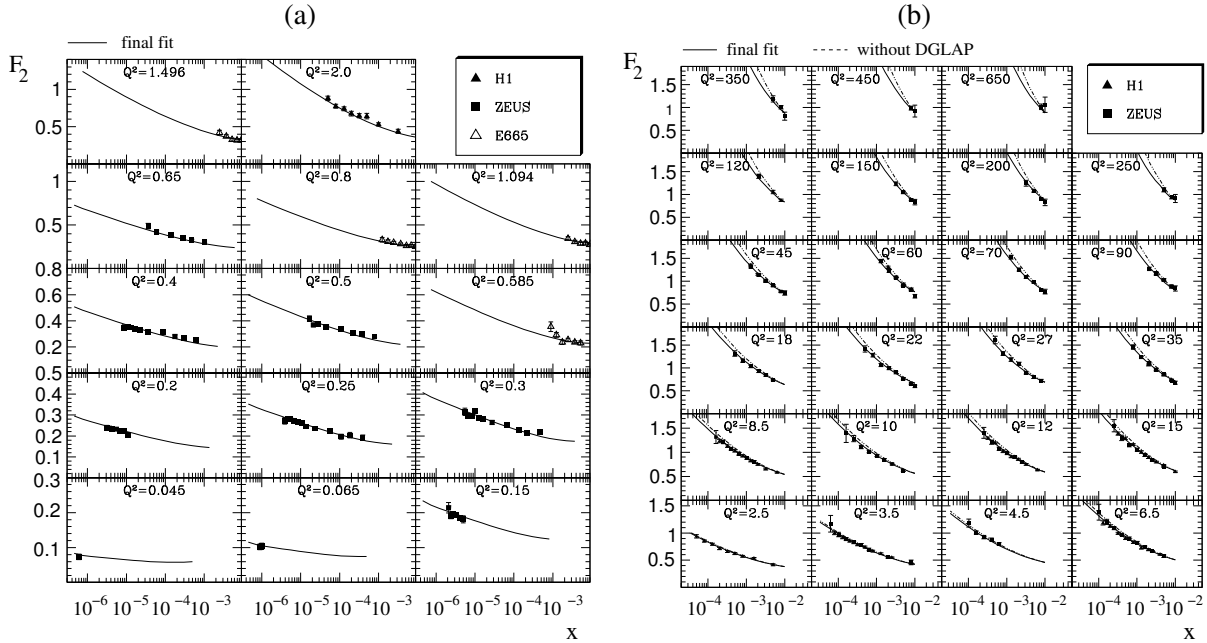


Fig. 10: Fit to the F_2 structure function.

intercept would eventually vanish in accord with the unitarity requirements. The band of our estimates for the value of saturation scale at LHC is displayed on Fig. 11b together with the most popular Golec-Biernat Wüsthoff saturation model [40]. Based on our analysis we predict much stronger saturation effects compared to the ones which could be anticipated from the GBW model. Though the power growth of the saturation scale in both cases is given by the very same exponent of the order $\lambda \simeq 0.3$, we had to take a much stronger saturation input at the beginning of the evolution.

⁴The initial condition for the BK equation is CTEQ gluon distribution. In the DGLAP-type equation for ΔN an initial condition at $r = r_0$ is required, which is set to zero and no modelling of the small x behavior is needed.

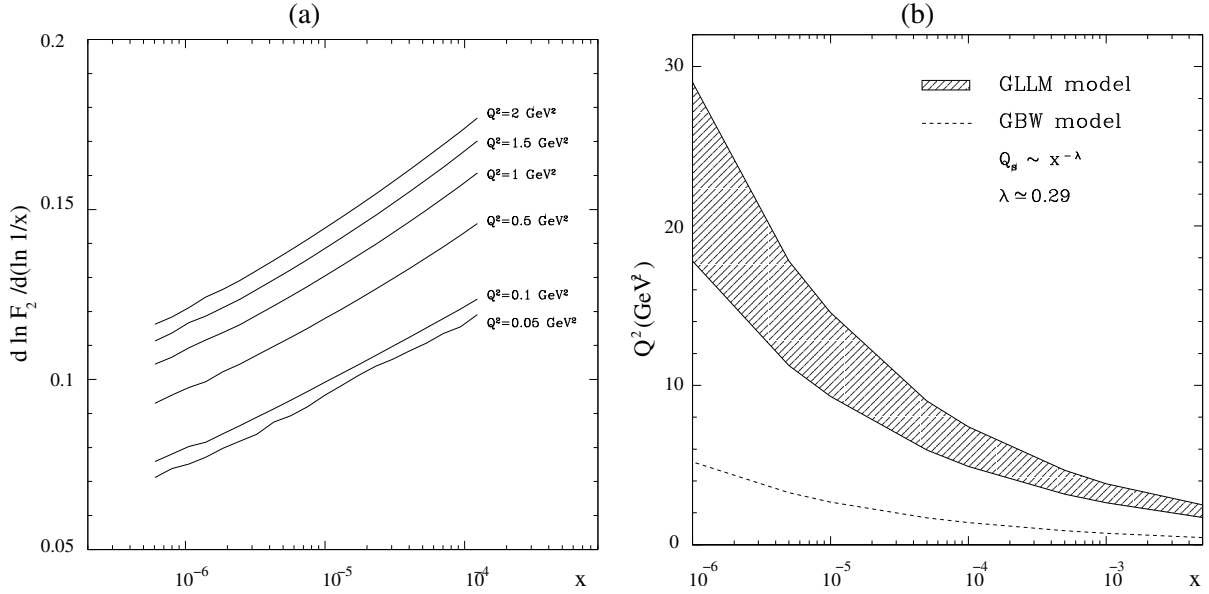


Fig. 11: (a) The logarithmic derivative $\lambda = \partial \ln F_2 / \partial \ln 1/x$ plotted at low Q^2 and very low x . (b) Saturation scale. the hatched area defines a prediction band of Ref. [37]; dashed line is the GBW model.

Model predictions for F_L at HERA and F_2 at LHC can be found in Ref. [37]. Having determined the dipole cross section we can relate it to the unintegrated gluon distribution $f(k, y)$:

$$\sigma^{dipole}(r, y) = \frac{4\pi^2}{N_c} \int \frac{dk^2}{k^4} [1 - J_0(kr)] \alpha_s(k^2) f(k, y). \quad (4)$$

The relation (4) can be inverted for f which can be then used as an input for any computation based on the k_t factorization scheme. The data set for the dipole cross section σ^{dipole} as well as for the unintegrated gluon f can be found in [24]. The uPDF is compared to other parameterizations in Fig.1.

3.3 Outlook

We have reported on, so far, the most advanced analysis of the F_2 data based on combined BK/DGLAP evolution equations. Though our approach incorporates most of the knowledge accumulated in saturation physics, it is not yet fully developed. The next essential steps would be to include NLO corrections both to BFKL and DGLAP. The quark sector should be also added into a unique scheme.

4 Generalized parton distributions⁵

The theoretical description of hard diffractive processes involves the gluon distribution in the proton. Such processes have a proton in the final state which carries almost the same momentum as the incident proton. Due to the small but finite momentum transfer, it is not the usual gluon distribution which appears, but its generalization to nonforward kinematics. Prominent example processes are the exclusive production of mesons from real or virtual photons (Figure 12a) when either the photon virtuality or the meson mass provides a hard scale, virtual Compton scattering $\gamma^* p \rightarrow \gamma p$, and the diffractive production of a quark-antiquark pair (Figure 12b) in suitable kinematics. The generalized gluon distribution depends on the longitudinal momentum fractions x and x' of the emitted and reabsorbed gluon (which differ because of the longitudinal momentum transfer to the proton) and on the invariant momentum transfer $t = -(p - p')^2$. In its “unintegrated” form it depends in addition on the transverse momentum k_t of the

⁵Authors: Markus Diehl and Thomas Teubner.

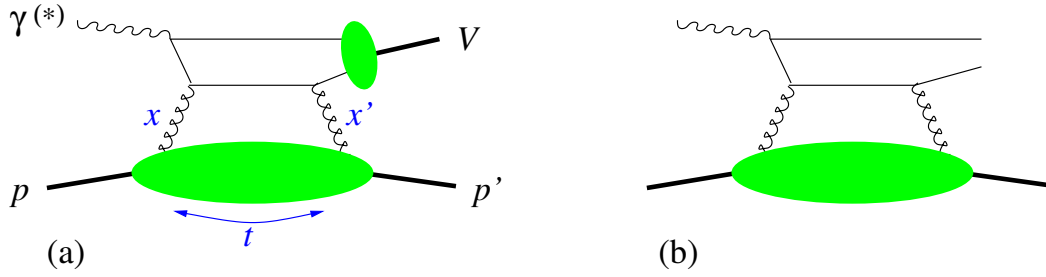


Fig. 12: Example graphs for the diffractive production of (a) a vector meson V or (b) a quark-antiquark pair. The large blob denotes the generalized gluon distribution of the proton and the small one the vector meson wave function.

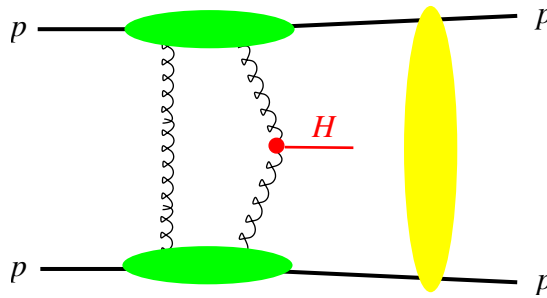


Fig. 13: Graph for the exclusive diffractive production of a Higgs boson, $p + p \rightarrow p + H + p$. The horizontal blobs indicate generalized gluon distributions, and the vertical blob represents secondary interactions between the projectiles.

emitted gluon. Another important process involving this distribution is exclusive diffractive production of a Higgs in pp scattering (Figure 13), discussed in detail in [41]. Note that the description of this process requires the gluon distribution to be unintegrated with respect to k_t , whereas the processes in $\gamma^{(*)}p$ collisions mentioned above can be treated either in k_t -factorization or in the collinear factorization framework, where k_t -integrated generalized parton distributions occur. Note also that Figures 12 and 13 show graphs for the process *amplitudes*: the cross section depends hence on the square of the gluon distribution for Figure 12, and on its fourth power for Figure 13.

To extract the generalized gluon distribution from vector meson production data requires knowledge of the meson wave function, which is an important source of uncertainty for the ρ^0 and ϕ and, to a lesser extent, for the J/Ψ . In this respect Υ production is by far the cleanest channel but experimentally challenging because of its relatively low production rate. An approach due to Martin, Ryskin and Teubner (MRT) [42] circumvents the use of the meson wave function by appealing to local parton-hadron duality, where the meson production cross section is obtained from the one for open quark-antiquark production, integrated over an interval of the invariant $q\bar{q}$ mass around the meson mass. The choice of that interval is then mainly reflected in an uncertainty in the overall normalization of the cross section. Virtual Compton scattering $\gamma^*p \rightarrow \gamma p$ does not involve any meson wave function and for sufficiently large Q^2 is again theoretically very clean.

By a series of steps one can relate the generalized gluon distribution to the usual gluon density, obtained for instance in global parton distribution fits.

1. The t dependence is typically parameterized by multiplying the distribution at $t = 0$ with an exponential $\exp(-b|t|)$, whose slope b has to be determined from measurement. In more refined models this slope parameter may be taken to depend on the other kinematic variables of the process.

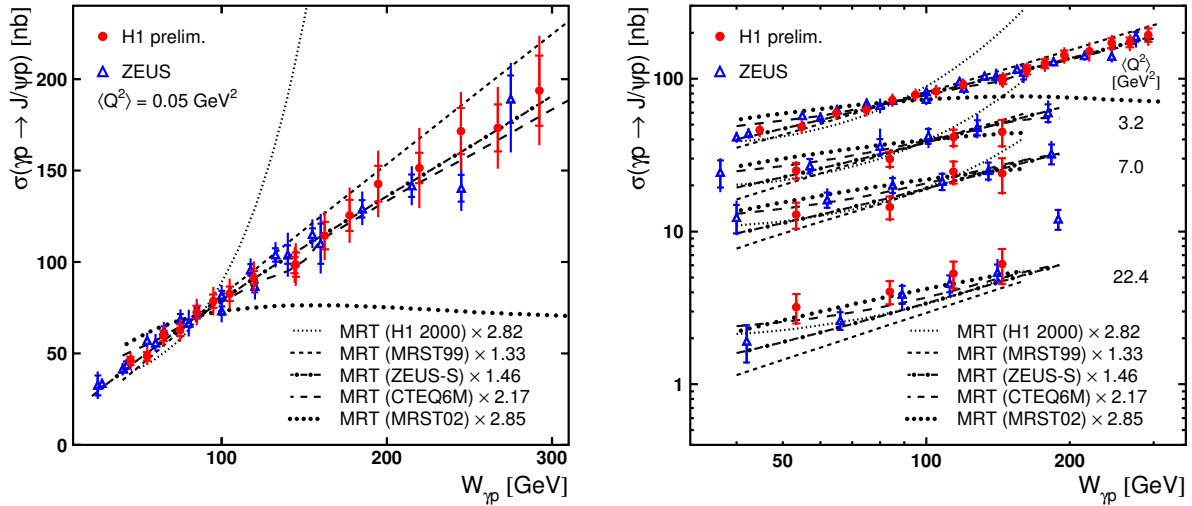


Fig. 14: Data for the $\gamma^*p \rightarrow J/\Psi p$ cross section from H1 [47] and ZEUS [48, 49] compared to calculations in the MRT approach [42, 46] with different gluon densities. The upper data points in the right panel correspond to those in the left one. The ZEUS data has been shifted to the Q^2 values of the H1 analysis using the Q^2 dependence measured by ZEUS, as described in [47]. Figure courtesy of Philipp Fleischmann (H1 Collaboration).

2. To leading logarithmic accuracy in $\log(1/x)$ one can neglect the difference between the longitudinal momentum fractions of the two gluons. The amplitude for meson production is then proportional to the usual gluon density evaluated at $x_g = (M_V^2 + Q^2)/W^2$, where M_V is the meson mass, Q^2 the photon virtuality, and W the γ^*p c.m. energy. For phenomenology this leading logarithmic approximation is however insufficient. A weaker approximation allows one to express the amplitude in terms of the gluon density at x_g times a correction factor for the kinematic asymmetry (“skewing”) between the two momentum fractions [43].
3. The problem to relate the k_t unintegrated gluon distribution to the k_t integrated one is quite analogous to the case of the usual forward gluon density (see Sect. 1.1), with some specifics concerning Sudakov form factors in the nonforward case [44].

An overview and discussion of theoretical aspects and uncertainties in describing vector meson production in this framework can be found in [45].

To illustrate the sensitivity of such processes to the gluon distribution we show in Figure 14 data for photo- and electroproduction of J/Ψ compared to calculations in the MRT approach [46], with different gluon densities taken as input to construct the generalized gluon distribution as just described. The potential of such processes to constrain the gluon distribution is evident from this plot.

We finally note that the theoretical description of diffractive Higgs production in pp collisions is very similar to the description of diffractive processes in ep scattering using k_t factorization (much more than to the description of, say, inclusive DIS in collinear factorization, which provides the main input to the determination of conventional gluon densities at small x), see [41, 50] for further discussion. The analysis of diffractive ep scattering is hence well suited to provide input to estimate the diffractive Higgs cross section at the LHC.

Acknowledgments

This work is supported in part (JC) by the U.S. DOE.

References

- [1] V. Gribov and L. Lipatov, Sov. J. Nucl. Phys. **15**, 438 and 675 (1972).
- [2] L. Lipatov, Sov. J. Nucl. Phys. **20**, 94 (1975).
- [3] G. Altarelli and G. Parisi, Nucl. Phys. **B 126**, 298 (1977).
- [4] Y. Dokshitzer, Sov. Phys. JETP **46**, 641 (1977).
- [5] E. Kuraev, L. Lipatov, and V. Fadin, Sov. Phys. JETP **44**, 443 (1976).
- [6] E. Kuraev, L. Lipatov, and V. Fadin, Sov. Phys. JETP **45**, 199 (1977).
- [7] Y. Balitskii and L. Lipatov, Sov. J. Nucl. Phys. **28**, 822 (1978).
- [8] M. Ciafaloni, Nucl. Phys. **B 296**, 49 (1988).
- [9] S. Catani, F. Fiorani, and G. Marchesini, Phys. Lett. **B 234**, 339 (1990).
- [10] S. Catani, F. Fiorani, and G. Marchesini, Nucl. Phys. **B 336**, 18 (1990).
- [11] G. Marchesini, Nucl. Phys. **B 445**, 49 (1995).
- [12] L. Gribov, E. Levin, and M. Ryskin, Phys. Rep. **100**, 1 (1983).
- [13] E. M. Levin, M. G. Ryskin, Y. M. Shabelski, and A. G. Shuvaev, Sov. J. Nucl. Phys. **53**, 657 (1991).
- [14] S. Catani, M. Ciafaloni, and F. Hautmann, Nucl. Phys. **B 366**, 135 (1991).
- [15] J. Collins and R. Ellis, Nucl. Phys. **B 360**, 3 (1991).
- [16] J. C. Collins, D. E. Soper, and G. Sterman, Nucl. Phys. **B250**, 199 (1985).
- [17] F. Landry, R. Brock, P. M. Nadolsky, and C. P. Yuan, Phys. Rev. **D67**, 073016 (2003).
hep-ph/0212159.
- [18] H. Jung and G. Salam, Eur. Phys. J. **C 19**, 351 (2001). hep-ph/0012143.
- [19] H. Jung, *Un-integrated updfs in ccfm*, 2004. hep-ph/0411287.
- [20] L. Lonnblad and M. Sjodahl, JHEP **05**, 038 (2005). hep-ph/0412111.
- [21] B. Andersson, G. Gustafson, and J. Samuelsson, Nucl. Phys. **B467**, 443 (1996);
B. Andersson, G. Gustafson, and H. Kharraziha, Phys. Rev. **D57**, 5543 (1998). hep-ph/9711403.
- [22] H. Jung, K. Kutak, K. Peters, and L. Motyka, *Nonlinear gluon evolution and heavy quark production at the lhc*. These proceedings, 2005.
- [23] K. Kutak and A. M. Stasto, Eur. Phys. J. **C41**, 343 (2005). hep-ph/0408117.
- [24] M. Lublinsky, *Parameterization of the dipole cross section and updf*.
<http://www.desy.de/~lublinm/>.
- [25] M. A. Kimber, A. D. Martin, and M. G. Ryskin, Phys. Rev. **D63**, 114027 (2001).
hep-ph/0101348.
- [26] H. Jung, Comput. Phys. Commun. **143**, 100 (2002). hep-ph/0109102.
- [27] H. Jung and G. P. Salam, Eur. Phys. J. **C19**, 351 (2001). hep-ph/0012143.
- [28] G. Watt, A. D. Martin, and M. G. Ryskin, Eur. Phys. J. **C31**, 73 (2003). hep-ph/0306169.
- [29] G. Watt, A. D. Martin, and M. G. Ryskin, Phys. Rev. **D70**, 014012 (2004). hep-ph/0309096.
- [30] J. C. Collins and X. Zu, JHEP **03**, 059 (2005). hep-ph/0411332.
- [31] J. Kwiecinski, A. D. Martin, and J. J. Outhwaite, Eur. Phys. J. **C9**, 611 (1999). hep-ph/9903439.
- [32] J. C. Collins, Acta Phys. Polon. **B34**, 3103 (2003). hep-ph/0304122.
- [33] J. Bartels, Z. Phys. **C60**, 471 (1993);
J. Bartels, Phys. Lett. **B298**, 204 (1993);
E. M. Levin, M. G. Ryskin, and A. G. Shuvaev, Nucl. Phys. **B387**, 589 (1992).
- [34] I. Balitsky, Nucl. Phys. **B 463**, 99 (1996).
- [35] Y. V. Kovchegov, Phys. Rev. **D 60**, 034008 (1999).
- [36] M. Lublinsky, E. Gotsman, E. Levin, and U. Maor, Nucl. Phys **A 696**, 851 (2001).

- [37] E. Gotsman, E. Levin, M. Lublinsky, and U. Maor, *Eur. Phys. J. C* **27**, 411 (2003).
- [38] M. Lublinsky, *Eur. Phys. J. C* **21**, 513 (2001).
- [39] A. M. Stasto, K. Golec-Biernat, and J. Kwiecinski, *Phys. Rev. Lett.* **86**, 596 (2001).
- [40] K. Golec-Biernat and M. Wusthoff, *Phys. Rev. D* **59**, 014017 (1999).
- [41] J. Forshaw, *Diffractive higgs production: theory*. These proceedings.
- [42] A. D. Martin, M. G. Ryskin, and T. Teubner, *Phys. Rev. D* **55**, 4329 (1997). [hep-ph/9609448](#);
A. D. Martin, M. G. Ryskin, and T. Teubner, *Phys. Lett. B* **454**, 339 (1999). [hep-ph/9901420](#);
A. D. Martin, M. G. Ryskin, and T. Teubner, *Phys. Rev. D* **62**, 014022 (2000). [hep-ph/9912551](#).
- [43] A. G. Shuvaev, K. J. Golec-Biernat, A. D. Martin, and M. G. Ryskin, *Phys. Rev. D* **60**, 014015 (1999). [hep-ph/9902410](#).
- [44] A. D. Martin and M. G. Ryskin, *Phys. Rev. D* **64**, 094017 (2001). [hep-ph/0107149](#).
- [45] M. Diehl, *Phys. Rept.* **388**, 41 (2003). [hep-ph/0307382](#).
- [46] T. Teubner. To appear in Proceedings of DIS05.
- [47] H. C. A. Aktas et al., *Elastic J/Ψ production at HERA*. [hep-ex/0510016](#), Submitted to *Eur Phys J.*
- [48] ZEUS Collaboration, S. Chekanov *et al.*, *Nucl. Phys. B* **695**, 3 (2004). [hep-ex/0404008](#).
- [49] ZEUS Collaboration, S. Chekanov *et al.*, *Eur. Phys. J. C* **24**, 345 (2002). [hep-ex/0201043](#);
ZEUS Collaboration, J. Breitweg *et al.*, *Eur. Phys. J. C* **6**, 603 (1999). [hep-ex/9808020](#);
ZEUS Collaboration, J. Breitweg *et al.*, *Z. Phys. C* **75**, 215 (1997). [hep-ex/9704013](#).
- [50] L. Motyka, *Talk at the workshop meeting 7–21 January 2005, CERN*.
<http://agenda.cern.ch/fullAgenda.php?ida=a045699>;
M. Diehl, *Talk at the workshop meeting 21–24 March 2005, DESY*.
<http://agenda.cern.ch/fullAgenda.php?ida=a05611>.

Resummation

A. Banfi¹, G. Corcella², M. Dasgupta³, Y. Delenda³, G.P. Salam⁴ and G. Zanderighi⁵.

¹ University of Cambridge, Madingley Road, Cambridge CB3 0HE, U.K

² Department of Physics, Theory Division, CH-1211 Geneva 23, Switzerland.

³ University of Manchester, Oxford Road, Manchester, M13 9PL, U.K

⁴ LPTHE, Universities of Paris VI and VII and CNRS, 75005, Paris, France.

⁵ Fermilab, Batavia, IL 60510, USA.

Abstract

We review the work discussed and developed under the topic “Resummation” at Working Group 2 “Multijet final states and energy flow”, of the HERA-LHC Workshop. We emphasise the role played by HERA observables in the development of resummation tools via, for instance, the discovery and resummation of non-global logarithms. We describe the event-shapes subsequently developed for hadron colliders and present resummed predictions for the same using the automated resummation program CAESAR. We also point to ongoing studies at HERA which can be of benefit for future measurements at hadron colliders such as the LHC, specifically dijet E_t and angular spectra and the transverse momentum of the Breit current hemisphere.

1 Introduction

Resummed calculations are an invaluable tool, both for the understanding of perturbative QCD dynamics at all orders as well as for extracting, as accurately as possible, QCD parameters such as the strong coupling, quark masses and parton distribution functions. These parameters, which cannot be directly computed from QCD perturbation theory itself, will be vital inputs in new physics searches at the LHC. Moreover, resummed expressions are also an important stepping stone to probing observable distributions in regions where non-perturbative power corrections make a significant contribution. In this region one may expect a smearing of the resummed perturbative result with a non-perturbative function (for which one can adopt, for example, a renormalon-inspired model), and the resulting spectrum can be confronted with data to test our understanding of non-perturbative dynamics. In all these aspects, HERA data and observables have played an important role (sometimes significantly underrated in the literature) in furthering our knowledge, without which accurate studies of several observables at the LHC would simply not be possible.

A concrete example of HERA’s important role in this regard is the case of event shape distributions [1, 2], theoretical studies of which led to the finding of non-global single-logarithmic [3] effects (discussed in more detail below). Prior to these studies it was widely believed that the HERA distributions, measured in the current hemisphere Breit frame, were trivially related to their e^+e^- counterparts. Had such ideas, based on independent soft gluon emission by the hard partons, been applied directly to similar variables at the LHC, such as energy flows away from jets, the accuracy of theoretical predictions would have been severely compromised leading almost certainly to erroneous claims and conclusions.

Another area where HERA has played a vital role is in the testing of renormalon inspired models for power corrections, most significantly the dispersive approach [4] to $1/Q$ power corrections, tested against HERA event-shape distributions and mean-values [5]. The fact that HERA data seem to confirm such models, where one can think of the power corrections as arising from the emission of a gluon with transverse momentum $\mathcal{O}(\Lambda_{\text{QCD}})$, is significant for the LHC. This is because the agreement of the renormalon model with data demonstrates that the presence of initial state protons does not affect significantly the form of $1/Q$ corrections. It thus sets limits on the additional non-perturbative contribution that may potentially be generated by the flight of struck partons through the proton cloud, which therefore does

not appear to be significant. Once again it is accurate resummed predictions [6] which have allowed us access to the non-perturbative domain hence strengthening our understanding of power corrections.

One important aspect of resummed studies, till date, is that stringent comparisons of next-to-leading logarithmic resummed predictions with data have only been carried out in cases involving observables that vanish in the limit of two hard partons. Prominent examples reflecting the success of this program are provided by $e^+e^- \rightarrow 2$ jet event shapes and DIS (1+1) jet event shapes as well as Drell-Yan vector boson transverse momentum spectra at hadron colliders. At the LHC (and hadron colliders in general) one already has two hard incoming partons and any observable dealing with final state jet production would take us beyond the tested two hard parton situation. Thus dijet event shapes at hadron colliders (discussed in detail later), which involve much more complicated considerations as far as the resummation goes, represent a situation where NLL resummations and power corrections are as yet untested. Bearing in mind the hadronic activity due to the underlying event at hadron colliders, it is important to test the picture of resummations and power corrections for these multiparton event shapes in cleaner environments. Thus LEP three-jet event shapes and similar $2 + 1$ jet event shapes at HERA become important to study in conjunction with looking at resummation of event shapes at hadron colliders.

Predictions for several LEP and HERA three-jet event shapes already exist (see e.g [7] and for a full list of variables studied Ref. [8]) and at this workshop a prominent development presented was the proposal of several dijet event-shapes in hadron-hadron collisions and the resummed predictions for their distributions [9].

Existing HERA data can also be usefully employed to study soft gluon radiation dynamics from multi-hard-parton ensembles, in the study of dijet E_t and angular spectra. These quantities are somewhat different from event shapes since one defines observables based on aggregate jet-momenta and angles rather than directly constructing them from final-state hadron momenta. Examples are the transverse energy, E_t , mismatch between the leading E_t jets in dijet production and the azimuthal correlation between jets ϕ_{jj} , once again referring to the highest E_t jets in dijet production. For the former quantity there are no direct experimental data as yet, but it is simply related to the dijet total rate in the region of symmetric E_t cuts for which data does exist. For the latter quantity similarly there are direct experimental data [10]. These observables have smaller hadronisation corrections scaling as $1/Q^2$ rather than $1/Q$ as for most event shapes. They thus offer a good opportunity to test the NLL perturbative predictions alone without necessarily probing non-perturbative effects at the same time ¹.

At this workshop developments were reported on extending existing calculations [11] for cone dijets, to different jet algorithms, such as the k_t algorithm, comparing to fixed order estimates and performing the leading order matching. Once the HERA data has been well described similar studies can be carried out for hadron-hadron dijets. In fact predictions already exist for hadron-hadron dijet masses near threshold [12] but are not in a form conducive to direct comparisons with data containing neither the jet algorithms in the form actually employed in experiment, nor the matching to fixed order. However these calculations provided a useful starting point for the calculations presented here, which should eventually lead to direct comparisons with data.

Another area where HERA may play an important role is to establish whether unaccounted for small x effects may be significant in comparing theoretical resummations for e.g. vector boson p_t spectra with experimental data. It has been suggested that a non-perturbative intrinsic k_t , growing steeply with x , is required to accommodate HERA data for semi-inclusive DIS processes [13]. When this observation is extrapolated to the LHC kinematical region there is apparently significant small x broadening in the vector boson p_t distribution. Similar effects may well arise in the case of the Higgs boson too. However DIS event shape studies in the Breit current hemisphere [6] apparently do not acquire such corrections since they are well described by conventional NLL resummations supported by dispersive

¹Although effects to do with intrinsic k_t will eventually have to be accounted for similar to the case of Drell-Yan vector boson p_t spectra.

power corrections [5], which are x independent ². However there are some important caveats:

- Unlike vector boson p_t spectra, event shapes receive $1/Q$ hadronisation corrections unrelated to intrinsic k_t . These could mask $1/Q^2$ terms originating from intrinsic k_t which may yet contain the x dependence in question.
- It has already been observed that including H1 data for $Q < 30$ GeV does spoil somewhat the agreement with the dispersive prediction of universal power corrections to event shapes [6]. The origin of this effect could well be extra non-perturbative k_t broadening related to the effects described above for vector boson p_t .

To get to the heart of this matter a useful variable that has been suggested (see plenary talk by G. Salam at the first meeting of this workshop) is the modulus of the vector transverse momentum $\sum_{i \in H_c} \vec{k}_{t,i}$ of the current hemisphere in the DIS Breit frame. This quantity is simply related to the Drell-Yan p_t spectra and comparing theoretical predictions, presented here, with data from HERA should help to finalise whether additional small- x enhanced non-perturbative terms are needed to accommodate the data. We begin by first describing the results for hadron-hadron event shape variables, discussed by G. Salam at this workshop. Then we describe the progress in studying dijet E_t and angular spectra (presented by M. Dasgupta and G. Corcella at the working group meetings). Finally we mention the results obtained thus far, for the Q_t distribution of the current hemisphere and end with a look at prospects for continuing phenomenology at HERA, that would be of direct relevance to the LHC.

2 Event shapes for hadron colliders

Event shape distributions at hadron colliders, as has been the case at LEP and HERA, are important collinear and infrared safe quantities, that can be used as tools for the extraction of QCD parameters, for instance α_s , by comparing theory and data. In contrast however to more inclusive sources of the same information (e.g the ratio of 3 jet to 2 jet rates), event shape distributions provide a wealth of other information, some of which ought to be crucial in disentangling and further understanding the different physics effects, relevant at hadron colliders. These range from fixed-order predictions to resummations, hadronisation corrections and, in conjunction with more detailed studies assessing the structure of, and role played by, the underlying event (beam fragmentation).

Until recently there have only been limited experimental studies of jet-shapes at hadron colliders [15] and no resummed theoretical predictions for dijet shape variables at hadron colliders. Rapid recent developments (see Ref. [9] and references therein) in the field of perturbative resummations have now made theoretical estimates possible for a number of such distributions, introduced in [9] which we report on below.

The three main theoretical developments that have led to the studies of Ref. [9] are:

- Resummation for hadron-hadron dijet observables depends on describing multiple soft gluon emission from a system of four hard partons. The colour structure of the resulting soft anomalous dimensions is highly non-trivial and was explicitly computed by the Stony Brook group in a series of papers (see e.g [12] and references therein).
- The discovery of non-global observables [3]. The realisation that standard resummation techniques based on angular ordering/independent-emission of soft gluons by the hard-parton ensemble, are not valid for observables that are sensitive to emissions in a limited angular range, has led to the introduction of observables that are made global by construction. This means that one can apply the technology developed by the Stony-Brook group to obtain accurate NLL predictions for these observables, without having to resort to large N_c approximations.

²An exception is the jet broadening [14] but the x dependence there is of an entirely different origin and nature.

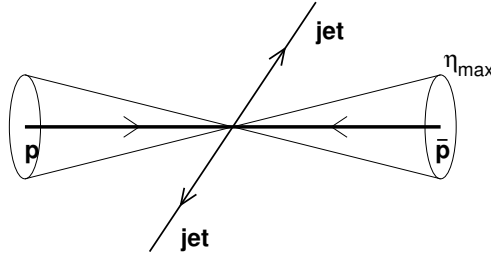


Fig. 1: Cut around the beam direction beyond rapidity η_{\max} corresponding to the maximum rapidity reach of the detectors.

- The advent of automated resummation [16]. The development of generalised resummation formulae and powerful numerical methods to determine the parameters and compute the functions thereof, has made it possible to study several variables at once rather than having to perform copious, and in some cases previously unfeasible, calculations for each separate observable.

We now discuss the different types of variables defined and resummed in [9]. The first issue one has to deal with is the fact that experimental detectors have a limited rapidity range, which can be modeled by a cut around the beam direction.

This cut would then correspond to a position in rapidity of the edge of the most forward detector with momentum or energy resolution and the relevant values of the maximum rapidity for measurements is 3.5 units at the Tevatron and 5 units at the LHC. One may then worry about gluon emissions beyond this rapidity (i.e. inside the beam cut, see Fig. 1) that emit softer gluons into the allowed rapidity range, outside the cones depicted in Fig. 1. Such a configuration would of course render the observable non-global.

To get around this potential problem, one can employ an idea suggested for 3-jet observables such as out-of-plane momentum flows in hadron-hadron collisions [17], which helps side-step the issue of non-globalness. We note that all the observables studied here have the following functional dependence on a soft emission, k , collinear to a given hard leg³ (common to all event shapes studied here and in other processes)

$$V(\tilde{p}, k) = d \left(\frac{k_t}{Q} \right)^a e^{-b\eta} g(\phi), \quad (1)$$

where k_t , η and ϕ are measured wrt a given hard leg and \tilde{p} represent the set of hard parton momenta including recoil against k while Q is the hard-scale of the process. We are particularly interested in emissions soft and collinear to the beam (incoming) partons. Then an emission beyond the maximum detector rapidity $\eta \geq \eta_{\max}$ corresponds to at most a contribution to the observable $V \sim e^{-(a+b_{\min})\eta_{\max}}$ with $b_{\min} = \min(b_1, b_2)$ and b_1 and b_2 are the values of b associated with collinear emission near beam-partons 1 and 2.

If one then chooses to study the observable over a range of values such that

$$L \leq (a + b_{\min})\eta_{\max}, \quad L \equiv \ln 1/V, \quad (2)$$

then emissions more forward than η_{\max} do not affect the observable in the measured range of values. One can thus include the negligible contribution from this region and do the calculation *as if the observable were global*, ignoring the cut around the beam. Including the region beyond η_{\max} does not alter the NLL resummed result in the suitably selected range Eq. 2.

³In general the values of parameters d, a, b and the function g depend on the observable considered. For more details and constraints on the various parameters that ensure globalness and infrared and collinear safety etc., see Ref. [16].

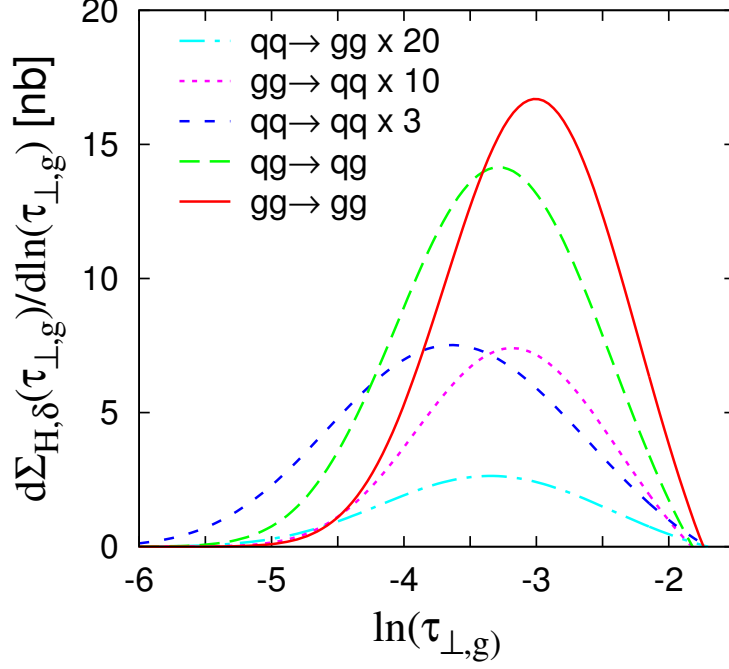


Fig. 2: The global transverse thrust distribution with the contribution from different partonic channels explicitly displayed.

The price one has to pay is to limit the range of the study of the observable V , such that emissions beyond η_{\max} make a negligible contribution. As we will mention later this is a more significant restriction for some variables compared to others (depending on the parameters a and b) but a range of study can always be found over which the observable can be treated as global.

2.1 Global event shapes

With the above caveat in place several variables can be safely studied (treated as global) over a wide range of values. An explicit example is the *global transverse thrust* defined as:

$$T_{\perp,g} \equiv \max_{\vec{n}_T} \frac{\sum_i |\vec{q}_{\perp i} \cdot \vec{n}_T|}{\sum_i q_{\perp i}}, \quad \tau_{\perp,g} = 1 - T_{\perp,g}, \quad (3)$$

where the thrust axis \vec{n}_T is defined in the plane transverse to the beam axis. The probability $P(v)$, that the event shape is smaller than some value v behaves as:

$$P(v) = \exp \left[-G_{12} \frac{\alpha_s}{2\pi} L^2 + \dots \right], \quad L = \ln 1/v, \quad (4)$$

with $G_{12} = 2C_B + C_J$, where C_B and C_J represent the total colour charges of the beam and jet (outgoing) partons. The above represents just the double-logarithmic contribution. The full result with control of up to next-to-leading single-logarithms in the exponent is considerably more complicated. It contains both the Stony-Brook colour evolution matrices as well as multiple emission effects (generated by phase-space factorisation). The automated resummation program CAESAR [16] is used to generate the NLL resummed result shown in Fig. 2. In this particular case the effect of the cut around the beam direction can be ignored for values $\tau_{\perp,g} \geq 0.15e^{-\eta_{\max}}$. We note that it is advisable to leave a safety margin between this value and the values included in measurement.

Other global variables studied include the *global thrust minor* and the three jet-resolution threshold parameter y_{23} . For detailed definitions and studies of these variables, the reader is referred to [9].

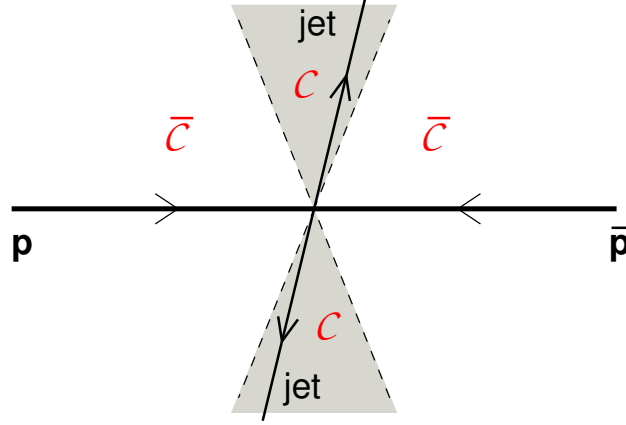


Fig. 3: Figure depicting the central region marked \mathcal{C} , containing the two hard jets.

We shall now proceed to look at two different ways of defining event shapes in a given central region, which on its own would lead to non-globalness, and then adding terms that render them global.

2.2 Forward suppressed observables

Here we shall examine event shapes defined in a chosen central region \mathcal{C} well away from the forward detector edges.

First we define central \perp momentum, and rapidity:

$$Q_{\perp, \mathcal{C}} = \sum_{i \in \mathcal{C}} q_{\perp i}, \quad \eta_{\mathcal{C}} = \frac{1}{Q_{\perp, \mathcal{C}}} \sum_{i \in \mathcal{C}} \eta_i q_{\perp i} \quad (5)$$

and an *exponentially suppressed forward term*,

$$\mathcal{E}_{\bar{\mathcal{C}}} = \frac{1}{Q_{\perp, \mathcal{C}}} \sum_{i \notin \mathcal{C}} q_{\perp i} e^{-|\eta_i - \eta_{\mathcal{C}}|}. \quad (6)$$

Then we can define an event shape in the central region \mathcal{C}^4 which on its own would be non-global since we measure emissions just in \mathcal{C} . The addition of $\mathcal{E}_{\bar{\mathcal{C}}}$ to the event-shape renders the observable global as this term includes suitably the effect of emissions in the remaining region $\bar{\mathcal{C}}$. The exponential suppression of the added term reduces sensitivity to emissions in the forward region which in turn reduces the effect of the beam cut η_{\max} considerably, pushing its impact to values of the observable where the shape cross-section is highly suppressed and thus too small to be of interest.

The event shapes are constructed as described stepwise below:

- Split \mathcal{C} into two pieces: *Up, Down*
- Define *jet masses* for each

$$\rho_{X, \mathcal{C}} \equiv \frac{1}{Q_{\perp, \mathcal{C}}^2} \left(\sum_{i \in \mathcal{C}_X} q_i \right)^2, \quad X = U, D. \quad (7)$$

Define sum and heavy-jet masses

$$\rho_{S, \mathcal{C}} \equiv \rho_{U, \mathcal{C}} + \rho_{D, \mathcal{C}}, \quad \rho_{H, \mathcal{C}} \equiv \max\{\rho_{U, \mathcal{C}}, \rho_{D, \mathcal{C}}\}. \quad (8)$$

⁴There is considerable freedom on the choice of the central region. For instance this could be a region explicitly delimited in rapidity or the two hard jets themselves.

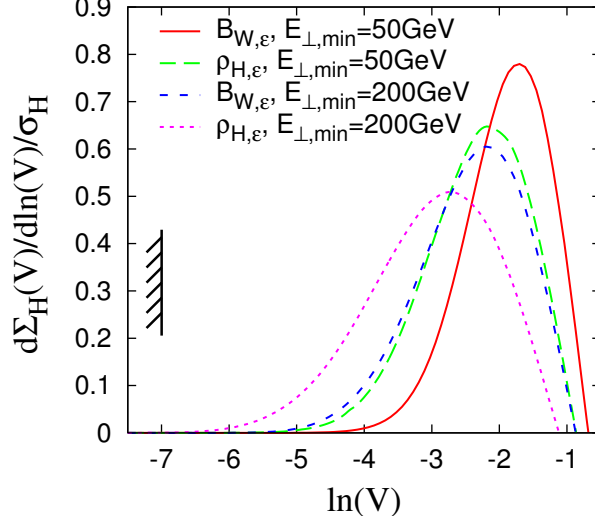


Fig. 4: NLL resummed predictions from CAESAR for the heavy jet-mass and the wide jet-broadening with the minimum jet transverse energy $E_{\perp,\min}$ values of 50 and 200 GeV as shown.

Define global extension, with extra forward-suppressed term

$$\rho_{S,\varepsilon} \equiv \rho_{S,C} + \mathcal{E}_{\bar{c}}, \quad \rho_{H,\varepsilon} \equiv \rho_{H,C} + \mathcal{E}_{\bar{c}}. \quad (9)$$

– Similarly: *total and wide jet-broadenings*

$$B_{T,\varepsilon} \equiv B_{T,C} + \mathcal{E}_{\bar{c}}, \quad B_{W,\varepsilon} \equiv B_{W,C} + \mathcal{E}_{\bar{c}}. \quad (10)$$

At the double-log level the results assume an identical form to Eq. 4 with G_{12} representing a combination of total incoming (beam) and outgoing (jet) parton colour charges [9]. The full NLL resummed results have a substantially more complex form and results from CAESAR [16] are plotted in Fig. 4.

2.3 Indirectly global recoil observables

Here we study observables that are defined exclusively in terms of particles in the central region but are global. Such observables are already familiar from HERA studies. As an example, although the current-jet broadening wrt the photon axis of the DIS Breit frame involves only particles that enter the current hemisphere, the current quark acquires transverse momentum by *recoil* against remnant hemisphere particles. This recoil means that the observable is indirectly sensitive to emissions in the remnant hemisphere which makes the observables global.

To construct similar observables in the hadron-hadron case we observe that by momentum conservation, the following relation holds :

$$\sum_{i \in \mathcal{C}} \vec{q}_{\perp i} = - \sum_{i \notin \mathcal{C}} \vec{q}_{\perp i} \quad (11)$$

which relates the sum of transverse momenta in \mathcal{C} to that in the complementary region. Then the central particles can be used to define a recoil term:

$$\mathcal{R}_{\perp, \mathcal{C}} \equiv \frac{1}{Q_{\perp, \mathcal{C}}} \left| \sum_{i \in \mathcal{C}} \vec{q}_{\perp i} \right|, \quad (12)$$

which contains an indirect dependence on non-central emissions.

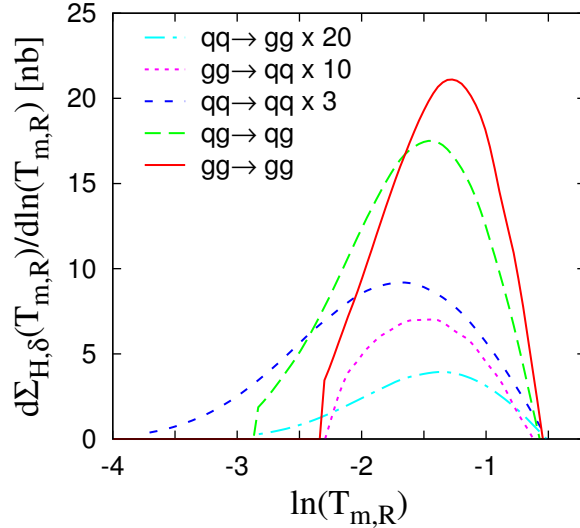


Fig. 5: The recoil thrust minor as predicted by CAESAR, with a cutoff before the divergence. Only a small fraction of the cross-section is beyond the cutoff.

Now we can define event shapes explicitly in terms of central particle momenta in \mathcal{C} . Examples are the recoil jet-masses and broadenings

$$\rho_{X,\mathcal{R}} \equiv \rho_{X,\mathcal{C}} + \mathcal{R}_{\perp,\mathcal{C}}, \quad B_{X,\mathcal{R}} \equiv B_{X,\mathcal{C}} + \mathcal{R}_{\perp,\mathcal{C}}, \dots \quad (13)$$

It is clear that since these observables are defined in terms of central particles alone, the cut around the beam direction is not an issue here. There is however another potential problem. Due to the addition of the recoil term we lose direct exponentiation of the result in variable space. Exponentiation to NLL accuracy only holds in impact-parameter or b space.

The physical effect in question here is similar to Drell-Yan Q_T spectra where there are two competing mechanisms that lead to a given small Q_T , Sudakov suppression of soft emissions and vectorial cancellation between harder emissions. Where the latter effect takes over (typically in the region where single-logs are large $\alpha_s L \sim 1$) we get a breakdown of the Sudakov result generated by CAESAR. This result is of the general form:

$$P(V) = e^{Lg_1(\alpha_s L) + g_2(\alpha_s L) + \dots} \quad (14)$$

The result for recoil observables produced by CAESAR will contain a divergence in the single-log function g_2 and is cut before the divergence. Again for some variables this cut is at a position that significantly reduces the range of possible phenomenological studies. For other variables the divergence is at values of the observable that are sufficiently small so that only a few percent of the cross-section is beyond the cutoff. An example of the former is the recoil transverse thrust where 15% of the cross-section lies beyond the cut-off. For the recoil thrust minor, in contrast, the cutoff has only a moderate effect and much less of the cross-section is cutoff, due to the divergence in g_2 .

Table 1 contains the different event shapes mentioned here and the impact of the two main limitations we discussed, the beam-cut η_{\max} and the breakdown of resummation due to divergences of g_2 . Additionally we mention the expected impact of hadronisation corrections (not yet computed in full) on the different observables as well as the form of the estimated contribution from the underlying event. The entries marked * are subject to uncertainty at present.

Further work is needed before the resummed expressions presented here can be compared with data including the matching to fixed order and computation of the power corrections for the various observables. This is currently in progress.

Table 1: Event shapes and their characteristics

Event-shape	Impact of η_{\max}	Resummation breakdown	Underlying Event	Jet hadronisation
$\tau_{\perp,g}$	tolerable*	none	$\sim \eta_{\max}/Q$	$\sim 1/Q$
$T_{m,g}$	tolerable	none	$\sim \eta_{\max}/Q$	$\sim 1/(\sqrt{\alpha_s}Q)$
y_{23}	tolerable	none	$\sim \sqrt{y_{23}}/Q^*$	$\sim \sqrt{y_{23}}/Q^*$
$\tau_{\perp,\mathcal{E}}, \rho_{X,\mathcal{E}}$	negligible	none	$\sim 1/Q$	$\sim 1/Q$
$B_{X,\mathcal{E}}$	negligible	none	$\sim 1/Q$	$\sim 1/(\sqrt{\alpha_s}Q)$
$T_{m,\mathcal{E}}$	negligible	serious	$\sim 1/Q$	$\sim 1/(\sqrt{\alpha_s}Q)$
$y_{23,\mathcal{E}}$	negligible	none	$\sim 1/Q$	$\sim \sqrt{y_{23}}/Q^*$
$\tau_{\perp,\mathcal{R}}, \rho_{X,\mathcal{R}}$	none	serious	$\sim 1/Q$	$\sim 1/Q$
$T_{m,\mathcal{R}}, B_{X,\mathcal{R}}$	none	tolerable	$\sim 1/Q$	$\sim 1/(\sqrt{\alpha_s}Q)$
$y_{23,\mathcal{R}}$	none	intermediate*	$\sim \sqrt{y_{23}}/Q^*$	$\sim \sqrt{y_{23}}/Q^*$

Having discussed the hadron-hadron event shapes we now move on to describe resummed studies concerning dijet production at HERA which can also be straightforwardly extended to hadron-hadron collisions.

3 Dijet p_t and angular spectra

It has been known for some time that dijet total rates cannot be predicted within fixed-order QCD if symmetric cuts are applied to the two highest p_t dijets [18]. While it was understood that the problems are to do with constraints on soft gluon emission, the exact nature of this constraint was only made clear in Ref. [11]. There it was pointed out that there are large double logarithms (aside from single logarithms and less singular pieces) in the slope $\sigma'(\Delta)$ of the total rate, as a function of Δ the difference in minimum p_t values of the two highest p_t jets. These logarithms were resummed and it was shown that the slope of the total rate $\sigma' \rightarrow 0$ as $\Delta \rightarrow 0$. This leads to a physical behaviour of the total rate as reflected by the data [10].

To perform the comparison to data accurately however, requires two improvements to be made to the calculations of Ref. [11]. Firstly the exact same jet algorithm has to be employed in the theoretical calculations and experimental measurements. The current algorithm used by H1 and ZEUS experiments is the inclusive k_t algorithm. At hadron colliders variants of the cone algorithm are used and it is in fact a cone algorithm that was employed in Ref. [11]. However the details of the calculation need to be amended to define the cones in η, ϕ space as is done experimentally and calculations concerning this were presented at the working group meeting. The second important step is matching to fixed order estimates. We report below on the leading order matching to DISENT [19] while a full NLO matching is still awaited.

We also introduce and study two variables of related interest, the first is the difference in p_t , between the highest p_t jets $\Delta p_{t,jj} = p_{t1} - p_{t2}$ (note that here we talk about the p_t difference rather than the difference in the minimum E_{cut} , that we mentioned earlier. The resummation of this distribution $\frac{d\sigma}{d\Delta p_{t,jj}}$ is essentially identical to that carried out in Ref. [11], except that here we compute the next-to-leading logarithms in different versions of the jet algorithm, which should help with direct experimental comparisons. We also perform the leading-order matching to DISENT.

Having developed the calculational techniques for $d\sigma/d\Delta p_{t,jj}$ it is then straightforward to generate the results for the distribution in azimuthal angle between jets $d\sigma/d\phi_{jj}$ which requires resummation in the region $\phi_{jj} = \pi$. These distributions have been measured at HERA and the Tevatron (most recently by the D0 collaboration). Comparing the resummation with data would represent an interesting challenge for the theory insofar as the status of resummation tools is concerned, and is potentially very instructive.

3.1 The $\Delta p_{t,jj}$ and ϕ_{jj} distributions

We shall consider dijet production in the DIS Breit frame. For the jet definition we can consider either an η, ϕ cone algorithm (such as the infrared and collinear safe midpoint cone algorithm) or the inclusive k_t algorithm. We shall point out to what level the two algorithms would give the same result and where they can be expected to differ. We shall use a four-vector recombination scheme where the jet four-momentum is the sum of individual constituent hadron four-momenta. We also impose cuts on the highest p_t jets such that $|\eta_{1,2}| \leq 1$ and $p_{t1,t2} \geq E_{\min}$.

We then consider the quantity $\Delta p_{t,jj} = p_{t1} - p_{t2}$ which vanishes at Born order and hence the distribution at this order is just $\frac{d\sigma}{dp_{t,jj}} \propto \delta(p_{t,jj})$.

Beyond leading order the kinematical situation in the plane normal to the Breit axis is represented as before [11]:

$$\vec{p}_{t1} = p_{t1}(1, 0) \quad (15)$$

$$\vec{p}_{t2} = p_{t2}(\cos(\pi \pm \epsilon), \sin(\pi \pm \epsilon)) \quad (16)$$

$$\vec{k}_t = k_t(\cos \phi, \sin \phi) \quad (17)$$

Thus we are considering a small deviation from the Born configuration of jets back-to-back in azimuth, induced by the presence of a soft gluon with transverse momentum $k_t \ll p_{t1,t2}$ (which is not recombined by the algorithm with either hard parton) and with azimuthal angle ϕ . In the above ϵ represents the recoil angle due to soft emission. We then have

$$\Delta p_{t,jj} = |p_{t1} - p_{t2}| \approx |k_t \cos \phi|, \quad (18)$$

which accounts for the recoil ϵ to first order and hence is correct to NLL accuracy. Thus for the emission of several soft gluons we have the p_t mismatch given by

$$\Delta p_{t,jj} = \left| \sum_{i \notin j} k_{xi} \right|, \quad (19)$$

where k_x denotes the single component of gluon transverse momentum, along the direction of the hard jets, which are nearly back-to-back in the transverse plane. The sum includes only partons not merged by the algorithm into the highest E_t jets.

Similarly for the dijet azimuthal angle distribution⁵, we have :

$$\pi - \phi_{jj} \approx \frac{1}{p_t} \left| \sum_{i \notin j} k_{yi} \right|. \quad (20)$$

where ϕ_{jj} is the azimuthal angle between the two highest p_t jets. Note that in the above we have set $p_{t1} = p_{t2} = p_t$ since we are considering a small deviation from the Born configuration and this approximation is correct to NLL accuracy. We also introduced k_y , the component of soft gluon momentum normal to the jet axis in the transverse plane.

In either of the above two cases, i.e the $\Delta p_{t,jj}$ or ϕ_{jj} distributions, an identical resummation is involved, due to the similar role of soft partons not recombined into jets. Henceforth we shall proceed with just the $\Delta p_{t,jj}$ resummation results, it being understood that similar considerations apply to ϕ_{jj} in the region $\phi_{jj} \sim \pi$.

Assuming independent emission of soft gluons by the hard three-parton system (the incoming parton and the two outgoing partons that initiate the dijets) and factorising the phase-space Eq. 19 as

⁵Note that the kinematical relations we derive here would be equally valid for dijets produced in hadron-hadron collisions at the Tevatron or LHC and just the dynamics of multisoft gluon emission would be more complex.

below⁶:

$$\Theta \left(\Delta p_{t,jj} - \left| \sum_{i \notin j} k_{x,i} \right| \right) = \frac{1}{\pi} \int_{-\infty}^{\infty} \frac{db}{b} \sin(b \Delta p_{t,jj}) \prod_{i \notin j} e^{i b k_{x,i}}, \quad (21)$$

the resummed result for the $\Delta p_{t,jj}$ distribution can be expressed as

$$\frac{d^3 \sigma}{dx dQ^2 d\Delta p_{t,jj}}(E_{\min}, \Delta p_{t,jj}) = \sum_{\delta=q,g} \int_x^1 \frac{d\xi}{\xi} \int_0^1 dz \sum_{a=T,L} F_a(y) C_\delta^a(\xi, z, E_{\min}) w_\delta(Q, \Delta p_{t,jj}). \quad (22)$$

In the above ξ and z are phase-space variables that parametrise the Born dijet configuration, $F_{a=T,L}$ denotes the $y = Q^2/xs$ dependence associated to the transverse or longitudinal structure function while C^a is the Born matrix-element squared. The function w represents the result of resummation.

The resummed expression w requires some explanation. Its form is as follows

$$w_\delta(p_{t,jj}) = \int_0^\infty \frac{db}{b} \sin(b \Delta p_{t,jj}) \exp[-R_\delta(b)] \mathcal{S}(b) q_\delta(x/\xi, 1/b^2). \quad (23)$$

Note the fact that the exponentiation holds only in b space where b is the impact parameter. The function $R(b)$ (we ignore the subscript δ which describes either incoming quarks or gluons) is the Sudakov exponent which can be computed up to NLL accuracy,

$$R(b) = L g_1(\alpha_s L) + g_2(\alpha_s L), \quad L \sim \ln(bQ). \quad (24)$$

while $S(b)$ is the non-global contribution that arises from soft partons inside the jet emitting outside it. q_δ is the incoming quark or gluon density and its scale depends on the variable b . The functions g_1 and g_2 are the leading-logarithmic and next-to-leading logarithmic resummed quantities.

For the leading logarithms g_1 and a subset of next-to-leading logarithms g_2 , generated essentially by exponentiation of the single-log result in b space, the cone and inclusive k_t algorithms would give the same result, which we have computed. Starting from terms that begin with $\alpha_s^2 \ln^2 b$ in g_2 (specifically two soft wide-angle gluons), the following two effects become important:

- For cone algorithms the implementation of the split/merge stage affects the g_2 piece. Present calculations [11] are valid to NLL accuracy if *all* the energy shared by overlapping jets is given to the jet that would have highest p_t . Note that this is different from merging the overlapping jets themselves. If other merging procedures are used the calculation becomes more complex but is still tractable.
- For the k_t algorithm it is just being realised that running the algorithm generates terms that start at $\alpha_s^2 \ln^2 b$ in the exponent, which are not correctly treated by naive Sudakov exponentiation. These terms, which are generated by the clustering procedure, can also be numerically accounted for in our case, but this is work in progress.

The effects that we mention above cause a similar impact on the final result as the non-global term $S(b)$ which was shown to be at around the 10% level in Ref. [11]. Hence the current results for the k_t algorithm that do not account for the recently found additional terms and only approximately for the non-global logs, can be expected to change by around 10% when these effects will be included correctly.

We present in Fig. 6 preliminary results for the $\Delta p_{t,jj}$ distribution matched to the leading order DISENT prediction, using the k_t algorithm. The matching at present combines quark and gluon channels whereas ideally one would like to separate the incoming quark and gluon channels with the right weights

⁶We compute here the cross-section for the observable to be less than $\Delta p_{t,jj}$ from which we can easily obtain the corresponding distribution.

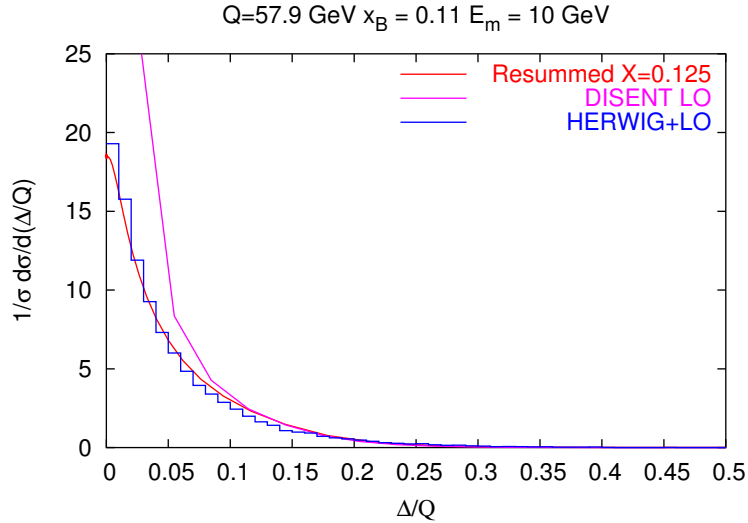


Fig. 6: Figure showing the resummed result matched to fixed-order DISENT results for the variable $\Delta = Q\Delta p_{t,jj}$. Also shown, for comparison, are HERWIG results with matrix-element corrections and the DISENT result alone.

($\mathcal{O}(\alpha_s)$ coefficient functions). This would be possible if, for instance, there was parton flavour information explicit in the fixed order codes, a limitation of the fixed-order codes that needs to be addressed also for hadron-hadron event shapes to be matched to NLO predictions.

We also present a comparison with HERWIG [20] results on the same quantity. The variable X in the figure merely refers to the effect of using the jet p_t as the hard scale rather than the photon virtuality Q^2 , formally a NNLL effect. It is amusing to note the very good agreement of the resummation with HERWIG but not too much can be read into it at this stage. Given the minor role of non-global effects we would expect HERWIG and our predictions to indeed have a broad resemblance. However we should mention that the resummed result in Fig. 6 is at present subject to change pending proper inclusion of non-global logs and the effect of independent soft emission at large angles. The latter is partly included in the results shown, through exponentiation of the one-gluon result as we pointed out before, but the clustering procedure changes this result at about the same level as the non-global logs ($\mathcal{O}(\alpha_s^2 \ln^2 b)$ in the exponent), and this feature needs to be accounted for still. Secondly the matching to LO DISENT combines channels and this spoils control over the $\alpha_s^2 \ln^2 Q/\Delta p_{t,jj}$ term in the expansion of the resummation to NLO. A full NLO matching with proper separation of the channels is awaited. The HERWIG curve also includes an intrinsic k_t component that lowers the height of the result at small $p_{t,jj}$, which can be easily included in the theoretical resummation but at present is excluded. Given these differences the very good agreement one sees with HERWIG is expected to change to some extent although broadly speaking the shapes of the two curves are expected to be similar. Similar conclusions apply for the ϕ_{jj} observable.

4 The vector Q_t of the current hemisphere

Next we examine a quantity that, as mentioned in the introduction, makes a very good analogy with Drell-Yan transverse momentum, Q_t , distributions. Comparison of the resummation of this observable with data could help to understand whether extra broadening of conventionally resummed Q_t spectra, is generated at small x . If so this will be a significant factor at the LHC. The observable in question is the (modulus of) the vectorially summed transverse momenta of all particles in the Breit frame current hemisphere:

$$Q_t = \left| \sum_{i \in \mathcal{H}_c} \vec{k}_{t,i} \right|. \quad (25)$$

Using momentum conservation this quantity is simply equal to the modulus of the transverse momenta of emissions in the remnant hemisphere. These emissions can all be ascribed to the incoming quark to NLL accuracy, *apart* from the soft wide-angle component where large-angle emissions in the current hemisphere can emit softer gluons into the remnant hemisphere (the by now familiar non-global logarithms).

The resummed result for this observable can be expressed as :

$$\frac{d\sigma}{dQ_T^2} \sim \sigma_0 \int_0^\infty b db J_0(bQ_t) \exp[-R(b)] S(b) q(x, 1/b^2) \quad (26)$$

where J_0 is the zeroth order Bessel function, $R(b)$ is the Sudakov exponent (the ‘‘radiator’’), $S(b)$ the non-global contribution and q denotes the quark distribution summed over quark flavours with appropriate weights (charges).

The result for the radiator to NLL accuracy can be expressed, as before, in terms of a leading-log and next-to-leading log function:

$$R(b) = L g_1(\alpha_s L) + g_2(\alpha_s L), \quad L = \ln(bQ). \quad (27)$$

We have

$$g_1 = \frac{C_F}{2\pi\beta_0\lambda} [-\lambda - \ln(1-\lambda)], \quad (28)$$

$$g_2 = \frac{3C_F}{4\pi\beta_0} \ln(1-\lambda) + \frac{KC_F}{4\pi^2\beta_0^2} \left[\frac{\lambda}{1-\lambda} + \ln(1-\lambda) \right] \quad (29)$$

$$+ \frac{C_F}{2\pi} \left(\frac{\beta_1}{\beta_0^3} \right) \left[-\frac{1}{2} \ln^2(1-\lambda) - \frac{\lambda + (1-\lambda)}{1-\lambda} \right],$$

where we have $\lambda = \beta_0\alpha_s \ln[Q^2(\bar{b})^2]$, $\bar{b} = be^{\gamma_E}/2$ and $K = (67/18 - \pi^2/6)C_A - 5/9n_f$.

It is straightforward to express the result directly in Q_t space and one has for the pure NLL resummed terms:

$$\frac{d\sigma}{dQ_T^2} \sim \frac{d}{dQ_T^2} \left[e^{-R(Q/Q_t) - \gamma_E R'(Q/Q_t)} \frac{\Gamma(1 - R'/2)}{\Gamma(1 + R'/2)} q(x, Q_T^2) S(Q/Q_t) \right] \quad (30)$$

where $R' = dR/d\ln(Q/Q_t)$. The result has a divergence at $R' = 2$ which is due to retaining just NLL terms and is of the same nature as that discussed before for certain hadron-hadron event shapes and the Drell-Yan Q_t distribution. However in the present case the divergence is at quite low values of Q_t , e.g for $Q = 100$ GeV, the divergence is at around 0.5 GeV (depending on the exact choice for Λ_{QCD}). Thus it is possible to safely study the distribution down to Q_t values of a few GeV using the simple form Eq. 30. We note that it is also possible to eliminate the divergence if one defines the radiator such that $R(b) \rightarrow R(b)\theta(\bar{b}Q - 1)$, which is a restriction that follows from leading-order kinematics (that one assumes to hold at all orders). The resultant modification has only a negligible impact in the Q_t range that we expect to study phenomenologically.

After the matching to fixed-order is performed, we can probe the non-perturbative smearing e^{-gb^2} that one can apply to the b space resummed result. Comparisons with data should hopefully reveal whether the NLL resummed result + ‘intrinsic k_t ’ smearing, mentioned above, is sufficient at smaller values of x or whether extra broadening is generated in the small x region, that has a significant effect on the result. Data from H1 are already available for this distribution [21] and this should enable rapid developments concerning the above issue.

5 Conclusions

In this article we have provided a summary of the developments discussed at the HERA-LHC workshop working group 2, concerning the topic of all-order QCD resummations. Specifically we have mentioned recent work carried out for hadronic dijet event shapes, dijet E_t and angular spectra and resummation of the current-hemisphere transverse momentum distribution in the DIS Breit frame.

We have stressed the important role of HERA studies in the development of the subject from the LEP era and the fact that, in this regard, HERA has acted as a bridge between LEP studies of the past (although LEP analysis of data continues and is an important source of information) and future studies at both the Tevatron and the LHC.

We have particularly tried to stress the continuing crucial role of HERA in testing all-order QCD dynamics, especially in the context of multi-hard parton observables where studies are currently ongoing. Careful experimental and theoretical collaborative effort is needed here in order to confirm the picture developed for NLL resummations and power corrections. If this program is successful it will greatly ease the way for accurate QCD studies at more complex hadronic environments, such as the LHC.

Acknowledgements

We would like to thank the convenors and organisers of the series of meetings which were a part of the HERA-LHC workshop, for their skillful organisation and for providing us all the necessary facilities needed to present and develop our respective contributions here.

References

- [1] H1 Collaboration, C. Adloff *et al.*, Eur. Phys. J. C **14**, 255 (2000).
- [2] H1 Collaboration, G. J. McCance (2000). hep-ex/0008009.
- [3] M. Dasgupta and G. Salam, Phys. Lett. B **512**, 323 (2001);
M. Dasgupta and G. Salam, JHEP **0203**, 017 (2002).
- [4] Y. Dokshitzer, G. Marchesini, and B. Webber, Nucl. Phys. B **469**, 093 (1996).
- [5] M. Dasgupta and B. Webber, Eur. Phys. J. C **1**, 539 (1998).
- [6] M. Dasgupta and G. Salam, JHEP **0208**, 032 (2002).
- [7] A. Banfi, Y. Dokshitzer, G. Marchesini, and G. Zanderighi, JHEP **0105**, 040 (2001);
A. Banfi, G. Marchesini, G. Smye, and G. Zanderighi, JHEP **0111**, 066 (2001).
- [8] M. Dasgupta and G. P. Salam, J. Phys. **G30**, R143 (2004). hep-ph/0312283.
- [9] A. Banfi, G. Salam, and G. Zanderighi, JHEP **0408**, 062 (2004).
- [10] ZEUS Collaboration, S. Chekanov *et al.*, Eur. Phys. J. **C23**, 13 (2002). hep-ex/0109029;
ZEUS Collaboration, S. Chekanov *et al.*, Phys. Lett. **B551**, 226 (2003). hep-ex/0210064.
- [11] A. Banfi and M. Dasgupta, JHEP **0401**, 027 (2004).
- [12] N. Kidonakis, G. Oderda, and G. Sterman, Nucl. Phys. B. **525**, 299 (1998).
- [13] S. Berge, P. Nadolsky, F. Olness, and C. P. Yuan, Phys. Rev. **D72**, 033015 (2005).
hep-ph/0410375.
- [14] M. Dasgupta and G. Salam, Eur. Phys. J. C **24**, 323 (2001).
- [15] D0 Collaboration, I. Bertram, Acta Phys. Polon. B **33**, 3141 (2002).
- [16] A. Banfi, G. Salam, and G. Zanderighi, JHEP **0503**, 073 (2005).
- [17] A. Banfi, G. Marchesini, G. Smye, and G. Zanderighi, JHEP **0108**, 047 (2001).
- [18] S. Frixione and G. Ridolfi, Nucl. Phys. B **507**, 315 (1997);
M. Klasen and G. Kramer, Phys. Lett. B **366**, 385 (1996).
- [19] S. Catani and M. Seymour, Nucl. Phys. B **485**, 291 (1997).
- [20] G. Corcella *et al.*, JHEP01 **01**, 010 (2001).
- [21] T. Kluge. Private Communication.

Matching Parton Showers and Matrix Elements

*Stefan Höche¹, Frank Krauss¹, Nils Lavesson², Leif Lönnblad², Michelangelo Mangano³,
Andreas Schälicke¹, Steffen Schumann¹*

¹Institut für Theoretische Physik, TU Dresden, Germany; ²Department of Theoretical Physics, Lund University, Sweden; ³CERN, Geneva, Switzerland.

Abstract

We compare different procedures for combining fixed-order tree-level matrix element generators with parton showers. We use the case of W-production at the Tevatron and the LHC to compare different implementations of the so-called CKKW scheme and one based on the so-called MLM scheme using different matrix element generators and different parton cascades. We find that although similar results are obtained in all cases, there are important differences.

1 Introduction

One of the most striking features of LHC final states will be the large number of events with several hard jets. Final states with 6 jets from $t\bar{t}$ decays will have a rate of almost 1Hz, with 10-100 times more coming from prompt QCD processes. The immense amount of available phase-space, and the large acceptance of the detectors, with calorimeters covering a region of almost 10 units of pseudorapidity (η), will lead to production and identification of final states with 10 or more jets. These events will hide or strongly modify all possible signals of new physics which involve the chain decay of heavy coloured particles, such as squarks, gluinos or the heavier partners of the top which appear in little-Higgs models. Being able to predict their features is therefore essential.

To achieve this, our calculations need to describe as accurately as possible both the full matrix elements for the underlying hard processes, as well as the subsequent development of the hard partons into jets of hadrons. For the complex final-state topologies we are interested in, no factorization theorem exists however to rigorously separate these two components, providing a constructive algorithm for the implementation of such separation. The main obstacle is the existence of several hard scales, like the jet transverse energies and dijet invariant masses, which for a generic multijet event will span a wide range. This makes it difficult to unambiguously separate the components of the event which belong to the “hard process” (to be calculated using a multiparton amplitude) from those developing during its evolution (described by the parton shower). A given $(N + 1)$ -jet event can be obtained in two ways: from the collinear/soft-radiation evolution of an appropriate $(N + 1)$ -parton final state, or from an N -parton configuration where hard, large-angle emission during its evolution leads to the extra jet. A factorization prescription (in this context this is often called a “matching scheme”) defines, on an event-by-event basis, which of the two paths should be followed. The primary goal of a matching scheme is therefore to avoid double counting (by preventing some events to appear twice, once for each path), as well as dead regions (by ensuring that each configuration is generated by at least one of the allowed paths). Furthermore, a good matching scheme will optimize the choice of the path, using the one which guarantees the best possible approximation to a given kinematics. It is possible to consider therefore different matching schemes, all avoiding the double counting and dead regions, but leading to different results in view of the different ways the calculation is distributed between the matrix element and the shower evolution. As in any factorization scheme, the physics is independent of the separation between phases only if we have complete control over the perturbative expansion. Otherwise a residual scheme-dependence is left. Exploring different matching schemes is therefore crucial to assess the systematic uncertainties of multijet calculations.

In this work we present a first comparison of the three approaches which have been proposed so far, the so-called CKKW scheme, the Lönnblad scheme, and the MLM scheme. After shortly reviewing them, we present predictions for a set of W +multijet distributions at the Tevatron collider and at the LHC.

2 Matching procedures

In general, the different merging procedures all follow a similar strategy:

1. A jet measure is defined and all relevant cross sections including jets are calculated for the process under consideration. I.e. for the production of a final state X in pp -collisions, the cross sections for the processes $pp \rightarrow X + n_{\text{jets}}$ with $n = 0, 1, \dots, n_{\text{max}}$ are evaluated.
2. Hard parton samples are produced with a probability proportional to the respective total cross section, in a corresponding kinematic configuration following the matrix element.
3. The individual configurations are accepted or rejected with a dynamical, kinematics-dependent probability that includes both effects of running coupling constants and of Sudakov effects. In case the event is rejected, step 2 is repeated, i.e. a new parton sample is selected, possibly with a new number of jets.
4. The parton shower is invoked with suitable initial conditions for each of the legs. In some cases, like, e.g. in the MLM procedure described below, this step is performed together with the step before, i.e. the acceptance/rejection of the jet configuration. In all cases the parton shower is constrained not to produce any extra jet; stated in other words: Configurations that would fall into the realm of matrix elements with a higher jet multiplicity are vetoed in the parton shower step.

From the description above it is clear that the merging procedures discussed in this contribution differ mainly

- in the jet definition used in the matrix elements;
- in the way the acceptance/rejection of jet configurations stemming from the matrix element is performed;
- and in details concerning the starting conditions of and the jet vetoing inside the parton showering.

2.1 CKKW

In the original merging description according to [1, 2], which has been implemented [3] in SHERPA [4] in full generality, the acceptance/rejection of jet configurations from the matrix elements and the parton showering step are well-separated.

In this realisation of what is known as the CKKW-prescription the phase space separation for the different multijet processes is achieved through a k_{\perp} -measure [5–7]. For the case of hadron–hadron collisions, two final-state particles belong to two different jets, if their relative transverse momentum

$$k_{\perp}^{(ij)2} = 2 \min \left\{ p_{\perp}^{(i)}, p_{\perp}^{(j)} \right\}^2 \left[\cosh(\eta^{(i)} - \eta^{(j)}) - \cos(\phi^{(i)} - \phi^{(j)}) \right] \quad (1)$$

is larger than a critical value, $k_{\perp,0}^2$. In addition, the transverse momentum of each jet has to be larger than $k_{\perp,0}$. The matrix elements are then reweighted by appropriate Sudakov and coupling weights. The task of the weight attached to a matrix element is to take into account terms that would appear in a corresponding parton shower evolution. Therefore, a “shower history” is reconstructed by clustering the initial and final state partons according to the k_{\perp} -algorithm. The resulting chain of nodal k_{\perp} -measures is interpreted as the sequence of relative transverse momenta of multiple jet production. The first ingredient of the weight are the strong coupling constants taken at the respective nodal values, divided by the value

of α_S used during the matrix element evaluation. The other part of the correction weight is provided by NLL-Sudakov form factors defined by

$$\Delta_{q,g}(Q, Q_0) := \exp \left[- \int_{Q_0}^Q dq \Gamma_{q,g}(Q, q) \right], \quad (2)$$

where the integrated splitting functions $\Gamma_{q,g}$ are given by

$$\Gamma_{q,g}(Q, q) := \begin{cases} \frac{2C_F\alpha_s(q)}{\pi q} \left[\log \frac{Q}{q} - \frac{3}{4} \right] \\ \frac{2C_A\alpha_s(q)}{\pi q} \left[\log \frac{Q}{q} - \frac{11}{12} \right] \end{cases} \quad (3)$$

and contain the running coupling constant and the two leading, logarithmically enhanced terms in the limit when $Q_0 \ll Q$. The two finite, non-logarithmic terms $-3/4$ and $-11/12$, respectively emerge when integrating the non-singular part of the corresponding splitting function in the limits $[0, 1]$. Potentially, when q/Q is not going to zero, these finite terms are larger than the logarithmic terms and thus spoil an interpretation of the emerging NLL-Sudakov form factor as a non-branching probability. Therefore, without affecting the logarithmic order of the Sudakov form factors, these finite terms are integrated over the interval $[q/Q, 1 - q/Q]$ rather than over $[q, Q]$. This way a Sudakov form factor determines the probability for having no emission resolvable at scale Q_0 during the evolution from a higher scale Q to a lower scale Q_0 . A ratio of two Sudakov form factors $\Delta(Q, Q_0)/\Delta(q, Q_0)$ then gives the probability for having no emission resolvable at scale Q_0 during the evolution from Q to q . Having reweighted the matrix element, a smooth transition between this and the parton shower region is achieved by choosing suitable starting conditions for the shower evolution of the parton ensemble and vetoing any parton shower emission that is harder than the separation cut $k_{\perp,0}$.

Within SHERPA the required matrix elements are provided by its internal matrix element generator AMEGIC++ [8] and the parton shower phase is handled by APACIC++ [9, 10]. Beyond the comparisons presented here the SHERPA predictions for W +multijets have already been validated and studied for Tevatron and LHC energies in [11, 12]. Results for the production of pairs of W -bosons have been presented in [13].

2.2 The Dipole Cascade and CKKW

The dipole model [14, 15] as implemented in the ARIADNE program [16] is based around iterating $2 \rightarrow 3$ partonic splitting instead of the usual $1 \rightarrow 2$ partonic splittings in a conventional parton shower. Gluon radiation is modeled as being radiated coherently from a color-anticolor charged parton pair. This has the advantage of eg. including first order correction to the matrix elements for $e^+e^- \rightarrow q\bar{q}$ in a natural way and it also automatically includes the coherence effects modeled by angular ordering in conventional showers. The process of quark antiquark production does not come in as naturally, but can be added [17]. The emissions in the dipole cascade is ordered according to invariant transverse momentum defined as

$$p_{\perp}^2 = \frac{s_{12}s_{23}}{s_{123}}, \quad (4)$$

where s_{ij} is the squared invariant mass of parton i and j , with the emitted parton having index 2.

When applied to hadronic collisions, the dipole model does not separate between initial and final state radiation. Instead all emissions are treated as coming from final state dipoles [18, 19]. To be able to extend the dipole model to hadron collisions, extended colored objects are introduced to model the hadron remnants. Dipoles involving hadron remnants are treated in a similar manner to the normal final-state dipoles. However, since the hadron remnant is considered to be an extended object, emissions with

small wavelength are suppressed. This is modeled by only letting a fraction of the remnant take part in the emission. The fraction that is resolved during the emission is given by

$$a(p_{\perp}) = \left(\frac{\mu}{p_{\perp}} \right)^{\alpha}, \quad (5)$$

where μ is the inverse size of the remnant and α is the dimensionality.

There are two additional forms of emissions which need to be included in the case of hadronic collisions. One corresponds to an initial state $g \rightarrow q\bar{q}$ [20]. This does not come in naturally in the dipole model, but is added by hand in a way similar to that of a conventional initial-state parton shower [20]. The other corresponds to the initial-state $q \rightarrow gq$ (with the gluon entering into the hard sub-process) which could be added in a similar way, but this has not been implemented in ARIADNE yet.

When implementing CKKW for the dipole cascade, the procedure is slightly different from what has been described above [21, 22]. First, rather than just reconstructing emission scales using the k_{\perp} -algorithm, a complete dipole shower history is constructed for each state produced by the Matrix Element generator, basically answering the question *how would ARIADNE have generated this state*. This will produce a complete set of intermediate partonic states, S_i , and the corresponding emission scales, $p_{\perp i}$.

The Sudakov form factors are then introduced using the Sudakov veto algorithm. The idea is that we want to reproduce the Sudakov form factors used in Ariadne. This is done by performing a trial emission starting from each intermediate state S_i with $p_{\perp i}$ as a starting scale. If the emitted parton has a p_{\perp} higher than $p_{\perp i+1}$ the state is rejected. This correspond to keeping the state according to the no emission probability in Ariadne, which is exactly the Sudakov form factor.

It should be noted that for initial-state showers, there are two alternative ways of defining the Sudakov form factor. The definition in eq. (2) is used in eg. HERWIG [23], while eg. PYTHIA [24, 25] uses a form which includes ratios of parton densities. Although formally equivalent to leading logarithmic accuracy, only the latter corresponds exactly to a no-emission probability, and this is the one generated by the Sudakov-veto algorithm. This, however, also means that the reconstructed emissions need not only be reweighted by the running α_S as in the standard CKKW procedure above, but also with ratios of parton densities, which in the case of gluon emissions correspond to the suppression due to the extended remnants in eq. (5) as explained in more detail in [22], where the complete algorithm is presented.

2.3 The MLM procedure

In this approach we match the partons from the ME calculation to the jets reconstructed after the perturbative shower. Parton-level events are defined by a minimum E_T threshold E_T^{min} for the partons, and a minimum separation among them, $\Delta R_{jj} > R_{min}$. A tree structure is defined in analogy with the CKKW algorithm, starting however from the colour-flow extracted from the matrix-element calculation [26], thus defining the scales at which the various powers of α_s are calculated. However, no Sudakov reweighting is applied. Rather, events are showered, without any hard-emission veto during the shower. After evolution, a jet cone algorithm with cone size R_{min} and minimum transverse energy E_T^{min} is applied to the final state. Starting from the hardest parton, the jet which is closest to it in (η, ϕ) is selected. If the distance between the parton and the jet centroid is smaller than R_{min} , the parton and the jet match. The matched jet is removed from the list of jets, and matching for subsequent partons is performed. The event is fully matched if each parton has a matched jet. Events which do not match are rejected. A typical example is when two partons are so close that they cannot generate independent jets, and therefore cannot match. Rejection removes double counting of the leading double logarithms associated to the collinear behaviour of the amplitude when two partons get close. Another example is when a parton is too soft to generate its own jet, again failing matching. This removes double counting of some single logarithms. For events which satisfy matching, it is furthermore required that no extra jet, in addition to those matching the partons, be present. Events with extra jets are rejected, a suppression replacing the Sudakov reweighting used in the CKKW approach. Events obtained by applying this procedure to the

parton level with increasing multiplicity can then be combined to obtain fully inclusive samples spanning a large multiplicity range. Events with extra jets are not rejected in the case of the sample with highest partonic multiplicity. The distributions of observables measured on this inclusive data set should not depend on the value of the parameters E_T^{min} and R_{min} , similar to the $k_{\perp,0}$ independence of the CKKW approach. This algorithm is encoded in the ALPGEN generator [27, 28], where evolution with both HERWIG and PYTHIA are enabled. In the following studies, the results quoted as ‘‘ALPGEN’’ employ the MLM matching scheme, and use ALPGEN for the generation of the parton-level matrix elements and HERWIG for the shower evolution and hadronisation.

3 Examples and comparisons

We present in this Section some concrete examples. We concentrate on the case of W +multijet production, which is one of the most studied final states because of its important role as a background to top quark studies at the Tevatron. At the LHC, W +jets, as well as the similar Z +jets processes, will provide the main irreducible backgrounds to signals such as multijet plus missing transverse energy, typical of Supersymmetry and of other manifestations of new physics. The understanding of W +multijet production at the Tevatron is therefore an essential step towards the validation and tuning of the tools presented here, prior to their utilization at the LHC.

For each of the three codes we calculated a large set of observables, addressing inclusive properties of the events (p_T spectrum of the W and of leading jets), geometric correlations between the jets, and intrinsic properties of the jets themselves, such as energy shapes. In view of the limited space available here we present only a subset of our studies, which will be documented in more detail in a future publication. An independent study of the systematics in the implementation of the CKKW prescription in HERWIG and PYTHIA was documented in [29].

The comparison between the respective results shows a reasonable agreement among the three approaches, but points also to differences, in absolute rates as well as in the shape of individual distributions, which underscore the existence of an underlying systematic uncertainty. The differences are nevertheless by and large consistent with the intrinsic systematic uncertainties of each of the codes, such as the dependence on the generation cuts or on the choice of renormalization scale. There are also differences due to the choice of parton cascade. In particular the ARIADNE cascade is quite different from a conventional parton shower, and it has been shown in this workshop [30] that ARIADNE eg. gives a much harder $p_{\perp W}$ spectrum than does HERWIG or PYTHIA. Now, although the hard emissions in the matching procedures should be described by the exact matrix element, the Sudakov formfactors in the ARIADNE matching (and indirectly in the MLM scheme) are generated by the cascade. In addition, the events in the ARIADNE matching are reweighted by PDF ratios in the same way as is done in the plain cascade. This means that some properties of the cascade may affect also the hard emissions in the matching procedure in these cases.

The existence in each of the codes of parameters specifying the details of the matching algorithms presents therefore an opportunity to tune each code so as to best describe the data. This tuning should be seen as a prerequisite for a quantitative study of the overall theoretical systematics: after the tuning is performed on a given set of final states (e.g. the W +jets considered here), the systematics for other observables or for the extrapolation to the LHC can be obtained by comparing the difference in extrapolation between the various codes. It is therefore auspicious that future analysis of Tevatron data will provide us with spectra corrected for detector effects in a fashion suitable to a direct comparison against theoretical predictions.

The following two sections present results for the Tevatron ($p\bar{p}$ collisions at 1.96 TeV) and for the LHC (pp at 14 TeV), considering events with a positively charged W . Jets are defined by Paige’s GETJET cone-clustering algorithm, with a calorimeter segmentation of $(\Delta\eta, \Delta\phi) = (0.1, 6^\circ)$ and a cone size of 0.7 and 0.4 for Tevatron and LHC, respectively. At the Tevatron (LHC) we consider jets with

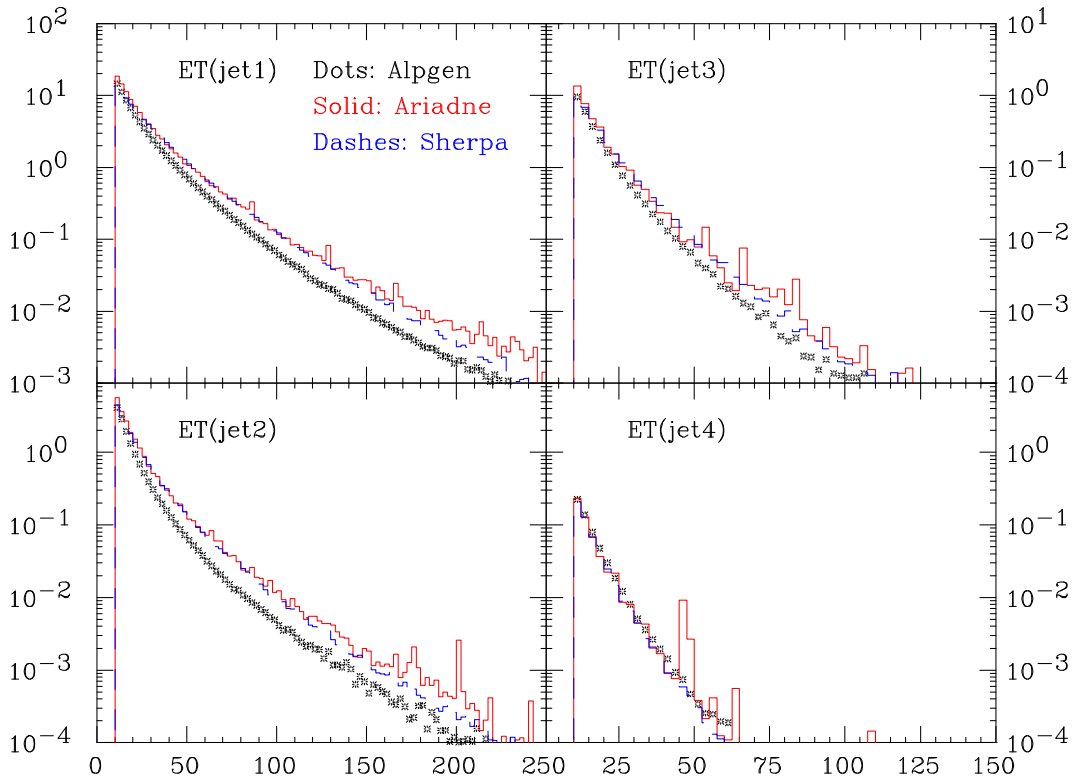


Fig. 1: Inclusive E_T spectra of the leading 4 jets at the Tevatron (pb/GeV).

$E_T > 10(20)$ GeV, within $|\eta| < 2(4.5)$. We use the PDF set CTEQ6L, with $\alpha_S(M_Z) = 0.118$.

For our default distributions, the ALPGEN results for the Tevatron (LHC) were obtained using parton level cuts of $p_{T,min} = 10(20)$ GeV, $|\eta| < 2.5(5)$, $R_{jj} < 0.7(0.4)$ and matching defined by $E_{Tmin} = 10$ GeV and $R = 0.7$. The SHERPA samples have been generated using matrix elements with up to four extra jets and the value of the merging scale has been chosen to $k_{\perp,0} = 10(20)$ GeV, respectively. Finally, for ARIADNE, the parton level cuts were $p_{T,min} = 10(20)$, $R_{jj} < 0.5(0.35)$ and, in addition, a cut on the maximum pseudorapidity of jets, $\eta_{j\max} = 2.5(5.0)$.

In all cases, the analysis is done at the hadron level, but without including the underlying event.

3.1 Tevatron Studies

We start by showing in fig. 1 the inclusive E_T spectra of the leading 4 jets. The absolute rate predicted by each code is used, in units of pb/GeV. We notice that the ALPGEN spectrum for the first two jets is softer than both SHERPA and ARIADNE, with the latter having even harder tails. The spectra for the third and fourth jet are instead in very good agreement, both in shape and normalization. As an indication of possible sources of systematics in these calculations, we rescaled the renormalization scale used in ALPGEN by a factor of 1/2. As seen in fig. 2 the distributions for the leading jets is now in perfect agreement with SHERPA, with an increase in rate for the third and fourth jet. These plots give us an idea of the level of flexibility which is intrinsic in the calculation of higher-order jet production. One should not forget that the rate for production of N jets is proportional to the N th power of α_s , and the absence of the full set of virtual corrections unavoidably leads to a large scale uncertainty.

Figure 3 shows the inclusive η spectra of the leading 4 jets, all normalized to unit area. The asymmetry for the first two jets is due to the W^+ , which preferentially moves in the direction of the proton (positive η). This is partially washed out in the case of the third and fourth jet. There is a good

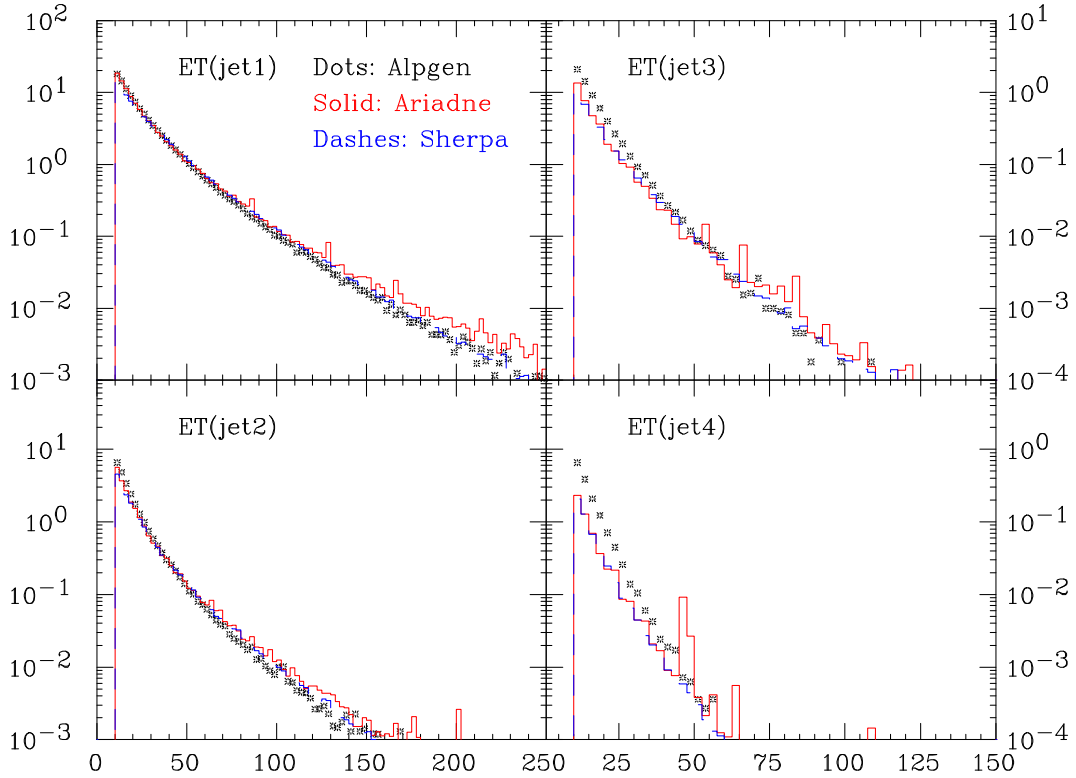


Fig. 2: Same as Fig. 1, but with the ALPGEN renormalization scale reduced by a factor 2.

agreement between the spectra of ALPGEN and SHERPA, while ARIADNE spectra appear to be broader, in particular for the subleading jets. This broadening is expected since the gluon emissions in ARIADNE are essentially unordered in rapidity, which means that the Sudakov form factors applied to the ME-generated states include also a $\log 1/x$ resummation absent in the other programs.

The top-left plot of fig. 4 shows the inclusive p_T distribution of the W^+ boson, with absolute normalization in pb/GeV. This distribution reflects in part the behaviour observed for the spectrum of the leading jet, with ALPGEN slightly softer, and ARIADNE slightly harder than SHERPA. The $|\eta|$ separation between the W and the leading jet of the event is shown in the top-right plot. The two lower plots show instead the distributions of $|\eta(\text{jet}_1) - \eta(\text{jet}_2)|$ and $|\eta(\text{jet}_2) - \eta(\text{jet}_3)|$. These last three plots are normalized to unit area. In all these cases, we observe once more a reflection of the behaviour observed in the inclusive η distributions of the jets: ALPGEN is slightly narrower than SHERPA, and ARIADNE is slightly broader.

3.2 LHC Predictions

In this section we confine ourselves to ALPGEN and SHERPA. It turns out that ARIADNE has a problem in the reweighting related to the fact that initial-state $g \rightarrow q\bar{q}$ emissions, contrary to the gluon emissions, are ordered both in p_\perp and rapidity. With the extra phase space available at the LHC this leads to unnatural reconstructions which, in turn, gives rise to a systematically too high reweighting. A solution for this problem is under investigation and a fuller comparison including ARIADNE will be documented in a future publication.

Following the same sequence of the Tevatron study, we start by showing in fig. 5 the inclusive E_T spectra of the leading 4 jets. The absolute rate predicted by each code is used, in units of pb/GeV. The relative behaviour of the predictions by ALPGEN and SHERPA follows the pattern observed in the

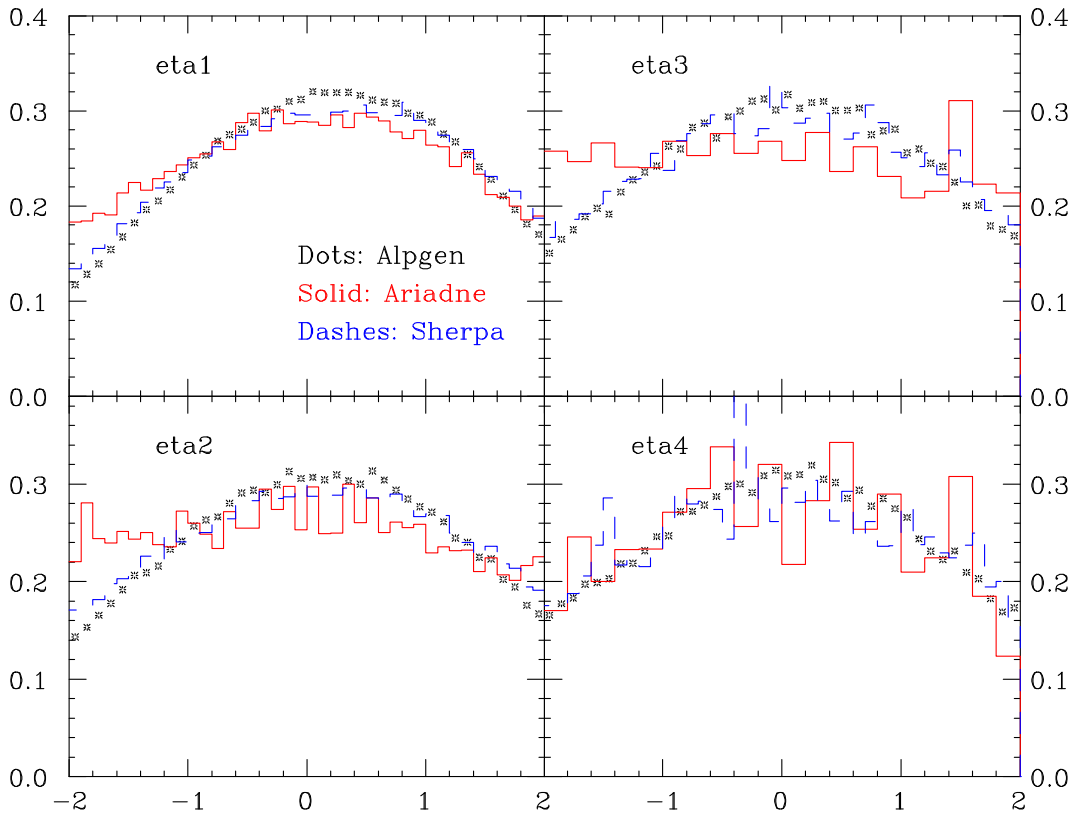


Fig. 3: Inclusive η spectra of the leading 4 jets at the Tevatron, normalized to unit area.

Tevatron case, with ALPGEN being softer in the case of the leading two jets. We do not notice however a deterioration of the discrepancy going from the Tevatron to the LHC, suggesting that once a proper tuning is achieved at lower energy the predictions of two codes for the LHC should be comparable.

Figure 6 shows the inclusive η spectra of the leading 4 jets, all normalized to unit area. The asymmetry now is not present, because of the symmetric rapidity distribution of the W^+ in pp collisions. As in the case of the Tevatron, jet production in ALPGEN is slightly more central than in SHERPA.

The top-left plot of fig. 7 shows the inclusive p_T distribution of the W^+ boson, with absolute normalization in pb/GeV. The $|\eta|$ separation between the W and the leading jet of the event is shown in the top-right plot. The two lower plots show instead the distributions of $|\eta(\text{jet}_1) - \eta(\text{jet}_2)|$ and $|\eta(\text{jet}_2) - \eta(\text{jet}_3)|$. These last three plots are normalized to unit area. As before, the features of these comparisons reflect what observed in the inclusive jet properties.

4 Conclusions

This document summarizes our study of a preliminary comparison of three independent approaches to the problems of merging matrix element and parton shower evolution for multijet final states. Overall, the picture shows a general consistency between the three approaches, although there are occasional differences. The origin of these differences is under study. It could be based on intrinsic differences between the matching schemes, as well as to differences between the different shower algorithms used in the three cases. We expect nevertheless that these differences be reconciled with appropriate changes in the default parameter settings for the matching schemes, as partly supported by the few systematic studies presented here. Validation and tuning on current Tevatron data is essential, and will allow to reduce the systematics.

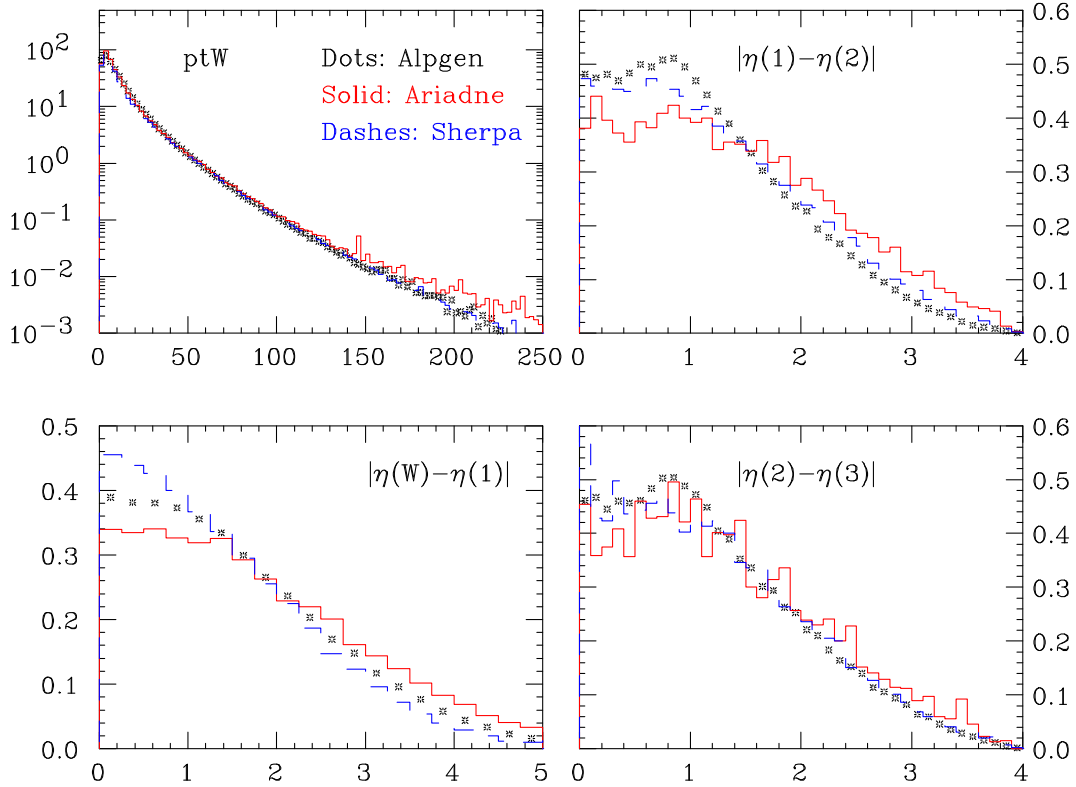


Fig. 4: Top left: inclusive $p_{\perp}(W^+)$ spectrum, pb/GeV. Bottom left: $|\eta(W^+) - \eta(\text{jet}_1)|$ (unit area). Top right: $|\eta(\text{jet}_1) - \eta(\text{jet}_2)|$ and bottom right: $|\eta(\text{jet}_2) - \eta(\text{jet}_3)|$ (unit area).

It is also important to compare these models to HERA data. However, besides some preliminary investigations for ARIADNE [31], there is no program which properly implements a CKKW or MLM matching scheme for DIS. The energy of HERA is, of course, lower, as are the jet multiplicities and jet energies, but HERA has the advantage of providing a large phase space for jet production which is not mainly determined by the hard scale, Q^2 , but rather by the total energy, giving rise to large logarithms of $x \approx Q^2/W^2$ which need to be resummed to all orders. This is in contrast to the Tevatron, where the phase space for additional jets in W -production mainly are determined by m_W . However, when going to the LHC there may also be important effects of the increased energy, and there will be large logarithms of $x \propto m_W/\sqrt{S}$ present, which may need to be resummed. The peculiar treatment of the available phase space in the plain ARIADNE cascade means that some logarithms of x are resummed in contrast to conventional initial-state parton cascades. This feature survives the matching procedure and is the reason for the broader rapidity spectra presented in the figures above. In DIS this is reflected by the increased rate of forward jets, and such measurements are known to be well reproduced by ARIADNE while conventional parton showers fail. It would be very interesting if the matching of these conventional showers with higher order matrix elements would improve the description of forward jets. In that case the extrapolation of the Tevatron results to the LHC would be on much safer grounds.

As our study of the LHC distributions suggests, the increase in energy exhibits the same pattern of discrepancies observed at the Tevatron. We therefore expect that if different algorithms are tuned on the same set of data, say Tevatron W +jets, they will extrapolate in the same way to the LHC or to different final states, for example multijet configurations without W bosons. While these systematic studies can be performed directly at the Monte Carlo level, only the availability of real measurements from the Tevatron can inject the necessary level of realism in these explorations. We look forward to the availability of such data.

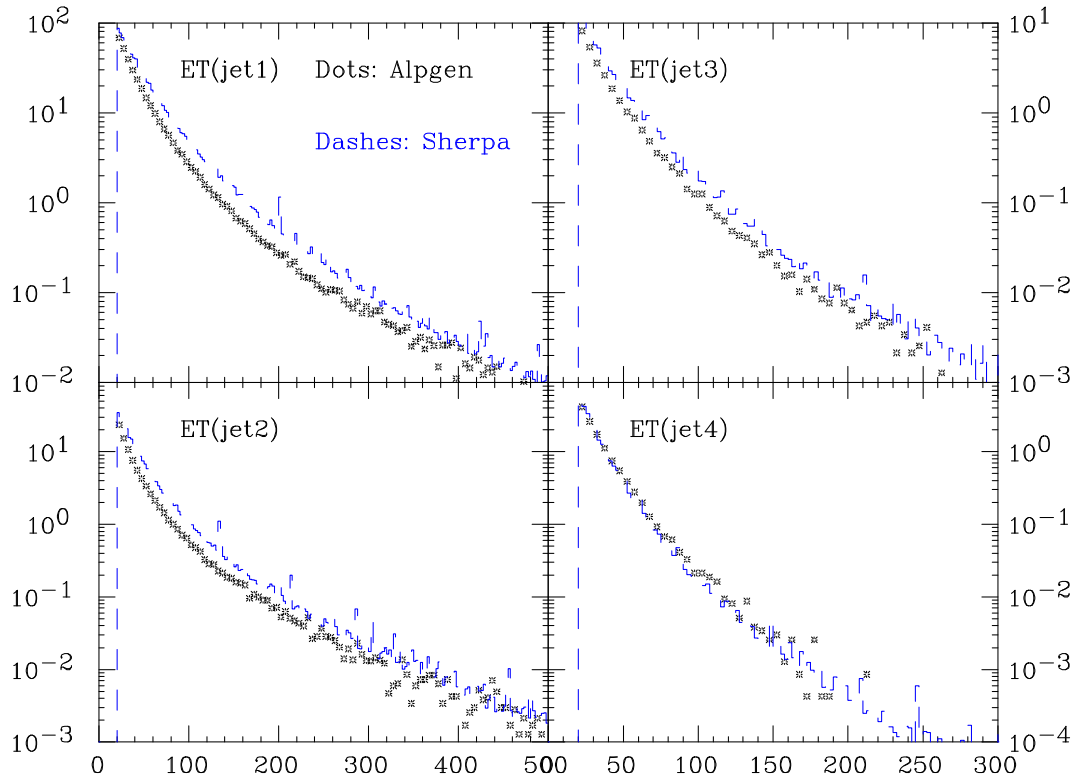


Fig. 5: Inclusive E_T spectra of the leading 4 jets at the LHC (pb/GeV).

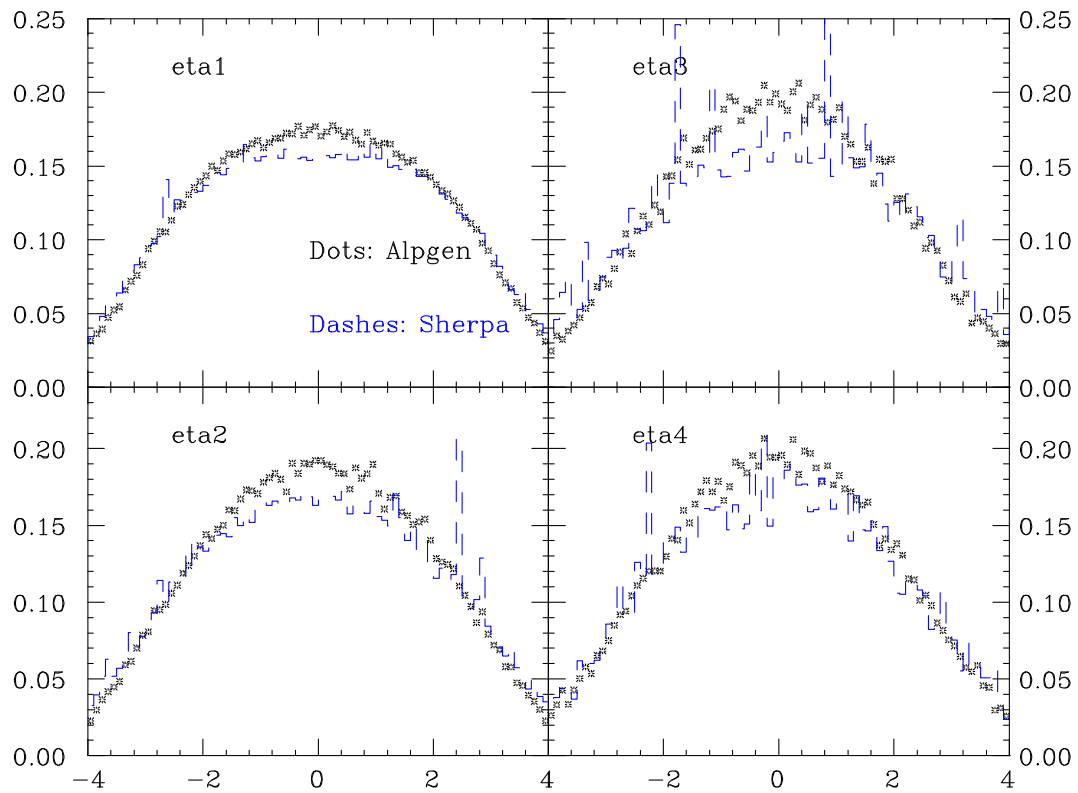


Fig. 6: Inclusive η spectra of the leading 4 jets at the LHC, normalized to unit area.

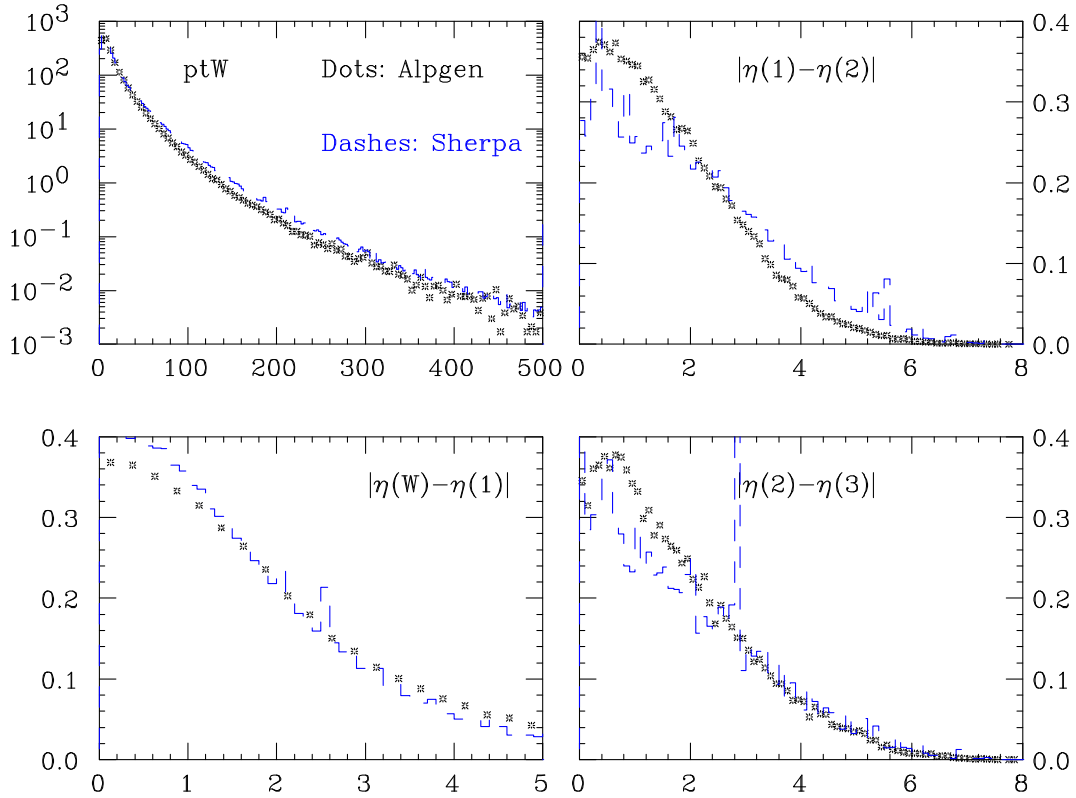


Fig. 7: Top left: inclusive $pt_T(W^+)$ spectrum, pb/GeV. Bottom left: $|\eta(W^+) - \eta(\text{jet}_1)|$ (unit area). Top right: $|\eta(\text{jet}_1) - \eta(\text{jet}_2)|$ and bottom right: $|\eta(\text{jet}_2) - \eta(\text{jet}_3)|$ (unit area).

References

- [1] S. Catani, F. Krauss, R. Kuhn, and B. R. Webber, *JHEP* **0111**, 063 (2001). [arXiv:hep-ph/0109231](#).
- [2] F. Krauss, *JHEP* **0208**, 015 (2002). [arXiv:hep-ph/0205283](#).
- [3] A. Schälicke and F. Krauss, *JHEP* **07**, 018 (2005). [hep-ph/0503281](#).
- [4] T. Gleisberg, S. Höche, F. Krauss, A. Schälicke, S. Schumann, and J. Winter, *JHEP* **0402**, 056 (2004). [arXiv:hep-ph/0311263](#).
- [5] S. Catani, Y. L. Dokshitzer, M. Olsson, G. Turnock, and B. R. Webber, *Phys. Lett. B* **269**, 432 (1991).
- [6] S. Catani, Y. L. Dokshitzer, and B. R. Webber, *Phys. Lett. B* **285**, 291 (1992).
- [7] S. Catani, Y. L. Dokshitzer, and B. R. Webber, *Nucl. Phys. B* **406**, 187 (1993).
- [8] F. Krauss, R. Kuhn, and G. Soff, *JHEP* **0111**, 044 (2002). [arXiv:hep-ph/0109036](#).
- [9] R. Kuhn, F. Krauss, B. Ivanyi, and G. Soff, *Comput. Phys. Commun.* **134**, 223 (2001). [hep-ph/0004270](#).
- [10] F. Krauss, A. Schälicke, and G. Soff, [hep-ph/0503087](#).
- [11] F. Krauss, A. Schälicke, S. Schumann, and G. Soff, *Phys. Rev. D* **70**, 114009 (2004). [hep-ph/0409106](#).
- [12] F. Krauss, A. Schälicke, S. Schumann, and G. Soff, *Phys. Rev. D* **72**, 054017 (2005). [hep-ph/0503280](#).
- [13] T. Gleisberg, F. Krauss, A. Schälicke, S. Schumann, and J.-C. Winter, *Phys. Rev. D* **72**, 034028 (2005). [hep-ph/0504032](#).

- [14] G. Gustafson and U. Pettersson, Nucl. Phys. **B306**, 746 (1988).
- [15] G. Gustafson, Phys. Lett. **B175**, 453 (1986).
- [16] L. Lönnblad, Comput. Phys. Commun. **71**, 15 (1992).
- [17] B. Andersson, G. Gustafson, and L. Lönnblad, Nucl. Phys. **B339**, 393 (1990).
- [18] B. Andersson, G. Gustafson, L. Lönnblad, and U. Pettersson, Z. Phys. **C43**, 625 (1989).
- [19] L. Lönnblad, Nucl. Phys. **B458**, 215 (1996). hep-ph/9508261.
- [20] L. Lönnblad, Z. Phys. **C65**, 285 (1995).
- [21] L. Lönnblad, JHEP **05**, 046 (2002). hep-ph/0112284.
- [22] N. Lavesson and L. Lönnblad, JHEP **07**, 054 (2005). hep-ph/0503293.
- [23] G. Corcella *et al.*, JHEP **01**, 010 (2001). hep-ph/0011363.
- [24] T. Sjöstrand, and others, Comput. Phys. Commun. **135**, 238 (2001). arXiv:hep-ph/0010017.
- [25] T. Sjöstrand, L. Lönnblad, S. Mrenna, and P. Skands (2003). hep-ph/0308153.
- [26] F. Caravaglios, M. L. Mangano, M. Moretti, and R. Pittau, Nucl. Phys. **B539**, 215 (1999). hep-ph/9807570.
- [27] M. L. Mangano, M. Moretti, and R. Pittau, Nucl. Phys. **B632**, 343 (2002). hep-ph/0108069.
- [28] M. L. Mangano, M. Moretti, F. Piccinini, R. Pittau, and A. D. Polosa, JHEP **07**, 001 (2003). hep-ph/0206293.
- [29] S. Mrenna and P. Richardson, JHEP **05**, 040 (2004). hep-ph/0312274.
- [30] B. Kersevan and E. Richter-Was., *The Monte Carlo Event Generator AcerMC and package AcderDET*. These Proceedings.
- [31] C. Aberg, *Correcting the colour dipole cascade with fixed order matrix elements in deep inelastic scattering*. Diploma thesis, Lund preprint LU-TP 04-25.

Constrained non-Markovian Monte Carlo modeling of the evolution equation in QCD*

S. Jadach and M. Skrzypek

Institute of Nuclear Physics, Academy of Sciences, ul. Radzikowskiego 152, 31-342 Cracow, Poland and CERN Department of Physics, Theory Division, CH-1211 Geneva 23, Switzerland

Abstract

A new class of the constrained Monte Carlo (CMC) algorithms for the QCD evolution equation was recently discovered. The constraint is imposed on the type and the total longitudinal energy of the parton exiting QCD evolution and entering a hard process. The efficiency of the new CMCs is found to be reasonable.

This brief report summarizes the recent developments in the area of the Monte Carlo (MC) techniques for the perturbative QCD calculations. Most of it was done at the time of the present HERA–LHC workshop, partial results being presented at several of its meetings. At present, two papers, [1] and [2], demonstrating the principal results are already available. Generally, these MC techniques concern the QCD evolution of the parton distribution functions (PDFs) $D_k(x, Q)$, where k denotes the type of the parton (quark, gluon), x the fraction of longitudinal momentum of the initial hadron carried by the parton, and the size of the available real/virtual emission phase space is Q . The evolution equation describes the response of the PDF to an increase of Q ; $D_k(x, Q)$ is an inclusive distribution and can be measured almost directly in hadron–lepton scattering. On the other hand, it was always known that there exists in QCD an *exclusive* picture of the PDF, the so-called parton-shower process, in which $D_k(x, Q)$ is the distribution of the parton exiting the emission chain and entering the hard process (lepton–quark for example). The kernel functions $P_{kj}(Q, z)$, that govern the differential evolution equations of PDFs are closely related to distributions governing a single emission process $(i - 1) \rightarrow i$ in the parton shower: $P_{k_i k_{i-1}}(Q_i, x_i/x_{i-1})$.

In other words, the evolution (Q -dependence) of PDFs and the parton shower represent two faces of the same QCD reality. The first one (inclusive) is well suited for basic precision tests of QCD at hadron–lepton colliders, while the second one (exclusive) provides realistic exclusive Monte Carlo modeling, vitally needed for experiments at high-energy particle colliders.

At this point, it is worth stressing that, so far, we were referring to DGLAP-type PDFs [3] and their evolution, and to constructing a parton-shower MC starting from them, as was done two decades ago and is still done today. This involves a certain amount of “backward engineering” and educated guesses, because the classical inclusive PDFs integrate over the p_T of the exiting parton. The so-called unintegrated PDFs (UPDFs) $D_k(x, p_T, Q)$ would be more suitable for the purpose, leading to higher-quality QCD calculations. UPDFs are, however, more complicated to handle, both numerically and theoretically. (It is still a challenge to construct a parton-shower MC based consistently on the theoretically well defined UPDFs.)

Another interesting “entanglement” of the evolution of PDFs on one side and of the parton shower (PS) MC on the other side is also present in the modeling of the showering of the incoming hadron — mostly for technical reasons and convenience. The Markovian nature of the QCD evolution can be exploited directly in the PS MC, where partons split/decay as long as there is enough energy to dissipate (final state) or the upper boundary Q of the phase space is hit (initial state). The multiparton distribution in such a MC is a product of the evolution kernels. However, such a direct Markovian MC simulation of a shower is hopelessly inefficient in the initial state, because the hard process accepts only certain types

*Supported in part by the EU grant MTKD-CT-2004-510126, in partnership with the CERN Physics Department.

and momenta of the incoming partons — most of the *shower histories* are rejected (zero MC weight) by the hard process, in particular when forming narrow resonances such as electroweak bosons or Higgs boson at the LHC. A well-known “workaround” is Sjöstrand’s backward evolution MC algorithm, used currently in all PS MCs, e.g., HERWIG [4] and PYTHIA [5]. Contrary to the forward Markovian MC, where the physics inputs are PDFs at low $Q_0 \sim 1$ GeV and the evolution kernels, in the backward evolution MC one has to know PDFs in the entire range (Q_0, Q) from a separate non-MC numerical program solving the evolution equation to provide look-up tables (or numerical parametrization) for them¹.

The following question has been pending in the parton-shower MC methodology for a long time: Could one invent an efficient “monolithic” MC algorithm for the parton shower from the incoming hadron, in which no external PDFs are needed and the only input are PDFs at Q_0 and the evolution kernel (the QCD evolution being a built-in feature of the parton shower MC)? Another question rises immediately: Why bother? Especially since this is a tough technical problem. This cannot still be fully answered before the above technique is applied in the full-scale (four-momentum level) PS MC. Generally, we hope that this technique will open new avenues in the development of the PS MC at the next-to-leading-logarithmic (NLL) level. In particular, it may help in constructing PS MCs closely related to unintegrated structure functions and, secondly, it may provide a better integration of the NLL parton shower (yet to be implemented!) with the NLL calculation for the hard process.

The first solution of the above problem of finding an efficient “constrained MC” (CMC) algorithm for the QCD evolution was presented in refs. [1, 6]. This solution belongs to what we call a CMC class II, and it relies on the observation that all initial PDFs at Q_0 can be approximated by $\text{const} \cdot x_0^{\eta-1}$; this is to be corrected by the MC weight at a later stage. This allows elimination of the constraint $x = \prod_i z_i$, at the expense of x_0 , keeping the factorized form of the products of the kernels. Simplifying phase-space boundaries in the space of z_i is the next ingredient of the algorithm. Finally, in order to reach a reasonable MC efficiency for the pure bremsstrahlung case out of the gluon emission line, one has to generate a $1/z$ singularity in the $G \rightarrow G$ kernel in a separate branch of the MC. The overall efficiency of the MC is satisfactory, as is demonstrated in Ref. [1] for the case of the pure bremsstrahlung out of the gluon and quark colour charge. Generalization to the quark–gluon transition is outlined, but not yet implemented. The main drawback of this method is its algebraic complexity. Further improvement of its relatively low MC efficiency is possible (even though it could lead to even more algebraic complexity).

The second, more efficient, CMC algorithm was presented in Ref. [2] (as well as during the October 2004 meeting of the workshop). It belongs to what we call a CMC class I. The main idea is to project/map points from the hyperspace defined by the energy constraint $x = \prod_i z_i$, into a simpler hyperspace, defined by the hardest emission, $x = \min z_i$. This mapping is accompanied by the appropriate MC weight, which compensates exactly for the deformation of the distributions involved, and the bookkeeping of the hyperspace boundaries is rigorous. The above describes a CMC for the pure bremsstrahlung segment of the gluon emission out of a quark or gluon chain. Many such segments are interconnected by the quark–gluon transitions. The algebraic hierarchic reorganization of the emission chain into a super-level of the quark–gluon transitions and sub-level of the pure bremsstrahlung is an important ingredient in all CMC algorithms and will be published separately [7]. The basic observation made in Ref. [8] is that the average number of super-level transitions is low, ~ 1 ; hence for precision of a 10^{-4} it is sufficient to limit it to three or four transitions. The integration/simulation of the super-level variables is done efficiently using the general-purpose MC tool FOAM [9, 10]. The above proof of the correctness of the CMC class I algorithm concept was given in Ref. [2] for the full DGLAP-type QCD evolution with the LL kernels (including quark–gluon transitions).

¹Backward evolution is basically a change in the order of the generation of the variables: Consider generating $\rho(x, y)$, where one generates first x according to $\rho(x) = \int dy \rho(x, y)$, and next y according to $\rho(x, y)$, by means of *analytical* mappings of x and y into uniform random numbers. However, such analytical mappings may not exist, if we insist on generating first x and next y ! Nevertheless, we may still proceed with the same method by “brute force”, if we pretabulate and invert numerically the functions $R(x) = \int^x \int dx' dy' \rho(x', y')$ and $R_x(y) = \int^y dy' \rho(x, y')$. This is what is done in a more dimensional case of the backward-evolution MC; it also explains why pretabulated PDFs are needed in these methods.

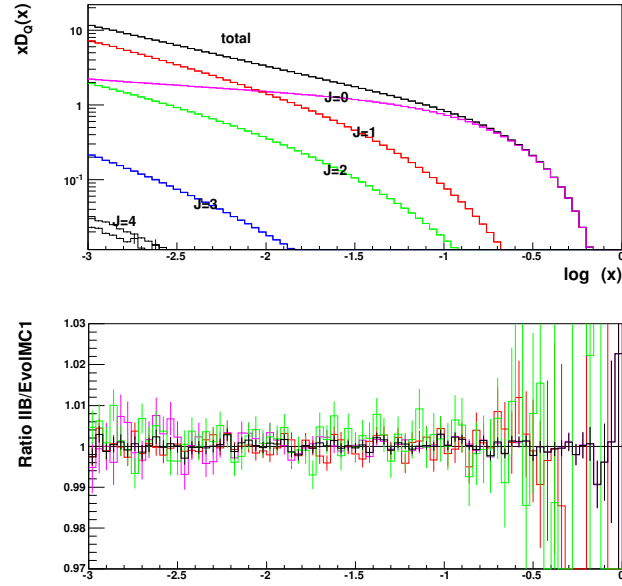


Fig. 1: CMC of the one-loop CCFM versus the corresponding MMC for quarks; number of quark–gluon transitions $J = 0, 1, 2, 3, 4$, and the total. The ratios in the lower plot are for $n = 0, 1$ and the total (blue).

Although our main aim is to construct the non-Markovian CMC class of algorithms, we have developed in parallel the family of Markovian MC (MMC) algorithms/programs, which provide numerical solutions of the QCD evolution equations with high precision, $\sim 10^{-3}$. We use them at each step of the CMC development as numerical benchmarks for the precision tests of the algorithms and their software implementations. The first example of MMC for DGLAP at LL was defined/examined in Ref. [8] and tested using the non-MC program QCDnum16 [11]². In some cases our MMC programs stand ahead of their CMC brothers; for instance, they already include NLL DGLAP kernels. A systematic description of the MMC family of our MC toolbox is still under preparation [13].

The last development at the time of the workshop was an extension of the CMC type-I algorithm from DGLAP to CCFM one-loop evolution [14] (also referred to as HERWIG evolution [15]), in which the strong coupling constant gains z -dependence, $\alpha_s(Q) \rightarrow \alpha_s(Q(1-z))$, as advocated in Ref. [16], confirmed by NLL calculations [17]. The above ansatz also compels introduction of a Q -dependent IR cutoff, $\varepsilon = Q_\varepsilon/Q$: another departure from DGLAP. This version of the CMC is still unpublished. Its version for the pure bremsstrahlung was presented at the March 2005 meeting of the workshop; in particular a perfect numerical agreement with the counterpart MMC was demonstrated. Recently both CMC and MMC for the one-loop CCFM were extended to quark–gluon transitions, and again perfect agreement was found.

For the detailed description of the new CMC algorithm, we refer the reader to the corresponding papers [1] and [2] and workshop presentations³. Here, let us only show one essential step in the development of the CMC for the one-loop CCFM model — the mapping of the Sudakov variables for the pure bremsstrahlung:

$$\begin{aligned}
 I &= \int_{t_0}^{t_1} dt \int_0^{z_1} dz \alpha(Q(1-z)) z P_{GG}^{\Theta}(z, t) \\
 &= \frac{2}{\beta_0} \int_0^{z_1} dz \int_{t_0}^{t_1} dt \frac{1}{\hat{t} + \ln(1-z)} \frac{\theta_{\ln(1-z) > \hat{t}_\varepsilon - \hat{t}}}{1-z} = \frac{2}{\beta_0} \int_0^{y_{\max}} dy(z) \int_0^1 ds(t).
 \end{aligned} \tag{1}$$

²It was also compared with the non-MC program APCheb [12].

³To be found at <http://jadach.home.cern.ch/jadach/>.

The short-hand notation $\hat{t} = \hat{t}(t) \equiv t - t_\Lambda$ and $v = \ln(1 - z)$ supplements that of Ref. [2] in use, and the mapping reads

$$\begin{aligned}
 y(z) &= \rho(v_1; \hat{t}_1, \hat{t}_0) = \rho(v_1 + \hat{t}_1) - \theta_{v_1 > t_\epsilon - t_0} \rho(v_1 + \hat{t}_0), & s(t) &= \frac{\ln(\hat{t} + v)}{\rho'(v; \hat{t}_1, \hat{t}_0)}, \\
 \rho'(v; \hat{t}_1, \hat{t}_0) &= \theta_{v < t_\epsilon - t_0} \rho'(v + \hat{t}_1) + \theta_{v > t_\epsilon - t_0} [\rho'(v + \hat{t}_1) - \rho'(v + \hat{t}_0)],
 \end{aligned}
 \tag{2}$$

where $\rho(t) \equiv \hat{t}(\ln \hat{t} - \ln \hat{t}_\epsilon) + \hat{t}_\epsilon - \hat{t}$. Once the above mapping is set, the same algorithm, with the parallel shift $y_i \rightarrow y_i + Y$, can be used in this case. The super-level of quark–gluon transitions is again implemented using FOAM⁴. A numerical comparison of the corresponding CMC and MMC programs is shown in fig. 1. The MC efficiency is comparable with that of the DGLAP case.

Summary: We have constructed and tested new, efficient, constrained MC algorithms for the initial-state parton-emission process in QCD.

References

- [1] S. Jadach and M. Skrzypek, report IFJPAN-V-04-06, hep-ph/0504205, Acta Phys. Pol. in press.
- [2] S. Jadach and M. Skrzypek, report IFJPAN-V-04-07, hep-ph/0504263.
- [3] L.N. Lipatov, *Sov. J. Nucl. Phys.* **20** (1975) 95;
V.N. Gribov and L.N. Lipatov, *Sov. J. Nucl. Phys.* **15** (1972) 438;
G. Altarelli and G. Parisi, *Nucl. Phys.* **126** (1977) 298;
Yu. L. Dokshitzer, *Sov. Phys. JETP* **46** (1977) 64.
- [4] G. Corcella *et al.*, *JHEP* **01** (2001) 010, hep-ph/0011363.
- [5] T. Sjöstrand *et al.*, *Comput. Phys. Commun.* **135** (2001) 238–259, hep-ph/0010017.
- [6] S. Jadach and M. Skrzypek, *Nucl. Phys. Proc. Suppl.* **135** (2004) 338–341.
- [7] S. Jadach, M. Skrzypek, and Z. Was, Report IFJPAN-V-04-09.
- [8] S. Jadach and M. Skrzypek, *Acta Phys. Polon.* **B35** (2004) 745–756, hep-ph/0312355.
- [9] S. Jadach, *Comput. Phys. Commun.* **152** (2003) 55–100, physics/0203033.
- [10] S. Jadach and P. Sawicki, physics/0506084.
- [11] M. Botje, ZEUS Note 97-066, <http://www.nikhef.nl/h24/qcdcode/>.
- [12] K. Golec-Biernat, APCheb33, the Fortran code to be obtained from the author; unpublished.
- [13] K. Golec-Biernat, S. Jadach, M. Skrzypek, and W. Placzek, report IFJPAN-V-05-03.
- [14] M. Ciafaloni, *Nucl. Phys.* **B296** (1988) 49;
S. Catani, F. Fiorani, and G. Marchesini, *Phys. Lett.* **B234** 339, *Nucl. Phys.* **B336** (1990) 18.
- [15] P. Nason, *JHEP* **11** (2004) 040, hep-ph/0409146.
- [16] D. Amati, A. Bassetto, M. Ciafaloni, G. Marchesini, and G. Veneziano, *Nucl. Phys.* **B173** (1980) 429.
- [17] G. Curci, W. Furmanski, and R. Petronzio, *Nucl. Phys.* **B175** (1980) 27.

⁴The z -independent $\alpha_s(t)$ is set in front of the relevant flavour-changing kernels to simplify the program.

QED \otimes QCD Exponentiation and Shower/ME Matching at the LHC*

B.F.L. Ward and S.A. Yost

Department of Physics, Baylor University, Waco, TX, USA

Abstract

We present the elements of QED \otimes QCD exponentiation and its interplay with shower/ME matching in precision LHC physics scenarios. Applications to single heavy gauge boson production at hadron colliders are illustrated.

In the LHC environment, precision predictions for the effects of multiple gluon and multiple photon radiative processes will be needed to realize the true potential of the attendant physics program. For example, while the current precision tag for the luminosity at FNAL is at the $\sim 7\%$ level [1], the high precision requirements for the LHC dictate an experimental precision tag for the luminosity at the 2% level [2]. This means that the theoretical precision tag requirement for the corresponding luminosity processes, such as single W,Z production with the subsequent decay into light lepton pairs, must be at the 1% level in order not to spoil the over-all precision of the respective luminosity determinations at the LHC. This theoretical precision tag means that multiple gluon and multiple photon radiative effects in the latter processes must be controlled to the stated precision. With this objective in mind, we have developed the theory of QED \otimes QCD exponentiation to allow the simultaneous resummation of the multiple gluon and multiple photon radiative effects in LHC physics processes, to be realized ultimately by MC methods on an event-by-event basis in the presence of parton showers in a framework which allows us to systematically improve the accuracy of the calculations without double-counting of effects in principle to all orders in both α_s and α .

Specifically, the new QED \otimes QCD exponentiation theory is an extension of the QCD exponentiation theory presented in Refs. [3]¹. We recall that in the latter references it has been established that the following result holds for a process such as $q + \bar{q}' \rightarrow V + n(G) + X \rightarrow \bar{\ell}\ell' + n(g) + X$:

$$d\hat{\sigma}_{\text{exp}} = \sum_n d\hat{\sigma}^n = e^{\text{SUM}_{\text{IR}}(\text{QCD})} \sum_{n=0}^{\infty} \int \prod_{j=1}^n \frac{d^3 k_j}{k_j} \int \frac{d^4 y}{(2\pi)^4} e^{iy \cdot (P_1 + P_2 - Q_1 - Q_2 - \sum k_j) + D_{\text{QCD}}} * \tilde{\beta}_n(k_1, \dots, k_n) \frac{d^3 P_2}{P_2^0} \frac{d^3 Q_2}{Q_2^0} \quad (1)$$

where gluon residuals $\tilde{\beta}_n(k_1, \dots, k_n)$, defined by Ref. [3], are free of all infrared divergences to all orders in $\alpha_s(Q)$. The functions $SUM_{\text{IR}}(\text{QCD})$, D_{QCD} , together with the basic infrared functions $B_{\text{QCD}}^{\text{nls}}$, $\tilde{B}_{\text{QCD}}^{\text{nls}}$, $\tilde{S}_{\text{QCD}}^{\text{nls}}$ are specified in Ref. [3]. Here $V = W^\pm, Z$, and $\ell = e, \mu$, $\ell' = \nu_e, \nu_\mu(e, \mu)$ respectively for $V = W^+(Z)$, and $\ell = \nu_e, \nu_\mu$, $\ell' = e, \mu$ respectively for $V = W^-$. We call attention to the essential compensation between the left over genuine non-Abelian IR virtual and real singularities between $\int dPh \tilde{\beta}_n$ and $\int dPh \tilde{\beta}_{n+1}$ respectively that really allows us to isolate $\tilde{\beta}_j$ and distinguishes QCD from QED, where no such compensation occurs. The result in (1) has been realized by Monte Carlo methods [3]. See also Refs. [5–7] for exact $\mathcal{O}(\alpha_s^2)$ and Refs. [8–10] for exact $\mathcal{O}(\alpha)$ results on the W,Z production processes which we discuss here.

*Work partly supported by US DOE grant DE-FG02-05ER41399 and by NATO grant PST.CLG.980342.

¹We stress that the formal proof of exponentiation in non-Abelian gauge theories in the *eikonal approximation* is given in Ref. [4]. The results in Ref. [3] are in contrast *exact* but have an exponent that only contains the leading contribution of the exponent in Ref. [4].

The new $QED \otimes QCD$ theory is obtained by simultaneously exponentiating the large IR terms in QCD and the exact IR divergent terms in QED, so that we arrive at the new result

$$\begin{aligned}
 d\hat{\sigma}_{\text{exp}} &= e^{\text{SUM}_{\text{IR}}(\text{QCED})} \\
 &\sum_{n,m=0}^{\infty} \int \prod_{j_1=1}^n \frac{d^3 k_{j_1}}{k_{j_1}} \prod_{j_2=1}^m \frac{d^3 k'_{j_2}}{k'_{j_2}} \int \frac{d^4 y}{(2\pi)^4} \\
 &e^{iy \cdot (p_1 + q_1 - p_2 - q_2 - \sum k_{j_1} - \sum k'_{j_2}) + D_{\text{QCED}}} \\
 &\tilde{\beta}_{n,m}(k_1, \dots, k_n; k'_1, \dots, k'_m) \frac{d^3 p_2}{p_2^0} \frac{d^3 q_2}{q_2^0},
 \end{aligned} \tag{2}$$

where the new YFS [11, 12] residuals, defined in Ref. [13], $\tilde{\beta}_{n,m}(k_1, \dots, k_n; k'_1, \dots, k'_m)$, with n hard gluons and m hard photons, represent the successive application of the YFS expansion first for QCD and subsequently for QED. The functions $\text{SUM}_{\text{IR}}(\text{QCED})$, D_{QCED} are determined from their analogs $\text{SUM}_{\text{IR}}(\text{QCD})$, D_{QCD} via the substitutions

$$\begin{aligned}
 B_{\text{QCD}}^{\text{nls}} &\rightarrow B_{\text{QCD}}^{\text{nls}} + B_{\text{QED}}^{\text{nls}} \equiv B_{\text{QCED}}^{\text{nls}}, \\
 \tilde{B}_{\text{QCD}}^{\text{nls}} &\rightarrow \tilde{B}_{\text{QCD}}^{\text{nls}} + \tilde{B}_{\text{QED}}^{\text{nls}} \equiv \tilde{B}_{\text{QCED}}^{\text{nls}}, \\
 \tilde{S}_{\text{QCD}}^{\text{nls}} &\rightarrow \tilde{S}_{\text{QCD}}^{\text{nls}} + \tilde{S}_{\text{QED}}^{\text{nls}} \equiv \tilde{S}_{\text{QCED}}^{\text{nls}}
 \end{aligned} \tag{3}$$

everywhere in expressions for the latter functions given in Refs. [3]. The residuals $\tilde{\beta}_{n,m}$ are free of all infrared singularities and the result in (2) is a representation that is exact and that can therefore be used to make contact with parton shower MC's without double counting or the unnecessary averaging of effects such as the gluon azimuthal angular distribution relative to its parent's momentum direction.

In the respective infrared algebra (QCED) in (2), the average Bjorken x values

$$\begin{aligned}
 x_{\text{avg}}(\text{QED}) &\cong \gamma(\text{QED}) / (1 + \gamma(\text{QED})) \\
 x_{\text{avg}}(\text{QCD}) &\cong \gamma(\text{QCD}) / (1 + \gamma(\text{QCD}))
 \end{aligned}$$

where $\gamma(A) = \frac{2\alpha_A \mathcal{C}_A}{\pi} (L_s - 1)$, $A = \text{QED}, \text{QCD}$, with $\mathcal{C}_A = Q_f^2, C_F$, respectively, for $A = \text{QED}, \text{QCD}$ and the big log L_s , imply that QCD dominant corrections happen an order of magnitude earlier than those for QED. This means that the leading $\tilde{\beta}_{0,0}$ -level gives already a good estimate of the size of the interplay between the higher order QED and QCD effects which we will use to illustrate (2) here.

More precisely, for the processes $pp \rightarrow V + n(\gamma) + m(g) + X \rightarrow \bar{\ell}\ell' + n'(\gamma) + m(g) + X$, where $V = W^\pm, Z$, and $\ell = e, \mu$, $\ell' = \nu_e, \nu_\mu(e, \mu)$ respectively for $V = W^+(Z)$, and $\ell = \nu_e, \nu_\mu$, $\ell' = e, \mu$ respectively for $V = W^-$, we have the usual formula (we use the standard notation here [13])

$$\begin{aligned}
 d\sigma_{\text{exp}}(pp \rightarrow V + X \rightarrow \bar{\ell}\ell' + X') &= \\
 \sum_{i,j} \int dx_i dx_j F_i(x_i) F_j(x_j) d\hat{\sigma}_{\text{exp}}(x_i x_j s),
 \end{aligned} \tag{4}$$

and we use the result in (2) here with semi-analytical methods and structure functions from Ref. [14]. A Monte Carlo realization will appear elsewhere [15].

We do not attempt in the *present* discussion to replace HERWIG [16] and/or PYTHIA [17] – we intend *here* to combine our exact YFS calculus with HERWIG and/or PYTHIA by using the latter to generate a parton shower starting from the initial (x_1, x_2) point at factorization scale μ after this point is provided by the $\{F_i\}$. This combination of theoretical constructs can be systematically improved with exact results order-by-order in α_s , where currently the state of the art in such a calculation is the work in Refs. [18] which accomplishes the combination of an exact $\mathcal{O}(\alpha_s)$ correction with HERWIG. We note that, even in this latter result, the gluon azimuthal angle is averaged in the combination. We note that the recent alternative parton distribution function evolution MC algorithm in Refs. [19] can also be used

in our theoretical construction here. Due to its lack of the appropriate color coherence [20], we do not consider ISAJET [21] here.

To illustrate how the combination with Pythia/Herwig can proceed, we note that, for example, if we use a quark mass m_q as our collinear limit regulator, DGLAP [22] evolution of the structure functions allows us to factorize all the terms that involve powers of the big log $L_c = \ln \mu^2/m_q^2 - 1$ in such a way that the evolved structure function contains the effects of summing the leading big logs $L = \ln \mu^2/\mu_0^2$ where we have in mind that the evolution involves initial data at the scale μ_0 . The result is therefore independent of m_q for $m_q \downarrow 0$. In the context of the DGLAP theory, the factorization scale μ represents the largest p_\perp of the gluon emission included in the structure function. In practice, when we use these structure functions with an exact result for the residuals in (2), it means that we must in the residuals omit the contributions from gluon radiation at scales below μ . This can be shown to amount in most cases to replacing $L_s = \ln \hat{s}/m_q^2 - 1 \rightarrow L_{\text{nls}} = \ln \hat{s}/\mu^2$ but in any case it is immediate how to limit the p_T in the gluon emission ² so that we do not double count effects. In other words, we apply the standard QCD factorization of mass singularities to the cross section in (2) in the standard way. We may do it with either the mass regulator for the collinear singularities or with dimensional regularization of such singularities – the final result should be independent of this regulator. This would in practice mean the following: We first make an event with the formula in (4) which would produce an initial beam state at (x_1, x_2) for the two hard interacting partons at the factorization scale μ from the structure functions $\{F_j\}$ and a corresponding final state X from the exponentiated cross section in $d\hat{\sigma}_{\text{exp}}(x_i x_j s)$; the standard Les Houches procedure [23] of showering this event (x_1, x_2, X) would then be used, employing backward evolution of the initial partons. If we restrict the p_T as we have indicated above, there would be no double counting of effects. Let us call this p_T matching of the shower from the backward evolution and the matrix elements in the QCED exponentiated cross section.

However, one could ask if it is possible to be more accurate in the use of the exact result in (2)? Indeed, it is. Just as the residuals $\tilde{\beta}_{n,m}(k_1, \dots, k_n; k'_1, \dots, k'_m)$ are computed order by order in perturbation theory from the corresponding exact perturbative results by expanding the exponents in (2) and comparing the appropriate corresponding coefficients of the respective powers of $\alpha^n \alpha_s^m$, so too can the shower formula which is used to generate the backward evolution be expanded so that the product of the shower formula's perturbative expansion, the perturbative expansion of the exponents in (2), and the perturbative expansions of the residuals can be written as an over-all expansion in powers of $\alpha^n \alpha_s^m$ and required to match the respective calculated exact result for given order. In this way, new shower subtracted residuals, $\{\hat{\tilde{\beta}}_{n,m}(k_1, \dots, k_n; k'_1, \dots, k'_m)\}$, are calculated that can be used for the entire gluon p_T phase space with an accuracy of the cross section that should in principle be improved compared with the first procedure for shower matching presented above. Both approaches are under investigation.

Returning to the general discussion, we compute, with and without QED, $r_{\text{exp}} = \sigma_{\text{exp}}/\sigma_{\text{Born}}$. For this ratio we do not use the narrow resonance approximation; for, we wish to set a paradigm for precision heavy vector boson studies. The formula which we use for σ_{Born} is obtained from that in (4) by substituting $d\hat{\sigma}_{\text{Born}}$ for $d\hat{\sigma}_{\text{exp}}$ therein, where $d\hat{\sigma}_{\text{Born}}$ is the respective parton-level Born cross section. Specifically, we have from (1) the $\tilde{\beta}_{0,0}$ -level result

$$\hat{\sigma}_{\text{exp}}(x_1 x_2 s) = \int_0^{v_{\text{max}}} dv \gamma_{\text{QCED}} v^{\gamma_{\text{QCED}}-1} F_{\text{YFS}}(\gamma_{\text{QCED}}) e^{\delta_{\text{YFS}}} \hat{\sigma}_{\text{Born}}((1-v)x_1 x_2 s) \quad (5)$$

where we intend the well-known results for the respective parton-level Born cross sections and the value of v_{max} implied by the experimental cuts under study. What is new here is the value for the QED \otimes QCD exponent

$$\gamma_{\text{QCED}} = \left\{ 2Q_f^2 \frac{\alpha}{\pi} + 2C_F \frac{\alpha_s}{\pi} \right\} L_{\text{nls}} \quad (6)$$

where $L_{\text{nls}} = \ln x_1 x_2 s/\mu^2$ when μ is the factorization scale.

²Here, we refer to both on-shell and off-shell emitted gluons.

The functions $F_{\text{YFS}}(\gamma_{\text{QCD}})$ and $\delta_{\text{YFS}}(\gamma_{\text{QCD}})$ are well-known [12] as well:

$$\begin{aligned} F_{\text{YFS}}(\gamma_{\text{QCD}}) &= \frac{e^{-\gamma_{\text{QCD}}\gamma_E}}{\Gamma(1 + \gamma_{\text{QCD}})}, \\ \delta_{\text{YFS}}(\gamma_{\text{QCD}}) &= \frac{1}{4}\gamma_{\text{QCD}} + (Q_f^2 \frac{\alpha}{\pi} + C_F \frac{\alpha_s}{\pi})(2\zeta(2) - \frac{1}{2}), \end{aligned} \quad (7)$$

where $\zeta(2)$ is Riemann's zeta function of argument 2, i.e., $\pi^2/6$, and γ_E is Euler's constant, i.e., 0.5772... Using these formulas in (4) allows us to get the results

$$r_{\text{exp}} = \begin{cases} 1.1901 & , \text{QCD} \equiv \text{QCD} + \text{QED}, \text{ LHC} \\ 1.1872 & , \text{QCD}, \text{ LHC} \\ 1.1911 & , \text{QCD} \equiv \text{QCD} + \text{QED}, \text{ Tevatron} \\ 1.1879 & , \text{QCD}, \text{ Tevatron}. \end{cases} \quad (8)$$

We see that QED is at the level of .3% at both LHC and FNAL. This is stable under scale variations [13]. We agree with the results in Refs. [5, 6, 8–10] on both of the respective sizes of the QED and QCD effects. The QED effect is similar in size to structure function results found in Refs. [24–28], for further reference.

We have shown that YFS theory (EEX and CEEX) extends to non-Abelian gauge theory and allows simultaneous exponentiation of QED and QCD, QED⊗QCD exponentiation. For QED⊗QCD we find that full MC event generator realization is possible in a way that combines our calculus with Herwig and Pythia in principle. Semi-analytical results for QED (and QCD) threshold effects agree with literature on Z production. As QED is at the .3% level, it is needed for 1% LHC theory predictions. We have demonstrated a firm basis for the complete $\mathcal{O}(\alpha_s^2, \alpha\alpha_s, \alpha^2)$ results needed for the FNAL/LHC/RHIC/ILC physics and all of the latter are in progress.

Acknowledgments

One of us (B.F.L.W.) thanks Prof. W. Hollik for the support and kind hospitality of the MPI, Munich, while a part of this work was completed.

References

- [1] S. Klimenko, in *Proc. HCP2002*, ed. M. Erdmann,(Karlsruhe, 2002) p.413.
- [2] M. Dittmar, F. Pauss and D. Zurcher,*Phys. Rev. D***56** (1997) 7284; M. Rijssenbeek, in *Proc. HCP2002*, ed. M. Erdmann,(Karlsruhe, 2002)p. 424; M. Dittmar, *ibid.*,p.431.
- [3] B.F.L. Ward and S. Jadach, *Acta Phys.Polon.* **B33** (2002) 1543; in *Proc. ICHEP2002*, ed. S. Bentvelsen *et al.*,(North Holland, Amsterdam, 2003) p. 275 and references therein.
- [4] J.G.M. Gatherall, *Phys. Lett.* **B133** (1983) 90.
- [5] R. Hamberg, W. L. van Neerven and T Matsuura, *Nucl. Phys.***B359** (1991) 343.
- [6] W.L. van Neerven and E.B. Zijlstra, *Nucl. Phys.* **B382** (1992) 11; *ibid.* **B680** (2004) 513; and, references therein.
- [7] C. Anastasiou *et al.*,*Phys. Rev. D***69** (2004) 094008.
- [8] U. Baur, S. Keller and W.K. Sakumoto, *Phys. Rev. D* **57** (1998) 199; U. Baur, S. Keller and D. Wackerroth, *ibid.***59** (1998) 013002; U. Baur *et al.*, *ibid.***65** (2002) 033007, and references therein.
- [9] S. Dittmaier and M. Kramer, *Phys. Rev. D***65** (2002) 073007, and references therein
- [10] Z. A. Zykunov,*Eur. Phys. J.***C3** (2001) 9, and references therein.
- [11] D. R. Yennie, S. C. Frautschi, and H. Suura,*Ann. Phys.* **13** (1961) 379; see also K. T. Mahanthappa, *Phys. Rev.* **126** (1962) 329, for a related analysis.

- [12] See also S. Jadach *et al.*, *Comput. Phys. Commun.* **102** (1997) 229; S. Jadach, M. Skrzypek and B.F.L. Ward, *Phys. Rev. D* **55** (1997) 1206; S. Jadach, B.F.L. Ward and Z. Was, *Phys. Rev. D* **63** (2001) 113009; S. Jadach, B.F.L. Ward and Z. Was, *Comp. Phys. Commun.* **130** (2000) 260; S. Jadach *et al.*, *ibid.* **140** (2001) 432, 475.
- [13] C. Glosser *et al.*, *Mod. Phys. Lett. A* **19** (2004) 2119.
- [14] A.D. Martin *et al.*, *Phys. Rev. D* **51** (1995) 4756.
- [15] S. Jadach *et al.*, to appear.
- [16] G. Corcella *et al.*, hep-ph/0210213, and references therein.
- [17] T. Sjostrand *et al.*, hep-ph/0308153.
- [18] S. Frixione and B. Webber, *J. High Energy Phys.* **0206**(2002) 029; S. Frixione, P. Nason and B. Webber, *ibid.* **0308** (2003) 007, and references therein.
- [19] S. Jadach and M. Skrzypek, *Acta Phys. Pol.* **B35** (2004) 735; hep-ph/0504263, 0504205.
- [20] Michelangelo Mangano, private communication, 2004.
- [21] F. Paige *et al.*, hep-ph/0312045, and references therein.
- [22] G. Altarelli and G. Parisi, *Nucl. Phys.* **B126** (1977) 298; Yu. L. Dokshitzer, *Sov. Phys. JETP* **46** (1977) 641; L. N. Lipatov, *Yad. Fiz.* **20** (1974) 181; V. Gribov and L. Lipatov, *Sov. J. Nucl. Phys.* **15** (1972) 675, 938.
- [23] E. Boos *et al.*, hep-ph/0109068.
- [24] S. Haywood, P.R. Hobson, W. Hollik and Z. Kunszt, in *Proc. 1999 CERN Workshop on Standard Model Physics (and more) at the LHC, CERN-2000-004*, eds. G. Altarelli and M.L. Mangano, (CERN, Geneva, 2000) p. 122.
- [25] H. Spiesberger, *Phys. Rev. D* **52** (1995) 4936.
- [26] W.J. Stirling, "Electroweak Effects in Parton Distribution Functions", talk presented at ESF Exploratory Workshop, *Electroweak Radiative Corrections to Hadronic Observables at TeV Energies* , Durham, Sept., 2003.
- [27] M. Roth and S. Weinzierl, *Phys. Lett.* **B590** (2004) 190.
- [28] W. J. Stirling *et al.*, in *Proc. ICHEP04*, eds. H. Chen *et al.* (World Sci. Publ., Singapore, 2005) p. 527.

PHOTOS as a pocket parton shower: flexibility tests for the algorithm*

Piotr Golonka and Zbigniew Was

CERN, 1211 Geneva 23, Switzerland, and Institute of Nuclear Physics, ul. Radzikowskiego 152, 31-342 Kraków, Poland

Abstract

PHOTOS is widely used for generation of bremsstrahlung in decays of particles and resonances in LHC applications. We document here its recent tests and variants. Special emphasis is on those aspects which may be useful for new applications in QED or QCD.

Recently version 2.14 of the PHOTOS Monte Carlo algorithm, written for bremsstrahlung generation in decays became available. In Ref. [1] detailed instructions on how to use the program are given. With respect to older versions [2,3] of PHOTOS, it now features: improved implementation of QED interference and multiple-photon radiation. The numerical stability of the code was significantly improved as well. Thanks to these changes, PHOTOS generates bremsstrahlung corrections in Z and W decays with a precision of 0.1%. This precision was established in [4] with the help of a multitude of distributions and of a specially designed numerical test (SDP), see Ref. [1], section 5 for the definition. The tests for other channels, such as semileptonic K decays and leptonic decays of the Higgs boson and the τ -lepton, are presented in [4] as well. In those cases the level of theoretical sophistication for the reference distribution was lower though.

In this note we will not repeat a discussion of the design properties, but we will recall the main tests that document robustness and flexibility of the PHOTOS design. The results of the comparisons of PHOTOS running with different options of separation of its physical content into functional parts of the algorithm will be shown. The design of the program, i.e. the relation between the parts of the algorithm remained unchanged for these tests. This aspect may be of broader use and may find extensions in future applications, also outside the simple case of purely QED bremsstrahlung in decays.

In the calculations that led to the construction of PHOTOS we had to deal with the diagrams generated by photon couplings to the charged fermions, scalars or vectors. They were definitely simpler than the ones required for the QCD, nonetheless they offered a place to develop solutions which may be of some use there as well. Having such possibility in mind, yet not having any extension to QCD at hand, we have called PHOTOS a *pocket parton shower*. We hope that the methods we developed would be useful for QCD at least as pedagogical examples.

We begin with a presentation of the components of the PHOTOS algorithm using operator language. The consecutive approximations used in the construction of the crude distribution for photon generation, and the correcting weights used to construct the physically complete distributions are listed, but can not be defined in detail here. Instead, we present the variations of the algorithm. Comparisons between different options of the algorithm provide an important class of technical tests, and also help to explore the limits of the universality of the PHOTOS solution. The results of some of these tests will be listed later in the contribution (for the remaining ones and the details we address the reader to refs. [1, 4]). In the comparisons we use the SDP universal test based on MC-TESTER [5] as in Ref. [1]. We skip its definition here as well.

The starting point for the development of PHOTOS was the observation that, at first order, the bremsstrahlung corrections in the $Z \rightarrow \mu^+ \mu^-$ process can be written as a convolution of the Born-level distribution with the single-photon emission kernels for the emission from μ^+ and μ^- .

*Supported in part by the EU grant MTKD-CT-2004-510126, in partnership with the CERN Physics Department, and the Polish State Committee for Scientific Research (KBN) grant 2 P03B 091 27 for the years 2004–2006.

The formulae for the emission kernels are 3-dimensional and can be parametrized using the angles and the invariant mass, which are the same variables as those used in the parametrization of the three-body phase space (the kernels use only a subset of the complete set of phase-space parametrization variables). The remaining two angular variables, not used in the kernels, can be identified as the angles defining the orientation of the μ^+ and/or μ^- directions (for a detailed definition, see e.g. [2]).

The principle of the single-photon algorithm working on n -body decay is to replace a point in the n -body phase space Ω_2 , with either the point in the original Ω_2 , or the point in the $(n + 1)$ -body phase space Ω_3 (with generated photon). The overall normalization of the decay rate has to change as well and, for example, in the case of $Z \rightarrow \mu^+ \mu^-$, due to the action of the single-photon algorithm, it needs to be multiplied by a factor of $1 + \frac{3}{4} \frac{\alpha}{\pi}$.

Subsequent steps of the PHOTOS algorithm are described in terms of the evolution operators. Let us stress the relations of these operators to the matrix elements and phase-space parametrizations. We will present the decomposition of the operators in the top-down order, starting with the definition of R_α , the operator describing the complete PHOTOS algorithm for single emission (which at least in the case of Z and leptonic τ decays originates from field theory calculations without any approximation). Then, we will gradually decompose the operators (they differ from decay channel to decay channel) so that we will end up with the single well-defined, elementary operator for the emission from a single charged particle in the final state. By aggregation of these elementary operators, the R_α may be reconstructed for any decay channel. Let us point out that the expression of theoretical calculations in the form of operators is particularly suitable in computer programs implementation.

We skip here a separate discussion of the factorization properties, in particular to define/optimize the way the iteration of R 's is performed in PHOTOS. Not only the first-order calculations are needed, but also higher-order ones, including mixed virtual-real corrections. For practical reasons, the R_α operator needs to be regularized with the minimum energy for the explicitly generated photons: the part of the real-photon phase space, under threshold, is integrated, and the resulting factor is summed with the virtual correction.

• 1

Let us define the five steps in R_α separation. In the first one, the R_α is replaced by (we use two-body decay as an example) $R_\alpha = R_I(R_S(\mu^+) + R_S(\mu^-))$, where R_I is a generalized interference operator and R_S is a generalized operator responsible for photon generation from a single, charged decay-product.

Let us point out here, that we use the word *interference* here having in mind its usual quantum-mechanical sense. The interference is introduced simultaneously for the real and the virtual photon correction. As a consequence, it changes, for instance, the hard-photon energy spectrum, and the action of R_I looks like kinematic reshuffling of events around the phase space. This interpretation of the interference was particularly clear in the case of the Z decays where the R_I operator can introduce *exact and complete* first-order radiative corrections.

It is important to firstly define the amplitudes, the sum of which is squared, in physically meaningful way, that is in gauge-invariant way, to produce interference. Our approach has changed with time, and we relaxed this requirement; at present we simply request that the action of R_I properly introduces interference effects. We also require that the generalized interference operator respects energy-momentum conservation, and also overall normalization of the distribution under construction. The freedom of choice in the separation of R_α into R_I and R_S we obtained this way is used to create different variants of the PHOTOS algorithm.

The R_S operator acts on the points from the Ω_2 phase space, and the results of its action belong either to Ω_2 or to Ω_3 . The domain of the R_I operator has to be $\Omega_2 + \Omega_3$, and the results are also in $\Omega_2 + \Omega_3$. In our solution we required that R_I acts as a unit operator on the Ω_2 -part of its domain and, with some probability, returns the points from Ω_3 back to the original points in Ω_2 , thus reverting the action of the R_S .

Let us stress that in practical applications, to ease the extension of the algorithm to “any” decay mode, we used in PHOTOS a simplification for R_I . Obviously, the exact representation of the first-order result would require R_I to be decay-channel-dependent. Instead, we used an approximation that ensures the proper behaviour of the photon distribution in the soft limit. Certain deficiencies at the hard-photon limit of the phase space appear as a consequence, and are the subject of studies that need to be performed individually for every decay channel of interest. The comparisons with matrix-element formulae, as in [6], or experimental data, have to be performed for the sake of precision; they may result in dedicated weights to be incorporated into PHOTOS. In principle, there is no problem to install a particular decay-channel matrix element, but there has not been much need for this yet. So far, the precision of the PHOTOS algorithm could always be raised to a satisfactory level by implementing some excluded parts of formulae, being the case of W decay [6] an exception.

The density generated by the R_S operator is normally twice that of real photons at the end of generation and all over the phase space; it can also overpopulate only those regions of phase space where it is necessary for R_I . The excess of these photons is then reduced by Monte Carlo with the action of R_I .

• 2

In the next step of the algorithm construction, we have separated $R_S = R_B R_A$, where R_B was responsible for the implementation of the spin-dependent part of the emission, and the R_A part was independent of the spin of the emitting final-state particle. Note that this step of the algorithm can be performed at the earlier stage of generation as well, that is before the full angular construction of the event. R_B is again, as R_I , it moves the hard bremsstrahlung events in excess back to the original no-bremsstrahlung ones. R_B operates on the internal variables of PHOTOS rather than on the fully constructed events.

• 3

The definition of the R_I , R_B , R_A operators was initially based on the inspection of the first-order matrix elements for the two-body decays. In the general solution for R_A , the process of multiple-body decay of particle X is temporarily replaced by the two-body decay $X \rightarrow CY$, in which particle X decays to the charged particle C , which “emits” the photon, and the “spectator system” Y . The action of the operator is repeated for each charged decay product: the subsequent charged particle takes the role of the photon emitter C ; all the others, including the photons generated in the previous steps, become a part of the spectator system Y . The independence of the emissions from each charged product then has to be ensured. This organization works well and can be understood with the help of the exact parametrization of multibody phase space. It is helpful for iteration in multiple-photon emission. It also helps to implement some genuine second-order matrix elements. This conclusion can be drawn from an inspection of the second-order matrix elements, as in [7].

• 4

In the next step, we decompose the R_A operator, splitting it in two parts: $R_A = R_a R_x$. The R_x operator generates the energy of the (to be generated) photon, and R_a generates its explicit kinematic configuration.

The R_x operator acts on points from the Ω_2 phase space, and generates a single real number x ; the R_a operator transforms this point from Ω_2 and the number x to a point in Ω_3 , or leaves the original point in Ω_2 . Note that again, as R_I , the R_a operator has to be unitary and has to conserve energy–momentum¹.

An analogy between R_x and the kernel for structure-function evolution should be mentioned. However, there are notable differences: the x variable is associated more with the ratio of the invariant mass of decay products of X , photon excluded, and the mass of X , than with the fraction of energy taken away by the photons from the outgoing charged product C . Also, R_x can be simplified by moving its parts to R_a , R_S or even R_I . Note that in R_x the contributions of radiation from all charged final states are summed.

• 5

The R_x operator is iterated, in the solutions for double, triple, and quartic photon emission. The iterated R_x can also be shifted and grouped at the beginning of the generation, because they are free from the phase-space constraints. The iterated R_x takes a form similar to a formal solution for structure-function evolution, but with exceptionally simple kernels. The phase-space constraints are introduced later, with the action of the R_a operators. Because of this, the iteration of R_x can go up to fixed or infinite order. The algorithm is then organized in two steps. At first, a crude distribution for the number of photon candidates is generated; then, their energies are defined. For that purpose we can perform a further separation: $R_x = R_f R_0 R_N$, where the R_0 operator determines whether a photon candidate has to be generated at all, and R_f defines the fraction of its energy (without energy–momentum-conservation constraint). From the iteration of R_0 , we obtain a Poisson distribution, but any other analytically solvable distribution would be equally good.

The overall factor, such as $1 + \frac{3}{4} \frac{\alpha}{\pi}$ in Z leptonic partial width, does not need to be lost. It finds its way to the R_N , which is a trivial overall normalization constant in the case of the final-state radiation discussed here. In the cases where precision requirements are particularly high, the users of PHOTOS should include this (process-dependent) factor into the decay tables in their main generator for decays. However, until now, the effects on the normalization due to R_N are too small and were usually neglected. We rise the attention to this point, because it may be important for generalizations, when different organization of R_f , R_0 and R_N may be enforced by the properties of the matrix elements.

The input data for the algorithm are taken from the event record, the kinematic configurations of all particles, and the mother–daughter relations between particles in the decay process (which could be a part of the decay cascade) should be available in a coherent way.

This wraps up, a basic, presentation of the steps performed by the PHOTOS algorithm. For more details see [1, 8].

Tests performed on the algorithm:

1. The comparison of PHOTOS running in the quartic-photon emission mode and the exponentiated mode for the leptonic Z and W decays may be found on our web page which documents the results of the tests [4]. The agreement in branching ratios and shapes of the distributions is better than

¹On the contrary, the R_x operator can not, in general, fulfill the unitarity requirement. For example, the part of R_a leading to $1 + \frac{3}{4} \frac{\alpha}{\pi}$ for the Z decay can not be placed elsewhere but in R_x . The energy–momentum conservation does not apply directly to R_x , as it does not change the kinematic configuration, but only supplements it with x , the energy of the photon to be generated. However, for multiple-photon generation, the limits for generated x for subsequent generated photons are the same as for the first photon, which may be in potential conflict with energy–momentum conservation constraint.

0.07% for all the cases that were tested. It can be concluded that changing the relative order for the iterated R_0 and the rest of R_α operators does not lead to significant differences. This test, if understood as a technical test, is slightly biased by the uncontrolled higher-than-fourth-order terms which are missing in the quartic-emission option of PHOTOS. Also, the technical bias, due to the minimal photon energy in generation, present in the fixed-order options of PHOTOS may contribute to the residual difference.

2. The comparison of PHOTOS with different options for the relative separation between R_I and R_S . The tests performed for the fixed-order and exponentiated modes indicated that the differences in results produced by the two variants of the algorithm are below the level of statistical error for the runs of 10^8 events. In the code these two options are marked respectively as VARIANT-A and VARIANT-B.
3. The comparisons of PHOTOS with different algorithms for the implementation of the R_I operator. In PHOTOS up to version 2.12, the calculations were performed using internal variables in the angular parametrization. This algorithm was limited to the cases of decays of a neutral particle into two charged particles. In later versions, the calculations are performed using the 4-momenta of particles, hence for any decay mode. The tests performed for leptonic Z decays indicated that the differences are below the statistical error of the runs of 10^8 events.
4. The comparisons of PHOTOS with different options for the relative separation between R_0 and R_x , consisting of an increase in the crude probability of hard emission at R_0 . The tests performed for the exponentiated mode of PHOTOS indicated that the differences are below the statistical error of the runs of up to 10^8 events.
5. The remaining tests, including new tests for the effects of the interference weights in cascade decays, are more about the physics content of the program than on the technical or algorithmic aspects. They are presented in Ref. [1] and the results are collected on the web page [4].

Multiple options for PHOTOS running and technical compatibility of results even for 10^8 event samples generated in a short CPU cycle time are encouraging. They indicate the potential for algorithm extensions. Note that PHOTOS was found to work for decays of up to 10 charged particles in the final state.

Acknowledgements: The authors are indebted to members of BELLE, BaBar, NA48, KTeV, ATLAS, CMS, D0, CDF collaborations for useful comments and suggestions.

References

- [1] P. Golonka and Z. Was, hep-ph/0506026.
- [2] E. Barberio, B. van Eijk, and Z. Was, *Comput. Phys. Commun.* **66** (1991) 115.
- [3] E. Barberio and Z. Was, *Comput. Phys. Commun.* **79** (1994) 291–308.
- [4] P. Golonka and Z. Was, see <http://cern.ch/Piotr.Golonka/MC/PHOTOS-MCTESTER>.
- [5] P. Golonka, T. Pierzchala, and Z. Was, *Comput. Phys. Commun.* **157** (2004) 39–62.
Also available as hep-ph/0210252.
- [6] G. Nanava and Z. Was, *Acta Phys. Polon.* **B34** (2003) 4561–4570.
Also available as hep-ph/0303260.
- [7] Z. Was, hep-ph/0406045.
- [8] P. Golonka, *In preparation*. PhD thesis, Institute of Nuclear Physics, Krakow, 2005/2006.
Written under the supervision of Z. Was.
A preliminary version will be available at <http://cern.ch/Piotr.Golonka/MC/PhD>.

